AN INVESTIGATION OF BLAST WAVES GENERATED BY CONSTANT VELOCITY FLAMES

by

Robert Thomas Luckritz

Dissertation submitted to the Faculty of the Graduate School
of the University of Maryland in partial fulfillment
of the requirements for the degree of
Doctor of Philosophy
1977

APPROVAL SHEET

Title of Dissertation: An Investigation of Blast Waves Generated by Constant Velocity Flames

Name of Candidate: Robert Thomas Luckritz

Doctor of Philosophy, 1977

Dissertation and Abstract Approved: Joseph M. Marchello

Joseph M. Marchello
Professor
Chemical Engineering
University of Maryland

Date Approved: February 9, 1977

ABSTRACT

Title of Dissertation: An Investigation of Blast Waves Generated by Constant Velocity Flames

Robert Thomas Luckritz, Doctor of Philosophy, 1977

Dissertation directed by: Joseph M. Marchello
Professor
Chemical Engineering

The relevant flow field parameters associated with the generation and propagation of blast waves from constant velocity flames were systematically studied through numerical integrations of the non-steady equations for mass, momentum, and energy. The flow was assumed to be that of an adiabatic inviscid fluid obeying the ideal gas law and the flame was simulated by a working fluid heat addition model.

The flame velocity was varied from infinitely fast (bursting sphere) through velocities characterized by the nearly constant pressure deflagration associated with low Mach number laminar flames. The properties noted included peak pressure, positive impulse, energy distribution, and the blast wave flow field.

Results were computed for the case of a methane-air mixture assuming an energy density, $q = 8.0$, an ambient specific heat ratio, $\gamma_o = 1.4$ and a specific heat ratio behind the flame, $\gamma_4 = 1.2$. In the source volume, as the flame

velocity decreased to Mach 4.0 the overpressure increased. For flame velocities below Mach 4.0 the overpressure decreased, and approach the acoustic solution originally developed by Taylor. In the far field the overpressure curves for supersonic flame velocities coalesced to a common curve at approximately 70% of Baker's pentolite correlation. Far field overpressures for subsonic flame velocities decreased as the flame velocity decreased.

For the flame velocities investigated the near field impulse was greater than the impulse from Baker's pentolite correlation. In the far field the flame generated impulse decreased to 60 to 75% of the pentolite impulse.

In cases where the flow was expected to reduce to a self-similar solution and/or show Rayleigh line behavior it did. The calculations showed that the flow field behaved normally where expected, and for flow velocities where steady state behavior is not expected, non-steady behavior was observed.

ACKNOWLEDGEMENTS

The author extends a special thank you to Professor Joseph M. Marchello and Professor Roger A. Strehlow for their help and guidance during all phases of this research.

To Mrs. Florence Goldsworthy who assisted in the prep-paration and typing of this manuscript, the author expresses his sincere gratitude.

Sincere appreciation is extended to the U.S. Coast Guard for the opportunity to pursue this degree and the financial support provided.

The computer time for this project was supported in part through the facilities of the Computer Science Center of the University of Maryland.

TABLE OF CONTENTS

APPENDIX

LIST OF TABLES

LIST OF ILLUSTRATIONS

I. INTRODUCTION

The increasing energy needs of the United States and other advanced technology countries have resulted in the handling, transportation, and storage of ever increasing quantities of highly volatile and highly combustible fuels. Present projections of energy needs for the future indicate a continued expansion of energy demands in these countries. As with any technological advance the luxuries provided by the use of large quantities of these energy sources are accompanied by an increased risk in the event of their accidental release.

In addition to the ever increasing need for additional fuel, the government and the public have become cognizant of the necessity for protection of the environment from pollution by the contaminants present in many of our more abundant fuel supplies. Natural Gas is one energy source which is presently available, easily distributed, and relatively low in pollution potential. However, the supply of easily accessible Natural Gas in the United States is limited and many existing distribution facilities in large metropolitan areas are unable to meet peak winter demands. To alleviate this situation many utilities are storing the natural gas in a liquefied state and/or providing for the importation of shipload quantities from such areas as Alaska, Algeria, Libya, and Indonesia.

The release of natural gas from accident, natural disaster, or sabotage could subject personnel and facilities near the release to great risk. Among these risks are the danger of fire and/or explosion if the release were ignited. The question which concerns both governmental decision makers and the public at large is precisely what would be the effects of large scale releases of a flammable gas such as Natural Gas.

Compounding this difficult question is the conclusions which can be extrapolated from accidents as a result of the release of similar exothermic compounds. A survey of accidental explosions that have occurred over the past 40 years was compiled by Strehlow[(1)]. He noted a sharp increase in annual damage from accidental explosions since 1964 and attributed this increase to larger spills of a variety of chemical substances with many spills occuring in the neighborhood of expensive process equipment. In his paper he recommended an investigation into the effects of the overall flame-propogation rate and the nature of the blast wave produced by the deflagrative combustion of a large unconfined vapor cloud.

There are also basic fundamental questions concerning the fluid dynamic flow field developed by an accidental explosion. The flow fields generated by high explosives have been investigated in detail for weapons applications and industrial blast technology. To date there has been only minimal effort directed to investigating the effects of accidental (non-ideal) explosions.

This dissertation addresses one aspect of accidental (non-ideal) explosions, namely the consequences of the propagation of constant velocity flames after delayed ignition. That is, what happens when there is a large scale release of flammable gas with widespread dispersion of the vapors, followed by ignition? Other related problems such as the effects of a burning pool of flammable fuel or the effects of rapid release which does not involve delayed ignition of the mixture are not addressed. The problem is presented in terms of a systematic study of the effects of constant Lagrangian velocity flame through a flammable, compressible mixture. The behavior of the flow is studied in the compressible medium surrounding the flammable mixture during and after heat addition.

A heat addition-working fluid model is used to replace the combustion process. This model and the equations of mass, momentum, and energy coupled with the equation of state are used to study the effects of heat addition waves. Both the near field and far field effects including peak pressure, impulse, and energy distribution were studied to show systematic trends and effects for an energy density approximating that of a stoichiometric mixture of natural gas in air, a common fuel.

A. Ideal (Point Source) Blast Waves

A blast wave is a pressure wave of finite amplitude generated by the rapid release of energy, such as an explosion. The structure will vary as a function of the energy source which produces it.

Nuclear and high explosive explosions generate what are known as ideal or point source blast waves. These explosions are described as a finite amount of energy deposited in an infinitely small increment of time at an infinitesimal point in a uniform atmosphere. They generate a shock wave which monotonically decreases in strength as it propagates from the energy source. The properties of the shock wave and the flow associated with it can be determined by solving the non-steady, non-linear equations of fluid mechanics.

The Eulerian pressure-time history at a reference point would show ambient conditions until the shock wave arrived at time t_a, with an almost discontinuous rise to the peak over-pressure of the shock wave, $p_s^+ + p_o$, as illustrated in figure 1 from Baker[(2)]. This peak overpressure, $p_s^+ + p_o$, would be followed by nearly exponential pressure decay through the ambient pressure, p_o, at time $t_a + t^+$, to a minimum pressure of less than ambient, $p_o - p_s^-$, then increasing until the pressure again reaches ambient, p_o, at time $t_a + t^+ + t^-$.

The time during which the pressure is greater than ambient, t_a through $t_a + t^+$, is know as the positive phase. The time during which the pressure is negative, $t_a + t^+$ through $t_a + t^+ + t^-$, is known as the negative phase.

As an ideal (point source) blast wave propagates away from its source there are three regions of interest:

(1) The near field wave where pressures are so large that external pressure can be neglected. In this region

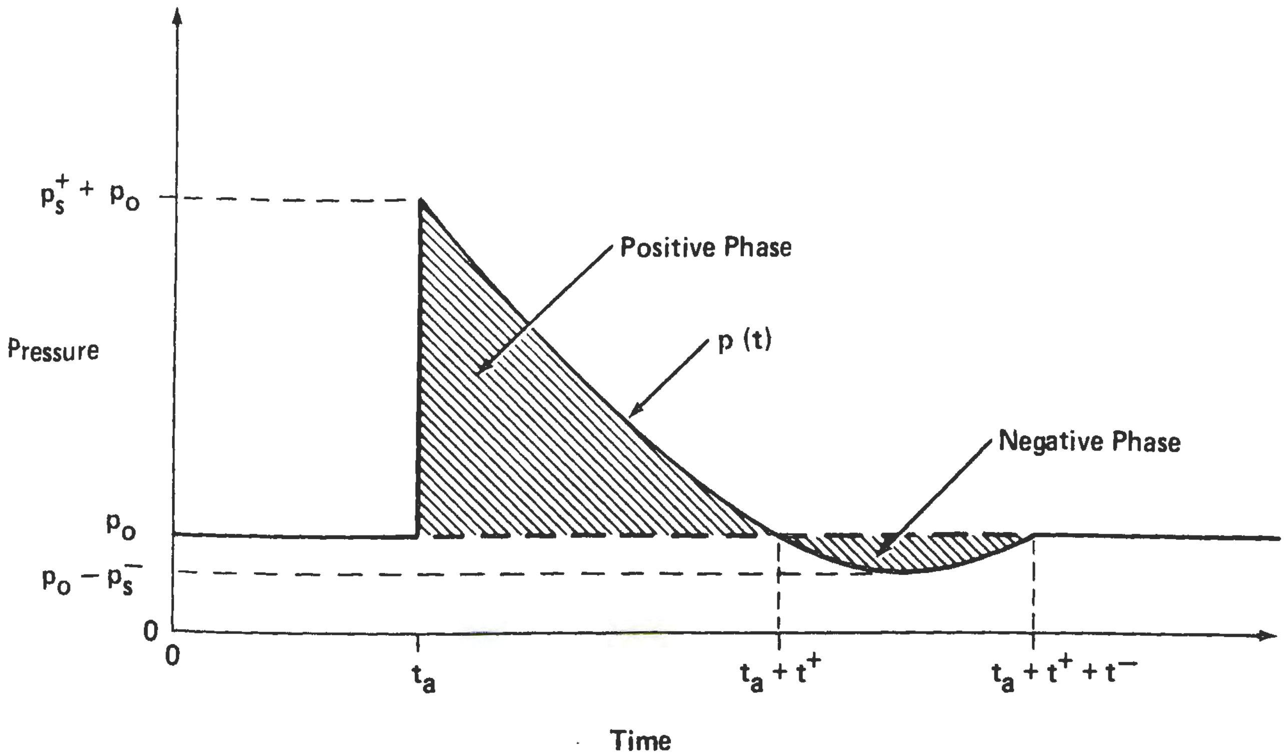

Figure 1. Pressure-time relationship for ideal blast wave.

self-similar solutions and analytical formulations are adequate. This is followed by

(2) An intermediate region of extremely practical importance because both the overpressure and impulse are sufficiently high to do significant damage. The flow field in this region cannot be solved analytically and must be solved numerically. This in turn is followed by

(3) A far field region which yields to an analytical approximation involving extrapolation of overpressure-time curves from one location to another. As the shock wave decays, its Mach number approaches unity and the lead wave nears the acoustic limit. There is theoretical evidence that an "N" wave which propagates as an acoustic level phenomena must form. However, atmospheric non-uniformities prevent the observation of this phenomena.

Assuming that the atmospheric counterpressure is small when compared to the shock overpressure, a constant value of specific heat, γ, and an instantaneous (over an infinitely small time) energy deposition at a point, Taylor(3), and Sedov(4) reduced the equations of fluid mechanics to non-linear differential equations with one independent variable. These differential equations were then solved to determine the blast wave behavior in the time-space domain. Their analysis determined the pertinent flow variables between the origin and the lead pressure wave and showed that: (1) the particle velocity and density decrease from a maximum value at the shock front to zero at the origin, (2) the pressure decreases, in a nearly exponential manner near the shock front, from a maximum value at the shock front, p_s^+, to a value of approximately 36% of p_s^+ at the origin (for γ=1.4 gas), and (3) the temperature increases without bound as the origin is approached.

While investigating these point source solutions, Bethe(5) observed from the shock relations:

$$\frac{\rho_2}{\rho_o} = \frac{(\gamma+1)M_1^{\ 2}}{(\gamma-1)M_1^{\ 2}+2} = \frac{(\gamma+1)}{(\gamma-1)+\dfrac{2}{M_1^{\ 2}}} \qquad \text{I-1}$$

where ρ_2 is the density of the fluid immediately behind the shock, ρ_o is the ambient density of the fluid, and M_1 is the approach fluid Mach number, that most of the mass in the system is concentrated near the shock. As gamma approaches one and the Mach number of the shock becomes large, the effect becomes more pronounced.

Using these same conditions it can be seen that in the limit as $\gamma\to1$, ρ_2/ρ_o approaches infinity, i.e. all the mass in the system bounded by the lead shock wave is located in or immediately adjacent to the wave.

B. Non-Ideal Blast Waves

Actual explosions do not generate ideal blast waves. Because of the explosive configuration, the finite reaction time, and the finite volume of the explosive, the pressure wave generated by a real explosion will not follow exactly the time-pressure distribution of an ideal blast wave. Near the energy source which is driving the pressure wave there may be a more gradual build-up in pressure than the nearly discontinuous pressure rise associated with ideal explosions. Other irregularities such as fragments, ground effects, reflections, etc. may cause pressure-time fluctuations inconsistent with ideal blast wave theory.

In general, non-ideal explosions are those where the source energy density is low and/or the energy deposition time is long. There are an infinite number of non-ideal source behaviors that yield blast waves with an infinite number of different structures, all non-ideal.

In point source analysis for ideal blast waves, the assumption is made that initially the energy is added to an infinitely small mass. Therefore, the total energy from the source is available to the surrounding gas to drive the lead shock wave. However, in a real explosion the energy is divided between the source volume and the surrounding atmosphere. Only the energy in the surrounding atmosphere drives the lead shock. This partitioning of energy causes the curves of overpressure vs. radius to lie below the curves from ideal or point source theory. However, as the energy density is increased and/or the time of deposition is decreased, as occurs in nuclear or high explosive explosions, the P_s - R_ε curves approach the ideal (point source) curves. This is attributed to the more efficient transmission of energy to the surrounding gas; thereby making more energy available to the shock and nearby flow field.

To model the rate of reduction of shock strength caused by the energy which remains in the source volume a non-similar solution in the form of series expansions of key non-dimensional flow parameters was developed by Sakurai[6]. He transformed the dependent and independent variables to another set where some of the variable were not as sensitive and then expanded each variable as a function of the Mach number squared. The variables were then incorporated into the conservation equations. Solutions, to various orders of accuracy, were obtained by collecting terms of like orders of magnitude and solving each set of differential equations produced, subject to applicable boundary conditions, and calculating the coefficients to the expansions. In the solution he used an energy source with an instantaneous energy deposition time, but indicated that sources with finite times of energy deposition could be modeled.

For the second order approximation Sakurai calculated the shock pressure for a $\gamma=1.4$ gas to be:

$$\frac{p_s}{p_o} = \begin{cases} 0.69\, R_\varepsilon^{-1} + 2.33 & j=0 \qquad \text{I-2} \\ 1.33\, R_\varepsilon^{-2} + 2.16 & j=1 \qquad \text{I-3} \\ 1.96\, R_\varepsilon^{-3} + 2.07 & j=2 \qquad \text{I-4} \end{cases}$$

where

$$R_\varepsilon = r_s / \left(\frac{E_j}{p_o}\right)^{\left(\frac{1}{1+j}\right)} \qquad \text{I-5}$$

$$E_j = \begin{cases} \text{Explosion energy per unit area} & j=0 \\ (\text{Explosion energy per unit line})(2\pi)^{-1} & j=1 \\ (\text{Explosion energy})(4\pi)^{-1} & j=2 \end{cases}$$

and j is the geometry factor (0,1, and 2 for planar, cylindrical and spherical flow fields respectively).

Data on shock arrival times were obtained by Oshima[7] from exploding wire experiments and were extensively compared with the predictions calculated by Sakurai. An increase in the range of validity was shown for the higher order approximations.

These analyses were performed with the assumption that the energy is deposited instantaneously. The heat release which occurs as a result of chemical reaction associated with a reactive fluid-dynamic process has both spatial and temporal dependence. In many cases this invalidates the simplifying self-similar assumptions and the theoritician must resort to numerical integration techniques to obtain a solution.

The conservation equations that describe blast waves are three non-linear partial differential equations. Two numerical techniques which have proven useful in the solution of numerous types of non-linear partial differential equations are the method of characteristics, a procedure from the theory of partial differential equations, and, with the development of high speed computers, finite differences.

When the finite differencing technique is used for the study of blast waves it is preferred to express the conservation equations of fluid dynamics in their Lagrangian form. In this method a fluid particle is followed from its initial position to a later position while its intensive properties vary as a function of time. The principle advantages are the computational grid does not distort with time and new grid points can be added as the lead wave uncovers new material.

One of the primary areas of interest on the study of blast waves is the generation and propagation of shock waves contained in the flow field and the deviation of these shock waves from those which would be generated in an ideal (point source) explosion. A shock wave can be described as a non-isentropic region in which the fluid properties rapidly change from their initial equilibrium states to a final state in which the temperature, density, and pressure are greater than ahead of the wave. The change in fluid properties occurs within a few mean free path lengths, the average distance a molecule must travel before it is influenced by the presence of another molecule. Because of the steep gradients in the non-isentropic region, the shock can be replaced by either a discontinuity satisfying the Rankine-Hugoniot "jump" relations[8] or, when using finite differencing procedures, by "spreading" this region to one of large but finite gradients over the length of a few computational cells. When performing numerical integrations using the finite differencing technique, gradients within the boundaries are assumed to the finite. Normally the shock is spread over the computational cells by incorporating into the momentum and energy equations a ficticious dissipative term developed by Von Neumann and Richtmyer[9] for their study of the propagation of plane shock waves. They incorporated a dissipation term which was proportional to the absolute value of the velocity gradient and only became significant in the shock region.

In a later analysis Lax and Wendroff[10] restricted the magnitude of gradients in strongly compressive regions by using the inherent dissipative mechanism in a modified central differencing scheme which attenuated the high frequency components of the solution.

The application of either dissipative mechanism to establish finite gradients does not violate the conservation of mass, momentum, or energy, as noted by Richtmyer and Morton[11]. The dissipated energy, which is only a minute amount of the total energy, appears as internal energy of the fluid.

Von Neumann[12] and Brode[13] were two of the first to apply the dissipative technique of Von Neumann and Richtmyer to the numerical solution of propagating spherical blast waves. By numerically integrating the differential equations of gas motion in Lagrangian coordinates, Brode determined the strong shock-point source solutions.

He determined that the strong shock-point source solutions of overpressure versus radius follows the inverse cube law down to an overpressure of approximately 10 atmospheres at which point actual overpressures are 3% higher than predicted.

Using a form of Sachs' scaling,[2] he proposed that the inverse cube relation be replaced by the following equation for pressures greater than 5 atmospheres:

$$P_s = 0.1567\ R_\varepsilon^{-3} + 1. \qquad \text{I-6}$$

For lower pressures he developed the following empirical fit:

$$P_s = \frac{0.137}{R_\varepsilon^{\ 3}} + \frac{0.119}{R_\varepsilon^{\ 2}} + \frac{0.269}{R_\varepsilon} - 0.019 \qquad \text{I-7}$$

$$0.1 < P_s < 10.$$

$$0.26 < R_\varepsilon < 2.8$$

where $$P_s = \frac{p_s - p_o}{p_o} \qquad \text{I-8}$$

$$R_\varepsilon = r_s/(E_T/p_o)^{1/3} \qquad \text{I-9}$$

and E_T is the total blast energy. He also solved for density, particle velocity, and particle position as functions of time and space.

Blast waves generated by the combustion of flammable vapors are of the non-ideal type. The mixing of the fuel with air gives an energy source dispersed over a large volume, i.e. the source has a low energy density. Also, the finite time required for the chemical reaction to reach end state conditions determines the time over which the energy is released.

An example of a strictly one-dimensional constant area, non-ideal blast wave generated by the deposition of a finite amount of energy over a finite volume is the rupture of a diaphram separating a high energy source gas from a low energy gas in a shock tube. At the instant the membrane is ruptured a wave system is generated at the edge of the pressure step as illustrated by figure 2. The wave system consists of a shock propagating into the low pressure gas while an expansion wave propagates through the high pressure source. Since the flow field is one-dimensional the pressure at the shock front can be determined by using the Rankine-Hugoniot jump conditions through the shock, the isentropic flow equations through the expansion fan, and matching the pressure and flow velocity at the contact surface. The procedure is outlined in Liepmann and Roshko[8] and other texts on compressible fluid flow.

From this analysis the overpressure at the shock front for one-dimensional, constant area flow is:

$$\frac{p_4}{p_1} = \frac{p_2}{p_1}\left[1-\frac{(\gamma_4-1)\left(\frac{a_o}{a_4}\right)\left(\frac{p_2}{p_1}-1\right)}{\sqrt{2\gamma_1\left[2\gamma_1+\left(\gamma_1+1\right)\left(\frac{p_2}{p_1}-1\right)\right]}}\right]^{\frac{-2\gamma_4}{\gamma_4-1}} \tag{I-10}$$

When the flow field geometry changes from planar (constant area) to cylindrical or spherical the one-dimensional, constant area solution is no longer valid. As the shock propagates through the surroundings there is a two or three dimensional relieving effect and the partial differential conservation equations can not be easily solved. Blast waves

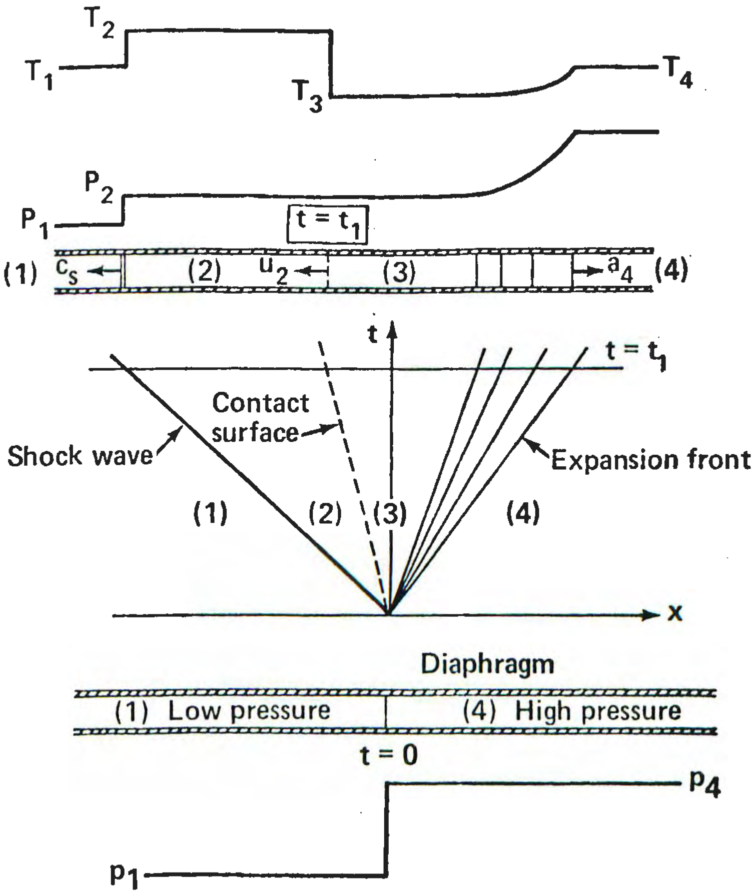

Figure 2. Motion in a shock tube.

from bursting pressurized gas spheres were studied by Ricker[14]. Using a Von Neuman/Richtmeyer type finite differencing procedure he obtained the relevant flow parameters by integrating the Lagrangrian, one-dimensional, non-steady fluid equations of motion. Blast damage (peak pressure and specific impulse vs radius) was calculated as a function of initial pressure, temperature, and the ratio of the specific heats of the gas in the source volume.

C. Homogeneous Energy Addition Blast Waves

In vapor and dust explosions the energy is deposited within a finite volume over a time period which is long in relation to the characteristic times of the system. Although bursting spheres have been extensively investigated, there has been little consideration to the case of homogeneous exothermic reactions which may occur when a highly dispersed cloud of combustible material is ignited.

An analysis of the pressure wave which is generated when a central core region containing a highly-exothermic mixture of hydrogen and oxygen begins to liberate heat was performed by Zajac and Oppenheim[15]. Using a constant timestep method of characteristic, they assumed a homogeneously reacting core region devoid of wave processes. An impermeable contact surface, across which the pressure and flow velocity was equal, separated the core region from the surroundings. The analysis incorporated the integration of the complete set of chemical-kinetic equations associated with the hydrogen-oxygen system for the core gas and the method of characteristics for the unreactive surrounding gas. Planar, cylindrical, and spherical flow field geometries were investigated and shock formation was predicted in both the planar and cylindrical flow with the distance greater in the cylindrical case. No shock formation was noted in the spherical case. This was attributed to the divergent effects of the expanding flow system.

Freeman[16] and Dabora[17] developed an analytical solution of self-similar flow fields which incorporated a variable rate of energy release as a function of time. In the analysis by Dabora the energy release was proportional to t^{β}. For β equal zero the energy release was instantaneous and for $\beta>0$ there was a gradual energy addition of finite power.

Adamczyk[18] performed a systematic study of the fluid dynamic and thermodynamic fields associated with the generation and propagation of blast waves from the homogeneous deposition of energy. Using a Von-Neumann/Richtmyer-type finite difference integration procedure, numerical solutions of the relevant flow parameters were generated by integrating the one-dimensional non-steady fluid dynamic equations of motion in Lagrangian form. Solutions were calculated for planar, cylindrical and spherical flow fields. Varying both the energy density of the source region and the time of energy deposition over two orders of magnitude he noted that they both affect the primary causes of structural damage, shock overpressure and positive phase impulse. A two-order of magnitude change in the time of energy deposition caused the near field, peak shock overpressure to vary by a factor of 80 and the near field positive-phase impulse to vary by a factor of 6. However, he found that the shock front "forgets" the influence of source non-idealities as it propagates from the origin.

D. Constant Velocity Flame Blast Waves

In the case of delayed ignition of a large volume of flammable gas the flow field will not be that of a bursting sphere as modeled by Brode(13) and Ricker(14) or a homogeneous reaction as studied by Zajac and Oppenheim(15) and Adamczyk(18). The flow field will develop from energy released as a flame front propagates from the ignition source through the combustible mixture to the edge of the source volume. Because of the finite source volume and the finite time required for the flame front to propagate from the ignition source to the edge of the kernel, the explosion will be non-ideal.

Combustion processes and non-steady one-dimensional flow in ducts were investigated by Rudinger(19). Assuming the chemical reaction takes place instantaneously as the unburned gas passes through an advancing flame front and the burning velocity is directly proportional to the absolute temperature of the unburned gas, he used the method of characteristics to calculate the properties of flame fronts with moderate, high, and detonative flame velocities. The conservation equations were reduced to a manageable form by omitting terms of small magnitude. Flow variables were then assumed to be uniformly distributed over any section of the duct leaving only time and one space coordinate as independent variables. The propagation of gas particles and pressure waves were then followed graphically in a coordinate system of these two variables on a plot called a wave diagram. Although this solution was strictly for one-dimensional flow, it led to the study of more complex flow fields.

A self-similar solution for evaluating the structure of blast waves was developed by Oppenheim[20], et al. The blast wave was assumed geometrically symmetrical and non-steady. The solution is in terms of two dimensionless independent variables, radius, R, and time, τ. The blast waves were examined in respect to two parameters, one describing the front velocity and the other the variation of the density immediately ahead of the front.

The evolution of pressure waves generated by steady flame propagating in an unbounded atmosphere with planar, cylindrical, and spherical geometry was studied by Kuhl Kamel, and Oppenheim[21]. They considered a self-similar flow field with both the deflagration and shock front propagating at constant velocity and constant gas dynamic parameters along lines of similarity $Y = r/r_s$. They introduced reduced blast wave parameters as phase-plane coordinates and determined the appropriate integral curves on this plane. A numerical solution for the case of a hydrocarbon-air mixture was developed which showed that the transition between the blast wave solution and the acoustic solution is continuous. Pressure curves were generated as a function of deflagrative burning velocity for an expansion ratio, ν_f, equal to 7.

A simplified method for calculating blast parameters generated by a propagating deflagration was developed by Strehlow[22]. Assuming that the pressure and density between the shock and the flame is spatially constant, regardless of geometry, the equations reduce to algebraic form allowing simple iterative solutions. Comparing his results with the exact self-similar solutions of Kuhl, et al., Strehlow showed his results were identical for the case of planar flow when the pressure between the shock and flame are known constant. However, when the geometry changes to cylindrical or spherical the divergence of the flow field causes the pressure to decrease from the flame to the shock and the results varied from the exact solution but were within acceptable limits.

E. Problem Definition

The classical problem of ideal or point source explosions has been extensively studied by many investigators. Ideal blast wave theory is well understood and conveniently summarized by Baker[28].

Non-ideal explosions are not well understood and many of the studies which have been done have not provided complete answers to the questions of interest. The solutions of Kuhl, et al. are limited by the self-similar assumption which applies only during the energy addition. There is no solution for the structure of the blast wave after the energy addition. Fishburn only investigated selected cases. Therefore his work did not show any trends. A systematic study of all the parameter affecting the generation and propagation of non-ideal blast waves is needed.

In the investigation of non-ideal explosions there are many parameters which affect the structure of the blast wave flow field. These parameters include the energy density of the source volume, the energy deposition time, the heat capacity ratio of the source volume and the surroundings, the flame velocity, and the flame thickness.

By considering these parameters as planes or dimensions in an n-dimensional space a convenient tool for visualizing this investigation in relation to other studies is available. Figure 3 illustrates three of the dimensions investigated:

(1) Energy density

(2) Energy deposition time

(3) Flame velocity (Plotted as the reciprocal)

An investigation of bursting spheres (infinitely fast energy wave with instantaneous deposition time) was performed by Ricker(14). His studies are located at various energy densities on the bursting sphere line in figure 3.

Adamczyk(18) expanded on the studies of Ricker. Adding energy uniformly throughout the source volume (infinite velocity, infinitely thick wave) he varied the energy density

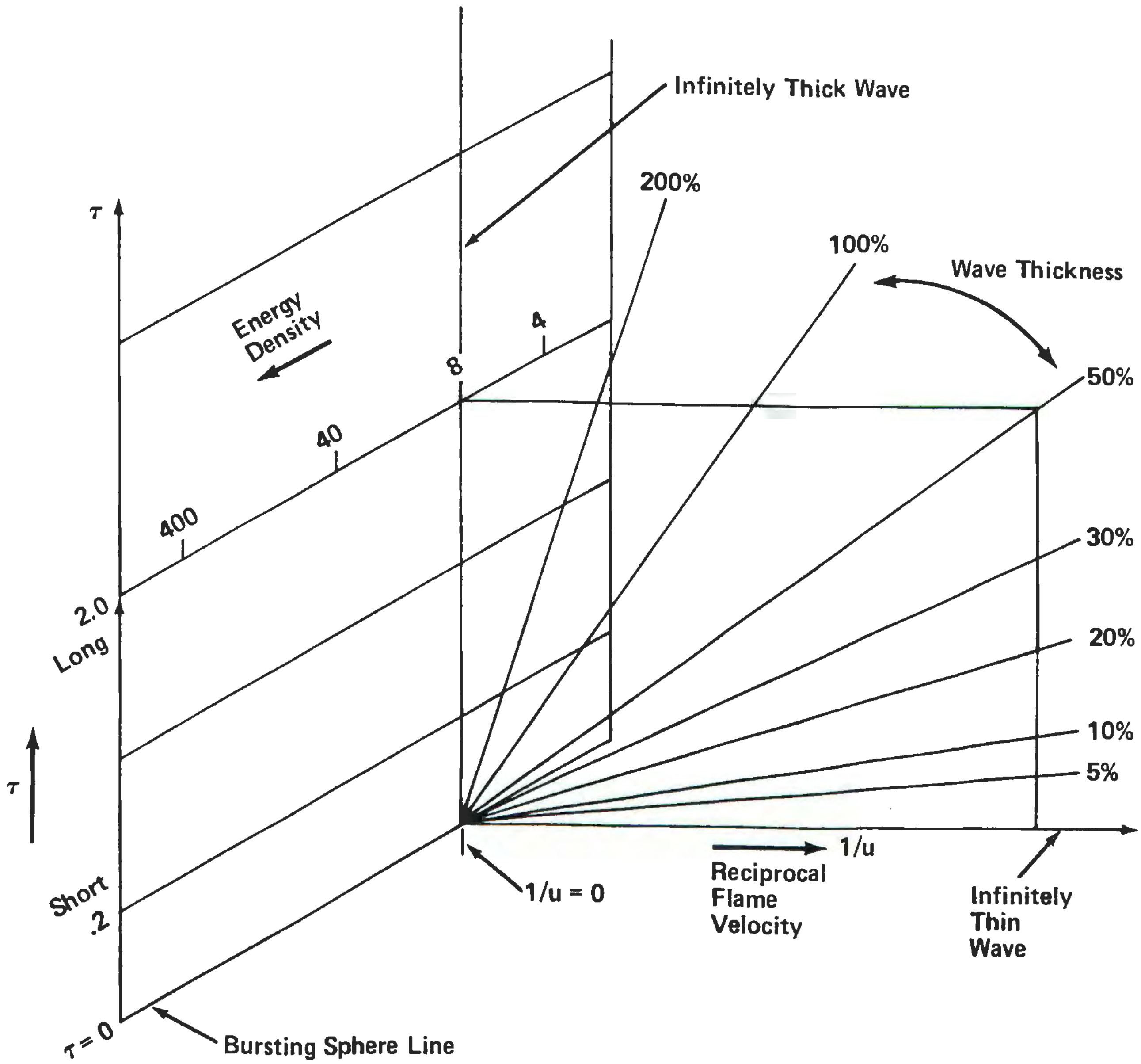

Figure 3. Three dimensional Diagram of three parameters affecting Non-ideal Blast Wave Behavior. (Not To Scale)

and energy deposition time, over two orders of magnitude.

This dissertation is part of a systematic study of the parameters affecting non-ideal explosions. In it the investigations of Ricker and Adamczyk are expanded into a third dimension, a study of the effects of a constant velocity flame propagating from the origin to the edge of the source volume. The investigation was done using the energy density of natural gas, a common fuel. Cases were systematically run at selected velocities and the results were then compared to the homogeneous energy addition and the common limit case of bursting sphere.

II. THEORETICAL CONSIDERATIONS

A. Governing Equations

Blast waves in air are non-steady flow fields propagating through a compressible fluid medium bounded by a gas dynamic discontinuity. To predict the effects of propagating blast waves it is essential to know the time history of the flow field properties at all locations within the medium. These properties are determined by the fundamental laws of nature applied to fluid flow. Air, at or near standard temperature and pressure, is considered to be an inviscid fluid. Shock waves that appear in the flow can be treated as discontinuities or by using an artificial viscosity technique. With these conditions the fundamental conservation equations can be expressed as:

$$\frac{\partial \rho}{\partial t} + \bar{\nabla}\cdot(\rho\bar{V}) = 0 \qquad \text{(Mass) II-1}$$

$$\frac{\partial \bar{V}}{\partial t} + \bar{V}\cdot\nabla\bar{V} = \frac{-(\nabla \cdot p)}{\rho} + \sum_i c_i \bar{f}_i \qquad \text{(Momentum) II-2}$$

$$\frac{\partial[\rho(e+\frac{V^2}{2})]}{\partial t} + \nabla\cdot[\rho(e+\frac{V^2}{2})\bar{V}] = -\nabla\cdot(p\bar{V})+\rho\mathring{Q}+\rho\Sigma c_i\bar{f}_i\bar{V}_i$$

(Energy) II-3

where ρ is the density, $\bar{V}$ is the flow velocity vector, p is the fluid pressure, e is the internal energy, $\mathring{Q}$ is the heat addition rate per unit mass, c_i is the mass concentration of species i, and $\bar{f}_i$ is the body force acting on species i.

Assuming an adiabatic inviscid fluid with no body forces, the terms involving $\bar{f}$ and $\mathring{q}$ become zero. Applying the thermodynamic equation of state, $p\nu = mR\theta$ with:

$$e = \sum_i c_i (e_i^\circ + \int_\circ^\theta c_{v_i} d\theta) \qquad \text{II-4}$$

where e_i° is the energy of formation and c_{v_i} is the constant volume heat capacity of species i, internal energy can be linked to temperature, θ, and density. There are then four equations to solve for the four prime variables of interest; u (local flow velocity), ρ (density), p (pressure), and e (internal energy per unit mass).

For simplification it is desirable to model the actual reactive fluid using a working fluid heat addition model. For a flow process the basic thermodynamic quantity is the enthalpy, h, explicitly defined by:

$$h = e + p\nu \qquad \text{II-5}$$

Enthalpy is used rather than internal energy, e, and equation II-4 is replaced by

$$h = \sum_i c_i h_i \qquad \text{II-6}$$

where $$h_i = \int_\circ^\theta c_{p_i} \, d\theta + (\Delta h_f^\circ)_i \qquad \text{II-7}$$

An actual flame process is an adiabatic process with no heat transfer to or from the system. However, large temperature changes occur within the system as a result of chemical reactions.

If the temperature is held constant during an exothermic chemical reaction heat must be removed from the system. The product enthalpy is then much less than the reactant enthalpy and the difference is Δh , the heat of reaction which was removed from the system. Since the system being modeled is an adiabatic system, the heat of reaction will not be removed but will become part of the system. Energy is conserved because the differing bond energies of the different molecules that appear or disappear lead to changes in the thermal energy of the system.

With these observations the chemical reactions of the system can be replaced by a simple heat addition to a working fluid. Assuming:

$$h_3 = h_3' = \int_0^{\Theta} c_{p_3} \, d\Theta \qquad \text{II-8}$$

$$h_4 = h_4' + \Delta h_f = \int_0^{\Theta} c_{p_4} \, d\Theta + \lambda \qquad \text{II-9}$$

where h_3 and h_4 represent the enthalpy before and after heat addition respectively, and a positive value of λ represents heat addition to the flow. The derivation of the full equations can be found in many texts on combustion, e.g. Williams[23] and Strehlow[24].

B. STEADY ONE-DIMENSIONAL FLOW DISCONTINUITY RELATIONSHIPS

Although details on steady one-dimensional flow discontinuities are available in most text books on combustion it is desirable to proceed with a brief review of basic principles and concepts for comparisons with non-steady behavior which are to be made in succeeding sections. Using the heat addition working fluid model there are four equations which, because of their complexity cannot be solved without certain assumptions and restriction. For the case under consideration, blast waves, a convenient simplification is that the shock in the blast wave can be approximated as being a one-dimensional phenomenon. Shock waves are extremely thin and fluid properties across the shock adjust within a few mean free path lengths. Thus in the scale under consideration the curvature of the shock approaches that of a planar wave and the one-dimensional relationships apply for the shock in plane-, line-, and point symmetrical blast waves.

The basic non-steady, one-dimensional conservation equations of fluid dynamics can then be expressed as:

$$\frac{\partial}{\partial t}(\rho r^j) + \frac{\partial}{\partial r}(\rho u r^j) = 0 \qquad \text{(Mass)} \quad \text{II-10}$$

$$\frac{\partial}{\partial t}(\rho u r^j) + \frac{\partial}{\partial r}(\rho u^2 r^j + p r^j) - j p r^{(j-1)} = 0 \qquad \text{(Momentum)} \quad \text{II-11}$$

$$\frac{\partial}{\partial t}[\rho r^j (e+\frac{u^2}{2})] + \frac{\partial[\rho u r^j (e+\frac{u^2}{2}) + p u r^j]}{\partial r} = 0 \qquad \text{(Energy)} \quad \text{II-12}$$

where

$$e \equiv c_v \Theta = \frac{p\nu}{\gamma - 1} \qquad \text{(State)} \quad \text{II-13}$$

and j = 0, 1, and 2 for planar, cylindrical, and spherical symmetry respectively.

Because shock waves are so thin the shock wave in blast wave structure can also be approximated as being quasi-steady. The equations of fluid dynamics can then be solved for the case of one-dimensional, constant area, inviscid flow to yield what are generally called the normal shock equations, i.e. the conditions for transition across a shock wave with heat addition:

$$\rho_1 u_1 = \rho_4 u_4 \qquad \text{(Mass)} \quad \text{II-14}$$

$$p_1 + \rho_1 u_1^2 = p_4 + \rho_4 u_4^2 \qquad \text{(Momentum)} \quad \text{II-15}$$

$$h_1' + u_1^2/2 = h_4' + u_4^2/2 + \lambda \qquad \text{(Energy)} \quad \text{II-16}$$

<u>Hugoniot</u>

Substituting the mass and momentum equation into the energy equation yields the Rankine Hugoniot equation.

$$h_4' - h_1' + \lambda = \tfrac{1}{2}(p_4 - p_1)(\nu_1 + \nu_4) \qquad \text{II-17}$$

With the enthalpy relationship, $h = C_p\Theta = \frac{\gamma R\Theta}{\gamma - 1}$ and the equation of state this becomes:

$$\left(\frac{\gamma_4}{\gamma_4 - 1}\right)\left(p_4\nu_4\right) - \left(\frac{\gamma_1}{\gamma_1 - 1}\right)\left(p_1\nu_1\right) + \lambda = \tfrac{1}{2}(p_4 - p_1)(\nu_1 + \nu_4) \qquad \text{II-18}$$

which represents the locus of final states, $p_4\nu_4$ for any initial conditions of p_1 and ν_1 with heat addition λ.

For the case of no chemical reaction λ is zero, γ is assumed constant, and equation II-18 becomes the shock Hugoniot, i.e. the locus of all possible solutions for normal shocks without chemical reactions for one set of upstream conditions, p_1 and ν_1.

$$\frac{\gamma}{\gamma-1}(p_2\nu_2 - p_1\nu_1) = \tfrac{1}{2}(p_2-p_1)(\nu_1+\nu_2) \qquad \text{II-19}$$

By algebraically manipulating the shock Hugoniot it can be shown that it will asymptotically approach p_2 and ν_2 as ν_2 and p_2 respectively approach infinity:

$$\left(\frac{p_2}{p_1}\right) \to -\left(\frac{\gamma-1}{\gamma+1}\right) \quad \text{as } \nu_2 \to \infty \qquad \text{II-20}$$

$$\left(\frac{\nu_2}{\nu_1}\right) \to \left(\frac{\gamma-1}{\gamma+1}\right) \quad \text{as } p_2 \to \infty \qquad \text{II-21}$$

Figure 4 is a plot of the shock Hugoniot. However it is physically known that the situation of pressure decrease across a shock wave does not exist. Therefore, in actuality the only physically real solution is the shock Hugoniot for increasing pressure and decreasing specific volume. This can be proven by an examination of the entropy change or by attempting to plot a discontinuous expansion for the shock Hugoniot by the Method of Characteristics.

For the case of heat addition to a constant gamma, ideal gas working fluid, Strehlow[24] determined that the reacted end state Hugoniot can be represented by a rectangular hyperbola

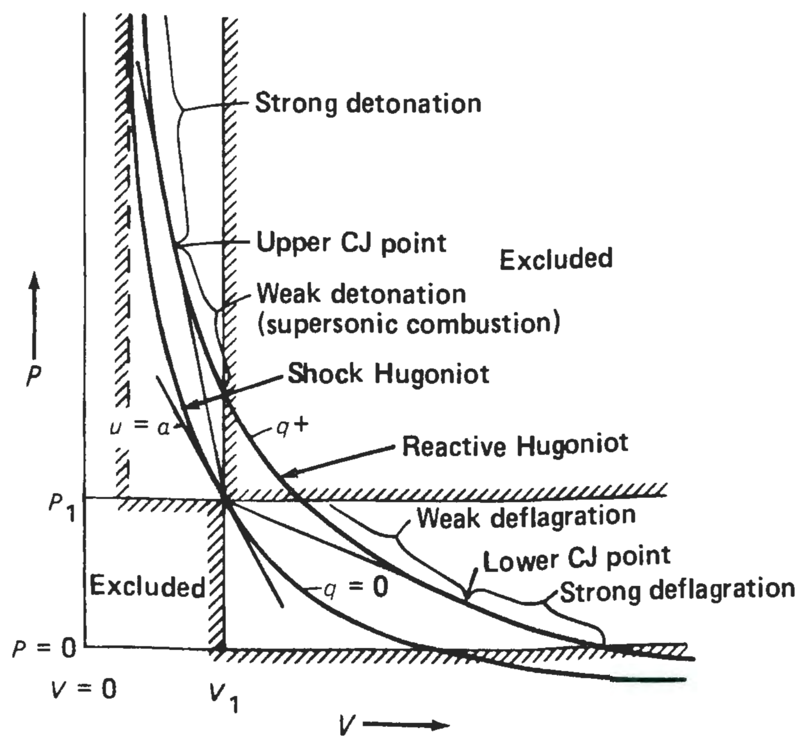

Figure 4. Pressure-volume plot of end states for a one-dimensional steady process with heat addition.

in the p-ν plane. Zajac and Oppenheim[25] have shown that this type of hyperbola accurately represents the shape of the real gas hugoniot. The assymptotes of the Reactive Hugoniot are:

$$\frac{p_4}{p_1} \rightarrow -\left(\frac{\gamma_4-1}{\gamma_4+1}\right) \qquad \text{as } \nu_4 \rightarrow \infty \qquad \text{II-22}$$

$$\frac{\nu_4}{\nu_1} \rightarrow \left(\frac{\gamma_4-1}{\gamma_4+1}\right) \qquad \text{as } p_4 \rightarrow \infty \qquad \text{II-23}$$

Two points for plotting the Reactive Hugoniot can be calculated by assuming a constant pressure expansion and a constant volume pressure rise:

$$\frac{p_4}{p_1} = \left(\gamma_4-1\right)\left(\frac{1}{\gamma_1-1} + \frac{\lambda}{p_1\nu_1}\right) \qquad \frac{\nu_4}{\nu_1} = 1 \qquad \text{II-24}$$

$$\frac{\nu_4}{\nu_1} = \left(\frac{\gamma_4-1}{\gamma_4}\right)\left(\frac{\gamma_1}{\gamma_1-1} + \frac{\lambda}{p_1\nu_1}\right) \qquad \frac{P_4}{P_1} = 1 \qquad \text{II-25}$$

Thus for the reactive Hugoniot the values of p_4 and ν_4 can be determined for plotting the curve. Since isotherms are hyperbolas that asymptotically approach the p=o, ν=o axis, the Hugoniot curves always cross the isotherms such that increasing p along a Hugoniot increases temperature. Since the temperature hyperbola asymptotes the axis, p = 0 represents a value of Θ = 0. This represents the hypothetical but impossible case where all the random kinetic energy of the molecules has been converted to ordered flow velocity.

Rayleigh Line

Manipulating further the normal shock equations by substituting the mass equation into the momentum equation, another relationship between the pressure and specific volume can be developed, the Rayleigh Line.

$$(\rho_1 u_1)^2 = -\left(\frac{p_4 - p_1}{\nu_4 - \nu_1}\right) \qquad \text{II-26}$$

The equation for the Rayleigh line specifies that the approach mass flow rate squared, $(\rho_1 u_1)^2$, is equal to the negative slope of a line in the p-ν plane connecting the initial and final states of the process under consideration. Thus if the initial conditions of p_1, ν_1, and u_1, are known, the final conditions p_4 and ν_4 can be determined by drawing a line through the initial point with a slope equal to $-(\rho_1 u_1)^2$. This straight line intersects the Hugoniot at the final state.

The Rayleigh line defines an important characteristic of steady state flow; since the density, ρ_1, and the flow velocity, u_1, are squared, their side of the equation will always be positive. Therefore, the slope of the steady state Rayleigh line must always be negative. Thus for steady state, one-dimensional flow, certain areas of the p-ν plane are excluded for final end states as illustrated by figure 4.

Equation II-26 can be rewritten in terms of the flow Mach number of the Rayleigh line process both ahead of the shock wave and behind the energy addition:

$$M_1{}^2 = \frac{1}{\gamma_1}\left[\frac{(p_4/p_1)-1}{1-\left(\frac{\nu_4}{\nu_1}\right)}\right] \qquad \text{II-27}$$

and

$$M_4{}^2 = \frac{\left(\frac{\nu_4}{\nu_1}\right)}{\gamma_4\left(\frac{p_4}{p_1}\right)}\left[\frac{\left(\frac{p_4}{p_1}\right)-1}{1-\left(\frac{\nu_4}{\nu_1}\right)}\right] \qquad \text{II-28}$$

When exothermic chemical reactions occur in a steady-state flow situation the Rayleigh line may intersect the Hugoniot in one, two, or no locations for both supersonic and subsonic incident flow velocity. Above a limiting subsonic velocity and below a limiting supersonic velocity the Rayleigh line does not intersect the Reactive Hugoniot and there are no possible steady-state solutions. Below the limiting subsonic velocity and above the limiting supersonic velocity the Rayleigh line intersects the Reactive Hugoniot twice, indicating two possible end states for both subsonic and supersonic velocities. For very low subsonic velocities the Rayleigh line can intersect the Reactive Hugoniot only once because the Hugoniot enters the imaginary region of negative pressure. The very low velocity subsonic solution corresponds to normal flame propagation. Physically, laminar flames are represented by this solution. For ordinary flames the flame velocity is very low and therefore there is only a very slight pressure drop across the wave.

At the tangency point of the Reactive Hugoniot and the Rayleigh line there exists only one propagation velocity. This velocity corresponds to exactly sonic velocity at station 4, and is called Chapman-Jouguet flow or CJ flow. The upper CJ point represents the proper end state for detonations. The existence of exactly sonic flow at the tangency point can be shown by differentiating the Hugoniot and equating this to the slope of the Rayleigh line

$$\left.\frac{d\left(\frac{p_4}{p_1}\right)}{d\left(\frac{\nu_4}{\nu_1}\right)}\right)_{\text{Hugoniot}} = -\left\{\frac{\gamma_4\left[\left(\frac{p_4}{p_1}\right)+1\right]+\left[\left(\frac{p_4}{p_1}\right)-1\right]}{\left[\left(\frac{\nu_4}{\nu_1}\right)+1\right]+\gamma_4\left[\left(\frac{\nu_4}{\nu_1}\right)-1\right]}\right\} \qquad \text{II-29}$$

$$\left.\frac{d\left(\frac{p_4}{p_1}\right)}{d\left(\frac{\nu_4}{\nu_1}\right)}\right)_{\text{Rayleigh}} = \frac{\left(\frac{p_4}{p_1}\right)-1}{\left(\frac{\nu_4}{\nu_1}\right)-1} \qquad \text{II-30}$$

The condition for tangency is then:

$$\left(\frac{p_4}{p_1}\right) = \frac{(\nu_4/\nu_1)}{\left(\frac{\nu_4}{\nu_1}\right)(\gamma_4+1) - \gamma_4} \qquad \text{II-31}$$

which can be rearranged to:

$$1 = \frac{(\nu_4/\nu_1)\left[\left(\frac{p_4}{p_1}\right) - 1\right]}{\gamma_4(p_4/p_1)[1 - (\nu_4/\nu_1)]} \qquad \text{II-32}$$

This is identical to Equation II-28, the equation for the Mach number of the Rayleigh line process at point 4, proving that the Mach number behind the shock at the upper and lower CJ points is sonic. For a strong detonation or a weak deflagration:

$$\left.\frac{d(p_4/p_1)}{d(\nu_4/\nu_1)}\right)_{\text{Hugoniot}} > \left.\frac{d(p_4/p_1)}{d(\nu_4/\nu_1)}\right)_{\text{Rayleigh}} \qquad \text{II-33}$$

and for a weak detonation or strong deflagration:

$$\left.\frac{d(p_4/p_1)}{d(\nu_4/\nu_1)}\right)_{\text{Hugoniot}} < \left.\frac{d(p_4/p_1)}{d(\nu_4/\nu_1)}\right)_{\text{Rayleigh}} \qquad \text{II-34}$$

Thus $M_4 < 1$ for a strong detonation or weak deflagration and $M_4 > 1$ for a weak detonation or strong deflagration.

Investigating further the characteristics of the upper CJ point, the Hugoniot equation and the Raleigh line can be combined to determine an explicit relationship for the pressure and volumetric ratio ahead of the shock and behind the energy addition:

$$\frac{P_4}{P_1} = \frac{(\gamma_4 M_1^2+1) \pm \gamma_1 \sqrt{(M_1^2-1)^2 + 2M_1^2\left[\frac{\gamma_1{}^2-\gamma_4{}^2}{\gamma_1(\gamma_1-1)} - \frac{\lambda(\gamma_4{}^2-1)}{a_1{}^2}\right] + \left[\left(\frac{\gamma_4}{\gamma_1}\right)^2 - 1\right]}}{\gamma_4 + 1} \qquad \text{II-35}$$

$$\frac{\nu_4}{\nu_1} = \frac{\frac{\gamma_4}{\gamma_1}\left(\gamma_1 M_1{}^2+1\right) \pm \sqrt{(M_1{}^2-1)^2+2M_1{}^2\left[\frac{\gamma_1{}^2-\gamma_4{}^2}{\gamma_1(\gamma_1-1)} - \frac{\lambda(\gamma_4{}^2-1)}{a_1{}^2}\right] + \left[\left(\frac{\gamma_4}{\gamma_1}\right)^2 -1\right]}}{(\gamma_4+1)M_1{}^2} \qquad \text{II-36}$$

The CJ point is the tangency point of the Rayleigh line and the Hugoniot curve. For this point there exists only one solution. Therefore, the expression under the radical sign must equal zero at the tangency point and can be expressed as follows:

$$\frac{(M_1{}^2-1)^2 + \left[\left(\frac{\gamma_4}{\gamma_1}\right)^2 -1\right]}{M_1{}^2} = 2\left[\frac{\lambda(\gamma_4{}^2-1)}{a_1{}^2} - \frac{(\gamma_1{}^2-\gamma_4{}^2)}{\gamma_1(\gamma_1-1)}\right] \qquad \text{II-37}$$

Knowing λ, the approach flow Mach number for the Chapman-Jouguet points can be evaluated:

$$M_{CJ} = \left\{ \left[1 + \frac{\lambda(\gamma_4^{\,2}-1)}{\gamma_1 p_1 \nu_1} - \frac{(\gamma_1^{\,2}-\gamma_4^{\,2})}{\gamma_1(\gamma_1-1)} \right] \pm \left[\left(1 + \frac{\lambda(\gamma_4^{\,2}-1)}{\gamma_1 p_1 \nu_1} - \frac{(\gamma_1^{\,2}-\gamma_4^{\,2})}{\gamma_1(\gamma_1-1)} \right)^2 - \left(\frac{\gamma_4}{\gamma_1}\right)^2 \right]^{\frac{1}{2}} \right\}^{\frac{1}{2}}$$

II-38

The pressure and specific volume can also be calculated from equations II-35 and II-36. At the CJ points the quantities within the radical signs of the equations become zero and the equations reduce to:

$$\left(\frac{p_4}{p_1}\right)_{CJ} = \frac{(\gamma_4 M_{CJ}^2 + 1)}{\gamma_4+1} \qquad \text{II-39}$$

$$\left(\frac{\nu_4}{\nu_1}\right)_{CJ} = \frac{\left(\frac{\gamma_4}{\gamma_1}\right)(\gamma_1 M_{CJ}^2+1)}{(\gamma_4+1)M_{CJ}^2} \qquad \text{II-40}$$

Even though one-dimensional steady-state heat addition is impossible over velocities which lie between the lower and upper CJ points, this investigation included the addition of energy at these forbidden velocities. This is possible since the calculation is fully non-steady. Therefore, the flow will follow a solution in accordance with the non-steady equations of mass, momentum, and energy, and will not be restricted by one-dimensional steady flow considerations.

C. ENERGY SCALING

Classical blast studies have been primarily directed to an investigation of the blast waves generated by either high explosives or nuclear weapons. When conducted on a large scale, experimental studies of blast waves are dangerous, expensive, and difficult to control. Large isolated areas are required where access and egress may be closely monitored and controlled to ensure the tests are conducted safely. In addition, the results are subject to the effects of atmospheric and topographical conditions which make the interpretation of data difficult and subject to error. The cost and other problems associated with large scale tests make their use in a systematic study of flow field behavior prohibitive.

Energy scaling is a tool which has been used extensively in the comparison and extrapolation of the results of tests involving different quantities and composition materials depositing energy in a source volume. The two most widely used methods of energy scaling involve Hopkinson's scaling law and Sachs' scaling law.

Hopkinson or "cube root" scaling is commonly used. This scaling, first formulated by Hopkinson[26] states that self-similar blast waves are produced when two similar explosive charges with characteristic dimensions varying by a length scaling factor, σ, are detonated in the same atmosphere, an observer whose location from the scaled explosive is σ times the distance from the standard, will feel a blast wave of similar form with amplitude P, duration σt, and impulse, σI. All characteristic times will be scaled by the same factor as the length scale factor, σ. Pressure, temperature, densities, and velocities are unchanged at homologous times. Hopkinson's scaling law requires that the model and prototype energy sources be of similar geometry and the same type of explosive or energy source. A more complete discussion of this scaling is available in Baker[2].

A more general blast scaling law than Hopkinson's was developed by Sachs to account for changes in ambient conditions and the effects of altitude. Sachs developed dimensionless groups that involve pressure, impulse, time, and ambient parameters as unique functions of the dimensionless distance parameter:

$$\left(\frac{p_s}{p_o}\,,\ \frac{(I_+)a_o}{\left(\frac{E_t}{p_o}\right)^{1/3}}\,,\ \frac{t\ a_o p_o{}^{1/3}}{E_t{}^{1/3}}\right) = f\left(r\left(\frac{p_o}{E_t}\right)^{\frac{1}{3}}\right) \qquad \text{II-41}$$

The Sachs' law identifies the blast source only by its total energy, E_t, and therefore is not restricted to similar geometry and explosive type as Hopkinson's law. However, it would not be expected to be consistent for scaling of close-in (near field) effects of non-ideal explosions.

Although the short comings in the use of these scaling parameters are obvious, they provide a convenient tool for comparing and analyzing theoretical and experimental data.

D. DAMAGE EQUIVALENCE

The concept of equivalence between non-ideal explosions is not fully understood. With equivalent far field overpressures, the near field behavior of non-ideal explosions may vary greatly. A means is needed to evaluate the effectiveness for blast damage of any particular accidental explosion and how this effectiveness varies with parameters affecting the development of the blast wave.

The common procedure in an actual accident is to observe the blast damage pattern to determine the weight of TNT (tri-nitro-toluene) required to develop blast wave overpressures to do similar damage at the same distance from the explosion center[27]. Next, the maximum equivalent TNT weight of the fuel or chemical is determined by calculating either the heat of reaction of the mixture or the heat of combustion of the substanced released. The mass equivalence of TNT is expressed as:

$$(W_{TNT})_{Equivalent} = \frac{\Delta H_c * m_c}{4.198 * 10^6} \qquad \text{II-42}$$

where ΔH_c is the heat of combustion of the hydrocarbon (cal/kgm), m_c is the total mass of the reactive mixture (kg), and 4.198×10^6 is the heat of explosion of TNT (joules). The common expression "per cent TNT equivalence" has been developed for comparison with data available from the testing of TNT and is determined by:

$$\%TNT = [(W_{TNT})_{damage} / (W_{TNT})_{equivalent}]*100. \qquad \text{II-43}$$

In an actual hydrocarbon explosion the damage as a function of scaled distance does not agree with that predicted from TNT equivalence. High explosives, such as TNT, contain internally much of the oxygen need for chemical reactions. Once initiated, the explosion proceeds almost instantaneously to completion.

Hydrocarbons, on the other hand, must react with the oxygen in the air, making mixing an important parameter. A finite time is required for the flame to propagate through the combustible mixture influencing the development of the blast wave. Also, the calculated heat of combustion is based on reactions to an equilibrium concentration of carbon dioxide and water. In actuality the reaction is not carried to equilibrium and at elevated temperatures the molecules may begin to dissociate, thereby further altering the effective heat release.

E. DAMAGE MECHANISMS

In the flow field associated with a blast wave there will be transient overpressures and wind induced drag forces.

The damage and injuries sustained by people, buildings, animals, and vegetation will vary, depending on the pressure-time history of the blast wave. Large overpressure of short duration may cause ear damage with little physical displacement of the body, whereas lower overpressure of longer-duration may cause lung damage and other severe body injuries. Similarly buildings may be constructed to resist overpressure of short duration, but may fail from the impulsive drag associated with lower overpressures of longer duration.

Damage and injuries are not restricted to the peak overpressure or impulsive drag alone, but to the combination and interaction of these effects. The exact relationships are quite complex, but a convenient simplification to correlate blast wave properties to damage effects on a wide variety of targets has been discussed by Baker, et al.(28). He states that for any object, levels of constant damage of one type can be plotted on a pressure-impulse (P-I) Diagram, or empirical or analytical equations can be developed to describe the pressure-impulse (P-I) relationship. An example is shown in figure 5.

To illustrate this concept, he considered the spring-mass system illustrated in figure 6 and subjected it to a specific time varying force to represent the dynamic response of a structure. The equations for a curve representing the combinations of scaled force and scaled impulse which cause the same scaled response X_{max} of the system were determined to be:

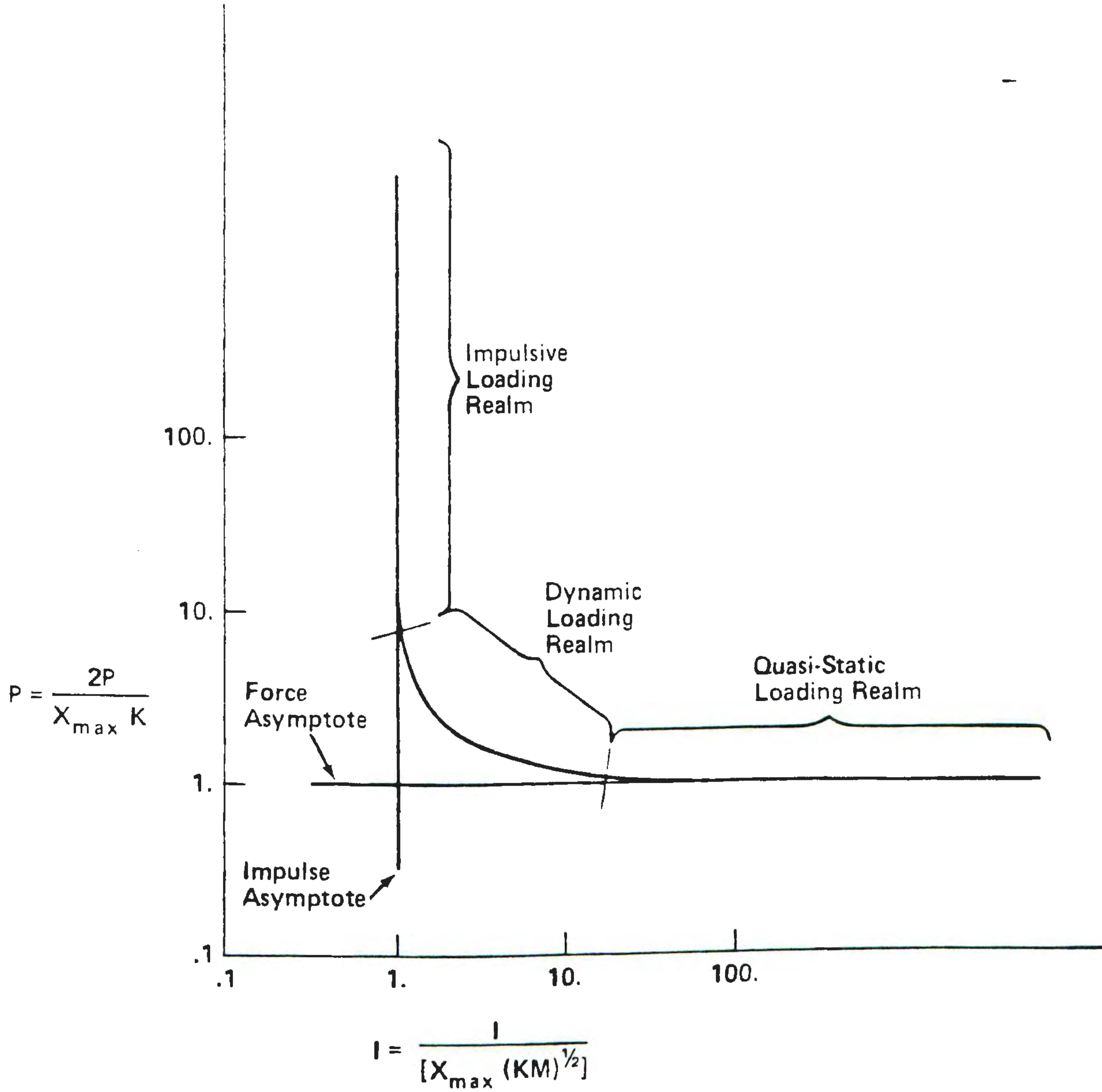

Figure 5. Scaled P—I Curve for Fixed Level of Damage.

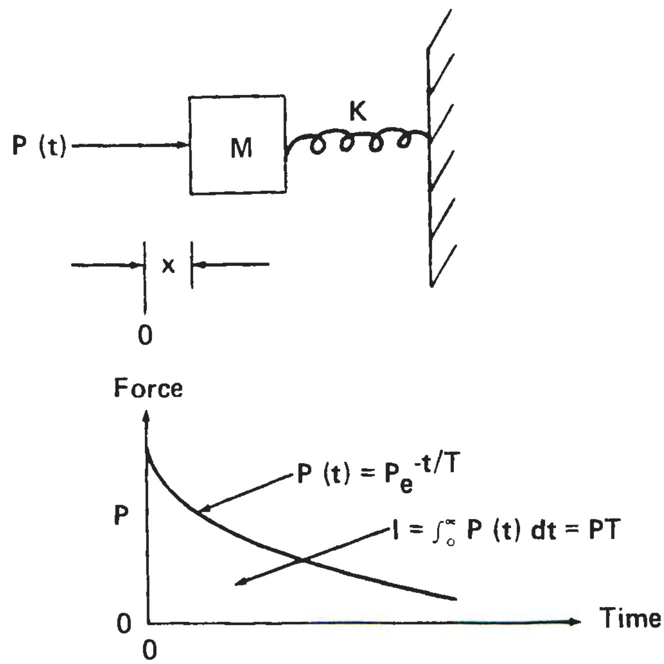

Figure 6. Schematic Diagram of Spring-Mass System to Model the Dynamic Response of a Structural Member.

$$\bar{P} = \frac{2P}{X_{max}K} = \frac{2}{[2-\exp(-\omega^2T^2/100)]\tanh \omega T} \qquad \text{II-44}$$

$$\bar{I} = \frac{I}{X_{max}(KM)^{1/2}} = \frac{\omega T}{[2-\exp(-\omega^2T^2/100)]\tanh \omega T} \qquad \text{II-45}$$

where X_{max} is the maximum displacement of the system, K is the spring rate, m is the mass, ω is the natural frequency of the system, and T is the characteristic loading time.

By varying ωT in these equations, a scaled response curve or Pressure Impulse (P-I) curve can be determined, similar to the curve in Figure 5. This curve represents the combinations of scaled force and scaled impulse which cause the same scaled response X_{max} of the system. This iso-response curve can be compared to an iso-damage curve of a building or similar structure. For a given structure varying levels of damage can be determined as functions of the pressure and impulse the structure is subject to. Predictions can then be made of the level of damage which the building would suffer based on the predicted pressure and impulse of the flow field associated with the blast wave. The causes of damage can be separated into regions on the iso-damage curve, the impulsive losding realm in which overpressure is controlling, the quasi-static loading realm in which impulse is controlling, and the dynamic loading realm in which the combination of overpressure and impulse determine the damage.

This technique has generality because once the pressure and impulse are known for any explosion, whether it is ideal or non-ideal, the P-I technique can be used to evaluate damage at any location. Sachs scaling and other methods of scaling do not have the flexibility of the P-I technique since they only relate pressure and impulse for high explosive and point source explosions. The P-I technique is a very general technique and more useful for accidental explosions than energy scaling or the TNT equivalency argument.

III. COMPUTATIONAL PROCEDURE

The computational techniques used are based on the Von Neuman-Richtmyer concept of artificial viscosity as developed by Brode[13] and Wilkins[29]. Using this technique Professor A.K. Oppenheim[30] of the University of California, Berkley, developed a computer program for studying the flow field of blast waves. The program is written for a one-dimensional, non-steady flow field in planar, cylindrical, and spherical geometry.

The system is idealized with several simplifying assumptions:

(1) The system is symmetrically one-dimensional.

(2) The high energy source volume is separated from the surroundings by a massless barrier and there is no transfer of mass between the high energy gas and the surroundings.

(3) The flow is inviscid with shock wave formation the only dissipative process in the surrounding atmosphere.

The computer program was modified by Adamczyk[18] of the University of Illinois to allow heat addition along particle paths by incorporating a homogeneous energy addition term with temporal and spatial dependence. The program was further modified by the author to incorporate a wave energy addition term and variable gamma, both with temporal and spatial dependence. In the computer program the conservation equations are expressed in Lagrangian coordinates, since through their inherent conservation of mass they lend themselves more easily to a computational scheme. Partial derivatives are taken along a particle path such that $u = \frac{\partial r}{\partial t}$ and the equations of mass, momentum, energy, and state are;

$$\text{Mass} \qquad \frac{\partial \nu}{\partial t} = \frac{\nu}{r^j} \frac{\partial (r^j u)}{\partial r} \qquad \text{III-1}$$

$$\text{Momentum} \qquad \frac{\partial u}{\partial t} = -\nu \frac{\partial p}{\partial r} \qquad \text{III-2}$$

$$\text{Energy} \qquad \frac{\partial e}{\partial t} = -p \frac{\partial \nu}{\partial t} - \lambda \qquad \text{III-3}$$

$$\text{State} \qquad e \equiv \frac{p\nu}{\gamma - 1} \qquad \text{III-4}$$

where ν is the specific volume, r is the radial position, j is the geometry coefficient (0, 1, 2 for planar, cylindrical, and spherical flow fields, respectively), p is the pressure, e is the internal energy, λ is the heat addition term assumed in the heat addition model, with spatial and temporal dependence, and γ is the ratio of specific heats, also with spatial and temporal dependence.

The properties of the flow field and their variation with time are determined by the integration of the governing conservation equations, the equation of state, and the kinematic equation coupled with the energy source term, λ, and subject to the appropriate boundary conditions at r=0, t=0, and ahead of the lead wave.

A. Boundary Conditions

For the cases studied the boundary conditions are:

1. At $t = 0$ and $0 \leq r \leq \infty$

$u = u(r,o) = 0$ III-5a

$p = p(r,o) = p_o$ III-5b

$e = e(r,o) = e_o$ III-5c

$\nu = \nu(r,o) = \nu_o$ III-5d

2. At $r=o$ and $0 \leq t \leq \infty$

$u = u(o,t) = 0$ III-6a

$\frac{\partial p}{\gamma r} = (\frac{\partial p}{\gamma r})_{(o,t)} = 0$ III-6b

$\frac{\partial e}{\partial r} = (\frac{\gamma e}{\partial r})_{(o,t)} = 0$ III-6c

$\frac{\partial \nu}{\partial r} = (\frac{\partial \nu}{\partial r})_{(o,t)} = 0$ III-6d

3. Ahead of the lead wave.

$u = o$ III-7a

$p = p_o$ III-7b

$e = e_o$ III-7c

$\nu = \nu_o$ III-7d

B. Dimensionless Variables

To aid in the computations, all variables are non-dimensionalized with respect to the thermodynamic state of the atmosphere into which the front propagates, $mR\Theta_o = p_o \nu_o$, and a reference point at the edge of the energy source volume. The non-dimensional independent variables are defined as:

$$\eta = r/r_o \qquad \text{III-8}$$

$$\tau = t/t_o \qquad \text{III-9}$$

where t_o is a characteristic time proportional to the time it takes an acoustic signal to propagate from the origin to the kernel edge when traveling at the ambient undisturbed sound speed, a_o, and r_o is the outermost edge of the source volume at a time $t = \tau = 0$:

$$t_o \equiv \frac{r_o\sqrt{\gamma_o}}{a_o} \qquad \text{III-10}$$

Using p_o to represent the ambient atmospheric pressure, ν_o the ambient value of the specific volume, and a_o the ambient speed of sound, the non-dimensional dependent variables can be expressed as:

$$U = \frac{u}{\sqrt{p_o \nu_o}} = \frac{u\sqrt{\gamma_o}}{a_o} \qquad \text{III-11}$$

$$\psi = \nu/\nu_o \qquad \text{III-12}$$

$$P = p/p_o \text{(for equation of state)} \qquad \text{III-13}$$

$$P^* = p/p_o - \Pi \text{(for conservation equations)} \qquad \text{III-14}$$

$$\Lambda = \lambda/p_o\nu_o \qquad \text{III-15}$$

$$E = e/p_o\nu_o \qquad \text{III-16}$$

In non-dimensional form the conservation equations are:

Mass $$\frac{\partial \psi}{\partial \tau} = \frac{\psi}{\eta^j} \frac{\partial (\eta^j U)}{\partial \eta} \qquad \text{III-17}$$

Momentum $$\frac{\partial U}{\partial \tau} = - \psi \frac{\partial P}{\partial \eta} \qquad \text{III-18}$$

Energy $$\frac{\partial E}{\partial \tau} = -P \frac{\partial \psi}{\partial \tau} + \Lambda \qquad \text{III-19}$$

State $$E = \frac{P\psi}{(\gamma-1)} \qquad \text{III-20}$$

where $$U = \frac{\partial \eta}{\partial \tau} \qquad \text{III-21}$$

and the boundary conditions become:

1. At $\tau = 0$ and $o \leq \eta \leq \infty$

   $U(\eta, o) = 0.0$ III-22a

   $P(\eta, 0) = 1.0$ III-22b

   $E(\eta, 0) = 2.5$ III-22c

   $\psi(\eta, 0) = 1.0$ III-22d

2. At $\eta = 0$ and $0 \leq \tau \leq \infty$

   $U(0, \tau) = 0.0$ III-23a

   $\frac{\partial P}{\partial \eta}(0, \tau) = \left(\frac{\partial P}{\partial \eta}\right)_{(0,\tau)} = 0.0$ III-23b

   $\frac{\partial E}{\partial \eta}(0, \tau) = \left(\frac{\partial E}{\partial \eta}\right)_{(0,\tau)} = 0.0$ III-23c

   $\frac{\partial \psi}{\partial \eta}(0, \tau) = \left(\frac{\partial \psi}{\partial \eta}\right)_{(0,\tau)} = 0.0$ III-23d

3. Ahead of the lead wave

$$U = 0.0 \qquad \text{III-24a}$$

$$P = 1.0 \qquad \text{III-24b}$$

$$E = 2.5 \qquad \text{III-24c}$$

$$\psi = 1.0 \qquad \text{III-24d}$$

C. Source Model

A major justification for replacing the chemical processes by the simple heat addition to the fluid model appears when examining the Hugoniot curve for strictly one-dimensional heat addition processes and comparing it to the real Hugoniot for the complete combustion of various fuels.

For the case of heat addition, λ, to a constant gamma, ideal-gas working fluid the reacted end state Hugoniot can be represented by a rectangular hyperbola in the p-v plane with asymptotes of $p/p_o = -(\gamma-1)/(\gamma+1)$ and $v/v_o = (\gamma-1)/(\gamma+1)$. Zajac and Oppenheim[25] showed that this type of hyperbola accurately represents the shape of the real gas Hugoniot.

For the pressure range $1.<p/p_o<20.$ Adamzcyk[18] performed a curve fit procedure using a least-squares technique and found the rectangular Hugoniot matched the real Hugoniot within an accuracy of 0.25%, yielding an effective q and γ for the particular source mixture. The quantity, q, is a dimensionless energy density:

$$q = \frac{E_T}{nC_v\Theta_o} \qquad \text{III-25}$$

$$q = \frac{p_4}{p_o} - 1 \qquad \text{III-26}$$

where E_T is the energy added per mole of mixture, n is the number of moles of mixture, $C_v = R/(\gamma-1)$ and Θ_o is the initial temperature of the gas at the ambient pressure p_o.

The values for q and γ for stoichiometric mixtures of six common fuels in air are given in Table 1. Both the values of q and γ vary with the equivalence ratio, and can be calculated for any combustible mixture, based on full chemical equilibrium in the final state.

1. Energy Addition Wave

To systematic study the effects of constant velocity wave addition of energy to a compressible fluid medium, energy was added to the flow field at various preselected Lagrangian velocities. In addition, bursting sphere and the kernel addition of energy, investigated by Adamczyk(18), were run to provide comparisons. A summary of the cases investigated is presented in Table 2.

The Lagrangian flame velocities of the different cases were non-dimensionalzed using the ambient velocity of sound, $a_o = \sqrt{\gamma_o p_o v_o}$. Supersonic velocities at Mach numbers of 2, 3, 4, 5.2 (steady-state CJ), and 8 were run. One run was done at a Lagrangian velcoity equal to the ambient velocity of sound (Mach number = 1.0), and subsonic cases of 0.5, 0.25, and 0.125, were also run. The subsonic cases were computed only until trends were established because they were found to be excessively expensive.

In this analysis the chemical energy release is modeled as a heat addition to a working fluid. The model incorporates

Table 1. Hugoniot Curve-Fit Data

Fuel	H_c Low Value J/Kg Moles Fuel	H_c Low Value MJ/Kg Fuel	Stoichiometric mixture				
			Q_c MJ/Kg Fuel	Q MJ/Kg Mix	q	γ_1	$\frac{Q_c}{H_c}$
H_2	241.8	120.00	140.80	3.989	5.864	1.173	1.174
CH_4	802.3	50.01	63.98	3.508	7.934	1.202	1.271
C_2H_2	1256.0	48.22	55.21	3.867	8.734	1.195	1.145
C_2H_4	1323.0	47.16	58.49	3.705	8.615	1.199	1.240
C_2H_4O	1264.0	28.69	34.41	3.890	9.593	1.203	1.159
C_3H_8	2044.0	46.35	61.60	3.695	9.169	1.208	1.329

Table 2. Summary of Parameters For Cases Investigated

Case	Energy Wave Mach Number	j	W	τ_c	τ_D	q	γ_o	γ_4
1	Bursting Sphere(∞)	2	∞	0.000	0.00	8.0	1.4	1.2
2	8.0	2	.1	0.011	0.12	8.0	1.4	1.2
3	5.2(CJ)	2	.1	0.016	0.18	8.0	1.4	1.2
4	4.0	2	.1	0.021	0.23	8.0	1.4	1.2
5	3.0	2	.1	0.028	0.31	8.0	1.4	1.2
6	2.0	2	.1	0.042	0.46	8.0	1.4	1.2
7	1.0	2	.1	0.085	0.93	8.0	1.4	1.2
8	0.5	2	.1	0.169	1.86	8.0	1.4	1.2
9	0.25	2	.1	0.338	3.72	8.0	1.4	1.2
10	0.125	2	.1	0.679	7.37	8.0	1.4	1.2
11	Bursting Plane(∞)	0	∞	0.000	0.00	8.0	1.4	1.2
12	4225.0	2	.1	0.000	0.00	8.0	1.4	1.2
13	5.2(CJ)	0	.1	0.016	0.18	8.0	1.4	1.2
14	4.0	2	.2	0.042	0.25	8.0	1.4	1.2
15	4.0	2	.05	0.011	0.22	8.0	1.4	1.2
16	4.0	2	.025	0.005	0.22	8.0	1.4	1.2
17	0.5	2	.2	0.338	2.03	8.0	1.4	1.2
18	0.5	2	.05	0.169	1.86	8.0	1.4	1.2
19	Kernel	2	∞	0.2	0.2	8.0	1.4	1.2
20	Kernel	2	∞	2.0	2.0	8.0	1.4	1.2
21	5.55(Fishburn)	2	.1	0.015	0.17	8.87	1.377	1.253
22	0.25(Kuhl,et al.)	2	.1	0.351	3.86	7.2	1.3	1.2

the fact that most chemical reactions do not take place instantaneously because they depend on particle collisions. In addition, the particles involved in the collision must have energy greater than the minimum activation energy for the reaction. These phenomena make the reaction rate highly dependent upon temperature and pressure. If the temperature increases, the average velocity and energy of the particles increases and a larger portion will have an energy above the activation energy. For a given volume, as the velocity increases the collision frequency also increases.

As the reaction procedes and the end products are produced the concentration of reactants will decrease. This results in a decrease in reaction rate until the final equilibrium concentration of reactants and products is obtained.

Therefore, the chemical reaction rate increases to a maximum followed by a rapid decrease as equilibrium concentrations are approached. A heat addition source term of the following form was chosen:

$$\Lambda = \xi_1(D) \quad \xi_2(D,\tau) \qquad \text{III-27}$$

where ξ_1 is a spatially dependent energy term and ξ_2 is both a temporal and spatial energy addition term.

The spatially dependent energy term, ξ_1, models the energy distribution of an ideal vapor cloud with stoichiometric concentration of fuel throughout the source volume with the concentration decreasing to zero at the edge.

$$\xi_1 = \begin{cases} 1.0 & \text{for} \quad D \leq D_1 \\ \Phi & \text{for} \quad D_1 \leq D \leq D_o \\ 0.0 & \text{for} \quad D_o \leq D \leq \infty \end{cases}$$ III-28a, III-28b, III-28c

where D_1 is the position in the source volume where the rounding function begins and D_o is the edge of the source volume and:

$$\Phi = \left\{\cos(3\pi\phi) - 9.0\cos(\pi\phi) + 8\right\} \Big/ 16.0 \qquad \text{III-29}$$

with $\phi = -\frac{D-D_o}{D_1-D_o}$ for the range $D_1 < D \leq D_o$.

The function Φ was chosen for the rounding function since it allows for a smooth transition from the inner region to the kernel edge. At $\phi = 0$ and $\phi = 1.0$ this function matches the values of the adjacent functions and also the first, second, and third derivatives with respect to D match the corresponding derivatives of the adjacent functions.

The energy function to represent the energy addition wave (flame front), $\xi_2(D,\tau)$, is similar to the cosine function used at the edge of the source volume. This cosine function was used since its power pulse, $\frac{\partial \Lambda}{\partial \tau}$, closely models the power function Zajac and Oppenheim[15] obtained when integrating the complete set of chemical kinetic equations for the hydrogen-oxygen chemical system.

This energy function can be expressed as:

$$\xi_2(D,\tau) = \begin{cases} 0.0 & \text{for} \quad \zeta \leq 0 \\ \Xi & \text{for} \quad 0 < \zeta \leq 1.0 \\ \frac{\lambda}{p_o v_o} & \text{for} \quad \zeta > 1.0 \end{cases}$$ III-30a, III-30b, III-30c

where: $\zeta(M_\Omega, \tau) = \dfrac{M_\Omega \tau - D}{W}$

and $$\Xi = \left\{\cos(3\tau\zeta) - 9.0 \cos(\pi\ \zeta) + 8.0\right\} / 16.0 \qquad \text{III-31}$$

The three-dimensional shape of the energy addition function is shown in figure 7. At time $\tau=0$ the system exhibits ambient conditions throughout. At time τ^+, energy addition begins at the center of the kernel in accordance with the energy source term until $\zeta=1.$, when all the energy has been added. At positions of increasing radius the start of the energy addition begins at later times in accordance with $M_\Omega = \frac{dD}{d\tau}$.

The energy addition is done in the energy wave in accordance with a selected wave width which can be varied to model the width of the flame. In this model the wave width, W, is the fraction of the source volume to which energy is being added at any time step as shown in figure 8:

$$W \equiv \frac{D_W}{D_o} \qquad \text{III-32}$$

This can also be visualized as the fraction of the transit time for the wave to propagate through the source volume, τ_T, that the energy is being added to a particular cell, τ_C, and can also be expressed as:

$$W = \frac{\tau_C}{\tau_T} \qquad \text{III-33}$$

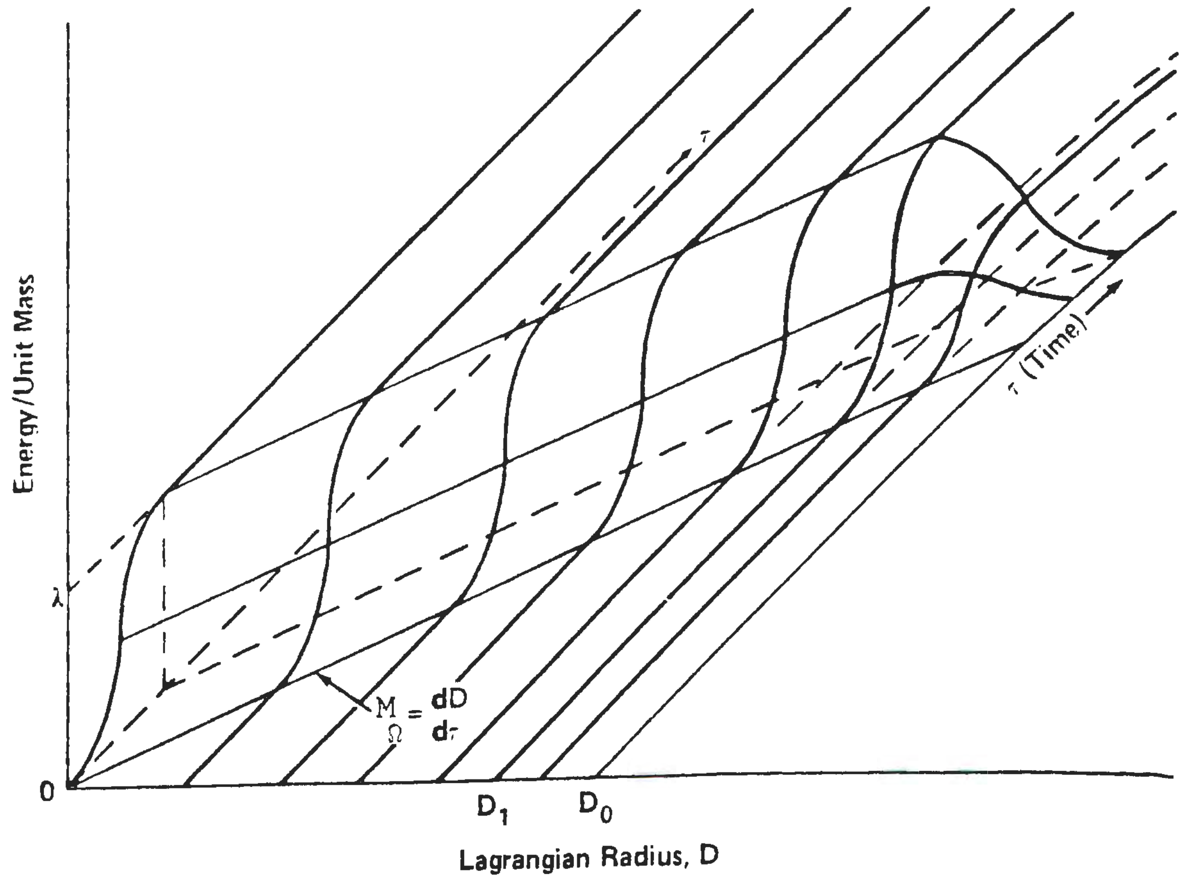

Figure 7. Energy Deposition Function.

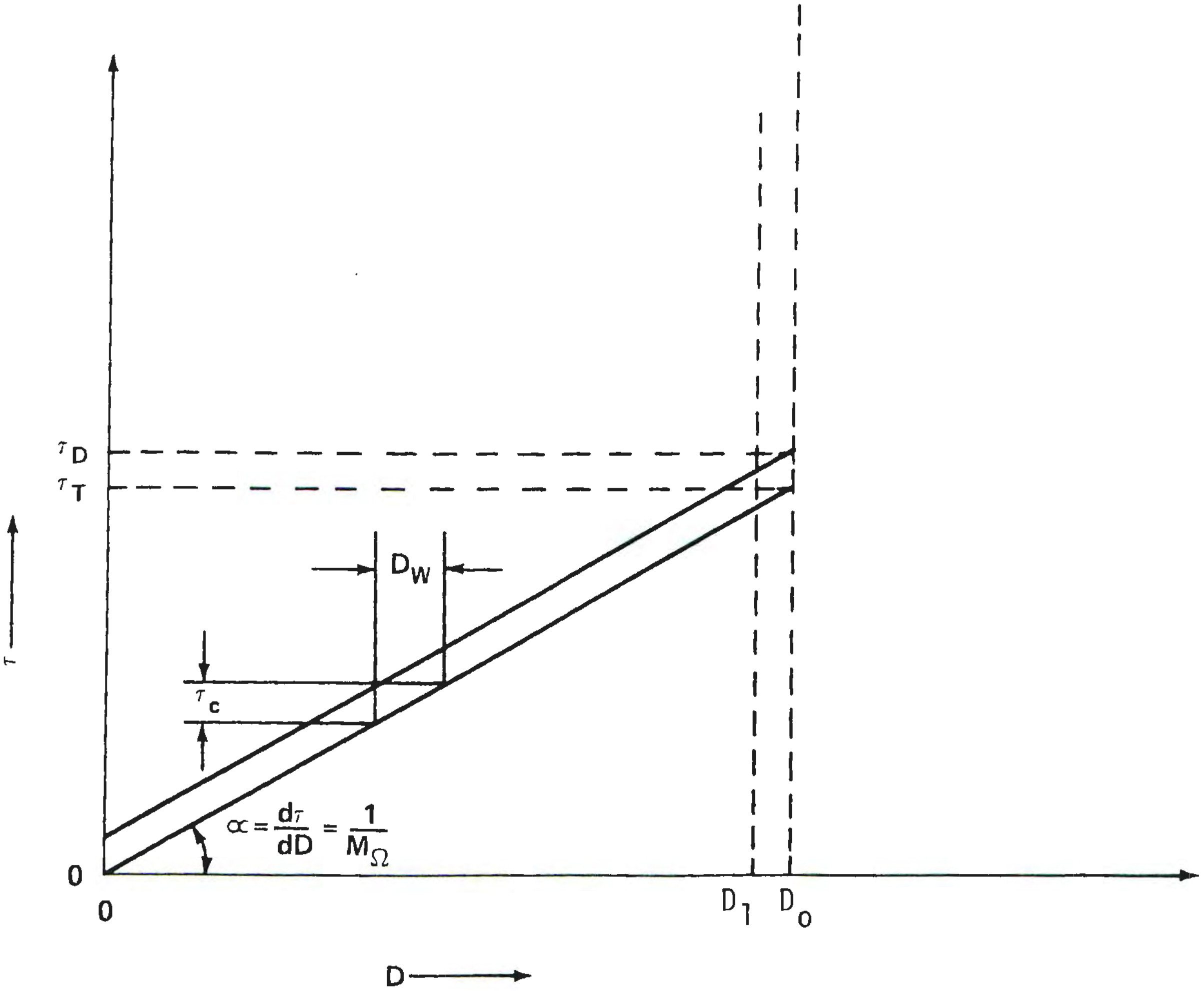

Figure 8. Wave Width of Energy Deposition Term.

The energy wave propagates at a constant Lagrangian velocity or Mach number, M_Ω, where:

$$M_\Omega = \frac{dD}{d\tau} = \frac{D_o}{\tau_T} \qquad \text{III-34}$$

The transit time of the energy wave through the source volume is inversely proportional to the velocity of the energy wave. For equal wave widths, as the velocity increases both the source volume transit time, τ_T, and the cell deposition time, τ_C, decrease.

Figure 9 shows the effects of wave width on cell deposition time. As the wave width increases, the cell deposition time increases for the same energy wave velocity.

The source volume deposition time, τ_D, is the sum of the transit time of the energy wave plus the cell deposition time at the edge of the source volume:

$$\tau_D = \tau_T + \tau_C \qquad \text{III-35}$$

This can also be expressed in terms of the energy wave Mach number:

$$\tau_D = \frac{1}{M_\Omega}(1+W) \qquad \text{III-36}$$

For an infinitely thin wave W=0 and the source volume deposition time equal the energy wave transit time. As the width of the energy wave becomes finite, energy is being added to

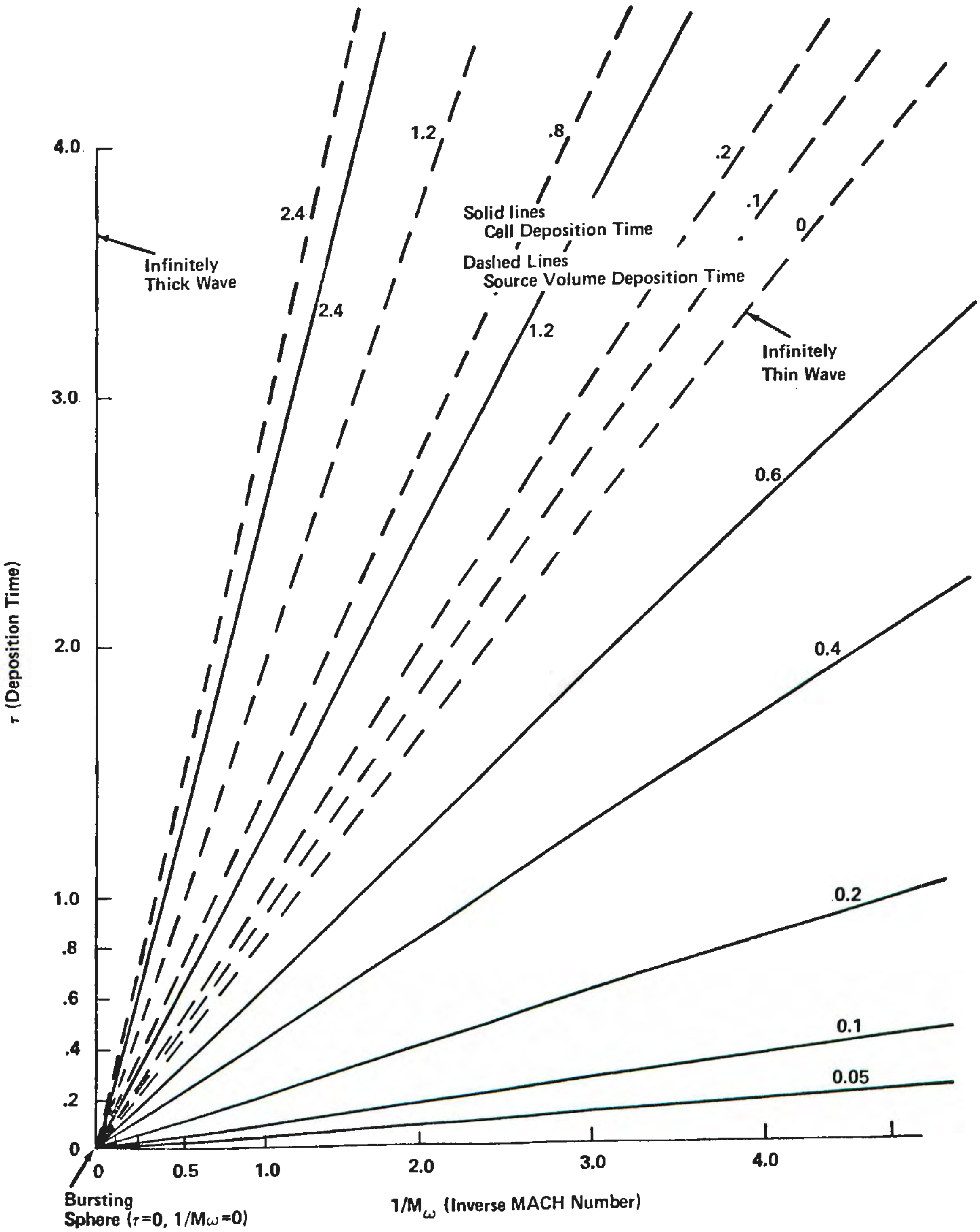

Figure 9. Deposition time vs. Inverse MACH Number as function of Wave Width.

the last cell after the leading edge of the energy wave reaches the edge of the source volume. Figure 9 shows that the greater the width of the energy wave the longer the source volume deposition time.

2. Change of Specific Heat Ratio

The ratio of specific heats, gamma, for a combustible mixture is known to vary from approximately 1.1 to 1.67 depending on the composition of the mixture and the complexity of the molecules in the individual components of the mixture. In addition, the value of gamma can also change as the chemical composition changes to maintain chemical equilibrium or as a function of temperature. As temperature increases, the species in air go through various changes including the dissociation and ionization of oxygen and nitrogen. At a temperature of 2500°K the dissociation of oxygen molecules begins. For the combustible mixture being investigated the temperature ratio is 9:1 which corresponds to a temperature of 2700°K behind the energy addition. Thus for the case under consideration the dissociation of oxygen begins, raising the heat capacity and lowering the heat capacity ratio, gamma.

An evaluation of an effective value of gamma and heat release associated with real combustion processes as a function of stoichiometry was performed by Adamczyk[18]. For the case which is being investigated a combustible mixture with an energy density approximating that of methane is used. For methane, Adamczyk calculated an effective gamma of 1.202, rounded off to 1.200 here. Before a vapor cloud is ignited, uniform ambient conditions exist throughout both the source volume and the surroundings. After ignition the flame front heats the medium through which it propagates and changes the chemical composition, lowering the heat capacity ratio. To model this change a variable gamma was developed in which the heat capacity ratio changes from an ambient condition of 1.4 to 1.2 when energy addition to the cell is completed.

$$\gamma = \gamma_o - (\gamma_o - \gamma_4)\left(\frac{\Lambda_i}{\Lambda}\right) \qquad \text{III-37}$$

where Λ_i/Λ is the fraction of the energy which has been added.

D. Numerical Integration

The numerical integration was done using a Von Neumann-Richtmyer/type, explicit, finite differencing technique. The equations of motion were integrated for an expanding flow field with constant Lagrangian distance spacing at finite times. The time steps were determined using the Courant Stability criteria as presented by Wilkins[29].

$$\Delta\tau^{n+\frac{1}{2}} = \min(\Delta\tau_R^{n+\frac{1}{2}},\ 1.4\ \Delta\tau^{n-\frac{1}{2}}) \qquad \text{III-38}$$

where $$\Delta\tau^{n} = \tfrac{1}{2}(\Delta\tau^{n+\frac{1}{2}} + \Delta\tau^{n-\frac{1}{2}}) \qquad \text{III-39}$$

and: $$\Delta\tau_R^{n+\frac{1}{2}} = \left[\frac{2}{3}\left(\frac{\Delta\eta_{\ i+\frac{1}{2}}}{\sqrt{Z_1^{\,2}+Z_2^{\,2}}}\right)\right] \text{min over all i's} \qquad \text{III-40}$$

where: $$\Delta\eta_{i+\frac{1}{2}} = \eta^{n}_{i+1} - \eta^{n}_{i} \qquad \text{III-41}$$

$$Z_1^2 = 64C_2^2 \left(\frac{\psi^{n}_{i+\frac{1}{2}} - \psi^{n-1}_{i+\frac{1}{2}}}{\psi^{n}_{i+\frac{1}{2}} + \psi^{n-1}_{i+\frac{1}{2}}}\right)^2 \left(\frac{\eta^{n}_{i+\frac{1}{2}} - \eta^{n}_{i}}{\Delta\tau^{n-\frac{1}{2}}}\right)^2 \qquad \text{III-42}$$

$$Z_2^2 = \gamma^{n}_{i+\frac{1}{2}} P^{n}_{i+\frac{1}{2}} \psi^{n}_{i+\frac{1}{2}} \qquad \text{III-43}$$

The computational grid for the finite differencing scheme is shown in figure 10. Velocity is evaluated at full steps in radius, cell boundaries, and half steps in time to maintain the proper relationship between the derivatives as demanded by the conservation equations. Thermodynamic properties, P, ψ, and E are evaluated at full steps in time and half steps in radius. Since Π is a relationship between the velocity and effective pressure, it is evaluated at both half steps in space and time. The sequence by which the equations are treated is first the momentum equation, followed by the kinematic equation, continuity equation, and energy equation. Using the nomenclature in figure 10, the conservation equations were written in finite difference form as follows:

Momentum Equation

$$U^{n+\frac{1}{2}}_{i} = U^{n-\frac{1}{2}}_{i} - \Delta\tau\left[\frac{\Delta P}{\Phi}\right] \qquad \text{III-44}$$

$$\Delta P = [P^{n} + \Pi^{n-\frac{1}{2}}]_{i+\frac{1}{2}} - [P^{n} + \Pi^{n-\frac{1}{2}}]_{i-\frac{1}{2}} \qquad \text{III-45}$$

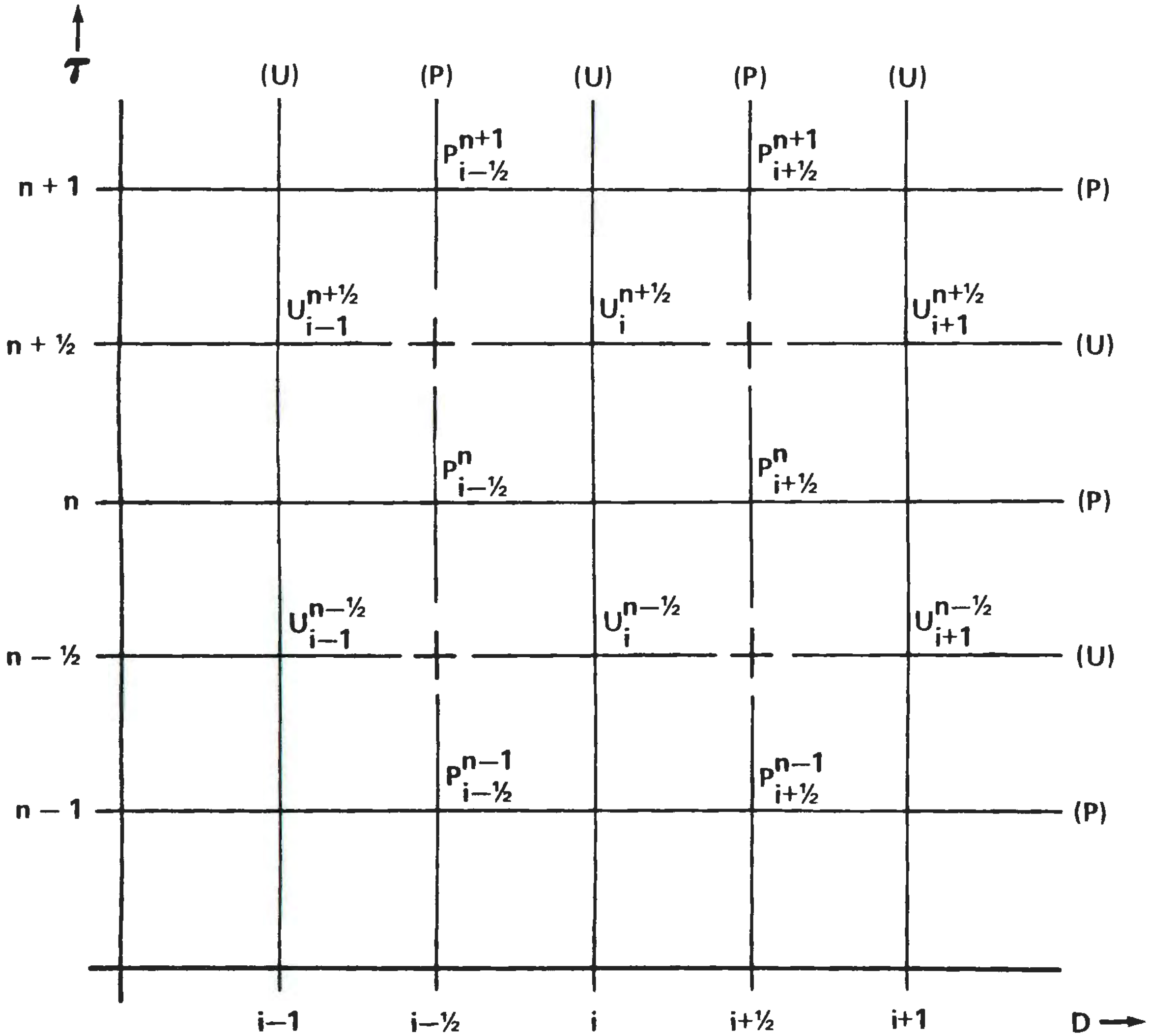

Figure 10. Computational Grid for finite differencing technique.

$$\Phi = \tfrac{1}{2}\left[\frac{\eta^n_{i+1} - \eta^n_i}{\psi^n_{i+\frac{1}{2}}} + \frac{\eta^n_i - \eta^n_{i-1}}{\psi^n_{i-\frac{1}{2}}}\right] \qquad \text{III-46}$$

and Π is normally zero except in regions of excessive pressure gradients (shock waves), in which case:

$$\Pi^{n-\frac{1}{2}}_{i\pm\frac{1}{2}} = \left\{ C_L\left[\frac{P^{n-1}_{i\pm\frac{1}{2}}}{2}\left(\psi^n_{i\pm\frac{1}{2}} + \psi^{n-1}_{i\pm\frac{1}{2}}\right)\right]^{\frac{1}{2}}\left(\frac{1}{\psi^n_{i\pm\frac{1}{2}}} + \frac{1}{\psi^{n-\frac{1}{2}}_{i\pm\frac{1}{2}}}\right)\left(\frac{U^{n-\frac{1}{2}}_{i\pm1} - U^{n-\frac{1}{2}}_i}{2}\right)\right]$$

$$+ C_o^2\left[\frac{\left(U^{n-\frac{1}{2}}_{i+1} - U^{n-\frac{1}{2}}_i\right)^2}{2}\left(\frac{1}{\psi^n_{i\pm\frac{1}{2}}} + \frac{1}{\psi^{n-1}_{i\pm\frac{1}{2}}}\right)\right]\Bigg\} \qquad \text{III-47}$$

Since the artificial vicosity is required only to smooth out the effects of excessive pressure gradients the condition is introduced that if

$$\psi^n_{i\pm\frac{1}{2}} \geq \psi^{n-1}_{i\pm\frac{1}{2}} \qquad \text{III-48}$$

or

$$\Delta U \geq 0 \qquad \text{III-49}$$

$$\Pi^{n-1}_{i\pm\frac{1}{2}} = 0 \qquad \text{III-50}$$

KINEMATIC EQUATION

$$\eta^{n+1}_i = \eta^n_i + U^{n+\frac{1}{2}}_i(\tau^{n+1} - \tau^n) \qquad \text{III-51}$$

CONTINUITY EQUATION

$$\psi^{n+1}_{i+\frac{1}{2}} = \psi^n_{i+\frac{1}{2}} + \frac{\{\tau^{n+1} - \tau^n\}\{U^{n+\frac{1}{2}}_{i+1}(\eta^{n+\frac{1}{2}}_{i+1})^j - U^{n-\frac{1}{2}}_i(\eta^{n+\frac{1}{2}}_i)^j + \underline{\overline{X}}\}}{M^n_{i+\frac{1}{2}}} \qquad \text{III-52}$$

where: $$M_{i+\frac{1}{2}}^{n} = \frac{(\eta_{i+1}^{n})^{j+1} - (\eta_{i}^{n})^{j+1}}{(j+1)\psi_{i+\frac{1}{2}}^{n}} \qquad \text{III-53}$$

and: $$\underline{\bar{X}} = \frac{j(j-1)}{24}\left\{(\tau^{n+1} - \tau^{n})^{2}\left([U_{i+1}^{n+\frac{1}{2}}]^{3} - [U_{i}^{n+\frac{1}{2}}]^{3}\right)\right\} \qquad \text{III-54}$$

where j is equal to 0, 1, or 2, for planar, cylindrical and spherical flow fields respectively.

ENERGY EQUATION

$$E_{i+\frac{1}{2}}^{n+1} = \left\{\frac{E_{i+\frac{1}{2}}^{n+1} - \left[\frac{P_{i+\frac{1}{2}}^{n}}{2} + \left(\frac{\Pi_{i+\frac{1}{2}}^{n+\frac{1}{2}} + \Pi_{i+\frac{1}{2}}^{n-\frac{1}{2}}}{2}\right)\right]\left[\psi_{i+\frac{1}{2}}^{n+1} - \psi_{i+\frac{1}{2}}^{n}\right] + \Lambda_{i+\frac{1}{2}}^{n+\frac{1}{2}}}{1 + \left[\frac{(\psi_{i+\frac{1}{2}}^{n+1} - \psi_{i+\frac{1}{2}}^{n})(\gamma_{i+\frac{1}{2}}^{n+1} - 1)}{\psi_{i+\frac{1}{2}}^{n+1}}\right]}\right\} \qquad \text{III-55}$$

and $$E_{i+\frac{1}{2}}^{n+1} = \frac{P_{i+\frac{1}{2}}^{n+1}\,\psi_{i+\frac{1}{2}}^{n+1}}{\gamma_{i+\frac{1}{2}}^{n+1} - 1} \qquad \text{III-56}$$

where $\Lambda_{i+\frac{1}{2}}^{n+\frac{1}{2}}$ is the energy addition term and γ is the local ratio of specific heats.

E. <u>Testing of Program</u>

To establish credibility of results and ensure that the computer program effectively models the system under evaluation test cases were run in which expected results were available to compare to computer output.

1. BURSTING PLANE

To test the computational technique of the program the case of one-dimensional, constant area flow similar to a membrane bursting in a shock tube was run. The initial conditions of a high temperature, high pressure constant gamma gas with a step change to ambient conditions at the membrane were used. The calculated results were then compared to result predicted by equation I-10. The results varied by less than 0.01%, establishing the validity of the calculation technique used.

2. BURSTING SPHERE

An infinite velocity energy wave propagating through the compressible fluid medium is a constant volume energy addition or bursting sphere. To test this case on the model, a wave velocity was selected at the maximum velocity which could be incorporated into the program, limited by the initial step size (this corresponds to a dimensionless Mach number, $M_{\Omega} = 4225$). Figure 11 is a pressure vs radius plot of the energy wave at dimensionless time increments of 0.0001. After the wave has propagated through the source volume, the pressure-radius distribution is a bursting sphere. The wave addition of energy yields a pressure difference of less than 0.001% from the energy distribution for a bursting sphere, but imparts a velocity to the particles of approximately 1.6×10^{-3}. These differences are considered well within the allowances of

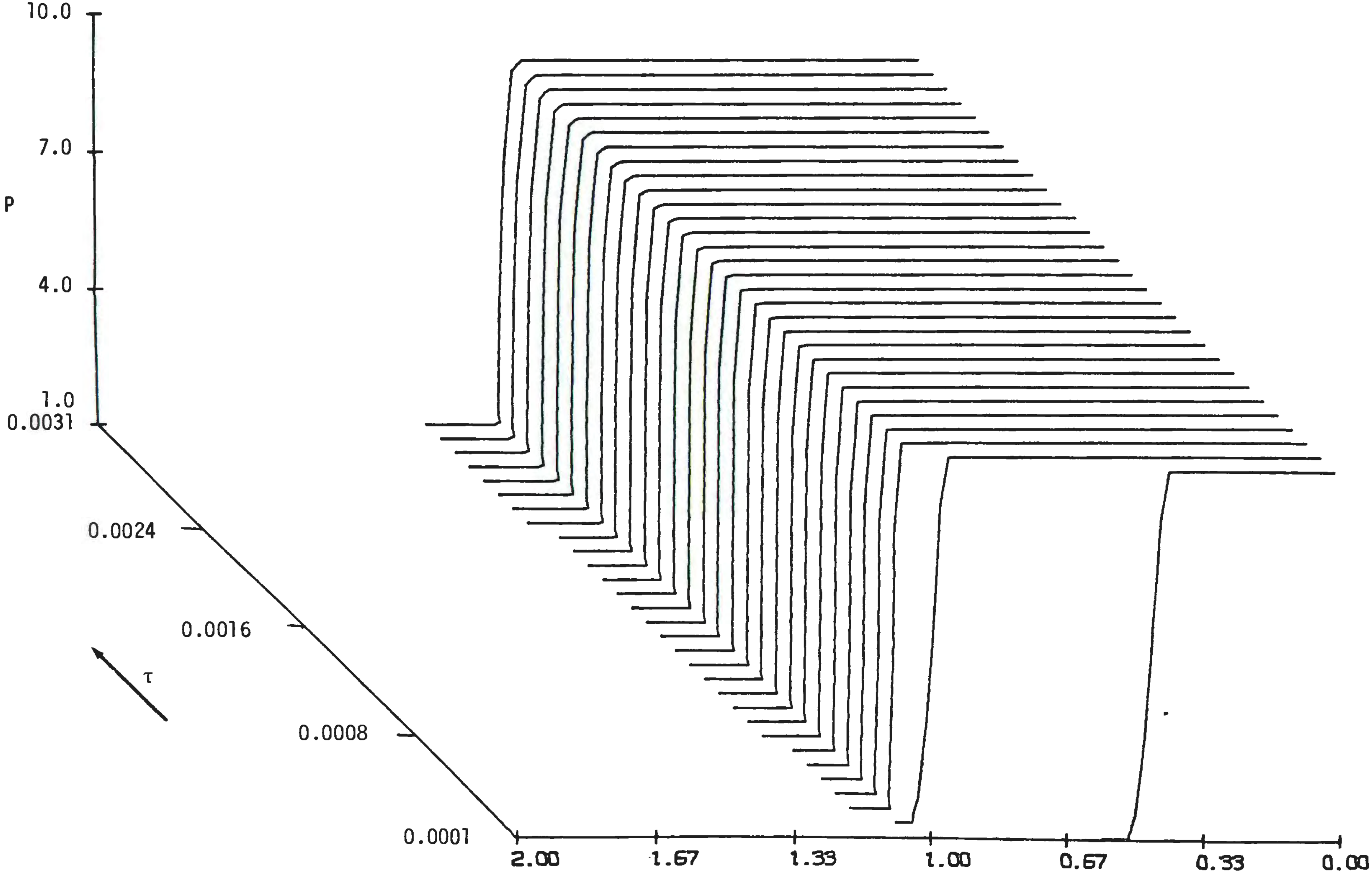

PRESSURE / PO DISTRIBUTION VS. DISTANCE / DO AND TIME / TO

Figure 11. Pressure distribution versus Eulerian distance and time from a Mach 4225.0 energy wave.

the problem under consideration.

2. Wave Width

In a flame the heat of reaction does not appear instantaneously but is controlled by the reaction rate of the chemical species. A flame propagating through a flammable mixture will have a finite time of deposition of energy to the individual particles as it passes. Therefore it is necessary to model the energy addition in the energy wave by adding the energy simultaneously over several cells. The wave width determines the number of cells to which energy is added.

In addition, the stability criteria used in determining the time increment relates the time step size used in the calculations to the energy being added to the cells. If the wave width limits energy addition to only one cell at a time, each cell would require a complete time cycle of energy additions and the energy addition would be effectively a series of explosions. If energy is added simultaneously to several cells the time step size is limited only by the most restrictive energy addition step. Thus, with energy addition simultaneously in several cells computer time is reduced in proportion to the number of cells within the energy addition wave. The wave width also affects the deposition time of energy addition to each cell. Figure 9 shows that as the wave width increases the time for energy deposition within the individual cell also increase.

A series of cases were run at a supersonic energy wave velocity of Mach 4 and a subsonic energy wave velocity of Mach 0.5 to investigate the effects of wave width on the model.

For the supersonic case (Mach 4) Figure 12 illustrates the effects of wave width on peak overpressure. During the energy addition there are significant fluctuations and differences in overpressure as the wave propagates through the source volume. For a wave width of 0.2 the energy is added to ten cells simultaneously and as the final energy is added to the last cell in the wave there has been some pressure transfer to adjoining cells during the relatively long deposition time. As the wave width decreases the number of cells in which energy is being added decreases with an accompanying decrease in the cell deposition time. Since the energy is added rapidly the increase in energy of the cell is reflected in a pressure rise with very little pressure transferred to adjoining cells. Also, in the finite differencing scheme all the cell properties are assumed to be concentrated at the cell center. For a narrow wave propagating through the kernel, i.e. containing 1 or 2 cells, the finite differencing scheme may result in large pressure and energy variations in adjoining cells because after energy addition is completed in one cell the energy addition in the adjoining cell may be only starting. During the time of energy addition to the new cell the energy (pressure) in the old cell will be transferred to adjoining cells. Thus there may be successive peaking of the pressure in the cells caused by the wave

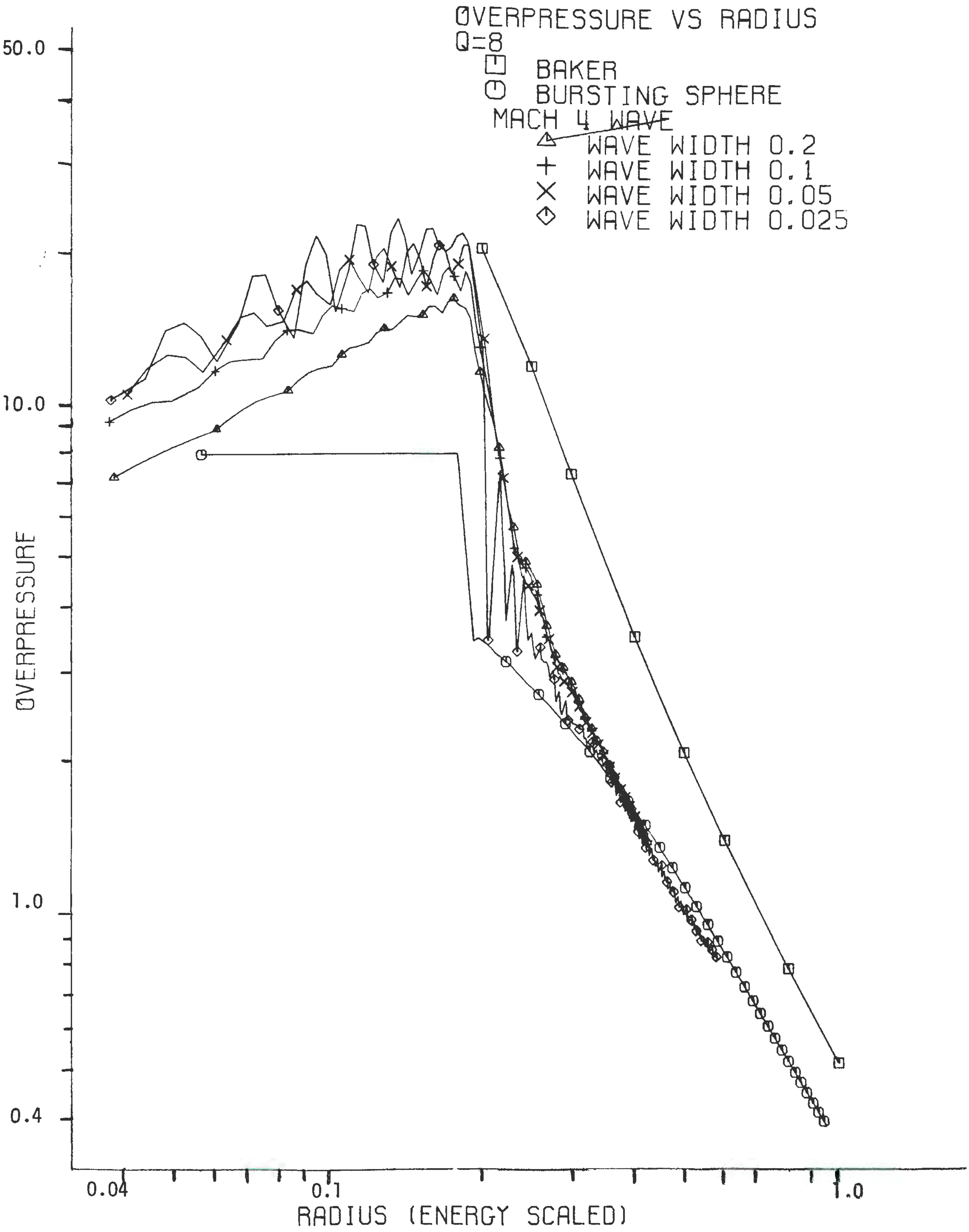

Figure 12. Overpressure versus energy scaled distance.

encompassing too few grid points as it propagates through the kernel.

This peaking is reflected by the overpressure waves for wave widths of 0.025 and 0.05 (2.5 and 1.25 cells respectively). However, it should be noted that as the pressure wave propagates from the source, the peak overpressures coalesce into the same overpressure curve. This implies that one of the effects of wave width is the rate at which the non-steady flow assymptotically approaches a maximum value of peak pressure during the energy addition.

For the subsonic wave velocity, Mach 0.5, figure 13 shows similar results, except at much lower overpressures. For a wave width of 0.2 the fluctuations in overpressure are much smaller than the 0.1 and 0.05 case; but all these cases approach similar overpressures at the edge of the kernel. The narrow wave width (0.05) initially has fluctuations in the overpressure, but as the wave propagates to the edge of the kernel the subsonic velocity of the wave allows equalization of the pressure. Also, the time of energy deposition per cell for the 0.05 wave width at Mach 0.5 is 8 times longer than the Mach 4-0.05 wave width, and twice as long as the Mach 4-0.2 wave width. However, in the far field the 0.2 wave width shows a noticeably lower overpressure than the case of a 0.1 and 0.05 wave width.

A wave width at 0.1 was chosen because:

(1) The solutions assymptotically approach the peak value before the energy wave has propagated an excessive

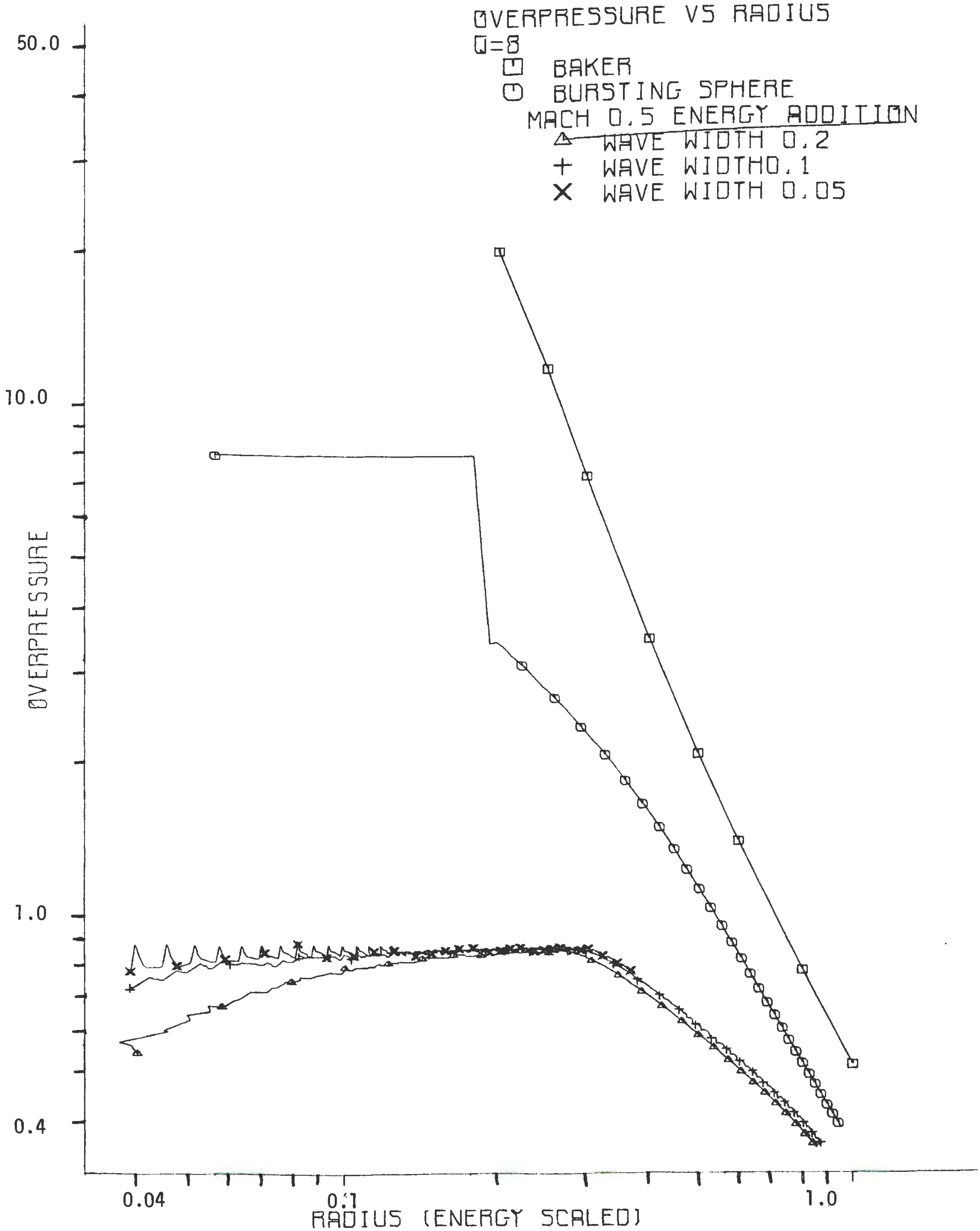

Figure 13. Overpressure versus energy scaled distance.

distance through the source volume,

(2) In the subsonic case, the expansion of the source volume was approximately the same for the 0.1 and smaller wave widths,

(3) The calculated results did not require excessive computer time, and

(4) This approximation reasonably modeled the physically realistic solution.

IV. RESULTS AND DISCUSSIONS

A. Flow Field Properties from One-Dimensional Steady State Theory.

Fuels at stoichiometric concentrations have an energy density ranging from 5.8 for hydrogen to 9.6 for ethylene oxide. Using an energy density of q=8.0 (approximately that of methane, q=7.93), a γ_4 of 1.2, and a γ_o of 1.4, the shock Hugoniot and reactive Hugoniot can be plotted and the system constants calculated. From equation III-26:

$$p_4/p_o = q + 1 \qquad \text{IV-1}$$

$$p_+/p_o = 9.0$$

For a constant volume energy addition equation II-24 can be rearranged to the following:

$$\Lambda = \frac{\lambda}{p_o v_o} = \frac{p_1 v_1}{p_o v_o}\left(\frac{p_4/p_1}{\gamma_4 - 1} - \frac{1}{\gamma_1 - 1}\right) \qquad \text{IV-2}$$

$$\Lambda = (45. - 2.5) = 42.5$$

For a constant pressure energy addition equation II-25 states:

$$\frac{\nu_4}{\nu_1} = \left(\frac{\gamma_4 - 1}{\gamma_4}\right)\left(\frac{\gamma_1}{\gamma_1 - 1} + \frac{\lambda}{p_1 \nu_1}\right) \qquad \text{IV-3}$$

and

$$\frac{\nu_4}{\nu_1} = 7.67$$

The approach flow Mach number for the Chapman-Jouget tangency point can be evaluated from equation II-38:

$$M_{CJ} = \left\{ \left[1 + \frac{\lambda(\gamma_4^2 - 1)}{\gamma_1 p_1 \nu_1} - \frac{(\gamma_1^2 - \gamma_4^2)}{\gamma_1(\gamma_1 - 1)}\right] \pm \left[\left(1 + \frac{\lambda(\gamma_4^2 - 1)}{\gamma_1 p_1 \nu_1} - \frac{(\gamma_1^2 - \gamma_4^2)}{\gamma_1(\gamma_1 - 1)}\right)^2 - \left(\frac{\gamma_4}{\gamma_1}\right)^2\right]^{\frac{1}{2}} \right\}^{\frac{1}{2}} \qquad \text{IV-5}$$

$M_{CJ} = 5.179$ & 0.165

The steady-state, one-dimensional flow properties at the Chapmen-Jouguet points can be evaluated from equations II-39 and II-40.

$$(p_4/p_1)_{CJ} = \frac{(\gamma_4 M_{CJ}^2 + 1)}{\gamma_4 + 1} \qquad \text{IV-6}$$

$$\left(p_4/p_1\right)_{CJ} = 15.08 \ \& \ 0.47$$

$$\left(\frac{v_4}{v_1}\right)_{CJ} = \frac{\frac{\gamma_4}{\gamma_1}(\gamma_1 M_{CJ}^2 + 1)}{(\gamma_4+1)M_{CJ}^2} \qquad \text{IV-7}$$

$$\left(\frac{v_4}{v_1}\right)_{CJ} = 0.56 \ \& \ 14.78$$

These steady state predictions will be compared with the results generated by the non-steady heat addition model.

B. <u>The Effects of Energy Wave Velocity</u>.

In this analysis, Lagrangian constant velocity energy waves were varied over several orders of magnitude to ascertain the flow field properties of the propagating wave system. These properties were then compared to those of bursting sphere. All cases were run with the same total energy and the variables are summarized in Table 2.

1. <u>Flow Field Properties</u>

The flow fields of the cases investigated were plotted to illustrate the results. Figure 14* is the Lagrangian pressure distribution as the energy wave reaches the edge of the source volume. Figures 15 through 27 show the Eulerian pressure distributions at various times. Figures 28 through 37 show the pressure - specific volume behavior of the individual particles. Figures 38 through 46 show the pressure versus time history at fixed Eulerian radius. Figures 47 through 55 show the displacement of the particles with time.

*Note: All figures in this chapter are collected at the end to simplify comparisons.

BURSTING SPHERE

In case 1 (bursting sphere) there is initially a constant pressure of 9.0 within the energy source volume, decreasing at the edge to an ambient pressure of 1.0 in the surroundings. Figure 15 shows that following the instant of burst an expansion wave begins to propagate into the high pressure source volume and a shock wave develops, propagating away from the source volume. The expansion wave propagates into the source volume at the local velocity of sound and reaches the center at a time of 0.257. The center of the sphere is a singularity point and the expansion wave reflects as another expansion wave. The pressure at the center drops to a minimum value of 0.0656 at τ=0.625. The system attempts to equilibrate the pressure by returning the mass removed by the expansion wave. The system over compensates and at τ=0.680 the pressure peaks at the center and is reflected as a shock wave.

This wave behavior can be seen in the particle path plot of figure 47. The initial expansion wave exhibits itself by the outward movement of the particles. Since the conditions within the source volume are initially uniform, the local velocity of sound is uniform and a straight line can be drawn from the source volume edge to the center along the front of the expansion wave. As time progresses the source volume has over expanded and the particles reverse there outward movement. At τ=0.680 the particle momentum reflects from the center as a shock wave. The second shock wave progression can be seen by the inflections in the particle paths. The decreasing strength of the shock wave is shown by the decrease in the inflection of the particle paths as the wave propagates outward. This second shock tranfers mass away from the center generating another expansion wave. This expansion wave generates a third shock at $\tau=1.85$. If the calculations had been run to longer times, the reflection of expansion waves and shock waves from the center would have continued, but figure 47 shows that successive shocks become much weaker. Both Boyer, et al.(31), and Huang and Chou(32), have reported similar multiple shock waves propagating away from bursting spheres.

The pressure-time behavior at fixed Eulerian radius is shown by figure 38. Inside the source volume ($\eta=0.825$) the pressure rises instaneously to 9.0 and remains until the expansion wave propagates from the edge. The pressure decreases to less than ambient at $\tau=0.38$. The second shock reflects from the center and passes at $\tau=0.9$.

At positions outside the source volume there is a rapid pressure rise as the lead shock arrives followed by a nearly exponential pressure decrease to less than ambient.

MACH 8.0

In case 2, the energy addition wave propagated at a dimensionless Mach number of 8.0, which for steady-state one-dimensional flow corresponds to supersonic combustion or a weak detonation. The energy wave movement is so rapid relative to the ambient velocity of sound that there is minimal reinforcement of pressure, even during energy addition, Figure 14 shows there is no pressure transferred ahead of the energy addition and the pressure peaks at the end of the energy addition. The peak pressure in the source volume is greater than bursting sphere because of the reinforcement of the energy (pressure) propagating with the energy wave.

Figure 16 shows the pressure distribution of the flow field. After the energy addition ends, the shock wave propagating from the source volume develops. Comparing this flow field to the flow field in figure 15 (bursting sphere), at equal radii in the far field the shock overpressures are equal and the flow fields behind the shock are similar.

The particle behavior during energy addition is shown by figure 28; in cell #1 the pressure initially rises and, due to the non-steady behavior, the cell expands to the Reactive Hugoniot in the excluded region for steady-state solutions. When the energy addition wave has progressed through five cells the energy addition begins to approach the steady-state solution and the exclude region is no longer entered during later energy addition. The p-ν behavior of cells 20 through 50 is a straight line which is indicative of a steady-state Rayleigh line.

Figure 48 shows that as the energy addition wave overrides the particles there is a small volumetric expansion during and shortly after the energy addition wave passes the particles. There is no further expansion until the energy addition wave reaches the edge of the source volume and the expansion wave propagates into the center.

The pressure-time history at a fixed Eulerian radius is shown by figure 39. Inside the source volume (η=0.825) the pressure changes from ambient to the peak within a time of 0.0106 because the wave velocity is so high that there is no pressure wave propagating ahead of the energy addition wave. After the energy wave passes there is a gradual pressure decrease until the expansion wave propagates through the position. The pressure continues to decrease until the expansion wave is reflected from the center and reaches the position. The pressure drops below ambient at τ=0.62, followed by a reflected shock which arrives at τ=1.05.

As the pressure wave propagates outside the source volume the peak pressure decreases at larger radii. However, at larger radii the pressure decrease behind the shock is not nearly as great as an exponential decrease and approaches a linear decay.

MACH 5.2 PLANAR GEOMETRY

Steady-state theory is based on the assumption of constant area flow. For comparison, the development of the flow field for Chapman-Jouguet conditions was first studied for the case of planar geometry (constant area). Figure 17 shows the development of the blast wave during energy addition. Of particular note is the p-v behavior shown by figure 29. When the energy addition wave passes through the last cell the pressure has reached the predicted steady-state value. The change in cell properties is a straight line from the initial to final conditions, implying Rayleigh line behavior. The cells at the edge of the kernel appear to tangent the isentropic behavior behind the energy addition. At the CJ point the Reactive-Hugoniot and isentrope are tangent verifying that the Mach 5.2 wave exhibits CJ behavior, as it should.

MACH 5.2 SPHERICAL GEOMETRY

In case 3 an energy addition wave of Mach 5.2, the Chapman-Jouguet value for steady-state conditions, was run in spherical coordinates. At this velocity the Rayleigh line for steady-state conditions tangents the Reactive Hugoniot.

Figure 14 shows very little pressure increase ahead of the energy wave with the pressure peaking at the end of energy addition. The development of the flow field is shown in figure 18. As the energy wave propagates the peak pressure rises and assymptotically approaches but does not reach the predicted CJ pressure of 15.08. This can be attributed to the divergence associated with the spherical flow field.

The p-ν behavior of the individual cells, shown in figure 30, is quite similar to the behavior for the Mach 8.0 addition. The center cells experience a pressure increase and expansion into the excluded region. As the flow field develops the cell behavior approaches Rayleigh line behavior. The cell at the edge of the source volume (cell 50) almost tangents the isentrope.

The particle displacement, shown in figure 49, is similar to the other supersonic cases. Before the energy wave arrives there is no displacement of the particles. During the energy addition there is some particle displacement caused primarily by the expansion behind the energy wave. After the particles expand to nearly equal pressure ($P \simeq 5.25$) behind the addition there is little particle movement until the wave has propagated through the source volume and the expansion wave propagates into the source volume. This is followed by a series of reflected shocks and expansion waves.

The pressure-time behavior of the flow field at Eulerian positions is shown in figure 40. Within the source volume ($\eta=0.825$) there is an almost discontinuous rise to the peak pressure decreasing to nearly uniform pressure behind the energy wave. The expansion wave propagates from the edge of the source volume, causing a rapid pressure decrease to less than ambient at $\tau=0.67$. A reflected shock arrives at $\tau=1.05$. At greater radii the sharp peak becomes more and more diffuse.

MACH 4.0

In case 4 the energy addition wave propagated at Mach 4.0. This is an impossible velocity according to steady-state theory. At this velocity the Rayleigh line for the steady-state solution does not intersect or tangent the Reactive Hugoniot.

The structure of the blast wave during and after energy addition is shown in figures 19 and 20. The energy addition wave moves supersonic relative to both ambient conditions and conditions behind the energy addition ($a_4/a_o=2.78$). Since the acoustic velocity behind the energy addition approaches the energy addition wave velocity the pressure is reinforced and peaks within the energy addition wave as shown by figure 14 (note: Figure 14 is based on Lagrangian positions. Fluid compression and expansion gives the Eulerian distribution of figure 19).

As the energy addition wave propagates through the source volume the peak pressure rises, reaching a maximum pressure of 19.7 at the edge of the source volume when the energy addition ends. The particles are displaced outward by the shock, reaching a particle velocity as great as 3.6 at the peak. When the energy addition reaches the edge of the source volume the pressure decreases and a shock wave is formed. As the shock wave propagates away from the source volume an expansion wave propagates into the source volume.

As the pressure peak goes through the transition from an energy addition wave to a shock wave, a "valley" in the pressure distribution can be seen at $\tau=0.25$. Since the peak pressure occurs at the middle of the energy addition wave, as the wave propagates through the edge of the source volume the pressure at the leading edges of the energy addition wave continues to propagate. However, in the center of the addition wave (tapered region of the source volume) the energy is less than at the edges of the source volume, resulting in a valley in the pressure distribution curve.

The pressure-time distribution at Eulerian radius is shown by figure 41. Within the source volume ($\eta=0.825$) there is a high ($P=15.0$) but very short pressure peak as the energy addition wave passes. The wave passage is followed by a pressure decrease approaching the uniform pressure ($P \simeq 5.45$) behind the energy wave. The propagation of the expansion wave into the source volume causes a rapid pressure drop with the pressure decreasing to below ambient at $\tau=0.68$.

Outside the source volume ($\eta=1.15$) the shock passage has a peak pressure of $P=10.6$ which rapidly decreases to $P=5.0$ followed by nearly exponential decay through ambient. At greater radii the high peak of short duration disappears and the blast wave structure becomes similar to that of a bursting sphere (Figure 15).

From the particle paths in figure 50 it can be seen that the effects of energy addition do not affect the flow field ahead of the energy addition wave. i.e., when the energy addition reaches the edge of the source volume ($\tau=0.21$) there has been no movement of the particle. As the energy addition wave propagates through the source volume the shock wave which is formed entraps particles and moves them outward. Behind the wave the particle velocity decreases and a nearly uniform pressure exists. When the energy addition ends an expansion wave propagates into the source volume. However, since the pressure behind the energy wave is lower than for the bursting sphere, the effects at the center singularity point are reduced.

From the pressure-specific volume plot of figure 31 it can be seen that since the approach flow Mach number is less than the Chapman Jouguet velocity, in the late stages of heat addition the pressure does not peak at the end of energy addition but decreases until the Reactive Hugoniot is reached. Examining the energy addition as it begins at the center, the first cell experiences a pressure increase and volumetric expansion until energy addition begins in the second cell. This prevents further expansion of the first cell and further energy addition results in a pressure increase, and specific volume decrease. The behavior of the second and third cells is quite similar. However, in the fourth and fifth cells there is some compression of the particle during the energy addition. In cells 10, 20 and 30 there is initially compression as the pressure rises until the properties reach the Reactive Hugoniot. The particles then experience an expansion and pressure decrease along the Reactive Hugoniot until energy addition ends. Cells 40 and 50 are subjected to a pressure rise before energy addition begins and do not reach the Reactive Hugoniot. At the end of the energy addition there is a specific volume increase to bring the cell properties to the Reactive Hugoniot.

These characteristics of the flow field indicate that the flow field remains non-steady, i.e., there is no steady-state solution. The flow approaches a quasi-steady-state, but because the p-v behavior during the energy addition is a curved line the addition is definitely not Rayleigh line behavior.

MACH 3.0

The Lagrangian pressure distribution for the Mach 3.0 energy wave has a pressure rise ahead of the energy addition as shown in figure 14. The pressure peaks at the leading edge of the energy addition wave and decreases during energy addition. Figures 21 and 22 show the flow field behavior of the Mach 3.0 is similar to the flow field generated by a Mach 4.0 energy wave, but at lower overpressures. The Mach 3.0 addition is an impossible steady-state solution for the ambient conditions. However, the pressure wave ahead of the energy wave raises the temperature to Θ/Θ_o=2.4, changing the properties.

The p-ν behavior in figure 32 shows the cells at the edge of the source volume exhibiting similar behavior with the pressure rise ahead of the energy wave greater as the edge is approached. The p-ν behavior during energy addition is not a straight line, indicating non-Rayleigh line behavior. But there is a pressure decrease during the energy addition indicating the energy addition is approaching deflagrative behavior.

MACH 2.0

In case 6 the energy addition wave propagated at Mach 2.0. This velocity is supersonic relative to the ambient conditions, but subsonic relative to the properties behind the energy addition wave (a_4/a_o=2.78). This permits energy to be transfered ahead of the energy addition wave and the pressure distribution assumes the form shown in figures 14 and 23. As the energy addition wave propagates through the source volume a pressure "hump" (P=8.0) develops ahead of the wave. With the arrival of the energy addition the pressure decreases to a nearly uniform pressure (P=4.0) behind the energy addition.

Since a pressure decrease across the energy addition is a characteristic of a deflagration, an examination of figure 33 will explain the behavior. Initially the acoustic velocity throughout the flow field is the same, ambient. When the energy addition begins in the first cell the energy wave is propagating supersonic relative to the entire flow field. For the first five cells there is no propagation of pressure ahead of the energy wave and during energy addition the cell properties change from nearly ambient to a pressure-specific volume relationship on the Reactive Hugoniot. When the energy wave reaches the tenth cell a pressure "hump" has begun to propagate ahead of the addition wave and the cell properties have been displaced along the shock Hugoniot ($P \simeq 1.4$) before the energy addition begins. As the energy wave reaches cell 20 the pressure wave ahead of the energy wave has changed the cell properties along the shock Hugoniot ($P \simeq 5.7$). For cells 30, 40 and 50, the pressure ahead of the energy wave approaches a uniform value of P=8.0, with a pressure drop and specific volume expansion across the energy wave. Since the p-ν-line for the energy addition in the final cells approaches a straight line which tangents the isentrope, this case approaches the special case of the lower Chapman-Jouget state for the pressure-specific volume properties ahead of the energy addition. The displacement of succesive plots of the Reactive Hugoniot is caused by transfer of energy away from the cell during the energy addition. Although an energy of

42.5 is added to each cell, the cell energy of the cells near the edge of the source volume at the end of energy addition is only 38. The other energy has been transferred into the flow field.

Figure 42 illustrates the pressure distribution of the flow field at fixed Eulerian radius. At a location inside the source volume, $\eta = 0.825$, there is a rapid pressure rise to $P=8.0$ at $\tau=0.26$ as the energy wave approaches. The pressure falls through the energy addition to a nearly uniform pressure ($P=4.0$) behind the energy addition. This pressure is nearly constant until the energy wave propagates past the edge of the source volume and an expansion wave propagates towards the center. The expansion wave causes a pressure decrease through ambient pressure at $\tau=0.85$.

At the position just outside the source volume, $\eta=1.15$, the expansion of the source volume during energy addition results in the energy wave traversing this Eulerian radius. The position is first subjected to the pressure field ahead of the energy wave followed by a pressure decrease during the energy addition. The expansion wave then causes the pressure to decrease to below ambient at $\tau=1.10$. At greater radii the peak pressure decreases and the blast wave begins to approach the form of a shock wave. However, the effects of the rapid pressure rise ahead of the energy addition can still be seen at the $\eta=1.6$ and $\eta=2.3$.

The particle displacements can be seen in figure 51. As the energy wave propagates through the source volume the particle movement occurs primarily ahead of the wave. The particle velocity is a maximum at the leading edge of the wave and decreases to a minimum at the end of the energy addition. After the energy addition is completed the flow field experiences a series of expansion and shock waves reflecting from the center.

MACH 1.0

In case 7 the energy addition wave propagated at the ambient velocity of sound. The addition of energy increases the local velocity of sound and energy (pressure) is transferred ahead of the energy addition as shown in figure 14. Figure 24 shows the flow field approaching a self-similar solution. As the energy addition wave propagates from the origin the flow field develops and the peak pressure asymptotes to P=3.5. The leading edge of the flow field experiences a rapid pressure rise at the limits of energy transfer. This is followed by a slow pressure rise to the peak pressure at the leading edge of the energy addition wave. Across the energy addition wave the pressure drops to a nearly uniform pressure of P=2.6 behind the wave.

This self-similar wave structure continues until τ=0.85 when the energy wave has propagated through the source volume. The wave structure changes with the peak moving to the leading edge of the pressure rise as the expansion wave is generated.

This can also be seen in figure 43. When energy addition is completed the edge of the source volume has expanded to a radius of 1.5. The positions η=0.825 and η=1.15 are both traversed by the energy wave. At position $\eta=0.825$ there is initially a rapid pressure rise when the pressure ahead of energy addition arrives. This is followed by a slow pressure rise to the peak pressure at the beginning of the energy addition wave. The pressure drops through the energy addition to a nearly uniform pressure behind the wave. This uniform pressure continues until the expansion wave forms at the end of the energy addition and propagates back into the source volume. Similar behavior is noted at $\eta=1.15$.

The position $\eta=1.6$ is located just beyond where energy addition ends. The pressure decrease through the energy addition has been replaced by an expansion wave. The leading edge of the blast wave is similar to the pressure profile ahead of the energy addition, however the expansion wave results in the pressure decreasing to below ambient behind the wave.

At greater radii the blast wave has a rapid rise to the peak pressure followed by a rapid decrease tapering to a nearly linear decrease through ambient pressure.

Most of the particle displacement shown on figure 52 takes place ahead of the energy addition wave. As an example, for the particle initially at D=0.8 the energy addition begins at $\tau=0.76$.

From figure 34 it can be seen that initially the particle p-ν behavior is definitely non-steady. When the energy addition wave has propagated through 20% of the source volume the flow field begins to approach a self-similar solution.

Initially the particle goes through a pressure rise along the shock Hugoniot. During energy addition the particle goes through a weak deflagration along a Rayleigh line.

MACH 0.5

For case 8 the energy wave is propagating subsonic relative to both ambient conditions and conditions behind the energy wave. Comparing figures 14 and 25, the compression and pressure rise ahead of the energy wave can be seen. As the pressure propagates ahead of the wave there is first a pressure rise along the shock Hugoniot followed by an isentropic compression to the beginning of the energy addition. There is an expansion and pressure decrease through the energy addition with nearly equal pressure behind the energy wave.

As the flow field develops the pressure increases and asymptotically approaches a final pressure of P=1.88. In the final stages of energy additions the flow field approaches self-similar behavior. Figure 35 shows the energy addition is a pressure decrease along a straight line in the p-v plane, implying Rayleigh line energy addition as a weak deflagration. The energy wave is propagating much slower than the lower CJ deflagration condition.

The low peak pressure associated with this energy addition results in a large expansion through the energy addition wave. This can be seen in the particle displacement curves of figure 53. The particles are initially displaced by the pressure rise ahead of the energy wave. As they go through the expansion associated with the energy addition their velocity decreases to nearly zero as shown by the nearly constant position after the initial displacement. The particle positions remain nearly constant until the expansion wave propagates through the source volume. Since the source volume has experienced considerable expansion during energy addition the secondary shocks are much weaker than for the cases of supersonic addition.

This is also shown by figure 44. Inside the source volume (η=0.825) there is initially a rapid pressure rise beginning at τ=0.55 followed by a slower rise until energy addition begins (P=1.85). The pressure decreases during energy addition to nearly constant (P=1.69) behind the energy addition, until the expansion wave at the end of energy addition (τ=1.69) propagates to the position (τ=1.96) causing a rapid pressure decrease to below ambient. A second shock is formed, but the pressure does not exceed ambient.

The expansion through the energy addition results in a large expansion of the source volume. When energy addition is completed (τ=1.69) the edge is at an Eulerian radius of 1.66. The expansion of the source volume causes the positions η=1.15 and η=1.6 to experience behavior similar to η=0.825, only the initial pressure rise occurs later and the propagation of the expansion wave into the source volume occurs earlier. At η=2.3 the pressure rise is similar to the rise ahead of the energy addition, however, at greater radii (η=3.2) the peak appears to be moving to the front of the shock.

MACH 0.25

The Mach 0.25 case is quite similar to the Mach 0.5 case except the lower energy wave velocity allows the solution to approach acoustic behavior. Figure 36 shows a slight compression and pressure rise to P=1.32 ahead of the energy wave and a Rayleigh line energy addition with pressure decrease to 1.25. This is indicative of a nearly constant pressure deflagration.

The edge of the source volume has expanded to η=1.84 when energy addition is completed. Figure 45 shows that at an Eulerian position inside the source volume (η=0.825) the pressure begins to rise at τ=0.71, the time required for an acoustic signal to propagate from the center. The pressure rises to P=1.31 ahead of the energy wave and decreases to P=1.25 behind the addition. The expansion of the source volume causes similar behavior at η=1.15 and η=1.6. Outside the source volume the pressure rise is similar to the pressure rise ahead of the energy wave. The overpressure decreases, but since the initial overpressures were low the shock wave decay is slowed.

There is a gradual expansion of the flow field as shown in figure 54.

MACH 0.125

For the Mach 0.125 the energy wave is propagating so slowly the energy addition approaches a nearly constant pressure deflagration. Figure 27 shows a nearly isentropic pressure rise to P=1.08 ahead of the energy wave. Through the energy addition the pressure decreases to P=1.075, a nearly constant pressure expansion. Similar behavior is seen in figure 46. At the time required for an acoustic wave to propagate to the Eulerian positions the pressure begins to rise. Figure 55 shows particle movement ahead of the energy wave, with a large expansion through the wave.

This case was run only until trends were established because excessive computer time was required.

2. Damage Parameters

Experimentally the parameters which are normally observed in blast wave studies are peak pressure, P_s, and positive impulse, I_+, calculated from the pressure-time history of the blast wave. Using these parameters and the P-I technique described earlier, accurate estimates of structural damage can be made.

The peak overpressure as a function of energy scaled distance for cases one through eight and Baker's pentolite data correlation are shown in figure 56. The behavior of the high explosive pentolite does not compare directly with the gas mixture under consideration but is plotted for illustrative comparison. These variables are plotted as they were defined in equations I-8 and I-9. In all cases the overpressures were considerably below the overpressure from an explosion of pentolite with the same total energy. This is caused by the non-ideal structure of the blast wave and the low energy density.

Bursting sphere (infinite wave velocity) is the limit case for the wave addition of energy and results in a constant overpressure from the center to the edge of the kernel. After energy addition, a shock front develops, propagating away from the source volume. Beyond the energy source volume the shock overpressure has a maximum value of P=3.40. In the far field the overpressure of the bursting sphere approaches 70% of the high explosive curve for the same energy scaled radius.

As the energy wave velocity decreases through Mach 4.0, the near field overpressure associated with the energy addition increases. Because of the large overpressure associated with the energy wave the shock propagating away from the source volume initially has a peak pressure greater than the bursting sphere case but decreases to 90% of bursting sphere in the intermediate field. In the far field the overpressure curves coalesce to approximately 70% of the pentolite correlation.

As the velocity decreases from Mach 4.0, the near field overpressure decreases. For each 50% decrease in the energy wave velocity the near field overpressure decreases by the following relationship:

overpressure (50% velocity)≈0.35*[overpressure (100% velocity)]

IV-8

In the near and intermediate field all the supersonic cases initially have an overpressure greater than bursting sphere. At an Eulerian radius of η=1.98 the overpressure curves of the supersonic cases intersect and at a radius of η=2.01 their pressures begin to drop below the bursting sphere overpressures. The overpressure in the Mach 2.0 addition decreases to approximately 75% of bursting sphere at a radius of η=2.73. The overpressure then approaches bursting sphere and reached 90% when the calculation was ended.

In the case of the energy wave propagating at the ambient velocity of sound, Mach 1.0, the expansion behind the energy addition results in shock wave ahead of the energy addition. When the energy addition ends, this shock wave continues to propagate with only a very gradual decrease in overpressure. Between a radius of η=1.96 and η=2.24 this case has the greatest overpressure. The overpressure then begins to drop rapidly as the expansion waves behind the shock decrease the shock overpressure. If the flow behavior behind the Mach 1.0 addition is similar to the Mach 2.0 the overpressure will begin to approach the bursting sphere in the far field, as it did in the Mach 2.0 case.

The subsonic energy additions exhibit expansions of the source volume behind the wave. However, as the velocity decreases the expansion does not produce the near field and intermediate field overpressures necessary to approach the overpressures from bursting sphere. The Mach 0.5 and Mach 0.25 overpressures approach, 84% and 23% of bursting sphere, respectively.

Figure 57 is a plot of non-dimensional impulse, $\bar{I}$, versus energy-scaled distance, R_ε. $\bar{I}$ is defined by Sachs' relationship and is expressed as:

$$\bar{I} = \frac{I_+ a_o}{(p_o)^{2/3}(E_T)^{1/3}} \qquad \text{IV-9}$$

where I_+ is the positive phase impulse, a_o and p_o are the ambient atmospheric values of sound speed and pressure, respectively, and E_T is the total energy deposited within the source volume. For comparison the impulse of a high explosive, pentolite, is also plotted.

Because impulse is the integral of overpressure with time, the overpressure and impulse plots exhibit similar behavior when plotted against similar parameters. For the supersonic energy addition, the impulse is higher in the near, intermediate and far field than the subsonic cases. As the energy wave velocity decreases the impulse decreases for the entire flow field.

In the near field the impulse from the theoretical energy addition is greater than the experimental correlation for pentolite because of the positive pressure behind the energy addition wave which exist until the end of the energy addition. In the far field the impulse varies from 60 to 75% of that for the high explosive (pentolite).

3. Energy Distribution

In an ideal or point source explosion all the energy is transferred to the surroundings and is available to drive the blast wave. In a non-ideal or diffuse explosion the source releases energy relatively slowly over a sizeable volume. In addition, the mass in the source volume retains a portion of the energy, reducing the amount of energy available to drive the blast wave through the surroundings. The energy which remains in the source volume can be used as a measure of the "effectiveness" of the explosive process relative to an ideal (point-source) explosion.

The concept of "waste energy" was introduced by Taylor[3] who surmised that some energy would remain or be "wasted" in the central core region of the blast zone. This energy which remains in the source volume after the shock passage and an adiabatic expansion to ambient pressure is unavailable to the pressure wave and has also been called "residual energy" by Strehlow and Baker[27]. They noted that the energy distribution in the system and how it shifts with time are two important properties in determining the behavior of an explosive process.

Adamczyk[18] analyzed his non-ideal explosions (produced by homogeneous addition of energy) and noted that the time over which energy is added to the source region determines the structure of the blast wave and the partitioning of energy between the source volume and the surroundings. He considered two idealized limit cases of constant volume energy addition and constant pressure expansion.

The first case of constant volume energy addition, bursting sphere, can be visualized as an infinitely fast energy addition wave with an instantaneous deposition time. Initially the source volume is at the ambient temperature and pressure of the surroundings. Energy is instantaneously added, raising the temperature and pressure of the source volume to the initial conditions of the bursting sphere. The energy added is:

$$\Lambda = n\left[C_{v_4}(\Theta_4-\Theta_o) + (C_{v_4}-C_{v_o})\Theta_o\right] \qquad \text{IV-10}$$

$$\Lambda = \frac{(p_4 - p_o)v_o}{\gamma_4 - 1} + \frac{(\gamma_o - \gamma_4)}{(\gamma_4 - 1)(\gamma_o - 1)} p_o v_o \qquad \text{IV-11}$$

and the energy density is given by:

$$q = \frac{p_4}{p_o} - 1 \qquad \text{IV-12}$$

$$q = \frac{\Theta_4}{\Theta_o} - 1 \qquad \text{IV-13}$$

where γ_4 is the constant gamma of the gas in the source volume after energy addition and γ_o is the initial gamma throughout the field. If the initial and final gamma's in the source volume are equal, the second term cancels and equation IV-11, is Brode's(33) formula for the energy stored in a bursting sphere.

If the bursting sphere undergoes an idealized isentropic expansion where the sphere expands slowly against a counter pressure equal to its instantaneous pressure, the fraction of the total energy remaining in the source volume is:

$$\frac{E_B}{E_T} = \frac{1}{q} \left[(1+q)^{1/\gamma} - 1 \right] \qquad \text{IV-14}$$

and the fraction of energy transferred to the surroundings is:

$$\frac{E_S}{E_T} = \frac{1}{q} \left[(1+q) - (1+q)^{1/\gamma} \right] \qquad \text{IV-15}$$

where E_S is the energy transferred to the surroundings, E_B

is the energy remaining in the source volume, and E_T is the total energy deposited. Equation IV-15 is Brinkley's[34] or Baker's[2] formula for the effective quantity of energy stored in the sphere, expressed as a fraction of Brode's energy. In the limit as $q \to \infty$ (point source), $E_s/E_T \to 1$ and as $q \to 0$, $E_s/E_T \to (\gamma-1)/\gamma$. For the conditions being investigated:

$$E_B/E_T = 0.48$$

and

$$E_S/E_T = 0.52$$

In the second limit case the energy is added infinitely slowly such that the energy of both the source volume and surroundings remain at p_o. The fraction of energy which remains in the source volume is:

$$\frac{E_B}{E_T} = \frac{C_v}{C_p} = \frac{1}{\gamma} \qquad \text{IV-16}$$

and the fraction of energy transferred to the surroundings is:

$$\frac{E_S}{E_T} = \frac{R}{C_p} = \frac{\gamma-1}{\gamma} \qquad \text{IV-17}$$

this is also the limit case for an infinitely rapid (constant volume), but infinitely small ($q \to 0$) energy addition. For the conditions investigated:

$$E_B/E_T = 0.83$$

$$E_s/E_T = 0.17$$

It should be noted that in both limit cases, $q \to o$ for bursting sphere and infinitely slow energy addition, there is no blast wave.

In the cases studied all internal properties are initially at their ambient values throughout the system. At the instant chemical reaction begins, the heat addition model adds energy to the volume encompassed by the heat addition wave. As time progresses this energy is redistributed as internal and kinetic energy throughout the system, where the system contains all materials out to the lead characteristic or lead shock wave.

The energy added to the system can be separated into four classifications:

(1) Internal Energy increase in the source volume:

$$(IE)_B = \int_o^{r_\varepsilon} \rho \frac{(\Theta - \Theta_o) r^j}{\gamma_4 - 1} \, dr - \int_o^{r_\varepsilon} \frac{\rho \Theta_o r^j}{\gamma_o - 1} \, dr \qquad \text{IV-18}$$

(2) Kinetic Energy of source volume:

$$(KE)_B = \int_o^{r_\varepsilon} \frac{\rho u^2 \, r^j}{2} \, dr \qquad \text{IV-19}$$

(3) Internal Energy increase in the surroundings:

$$(IE)_S = \int_{r_\varepsilon}^{r_\infty} \frac{\rho(\Theta-\Theta_o)r^j}{\gamma_4-1}\,dr - \int_{r_\varepsilon}^{r_\infty} \frac{\rho\Theta_o r^j}{\gamma_o-1}\,dr \qquad \text{IV-20}$$

(4) Kinetic Energy of surroundings:

$$(KE)_S = \int_{r_\varepsilon}^{r_\infty} \frac{\rho u^2 r^j dr}{2} \qquad \text{IV-21}$$

where 0 is the center of the sphere, r_ε is the position of the contact surface of the ball containing the high energy gas, and r_∞ is the limits of the flow field.

Figures 58 through 66 illustrate the energy distribution for the cases investigated and how it varies with time. Figure 58 shows an instantaneous addition of the total energy to the source volume. Since the instantaneous energy addition is a constant volume energy addition, initially 100% of the energy is internal energy in the source volume. As the flow field develops this internal energy shifts to kinetic energy in both the source volume and the surroundings, and internal energy in the surroundings. As the source volume expands its kinetic energy rises and peaks when the expansion fan reaches the center, followed by an oscillatory decay. The kinetic energy in the surroundings increases until there is a maximum in the rate of displacement of the source volume at $\tau \simeq 0.66$. The kinetic energy of the surroundings gradually decreases as the shock wave propagates into the flow field. The internal energy of the air continually rises and asymptotically approaches a final value of 36%. The internal energy of the source volume appears to asymptotically approach a final value of 66%.

In case 2(M_W = 8.0) the movement of the energy wave through the source volume generates kinetic energy of the entraped particles. Since the energy wave moves supersonic there is no energy transfer to the surroundings until the energy addition wave reaches the edge of the source volume (τ=0.116). There is a rapid rise in the internal and kinetic energy of the surroundings as the energy wave propagates into the surroundings and continues as a shock wave. The expansion wave which propagates into the source volume develops a large value of kinetic energy in the source volume. The internal energies approach final values of 63% in the source volume and 37% in the surroundings.

In case 4 (M_W = 4.0), the large overpressure of the energy wave imparts considerable kinetic energy to the particles in the source volume. This kinetic energy maximizes and decreases abruptly when the shock enters the surroundings (τ=0.23). The expansion wave then increases the kinetic energy of the source volume until the wave reflects from the center. Subsequent expansion waves reflecting between the center and the shock have less kinetic energy. The internal energy of the source volume decreases from a value of 98% when the addition wave reaches the edge of the source volume to a final value of 60%. The internal energy of the surroundings approaches 40% of the energy added.

In cases 6(M_W = 2.0), 7(M_W = 1.0), 8(M_W = 0.5), and 9(M_W = 0.25), figures 62, 63, 64, and 65 respectively, there is energy transfer ahead of the energy addition wave. This causes a movement (displacement) of the particles resulting in an increase in the kinetic energy. As the energy wave approaches the edge of the source volume the particle movement ahead of the wave moves into the surroundings with the kinetic energy abruptly decreasing in the source volume and increasing in the surroundings. As the expansion wave propagates into the source volume the kinetic energy increases, but not to the level reached during the passage of the heat addition wave. At later times the kinetic energy of the source volume decreases as successive expansion waves become weaker. The final distribution of energy is; for case 6, 61% source volume, 39% surroundings; case 7, 66% source volume, 34% surroundings; case 8, 74% source volume, 26% surroundings; and in case 9, 77% source volume, 23% surroundings.

As the Mach number of the energy addition wave decreases, the overpressure also decreases resulting in a weaker shock wave propagating into the surroundings and consequently there is less energy transfer.

In a non-steady heat addition the limit case of a constant pressure expansion can not be reached since any heat addition, even at very low subsonic velocities will result in a pressure rise ahead of the energy addition wave and pressure decrease through the energy addition. For the cases run the energy distribution approached 77% in the source volume and 23% in the surroundings for very slow flame propagation velocities. The energy distribution for case 10 (M_W = 0.125) was not calculated since the complete energy addition was not run.

Examining the energy distribution for the cases which were run it can be seen that for a constant energy density the energy distribution is significantly affected by the Mach number of the energy wave. The principle mechanism for transfer of energy to the surroundings is the propagation of the shock wave through the flow field. For the cases of a highly supersonic energy addition wave, there is very little kinetic energy in the flow field as the wave propagates. When the energy addition stops there has been only minimal development of the flow field.

The distribution of energy between the source volume and the surroundings and how this distribution shifts with time as a function of the flame velocity is summarized by figure 67. For the limit case of infinite energy wave velocity, bursting sphere, 37% of the energy is transfered to the surroundings by the final time line calculation. The energy transfer to the surroundings increases to 41% as the velocity decreases to M_W = 4.0. As the velocity is decreased further the energy transfer to the surroundings decreases to 23% in case 9(M_W = 0.25), the lowest velocity for which the energy distribution is calculated.

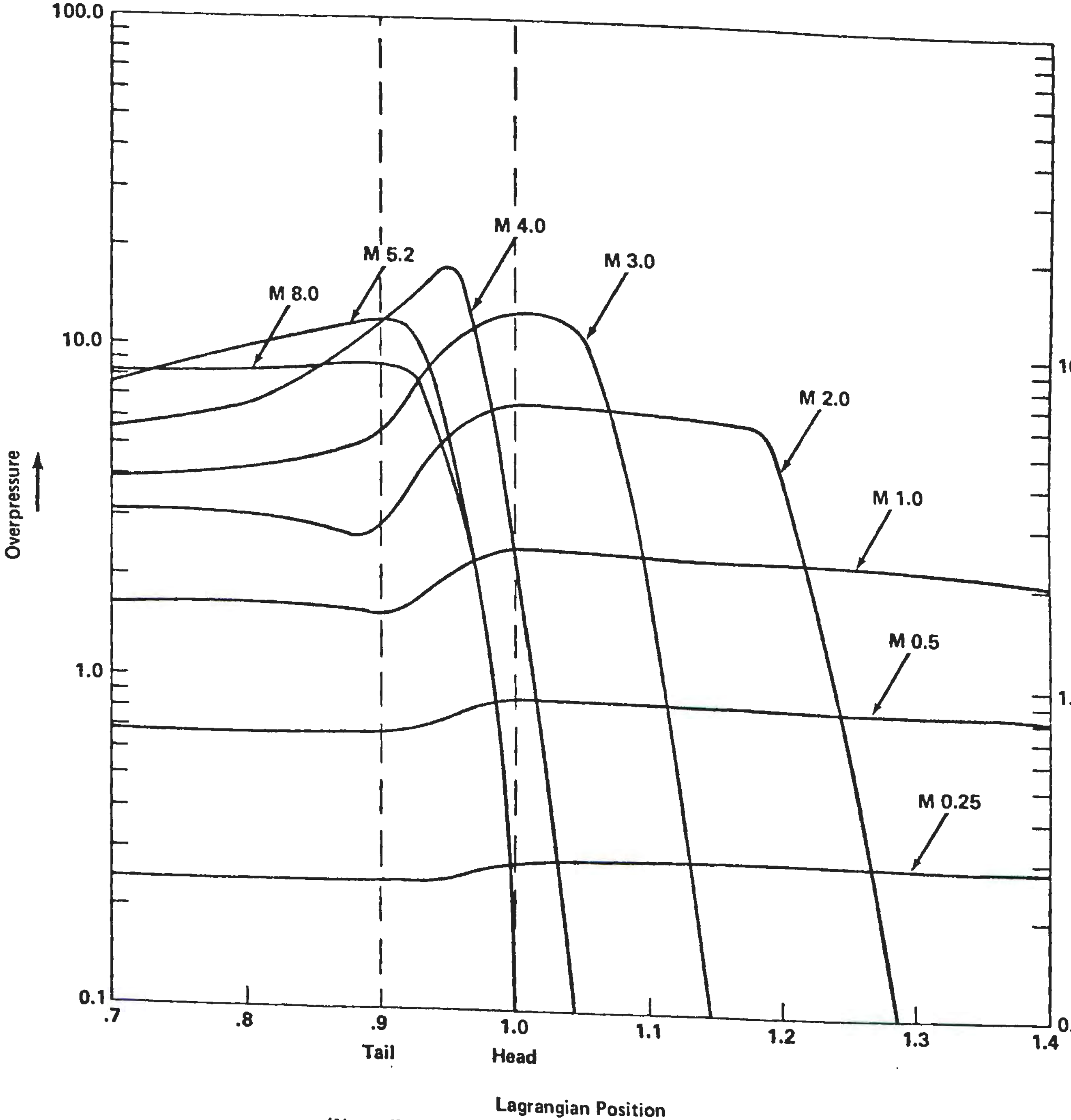

Figure 14. Overpressure Distribution Through Energy Addition Wave

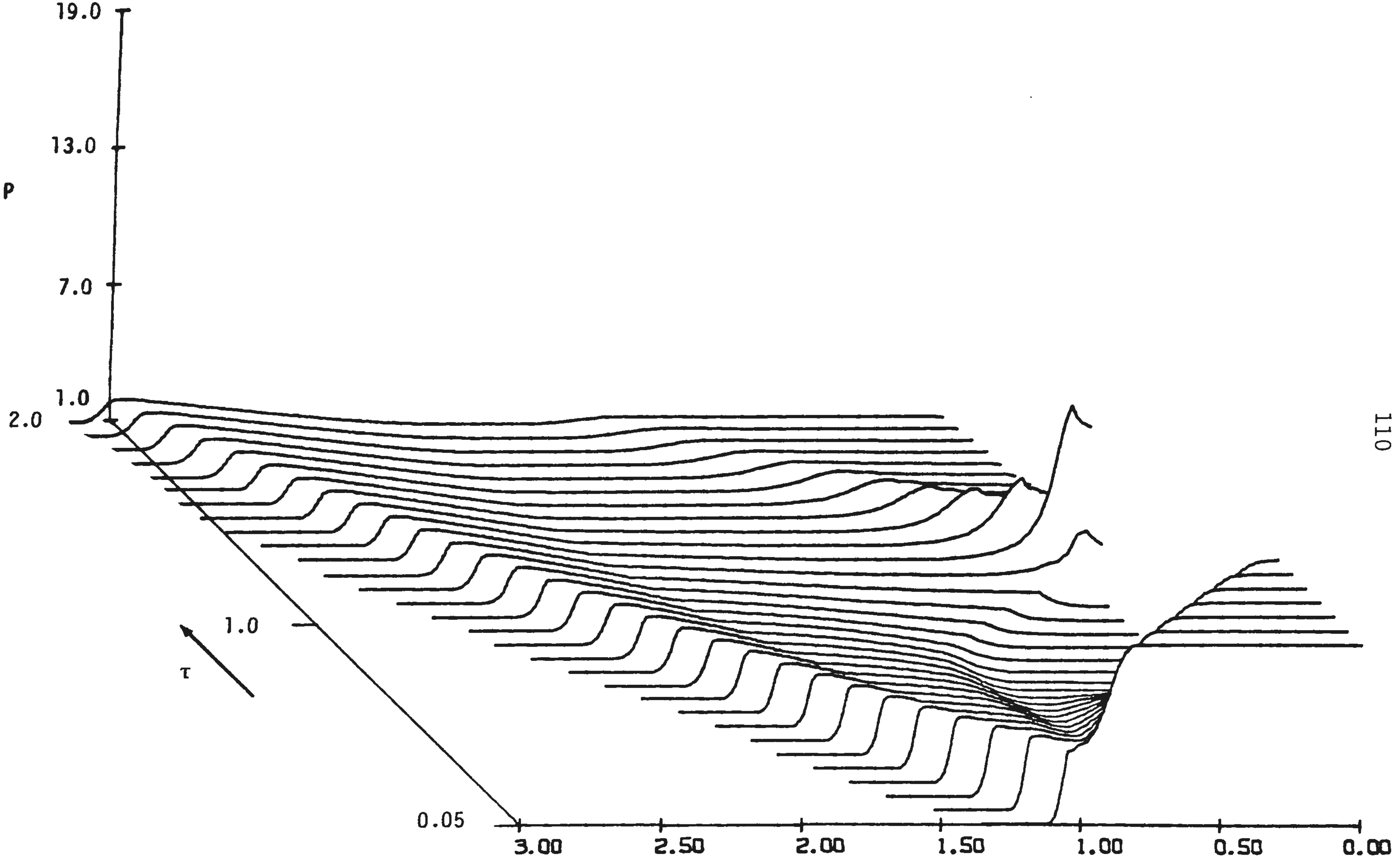

PRESSURE / PO DISTRIBUTION VS. DISTANCE / DO AND TIME / TO

Figure 15. Pressure distribution versus Eulerian distance and time for blast system generated by an infinite velocity energy

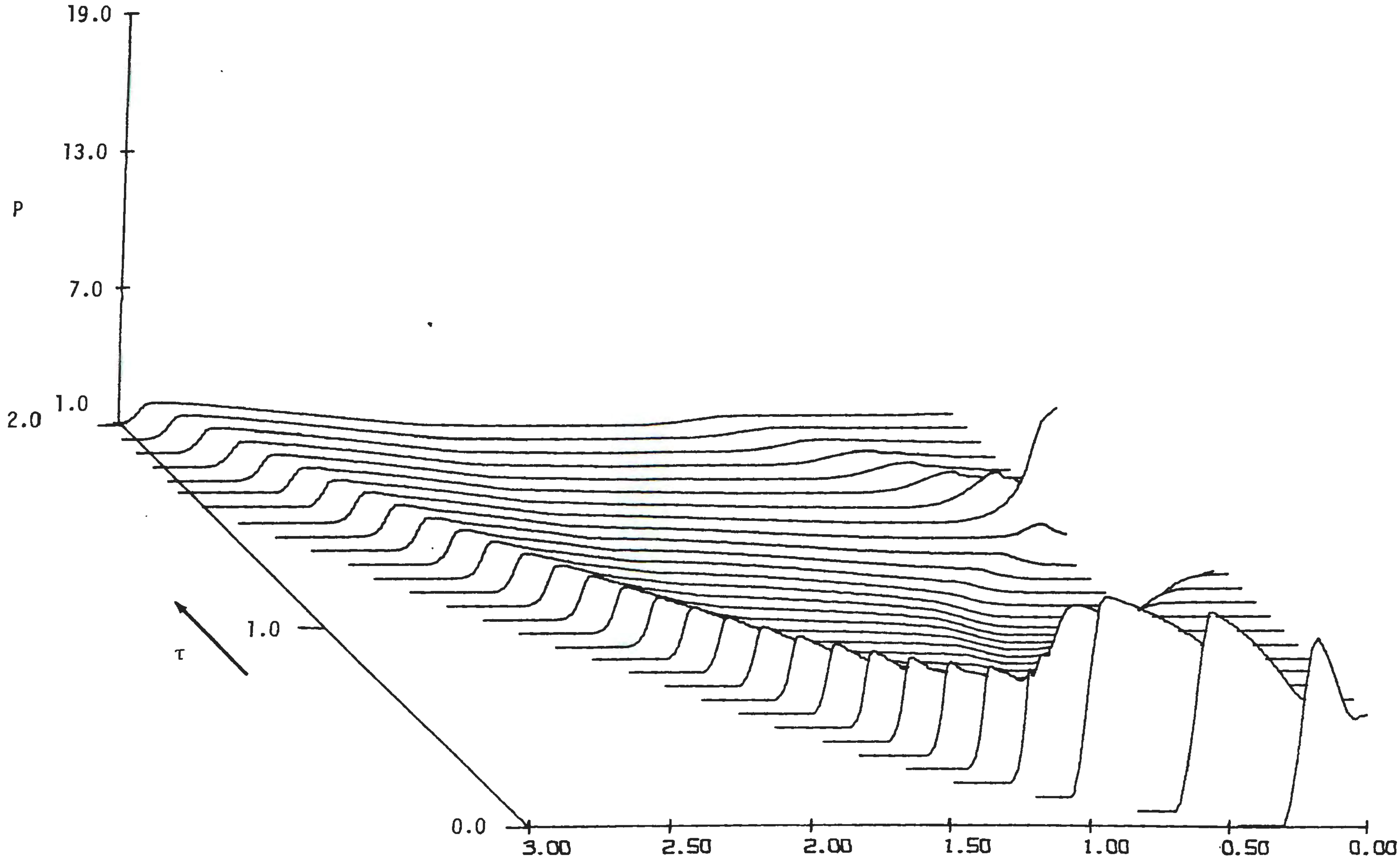

PRESSURE / PO DISTRIBUTION VS. DISTANCE / DO AND TIME / TO

Figure 16. Pressure distribution versus Eulerian distance and time for a blast system generate by a Mach 8.0 energy addition wave.

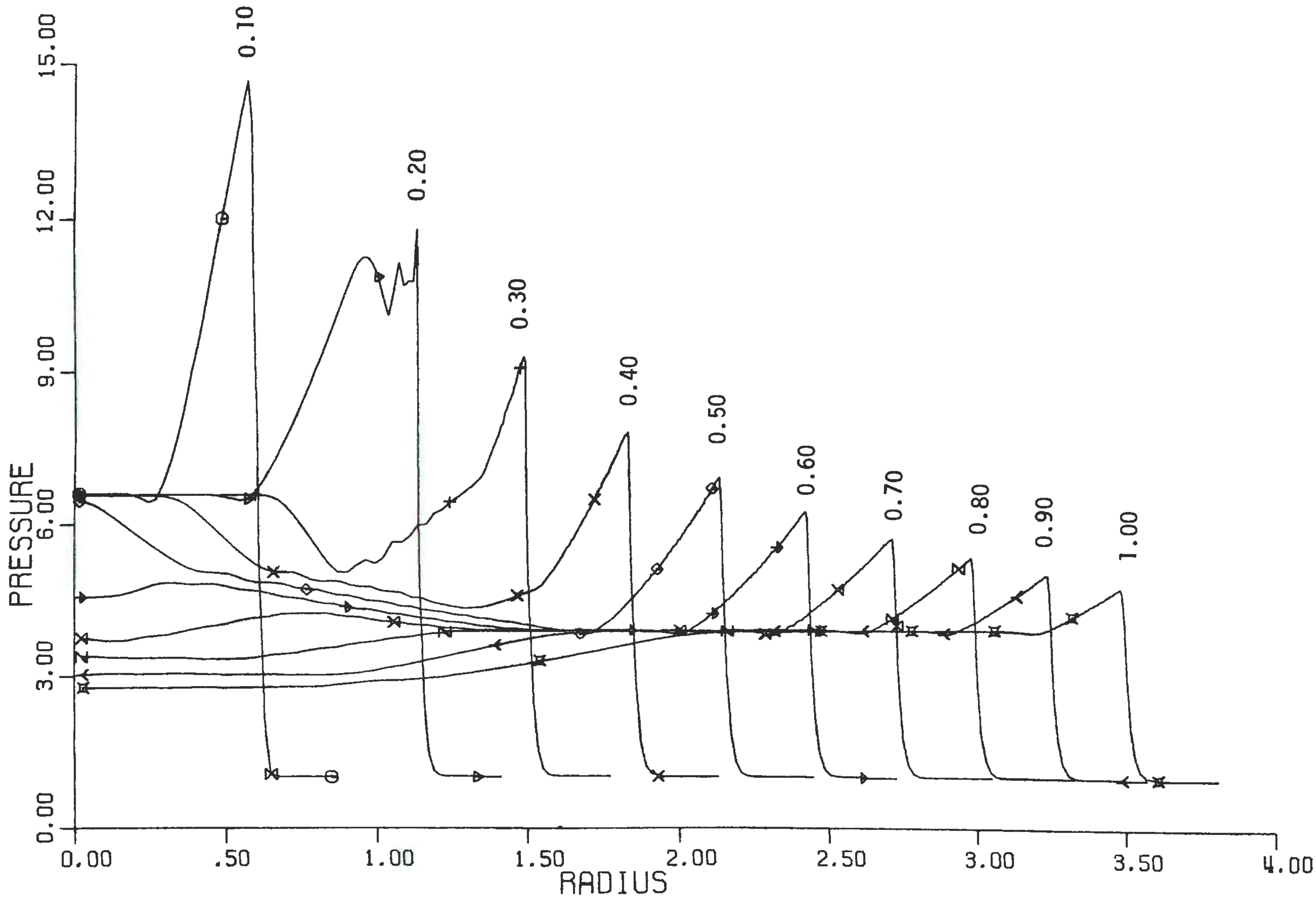

Figure 17. Pressure distribution versus Eulerian distance and time from a blast system generated by a Mach 5.2 (CJ) energy wave in planar geometry.

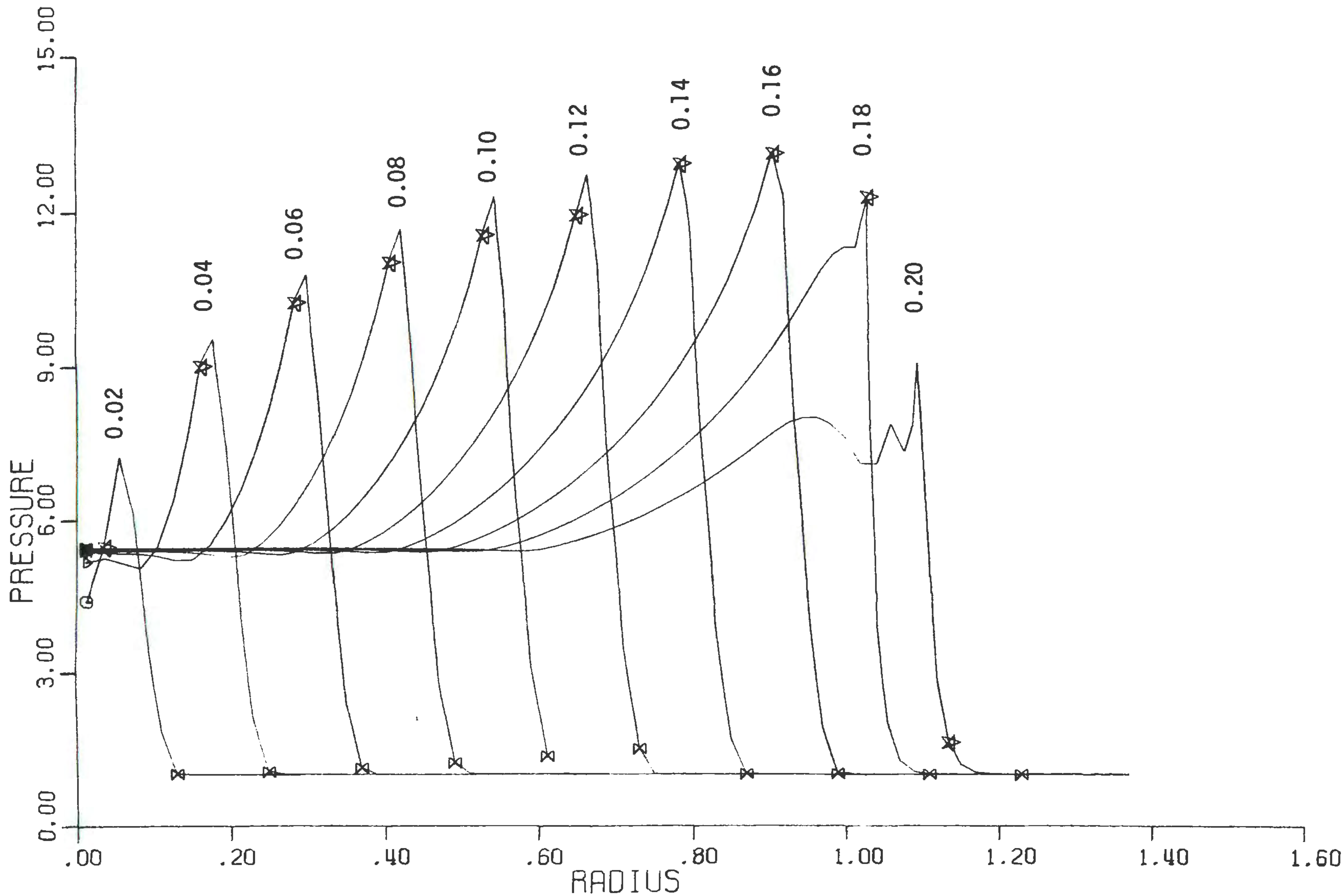

Figure 18. Pressure Distribution Versus Eulerian Distance And Time From a Blast System Generated By A Mach 5.2 (CJ) Energy Wave in Spherical Geometry.

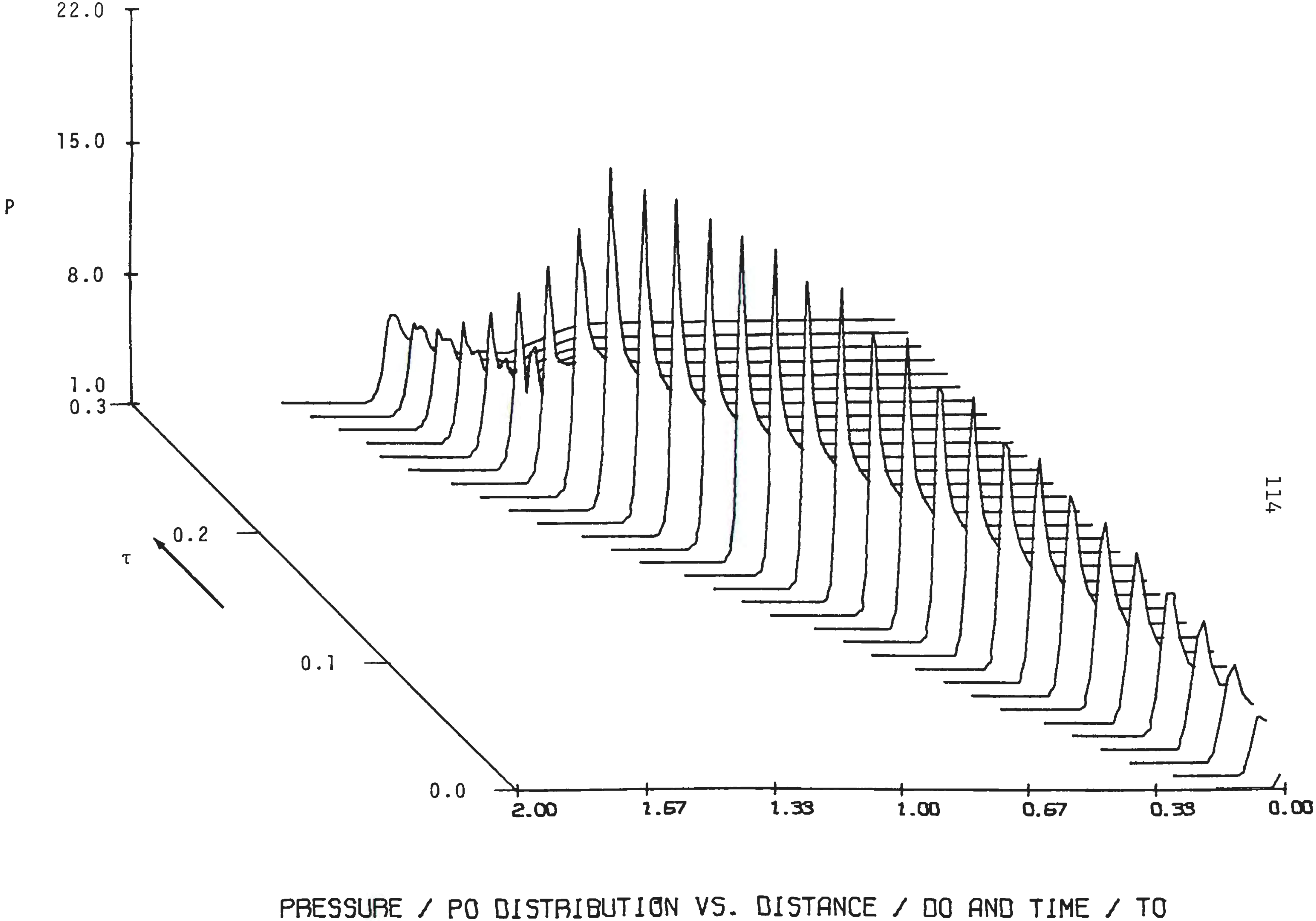

Figure 19. Pressure distribution versus Eulerian distance and time for a blast system generated by a Mach 4.0 energy wave.

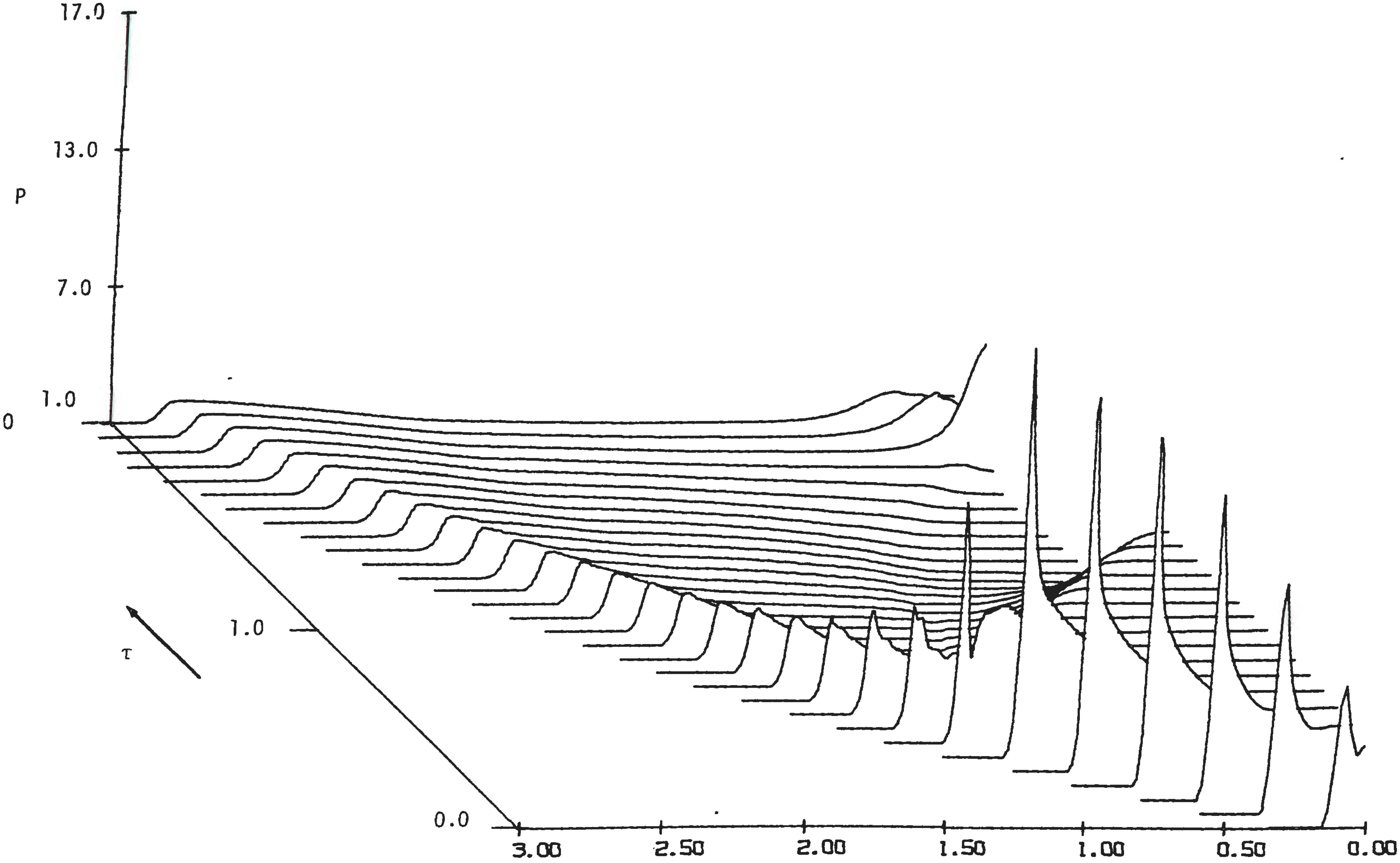

Figure 20. Pressure distribution versus Eulerian distance and time for a blast system generated by a Mach 4.0 energy addition wave.

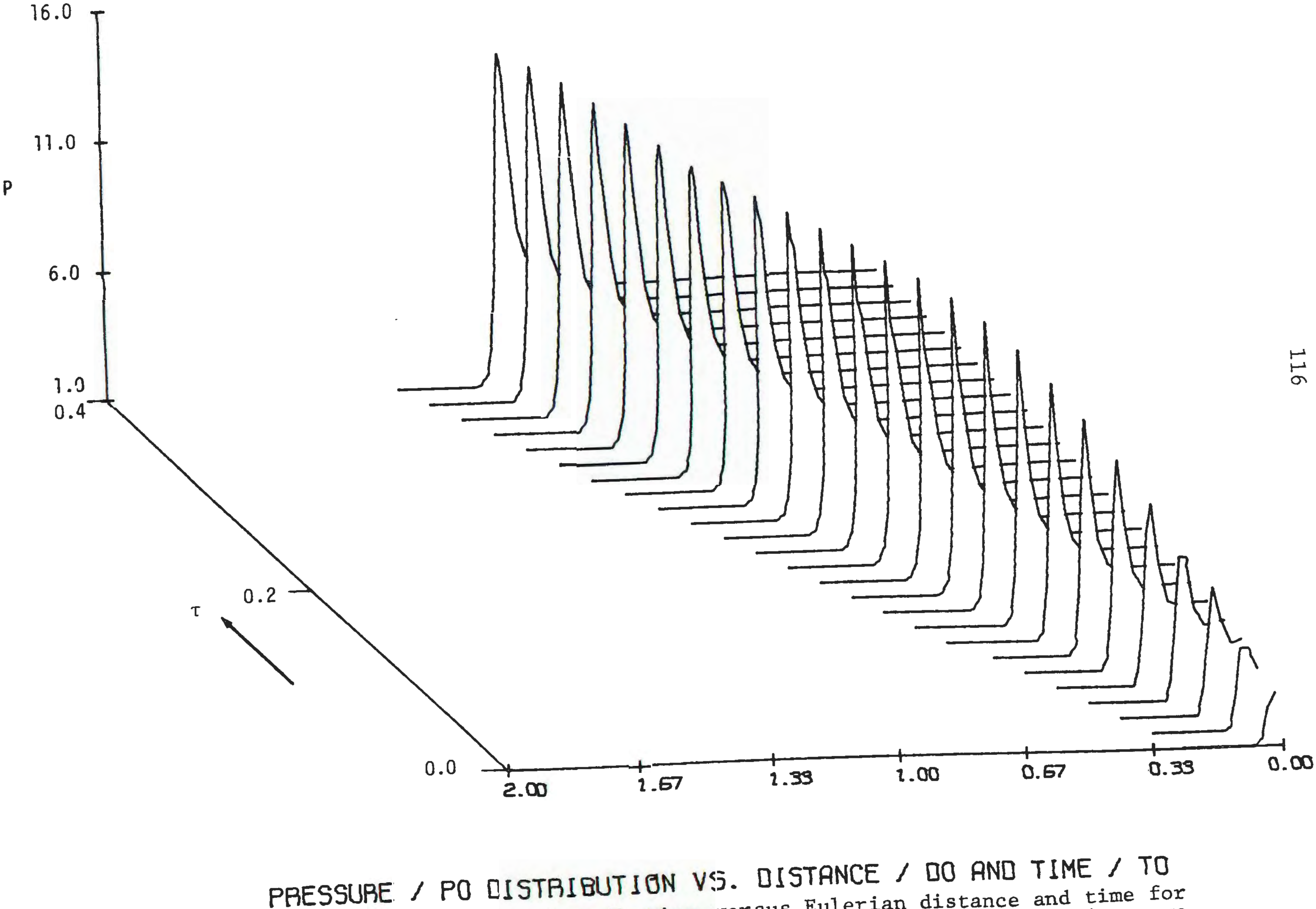

Figure 21. Pressure distribution versus Eulerian distance and time for a blast system generated by a Mach 3.0 energy addition wave.

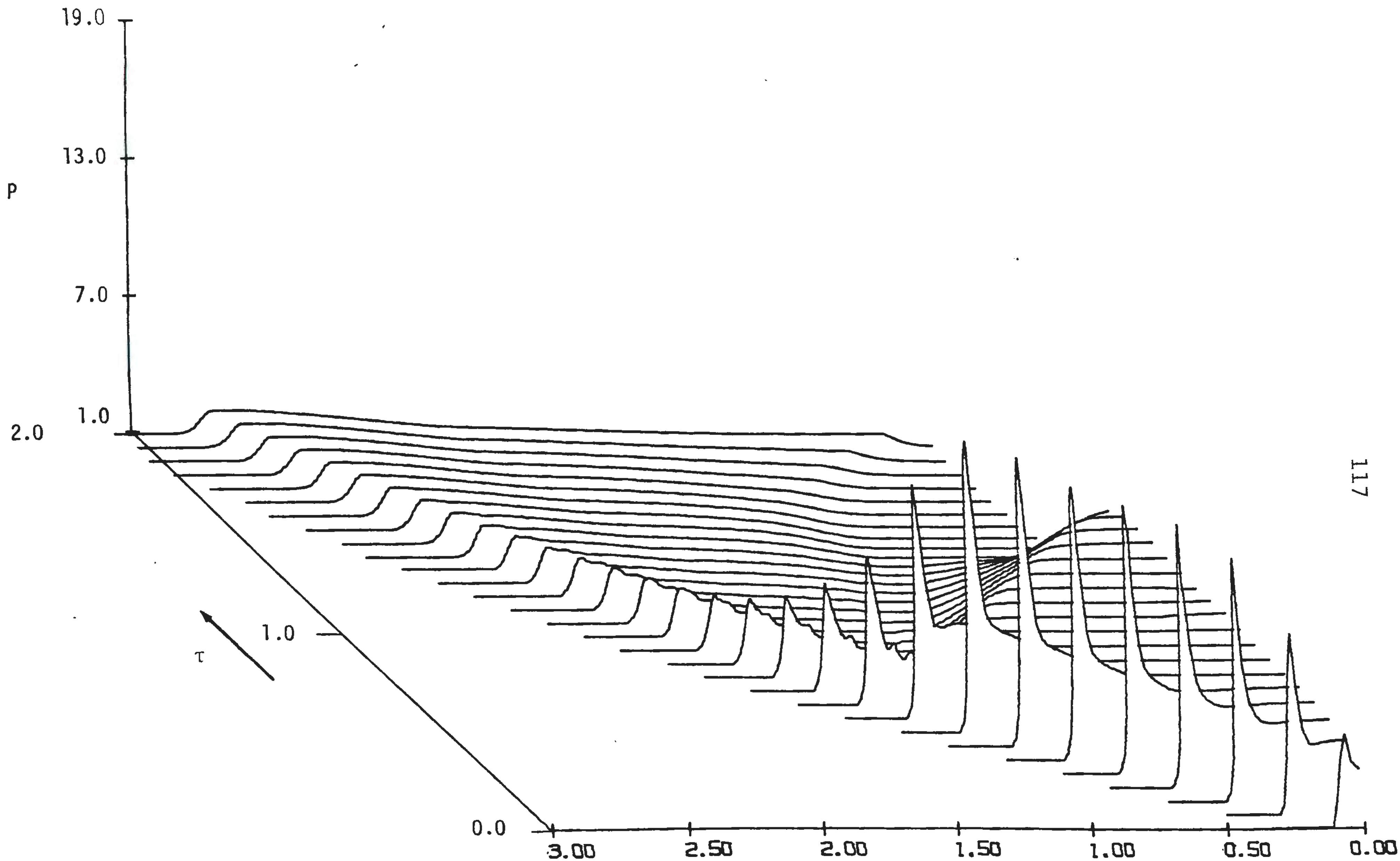

Figure 22. Pressure distribution versus Eulerian distance and time from a blast system generated by a Mach 3.0 energy addition wave.

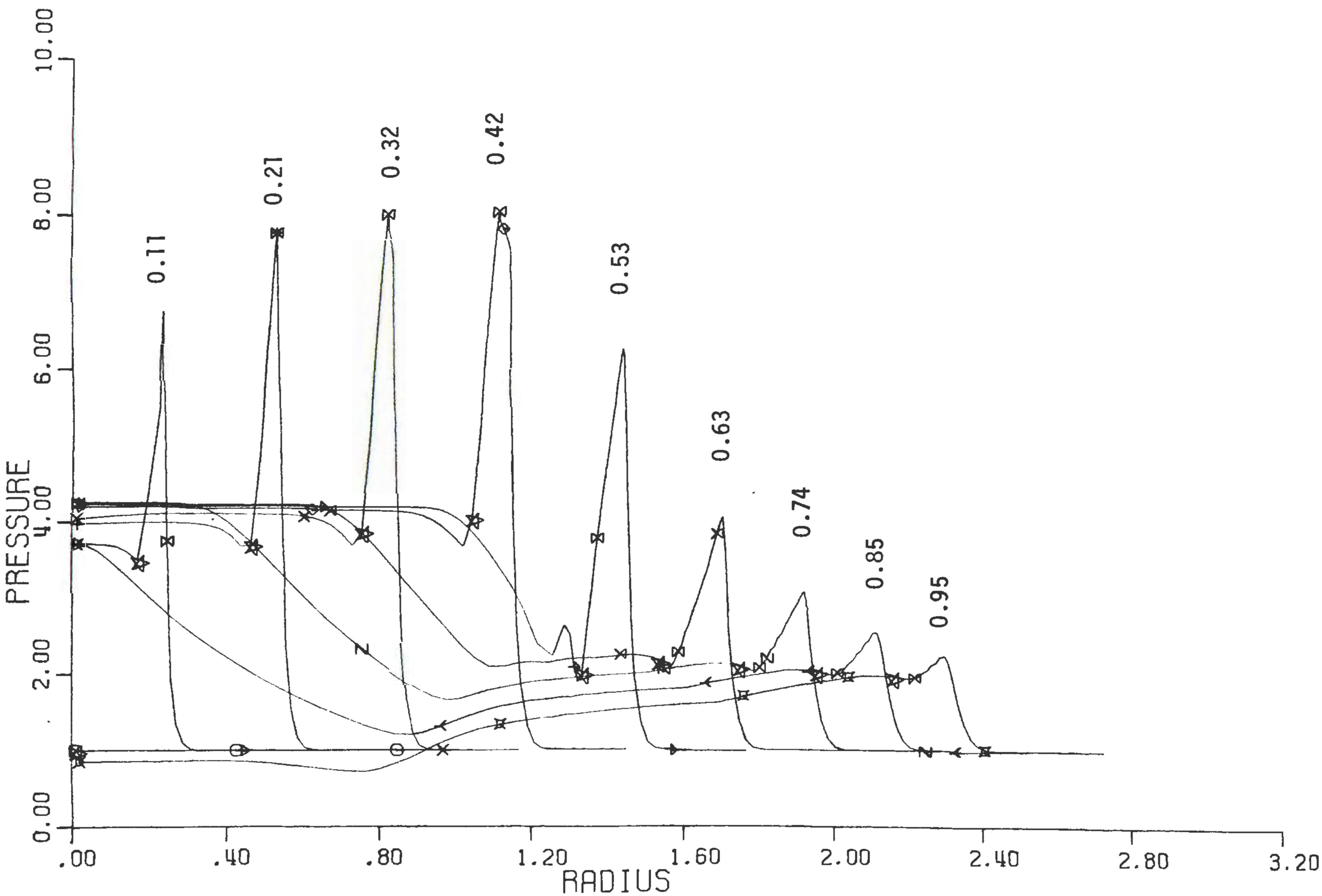

Figure 23. Pressure distribution versus Eulerian distance and time for a blast system generated by a Mach 2.0 energy addition wave.

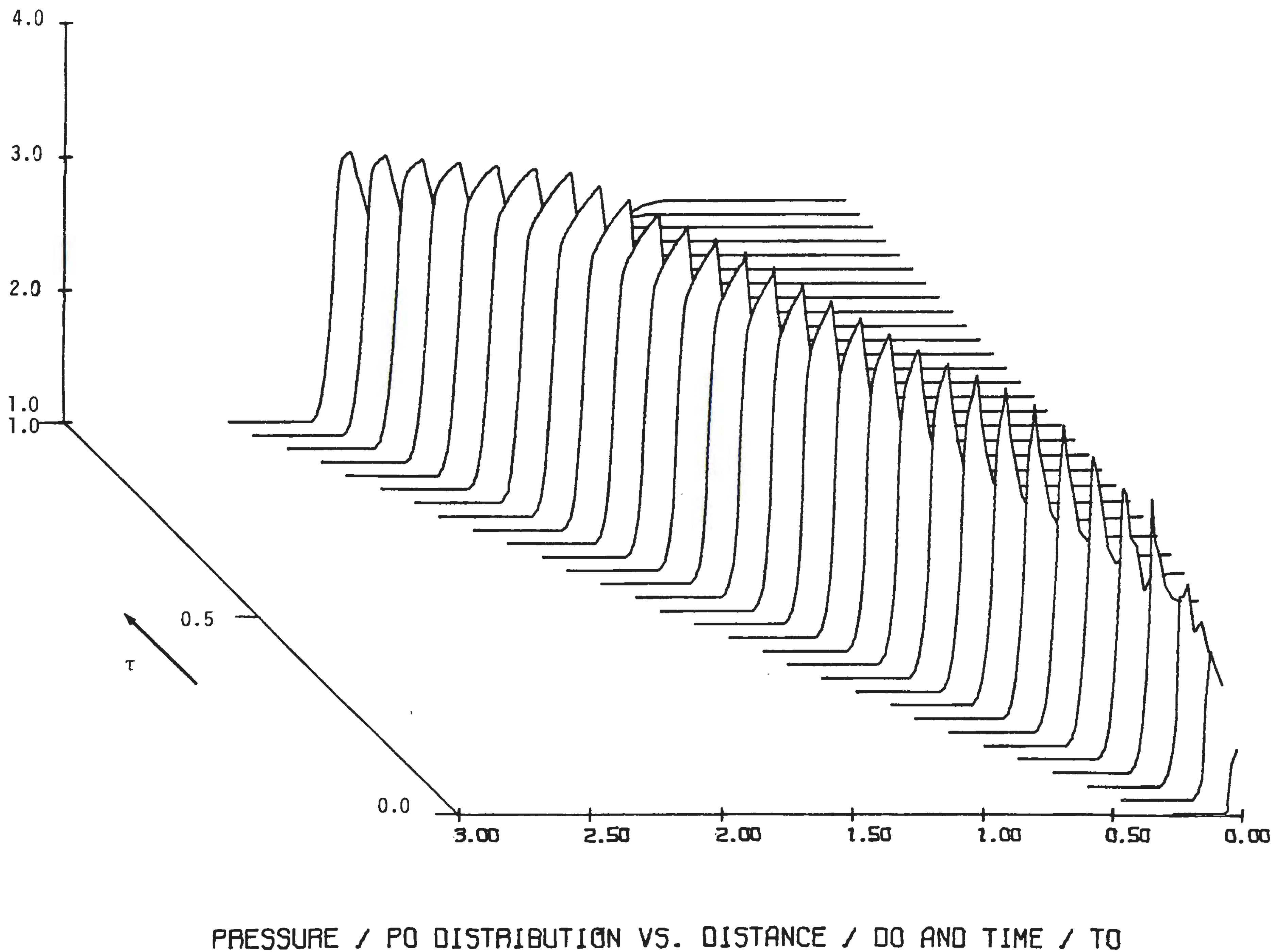

Figure 24. Pressure distribution versus Eulerian distance and time for a blast system generated by a Mach 1.0 energy addition wave.

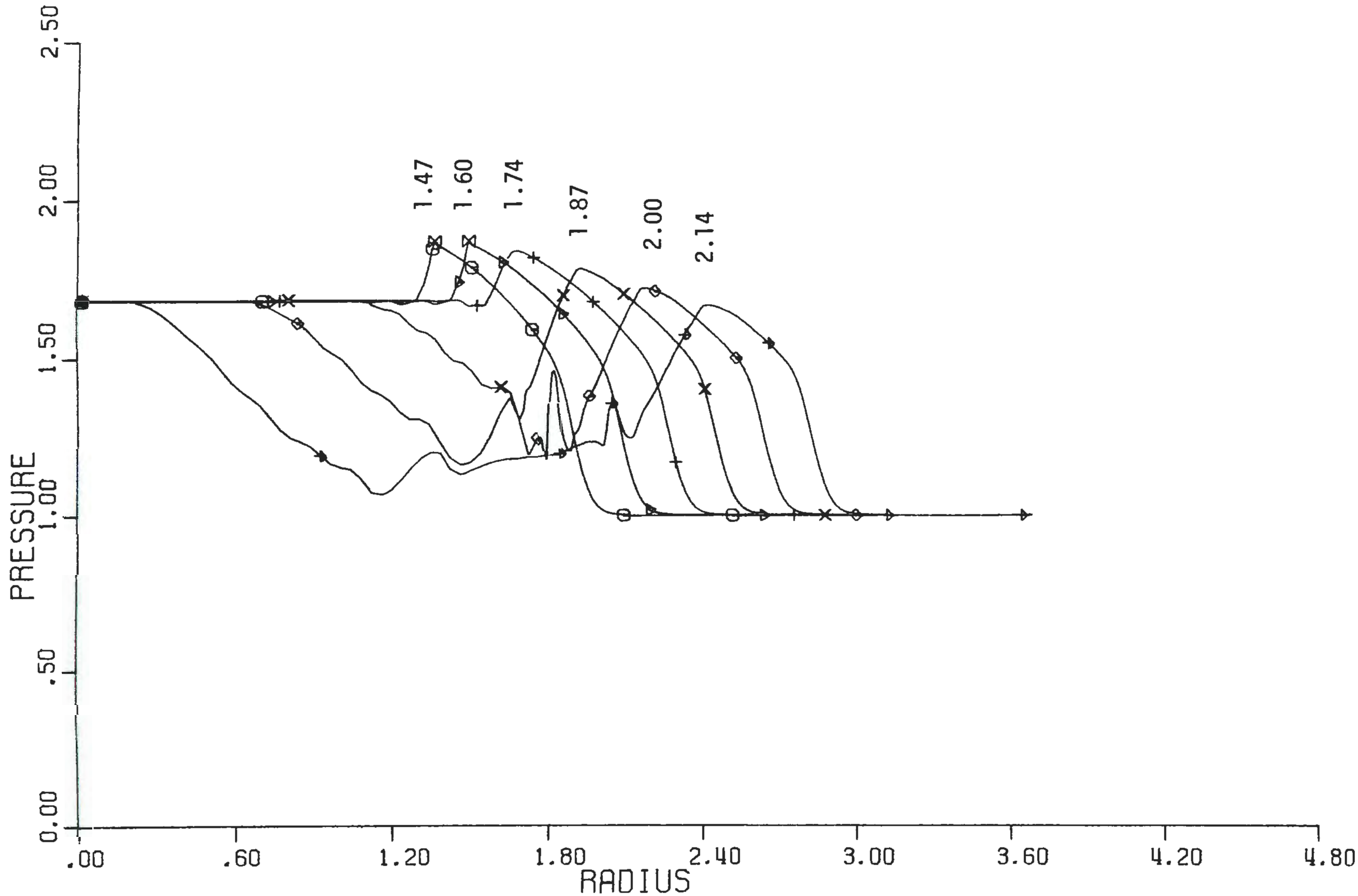

Figure 25. Pressure distribution versus Eulerian distance and time from a blast system generated by a Mach 0.5 energy wave.

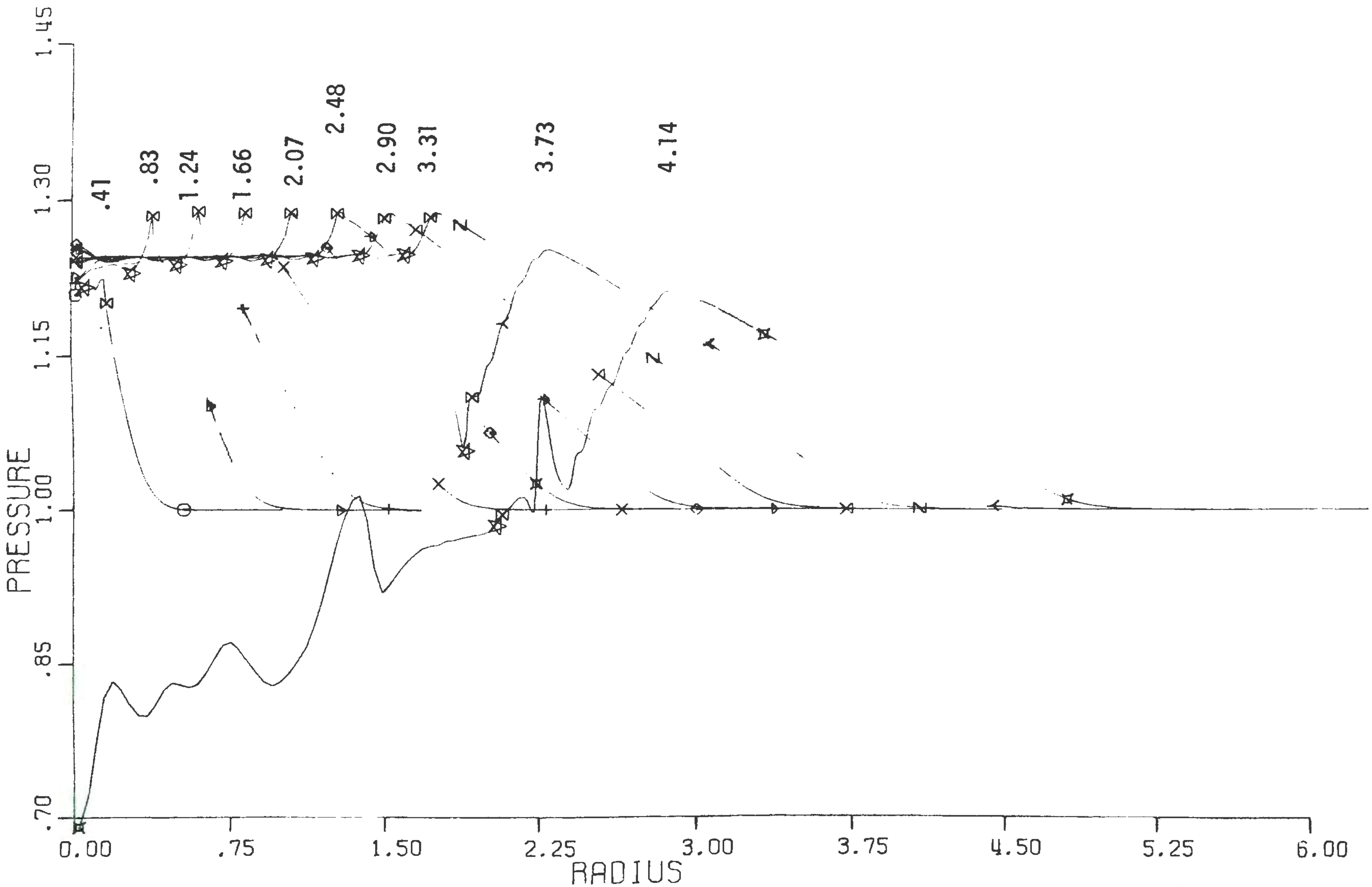

Figure 26. Pressure distribution versus Eulerian distance and time from a blast system generated by a Mach 0.25 energy addition wave.

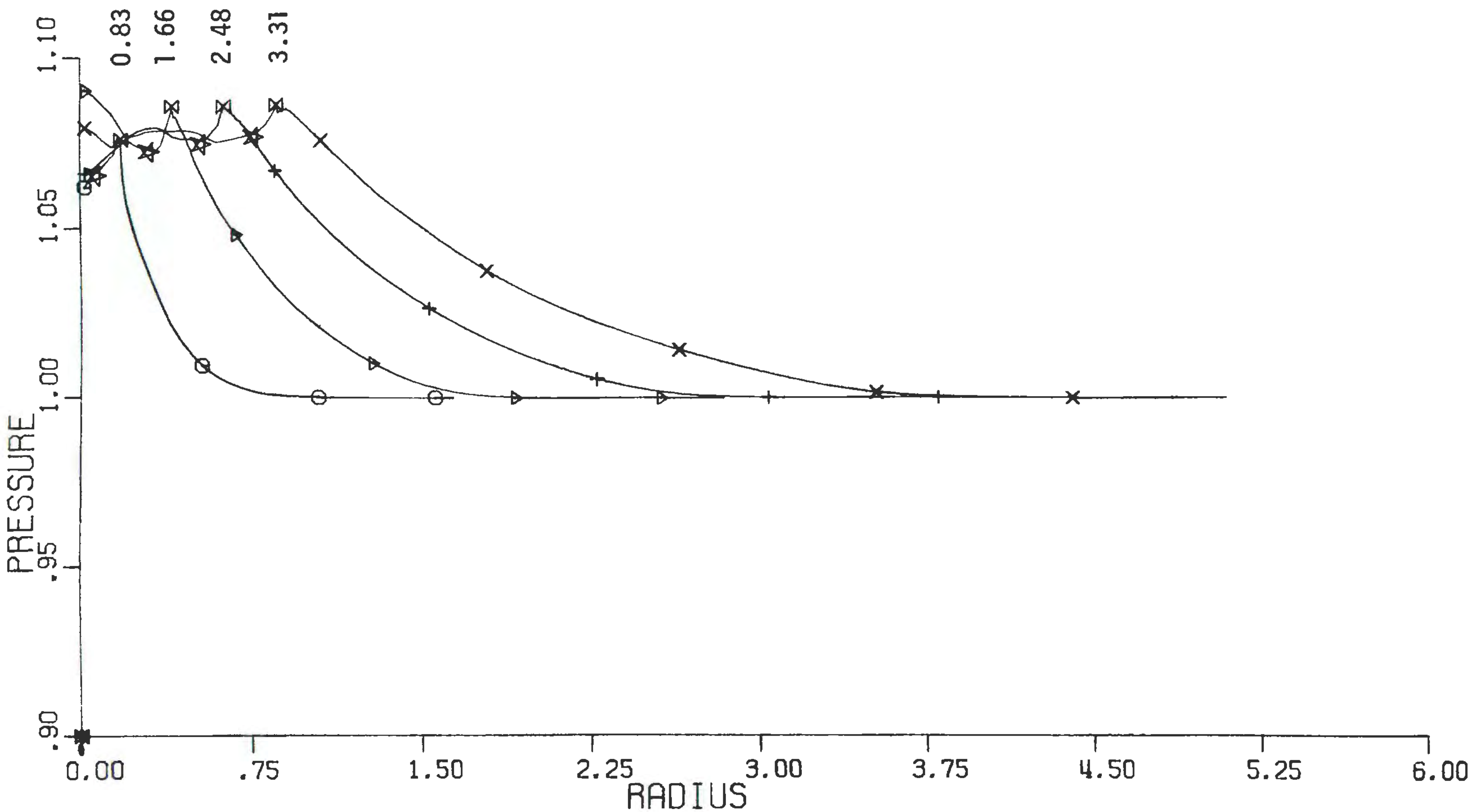

Figure 27. Pressure distribution versus Eulerian distance and time for a blast system generated by a Mach 0.125 energy addition wave.

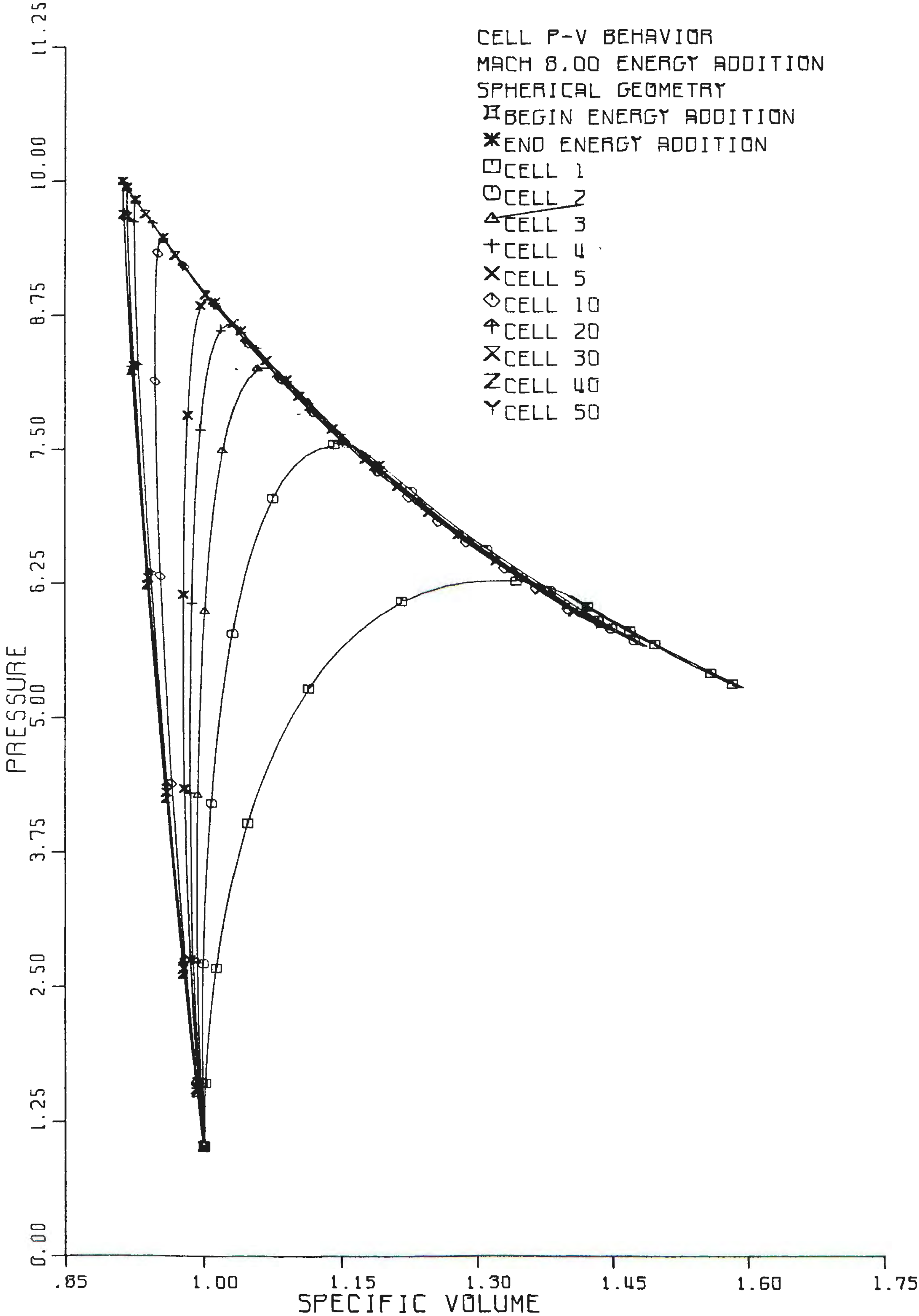

Figure 28. Pressure versus specific volume behavior from a Mach 8.0 energy wave (D = 1.0 at cell 50)

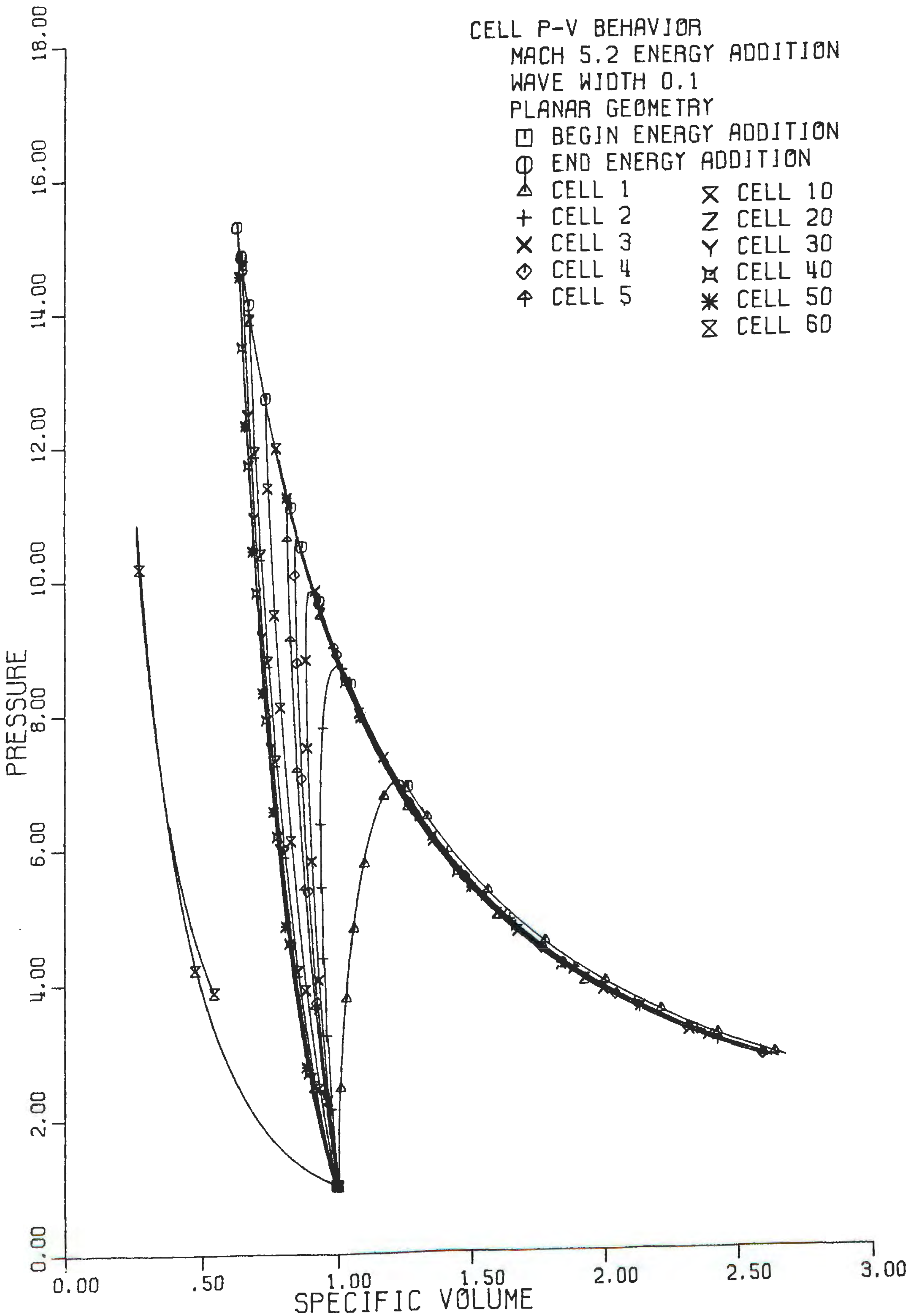

Figure 29. Pressure versus specific volume behavior from a Mach 5.2 (CJ) energy wave in planar geometry

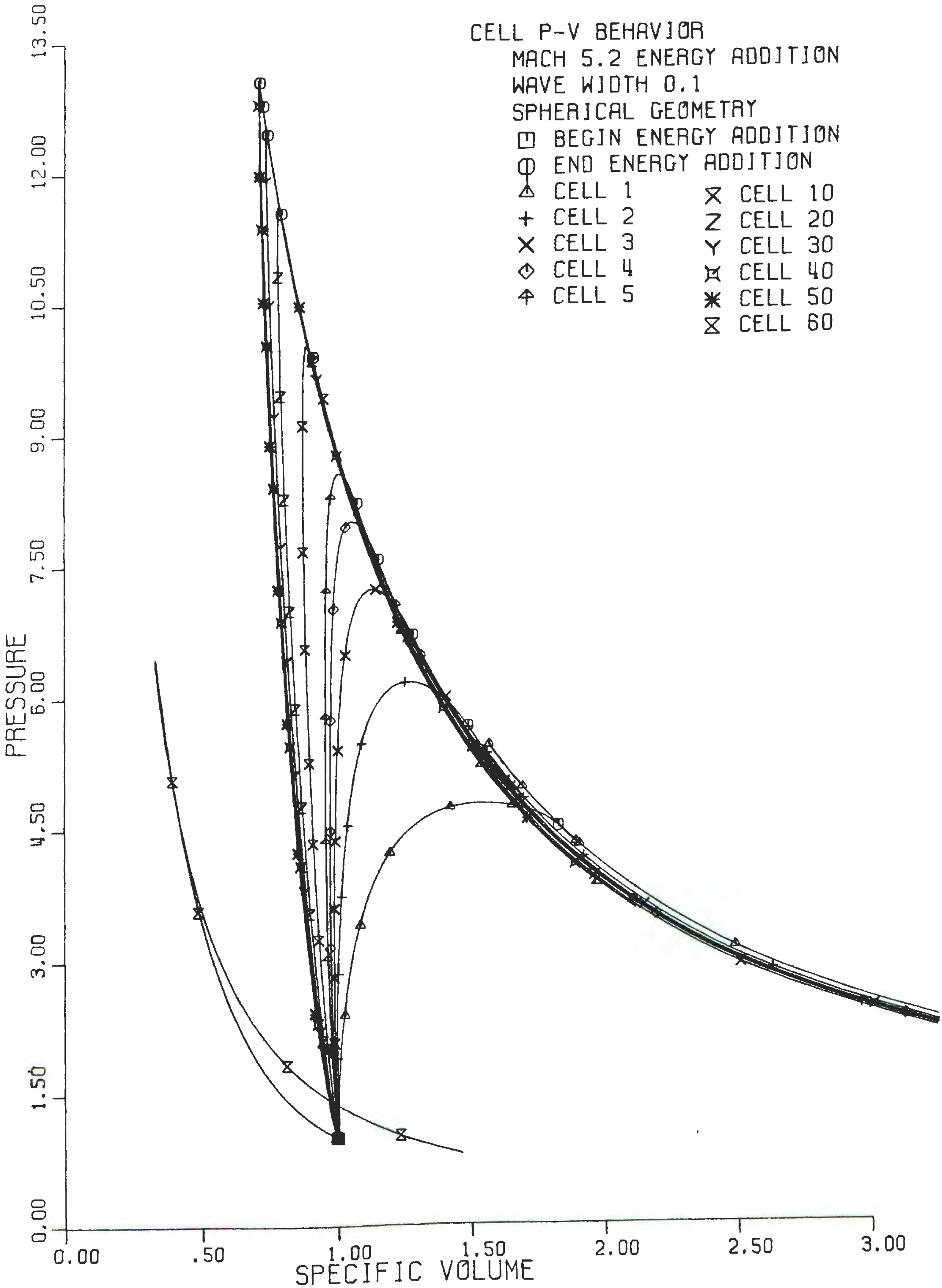

Figure 30. Pressure versus specific volume behavior from a Mach 5.2 (CJ) energy wave in spherical geometry

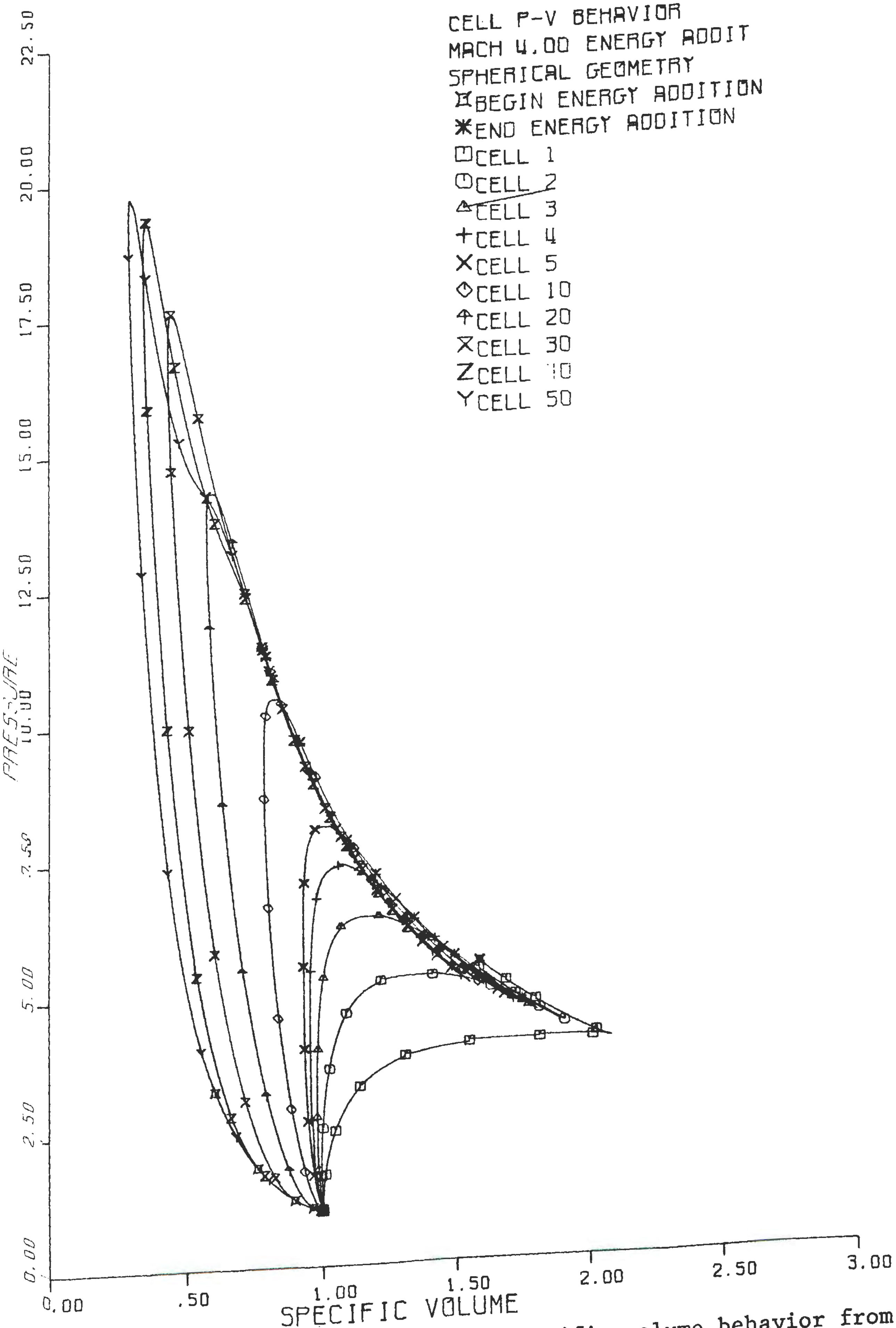

Figure 31. Pressure versus specific volume behavior from Mach 4.0 energy wave.

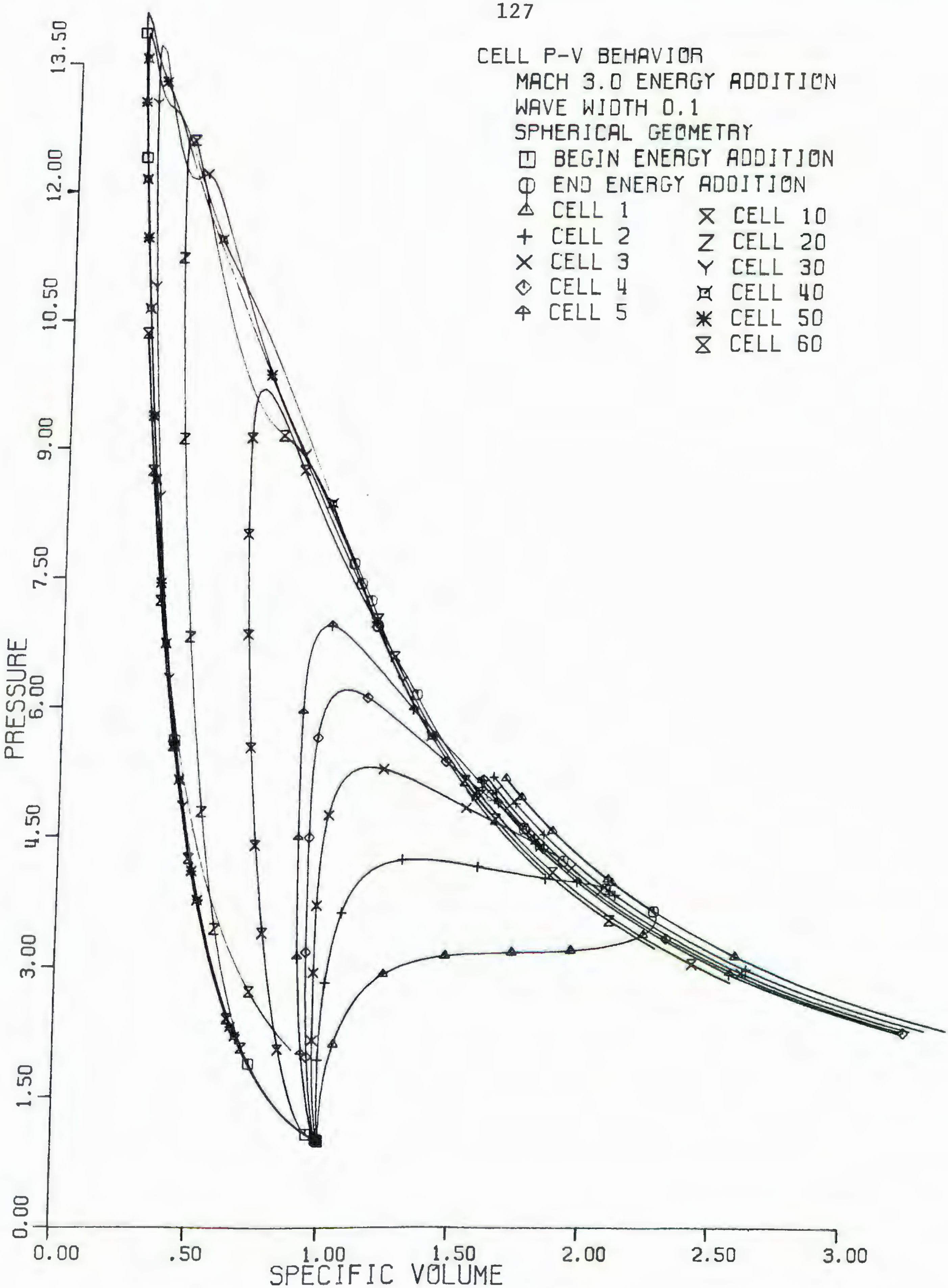

Figure 32. Pressure versus specific volume behavior from a Mach 3.0 energy wave (D = 1.0 at cell 50).

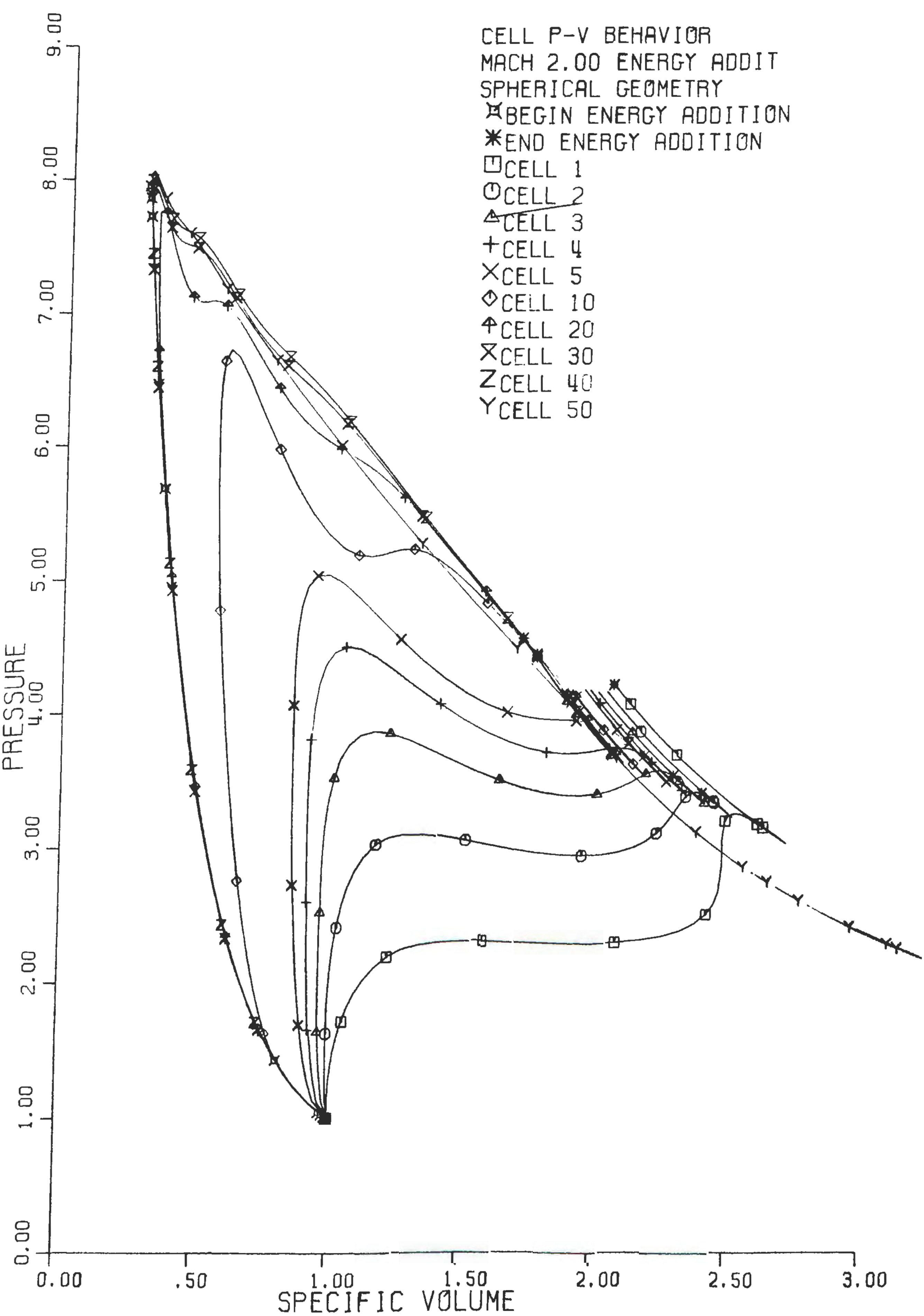

Figure 33. Pressure versus specific volume behavior from Mach 2.0 energy wave.

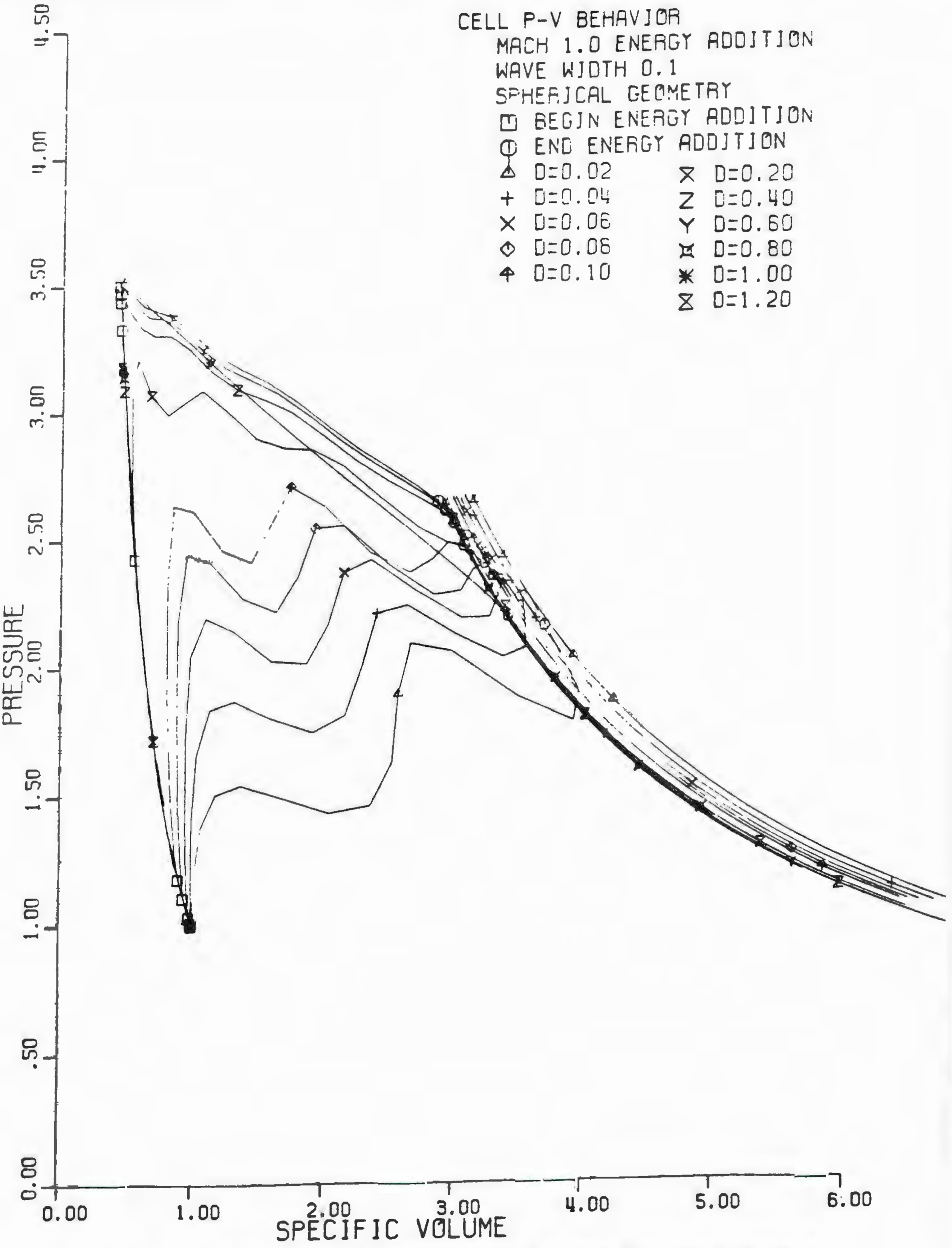

Figure 34. Pressure versus specific volume behavior from a Mach 1.0 energy wave.

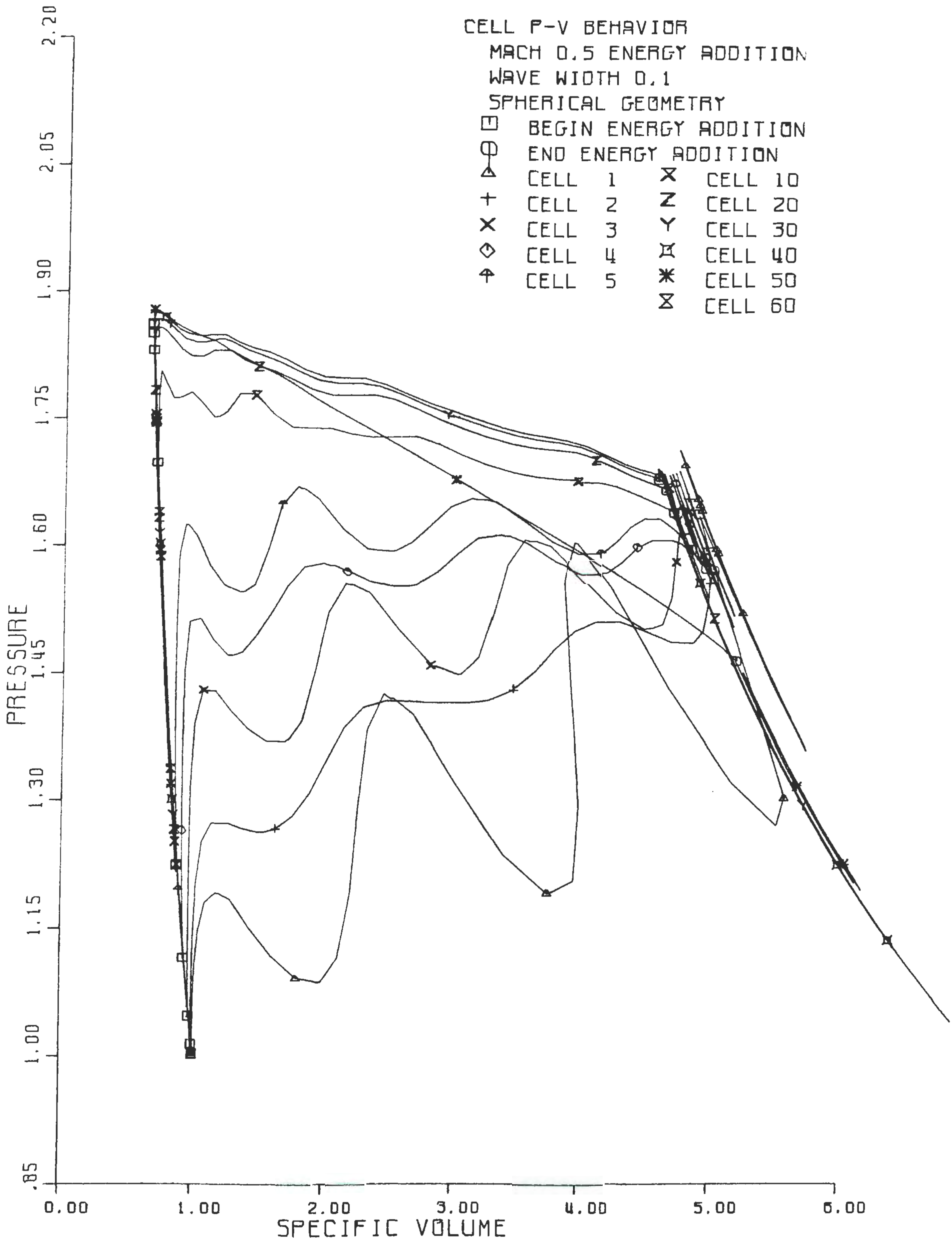

Figure 35. Pressure versus specific volume behavior from Mach 0.5 energy wave.

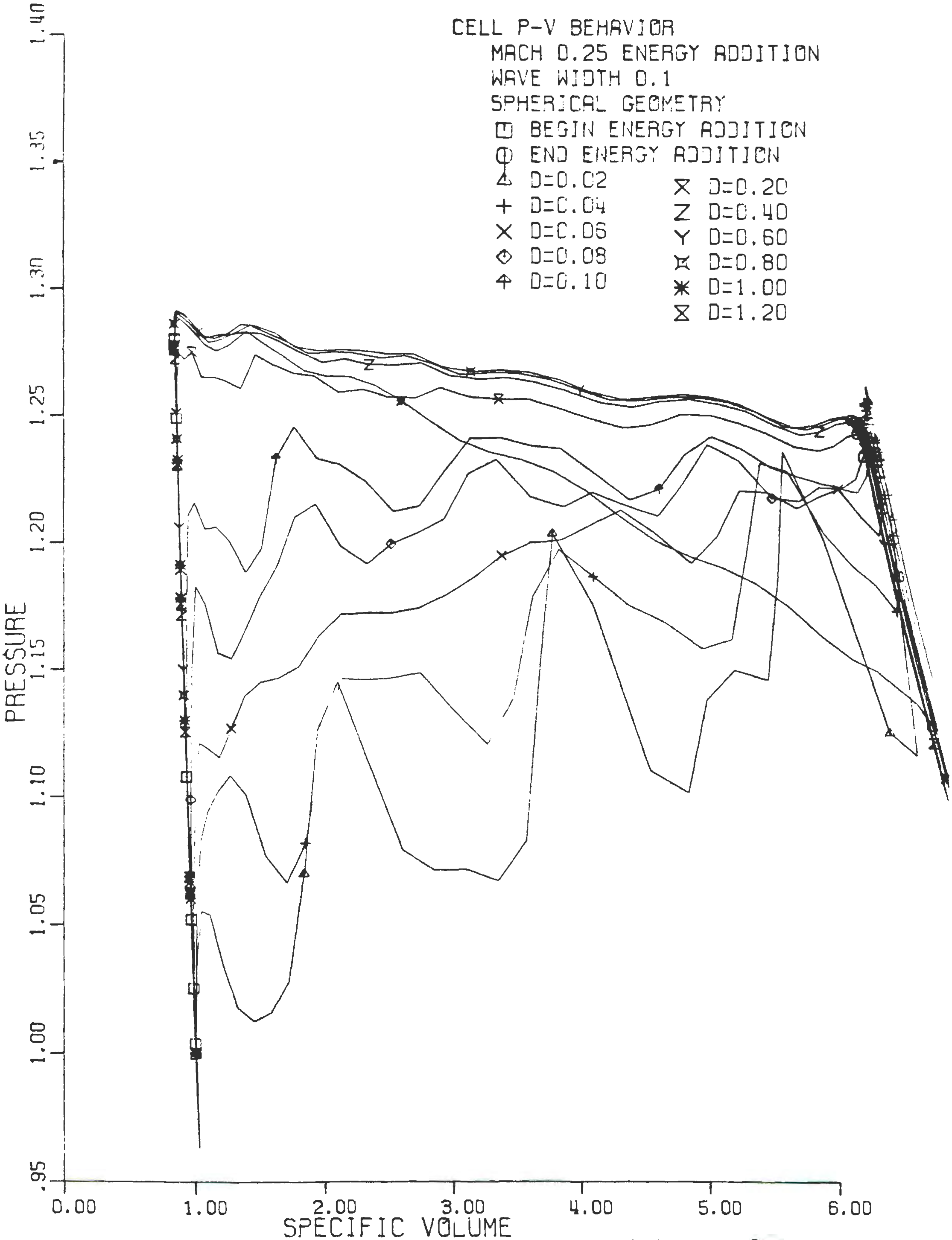

Figure 36. Pressure versus specific volume behavior from a Mach 0.25 energy wave.

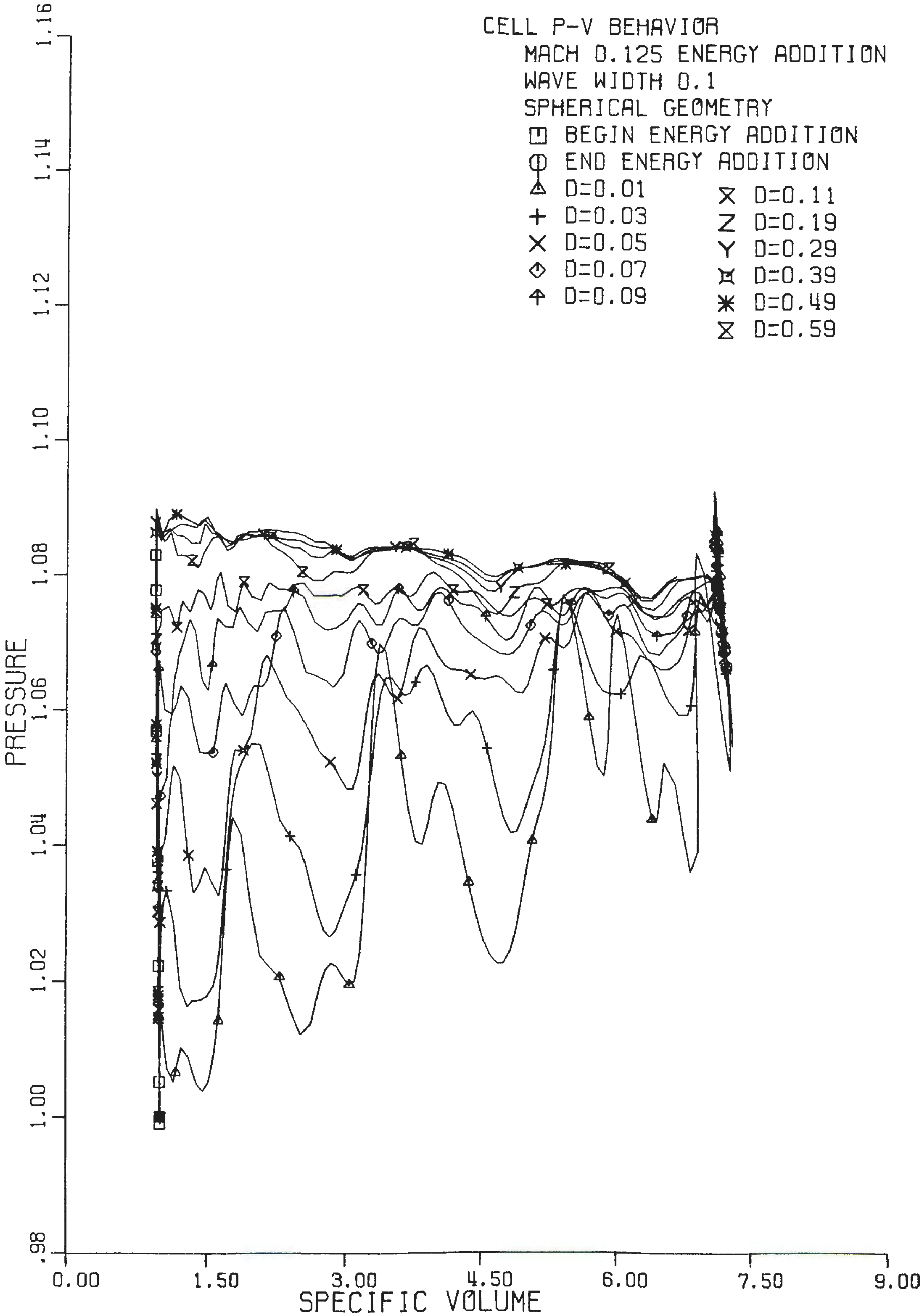

Figure 37. Pressure versus specific volume behavior from a Mach 0.125 energy wave.

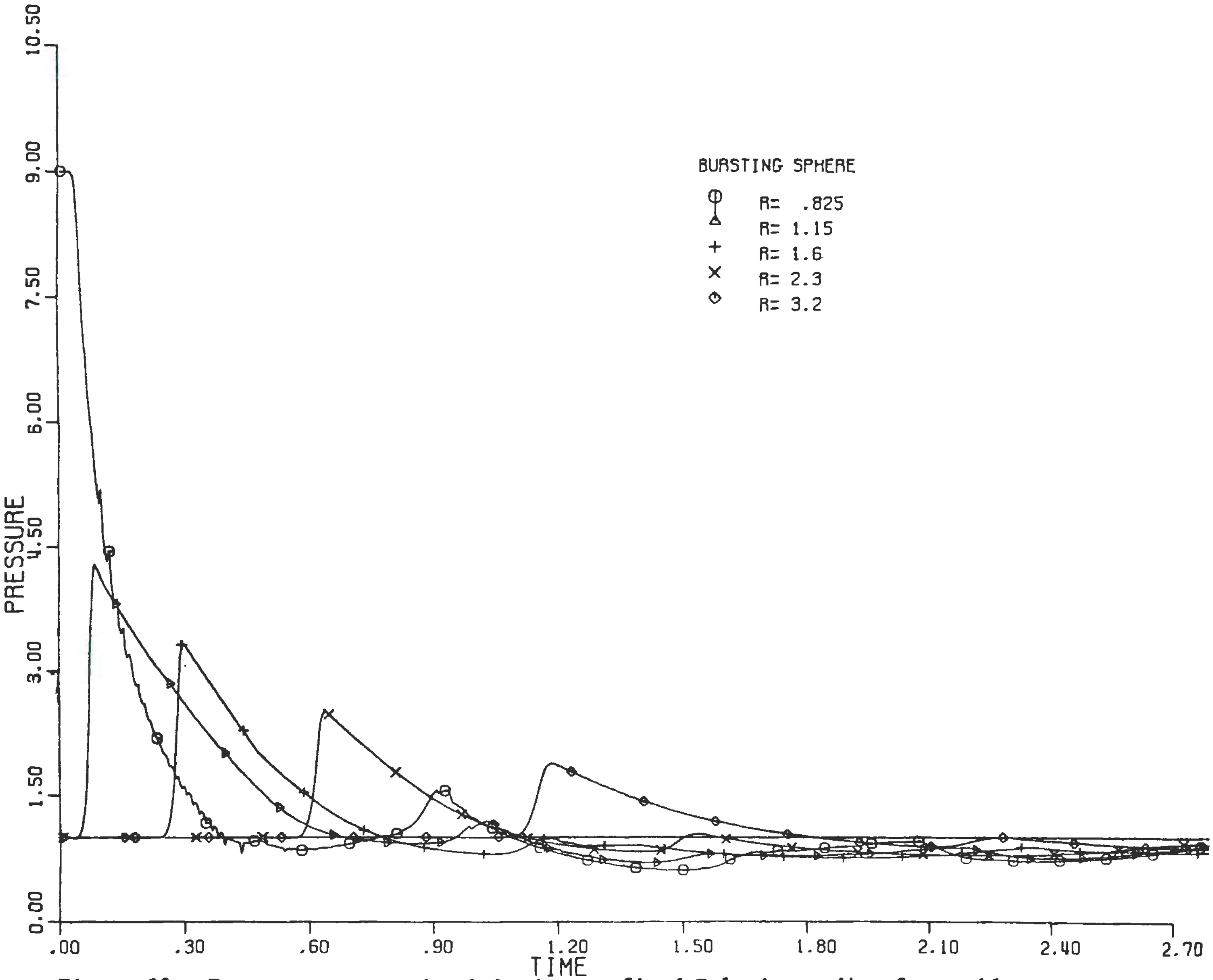

Figure 38. Pressure versus time behavior at fixed Eulerian radius from a blast system generated by an infinite velocity energy wave (bursting sphere).

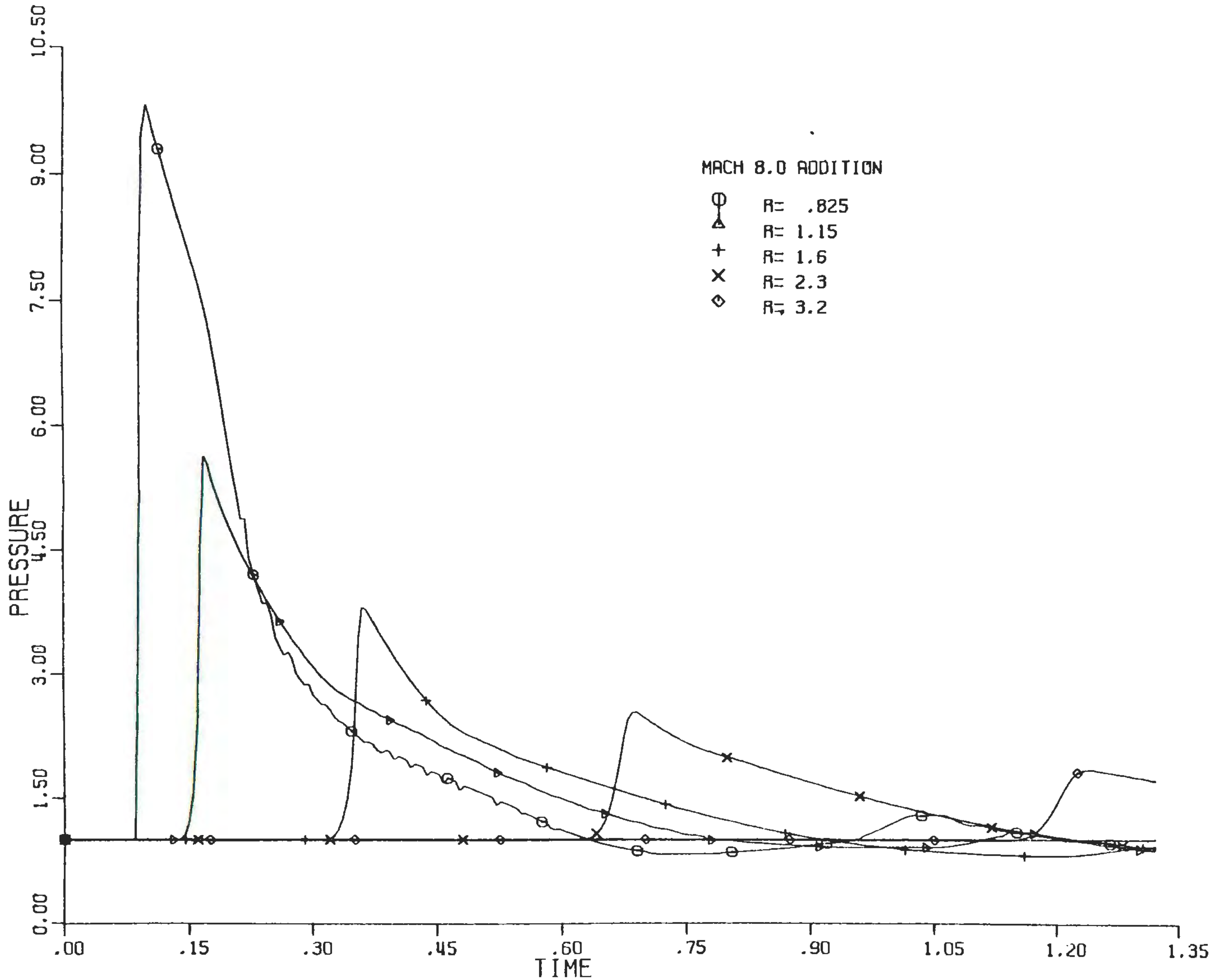

Figure 39. Pressure versus time behavior at fixed Eulerian radius from a blast system generated by a Mach 8.0 energy wave.

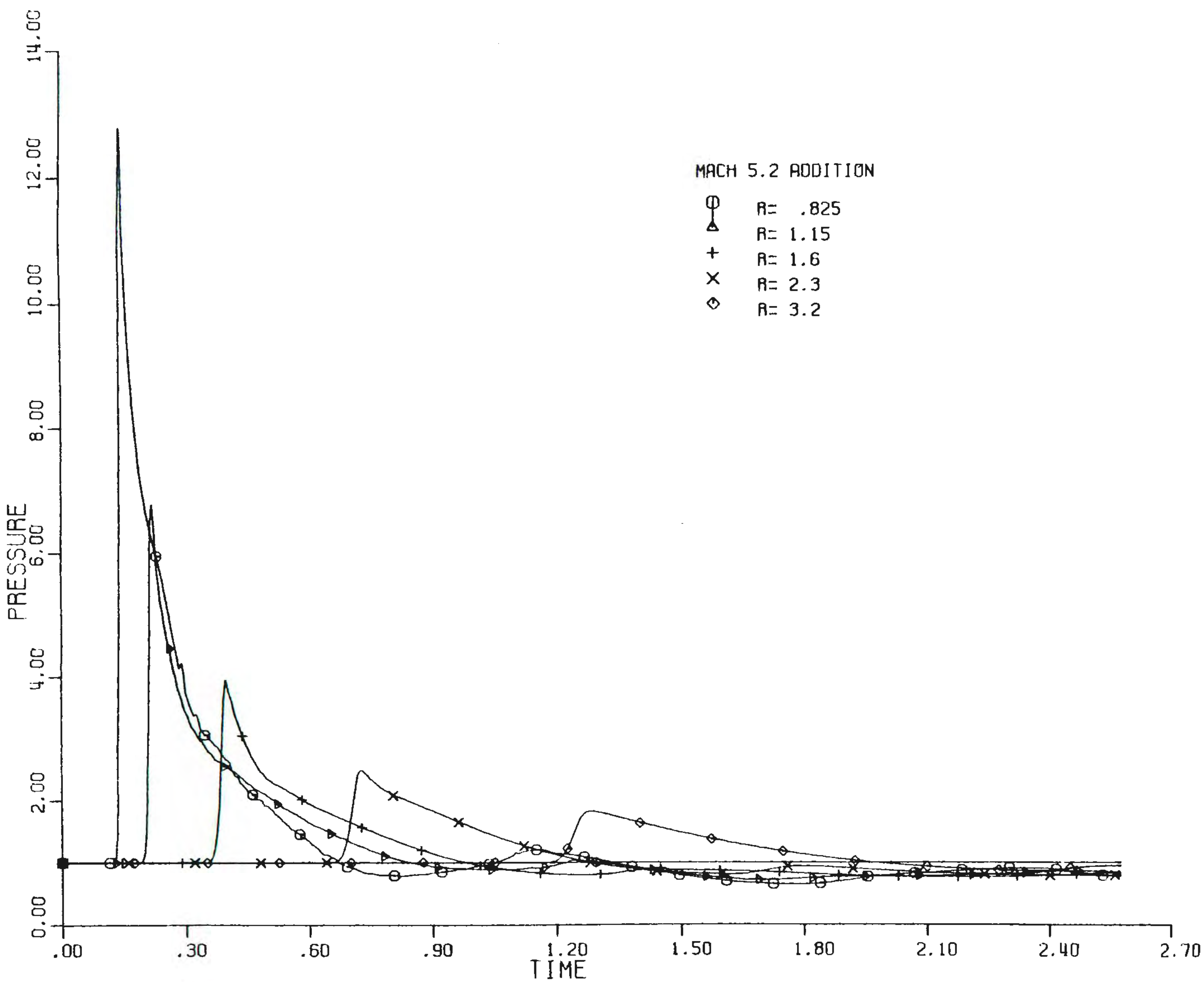

Figure 40. Pressure versus time behavior at fixed Eulerian radius from a blast system generated by a Mach 5.2 (CJ) energy wave.

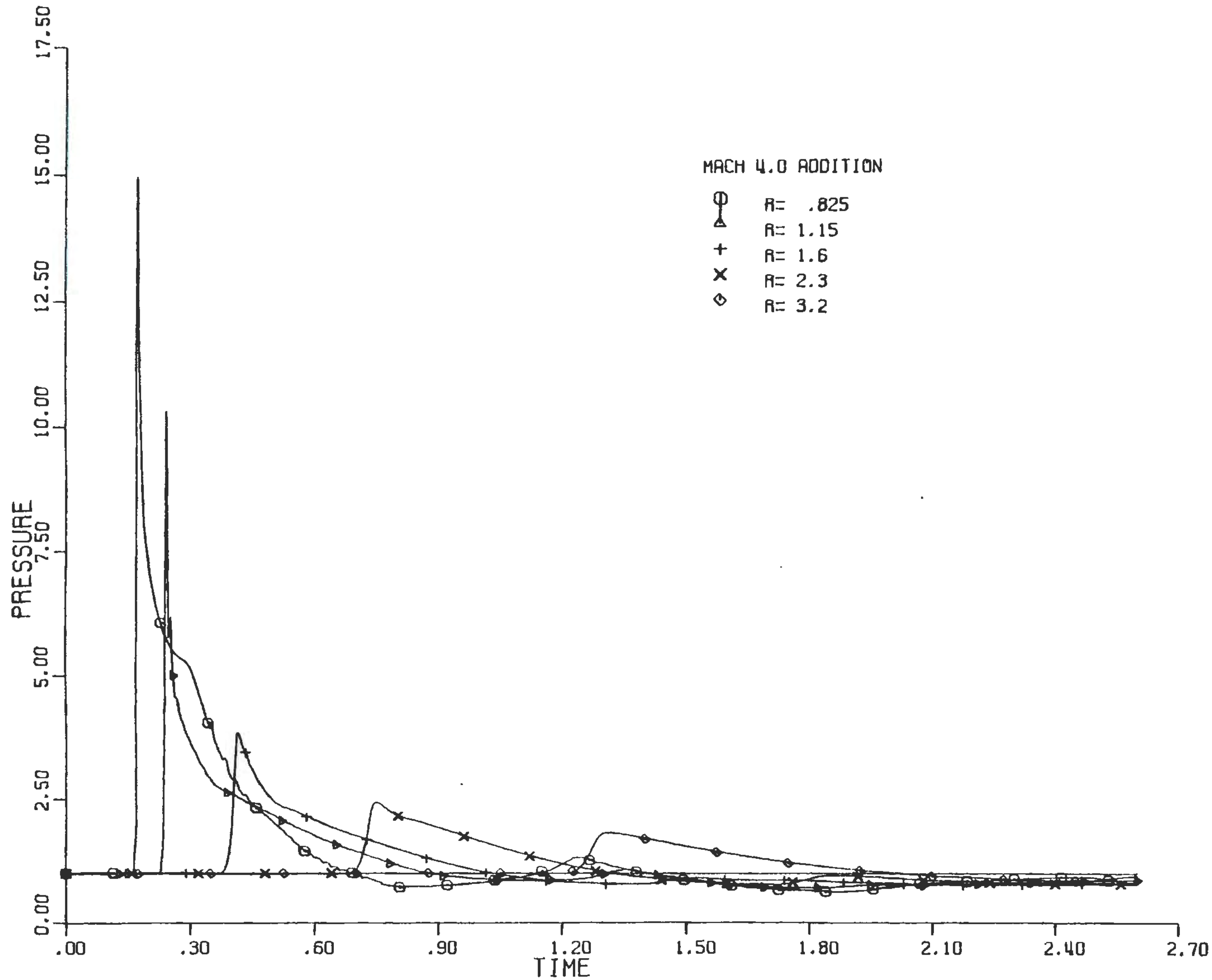

Figure 41. Pressure versus time behavior at fixed Eulerian radius from a blast system generated by a Mach 4.0 energy wave.

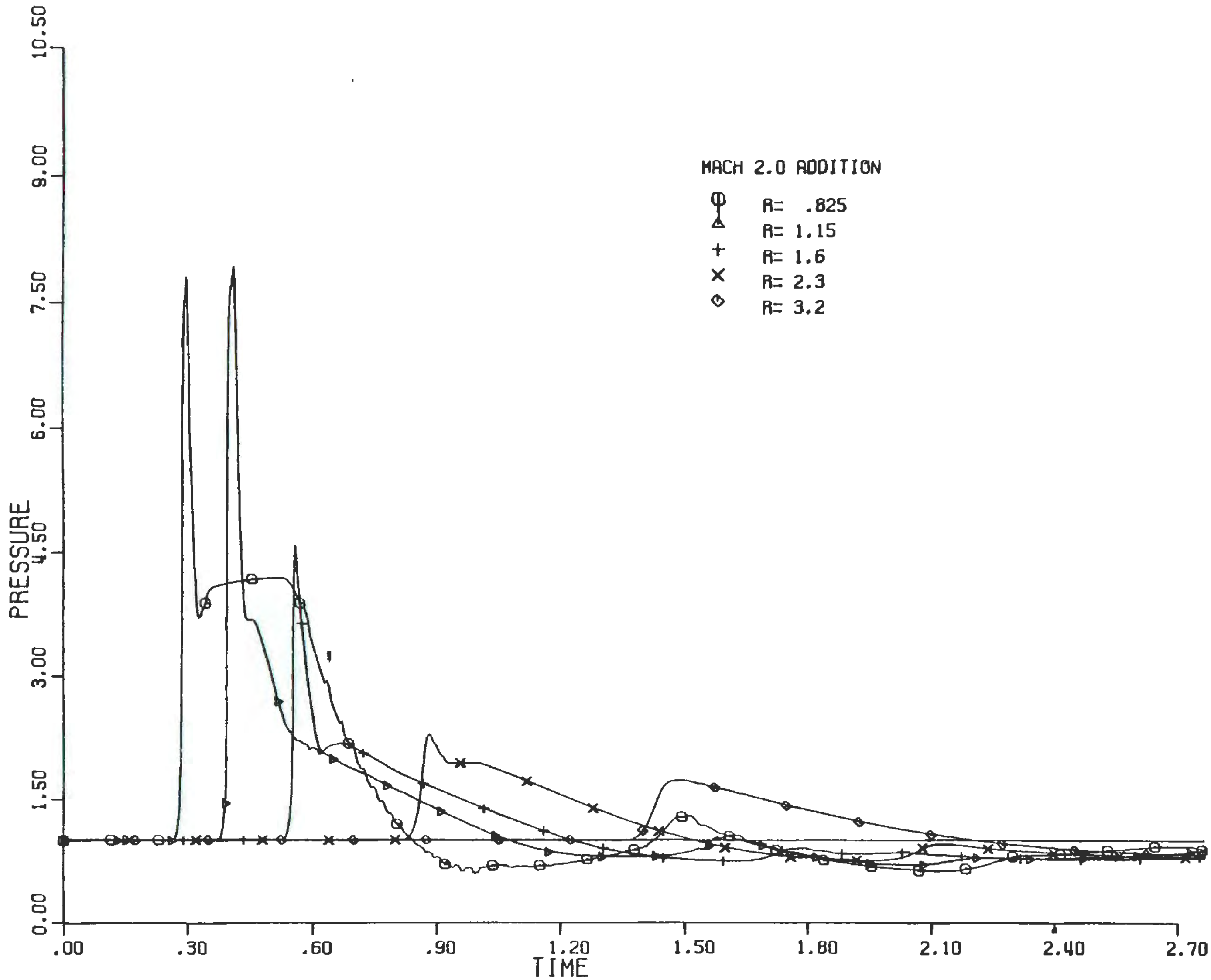

Figure 42. Pressure versus time behavior at fixed Eulerian radius from a blast system generated by a Mach 2.0 energy wave.

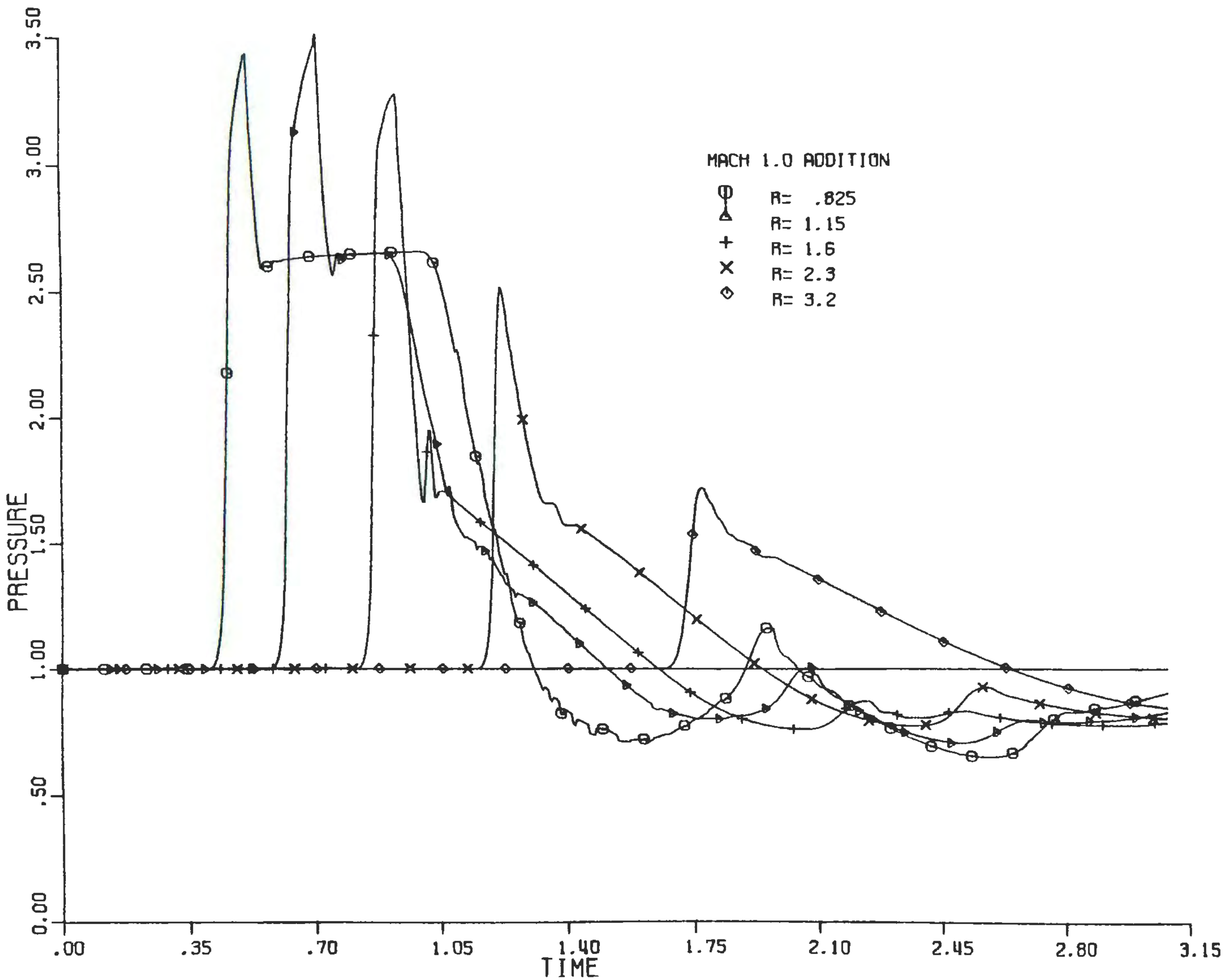

Figure 43. Pressure versus time behavior at fixed Eulerian radius from a blast system generated by a Mach 1.0 energy wave.

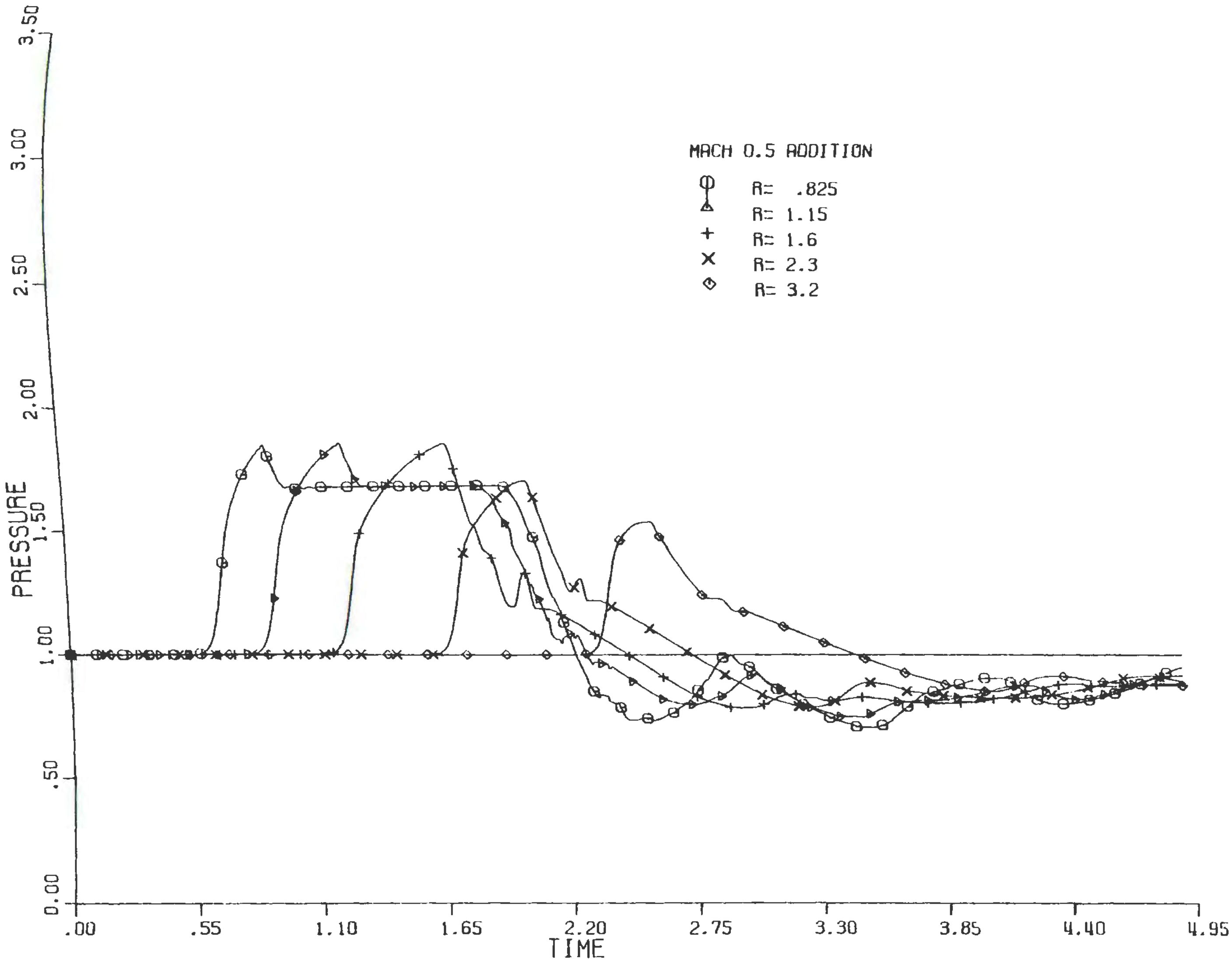

Figure 44. Pressure versus time behavior at fixed Eulerian radius from a blast system generated by a Mach 0.5 energy wave.

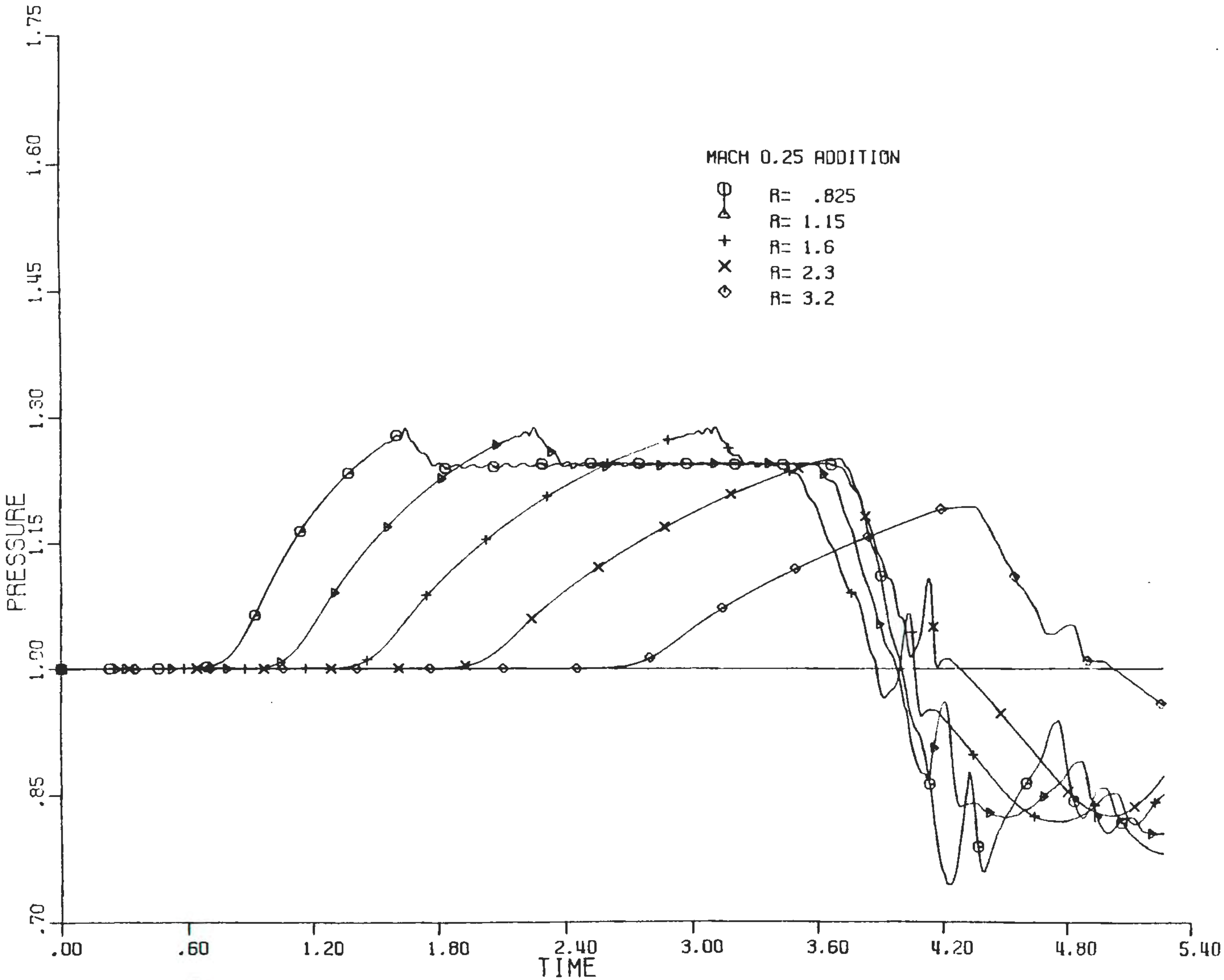

Figure 45. Pressure versus time behavior at fixed Eulerian radius from a blast system generated by a Mach 0.25 energy wave.

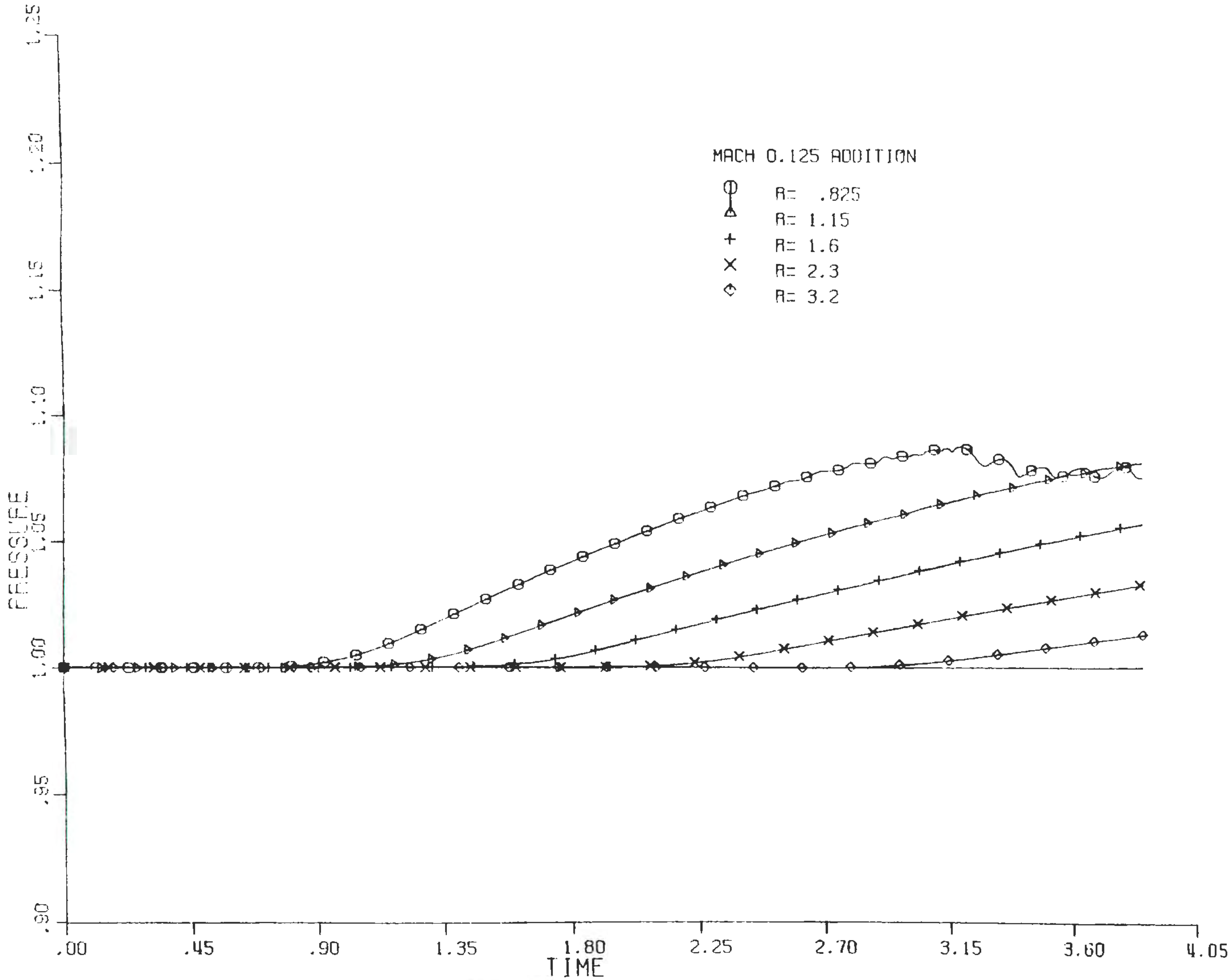

Figure 46. Pressure versus time behavior at fixed Eulerian radius from a blast system generated by a Mach 0.125 energy wave.

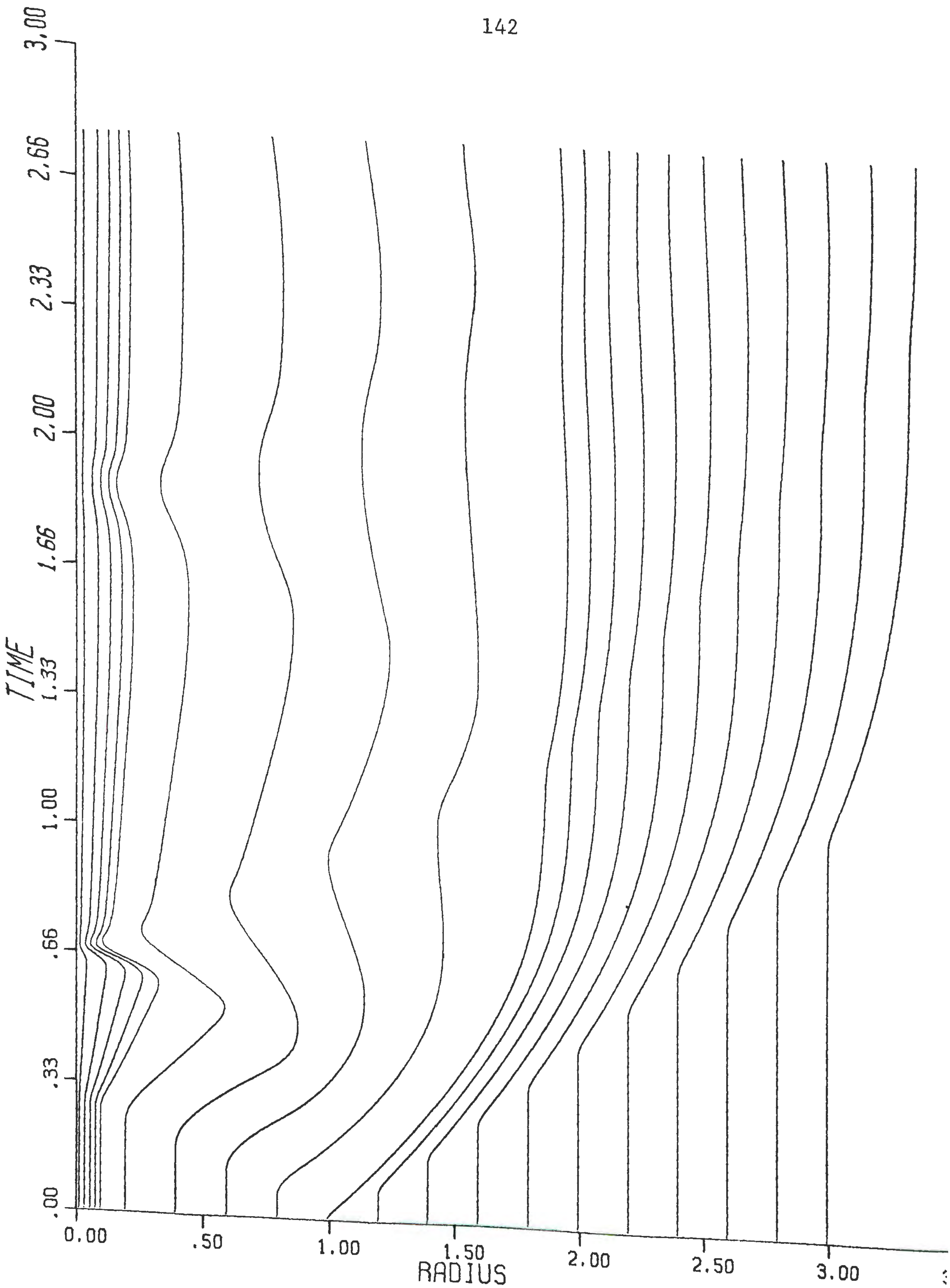

Figure 47. Particle position versus time in a blast system generated by an infinite velocity energy

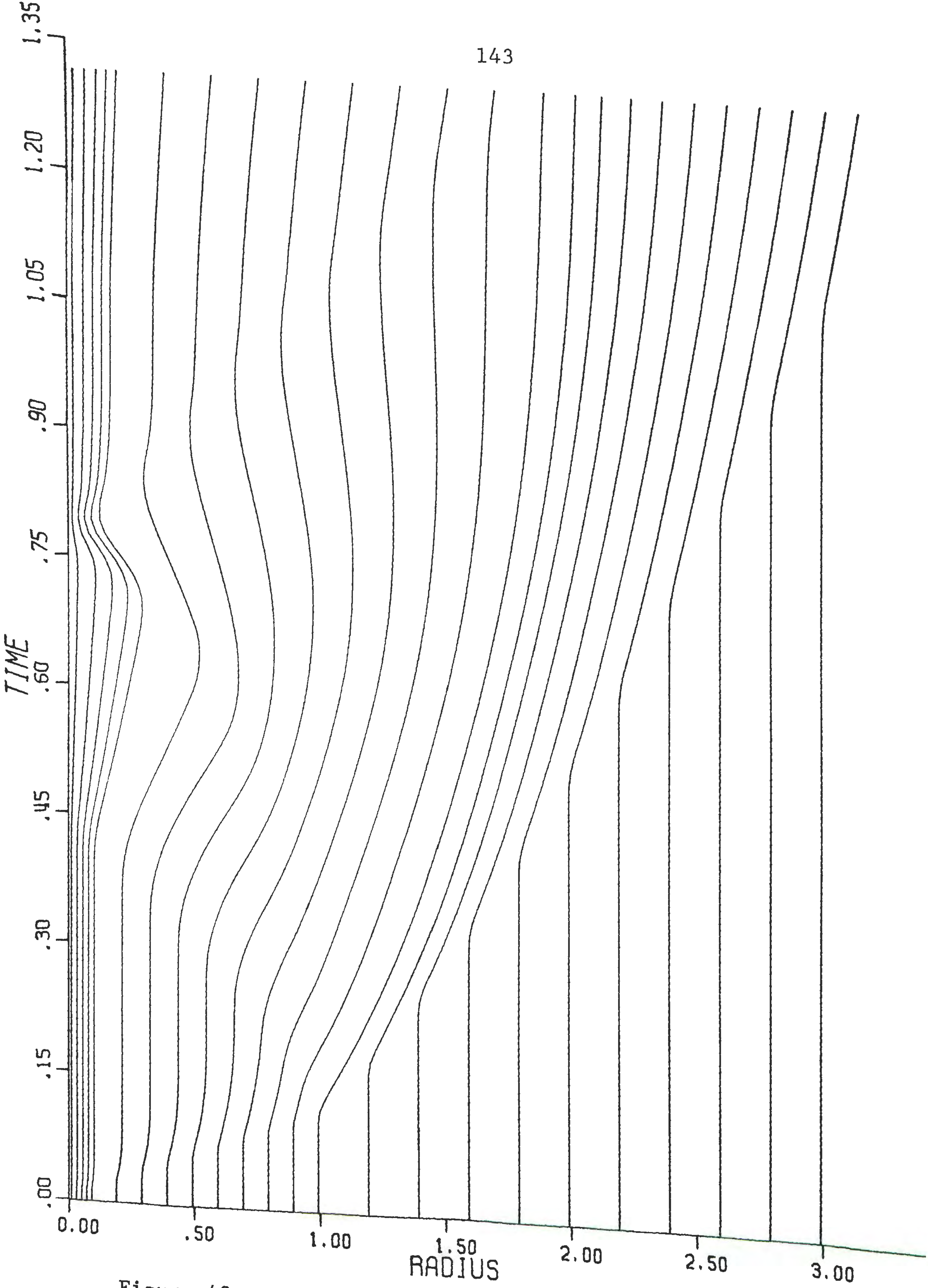

Figure 48. Particle position versus time in a blast system generated by a Mach 8.0 energy wave.

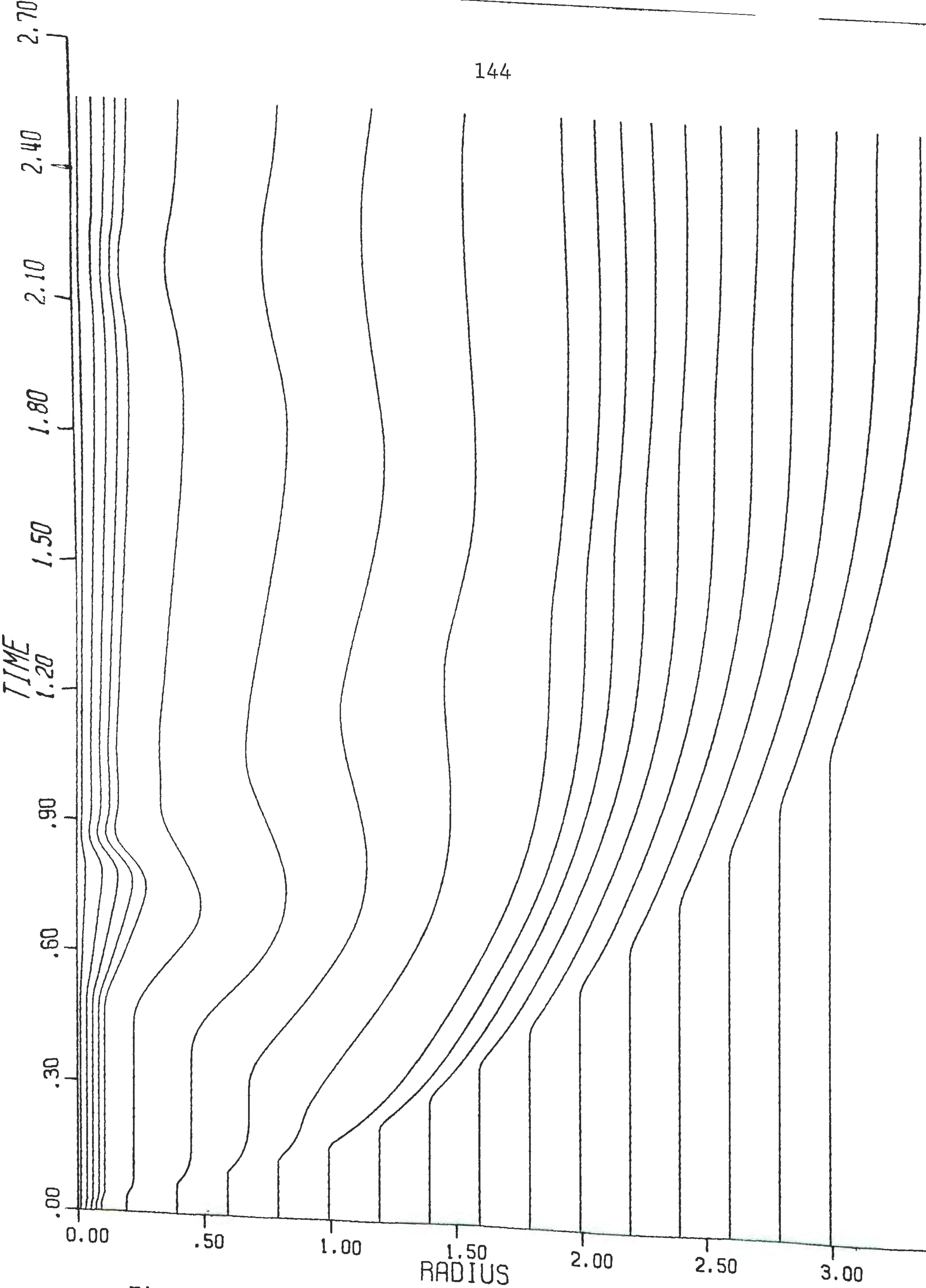

Figure 49. Particle position versus time in a blast system generated by a Mach 5.2 (CJ) energy wave.

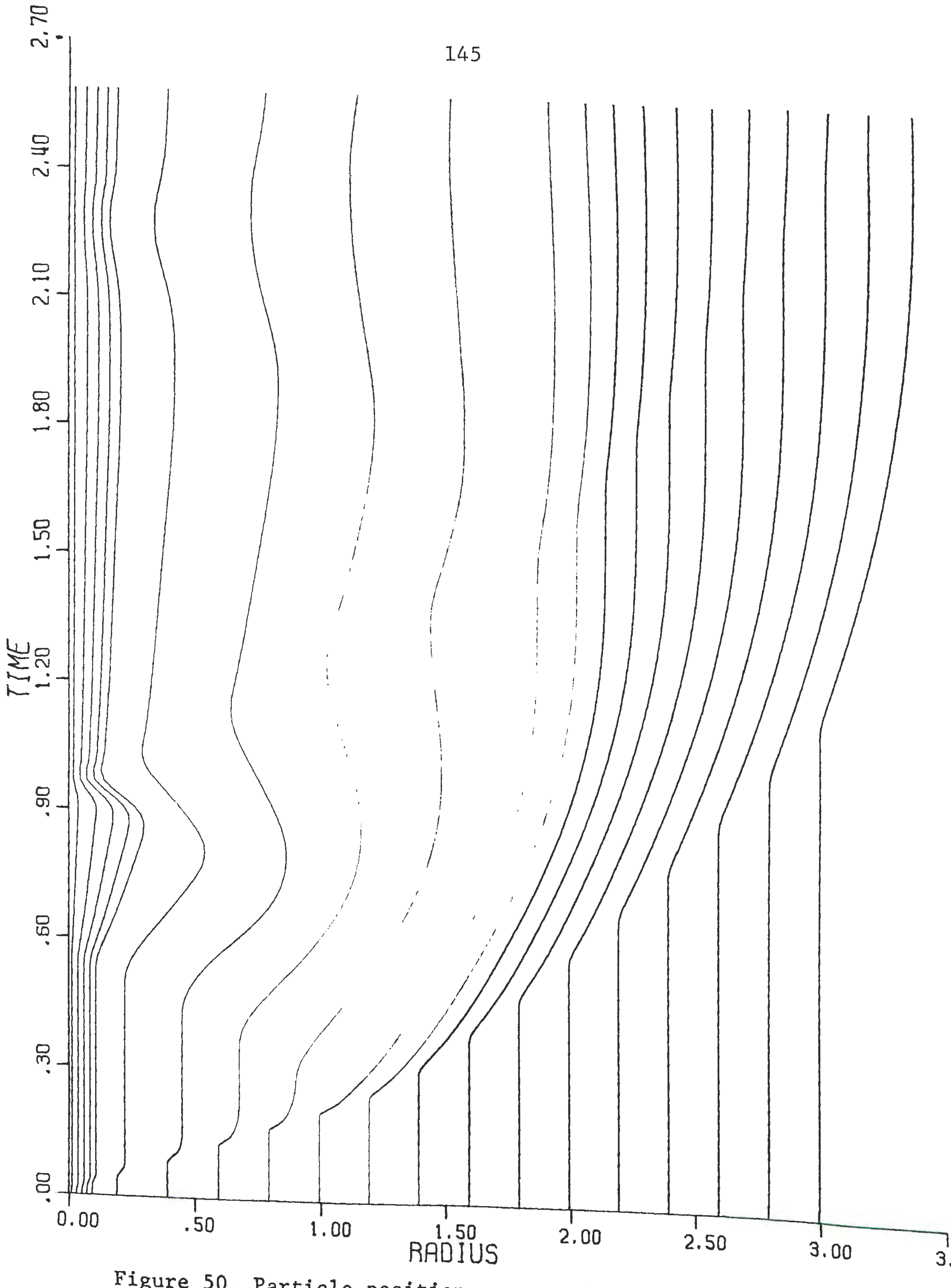

Figure 50. Particle position versus time in a blast system generated by a Mach 4.0 energy wave.

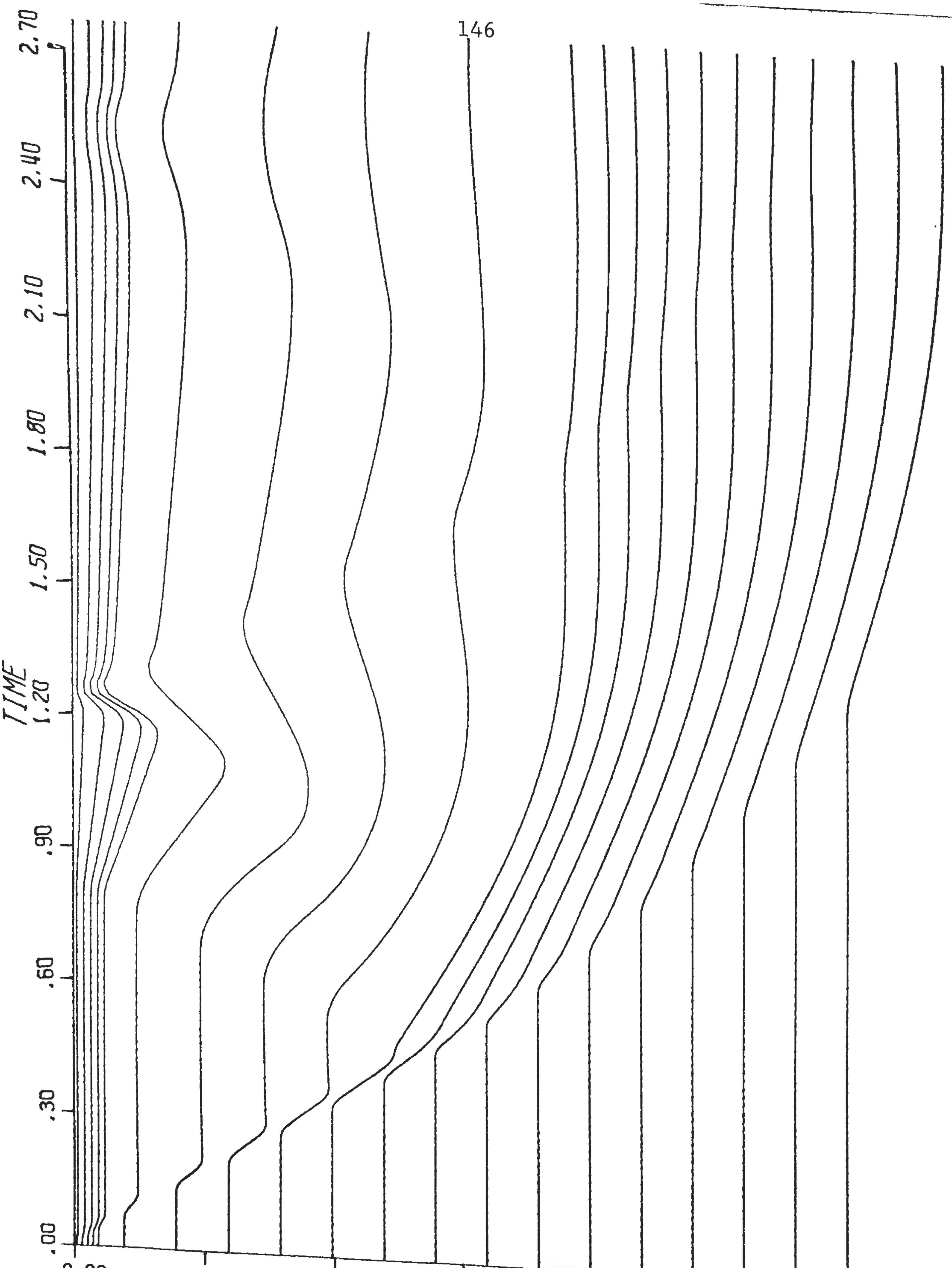

Figure 51. Particle position versus time in a blast system generated by a Mach 2.0 energy wave.

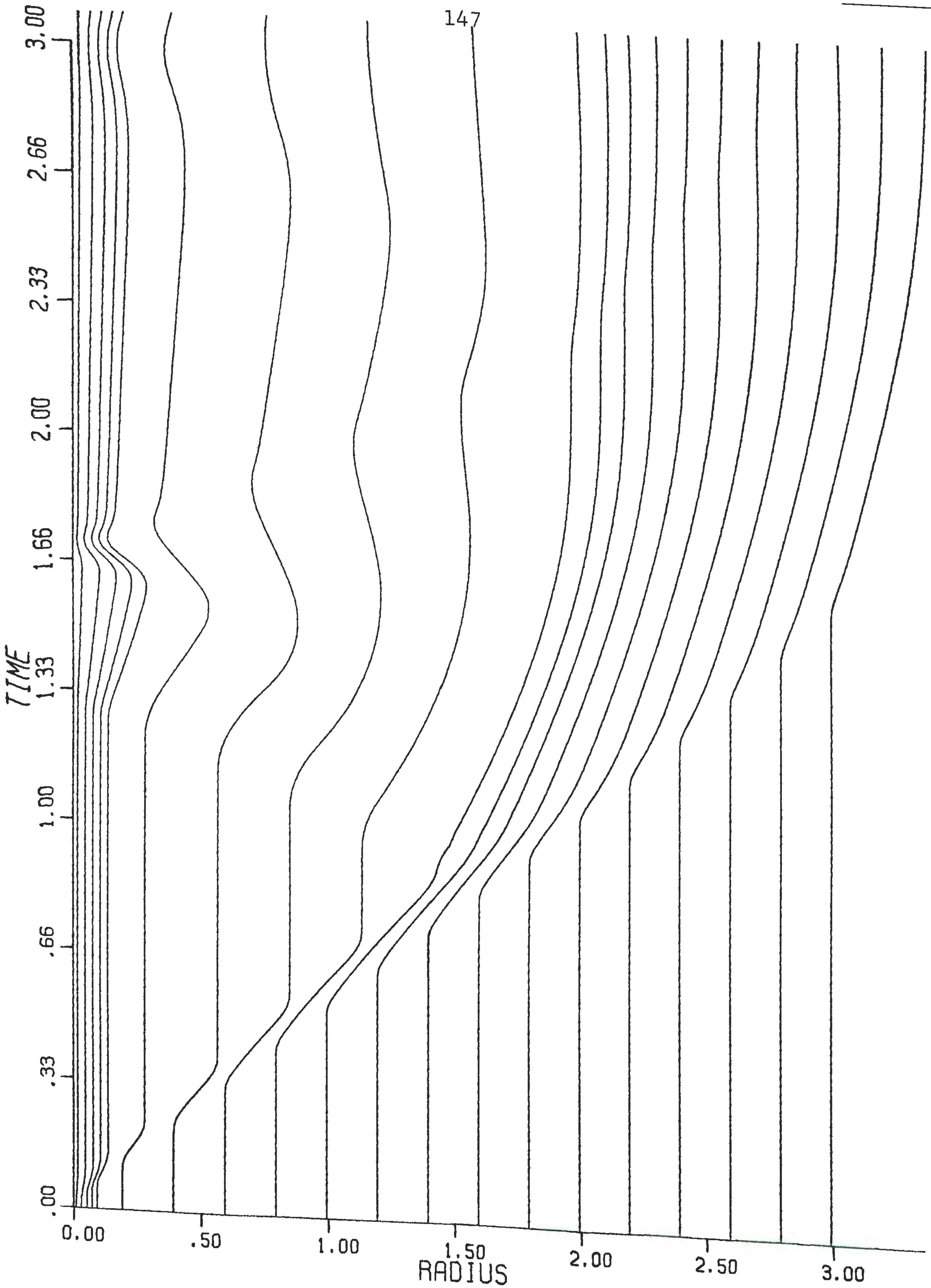

Figure 52. Particle position versus time in a blast system generated by a Mach 1.0 energy wave.

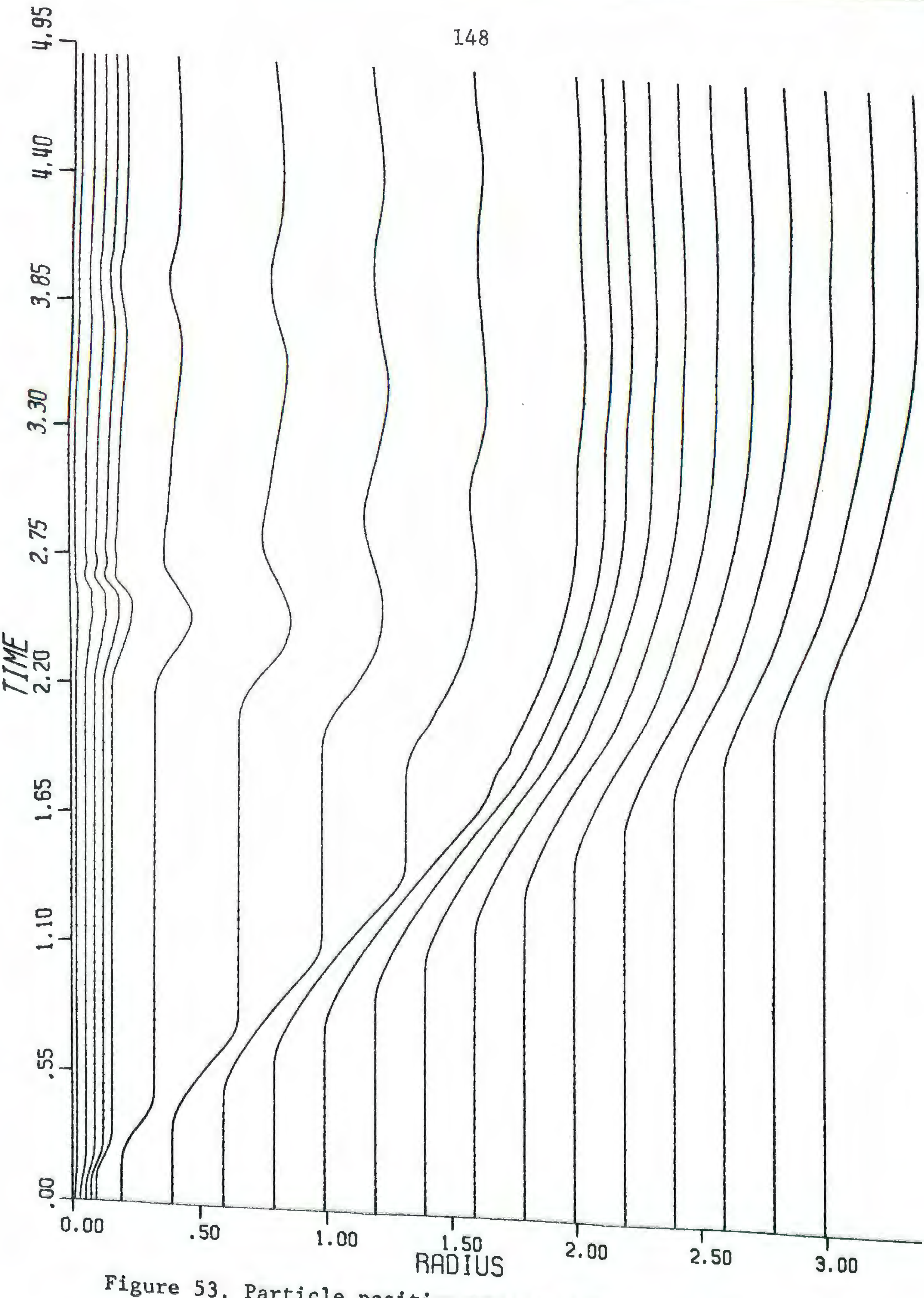

Figure 53. Particle position versus time in a blast system generated by a Mach 0.5 energy wave.

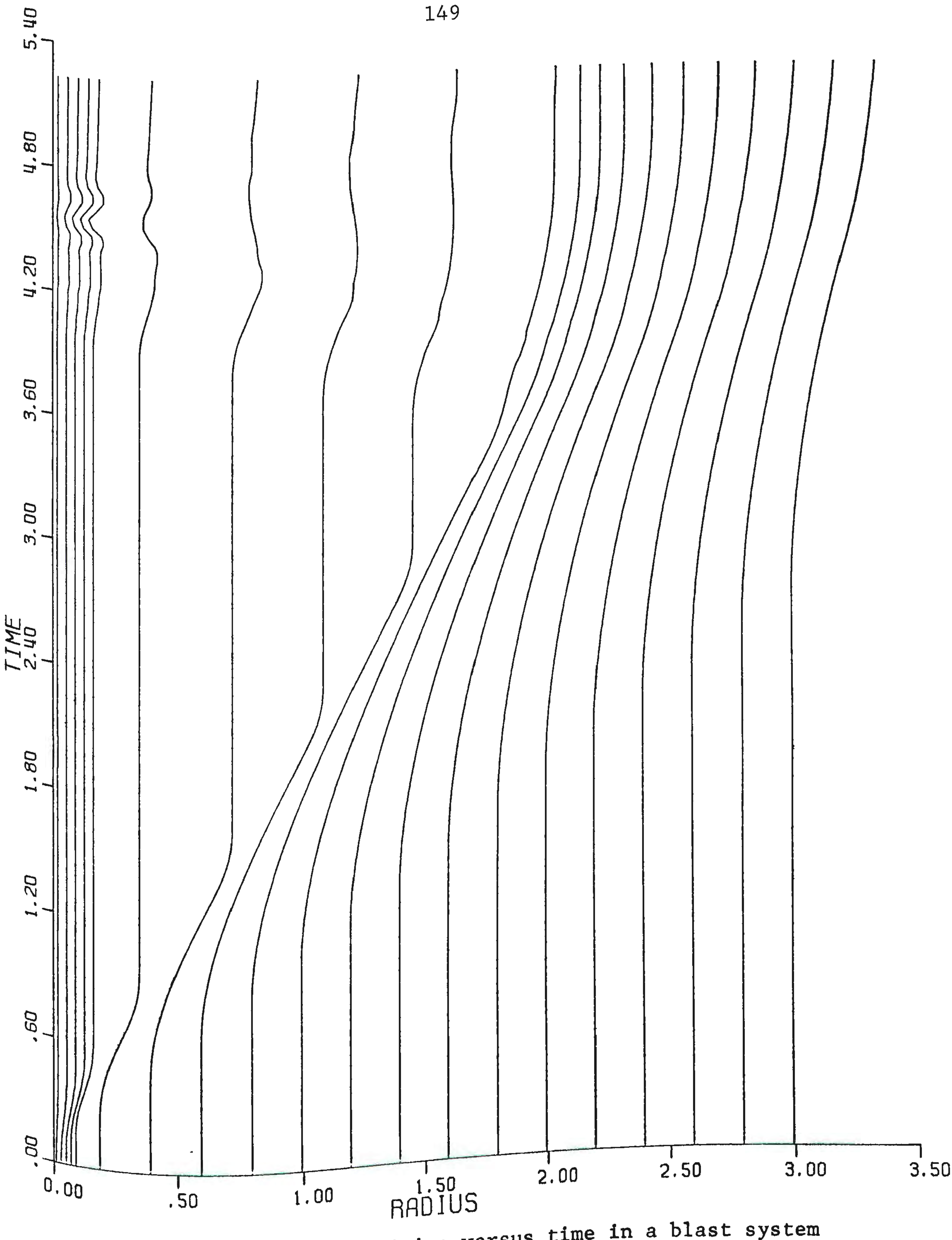

Figure 54. Particle position versus time in a blast system generated by a Mach 0.25 energy wave.

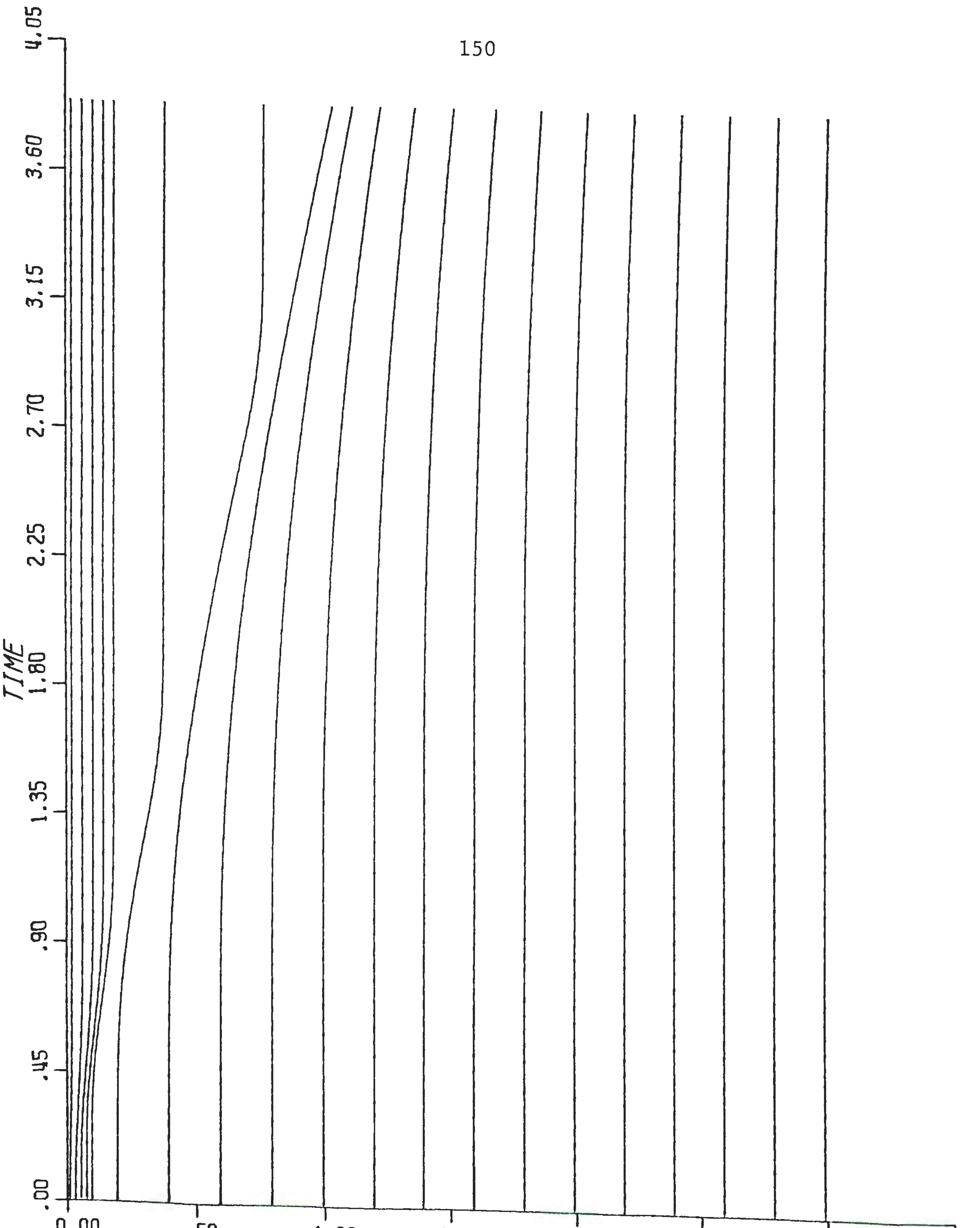

Figure 55. Particle position versus time in a blast system generated by a Mach 0.125 energy wave.

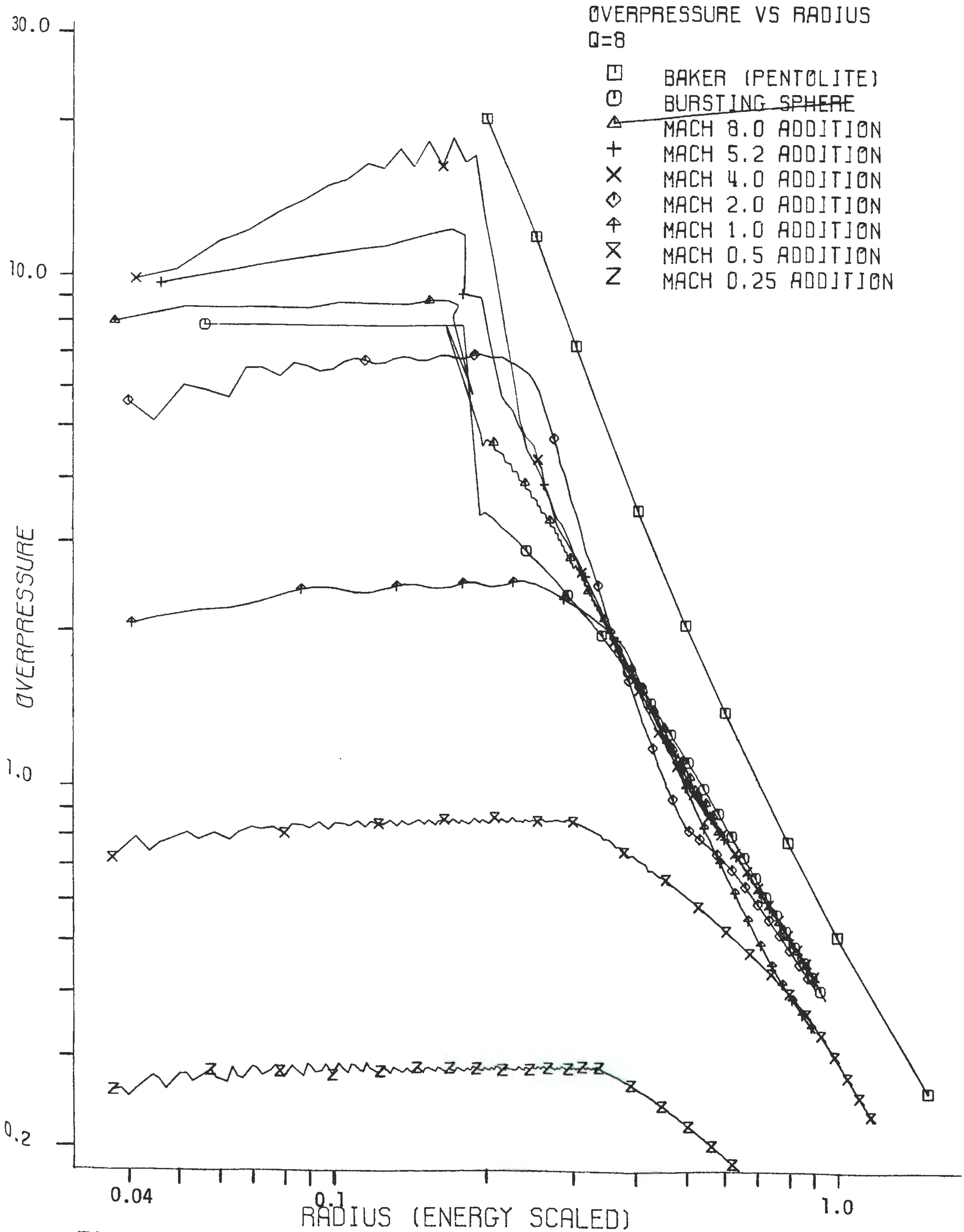

Figure 56. Overpressure versus energy scaled distance.

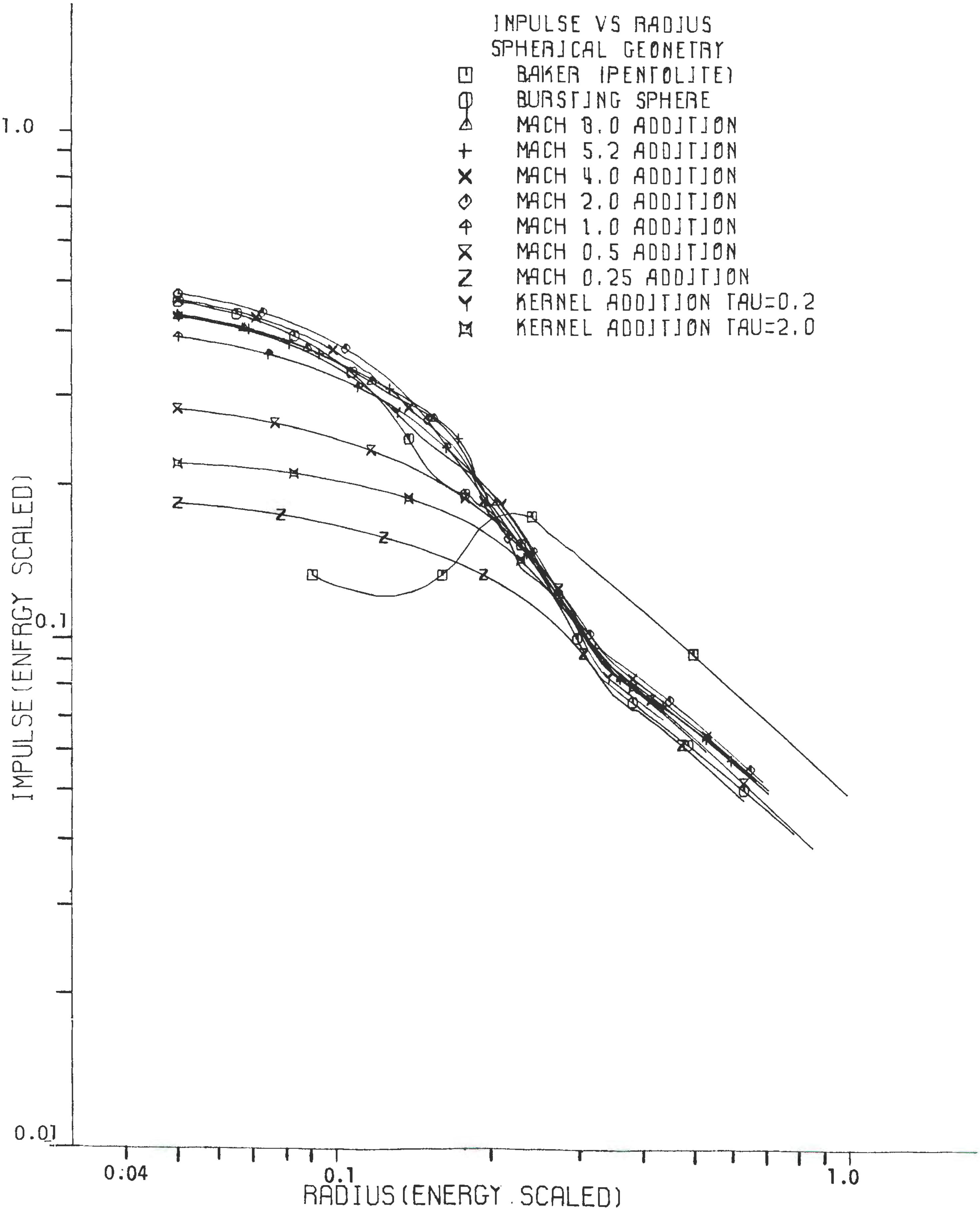

Figure 57. Impulse versus energy scaled distance.

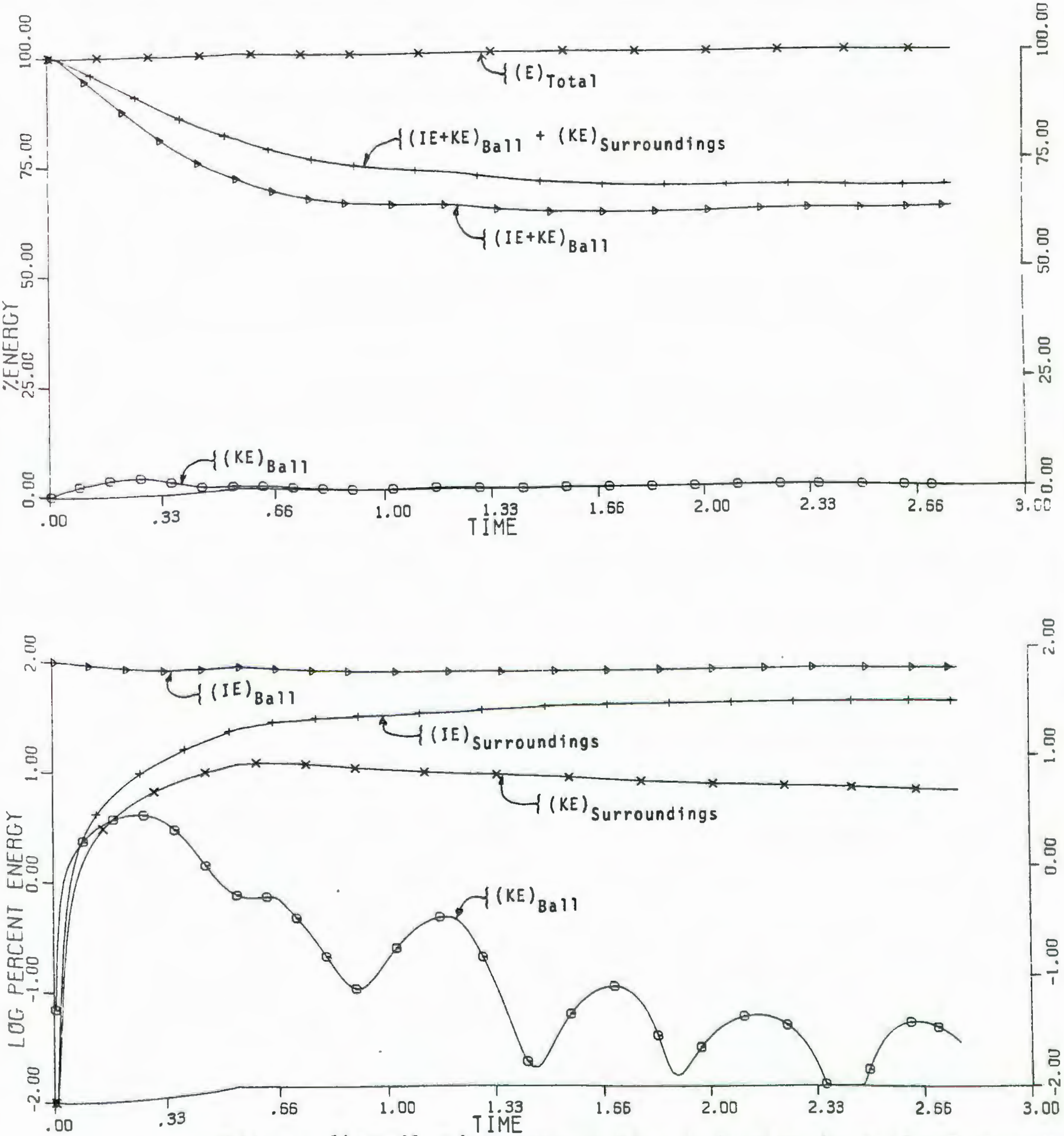

Figure 58. Energy distribution versus time behavior in a blast system generated by an infinite velocity energy wave (bursting sphere)

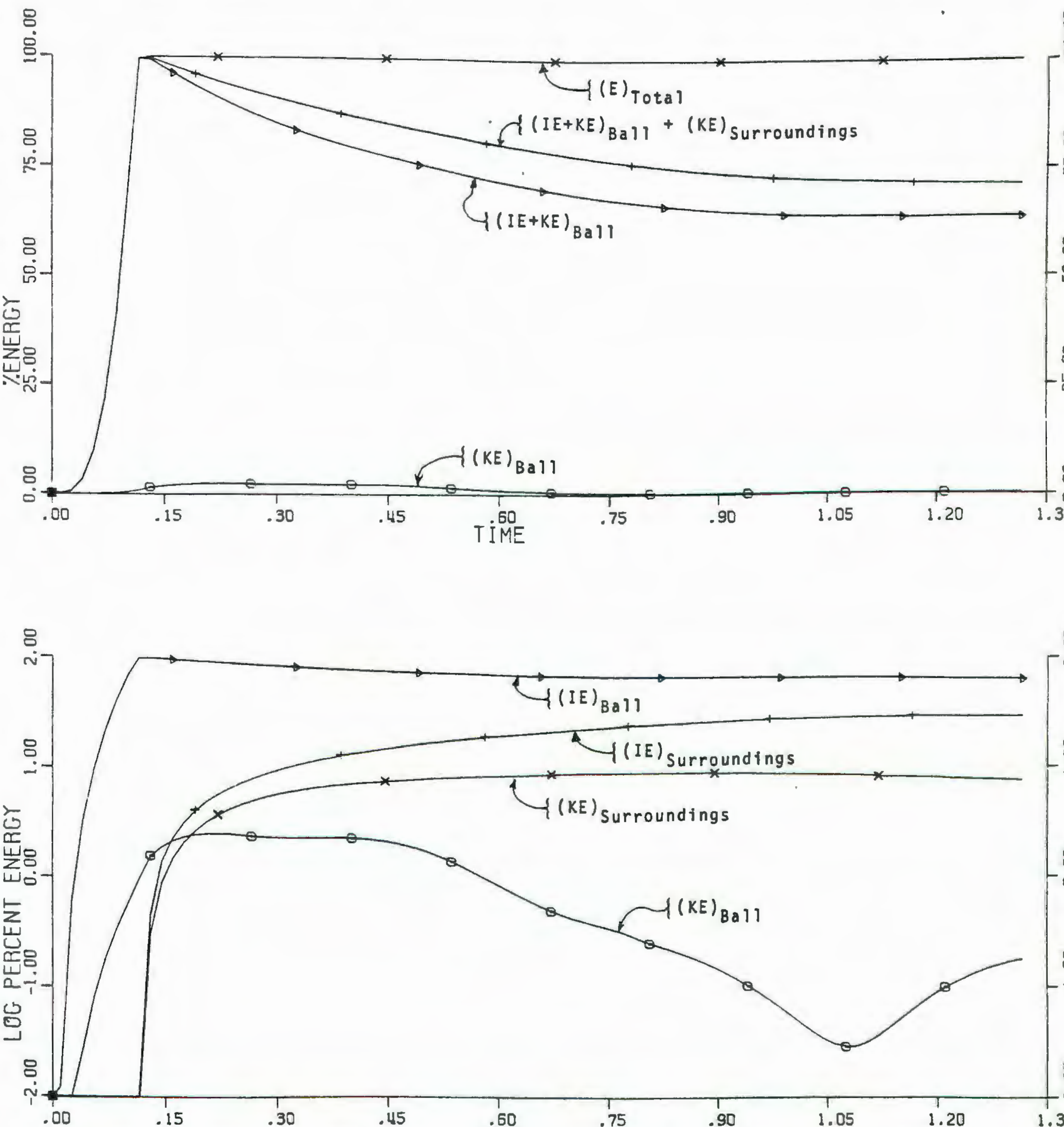

Figure 59. Energy distribution versus time behavior in a blast system generated by a Mach 8.0 energy wave.

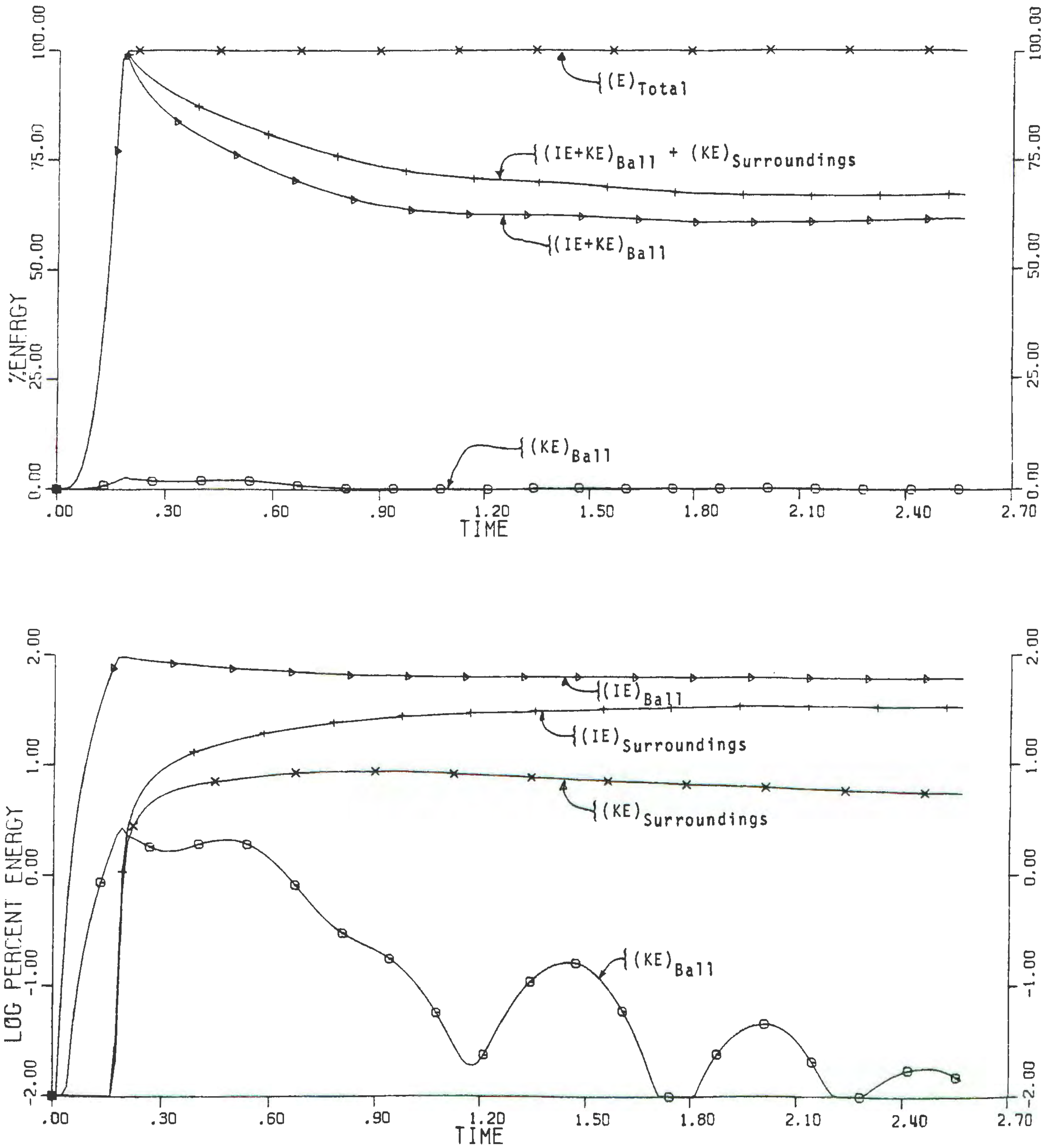

Figure 60. Energy distribution versus time behavior in a blast system generated by a Mach 5.2 (CJ) energy wave.

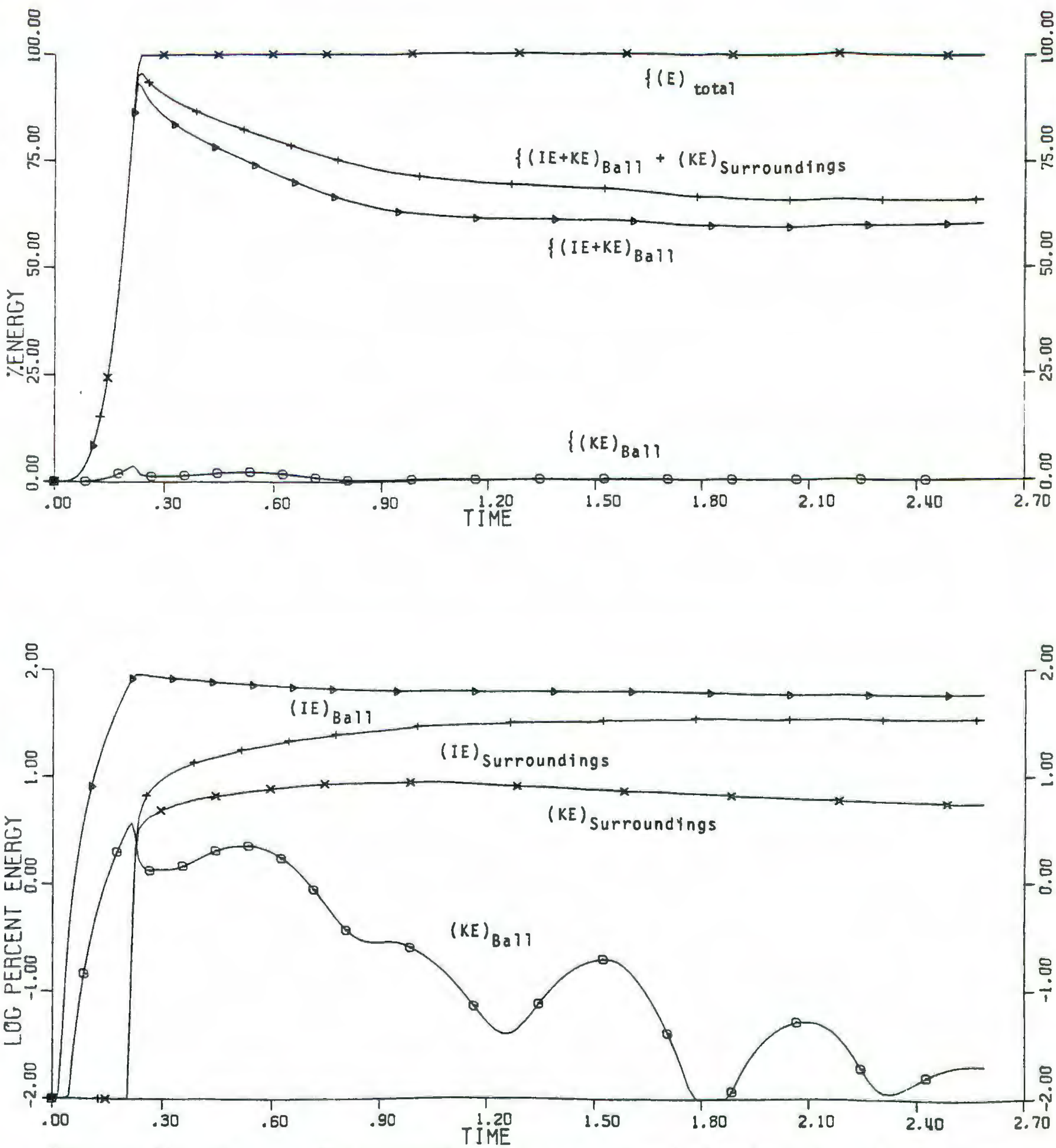

Figure 61. Energy distribution versus time behavior in a blast system generated by a Mach 4.0 energy wave.

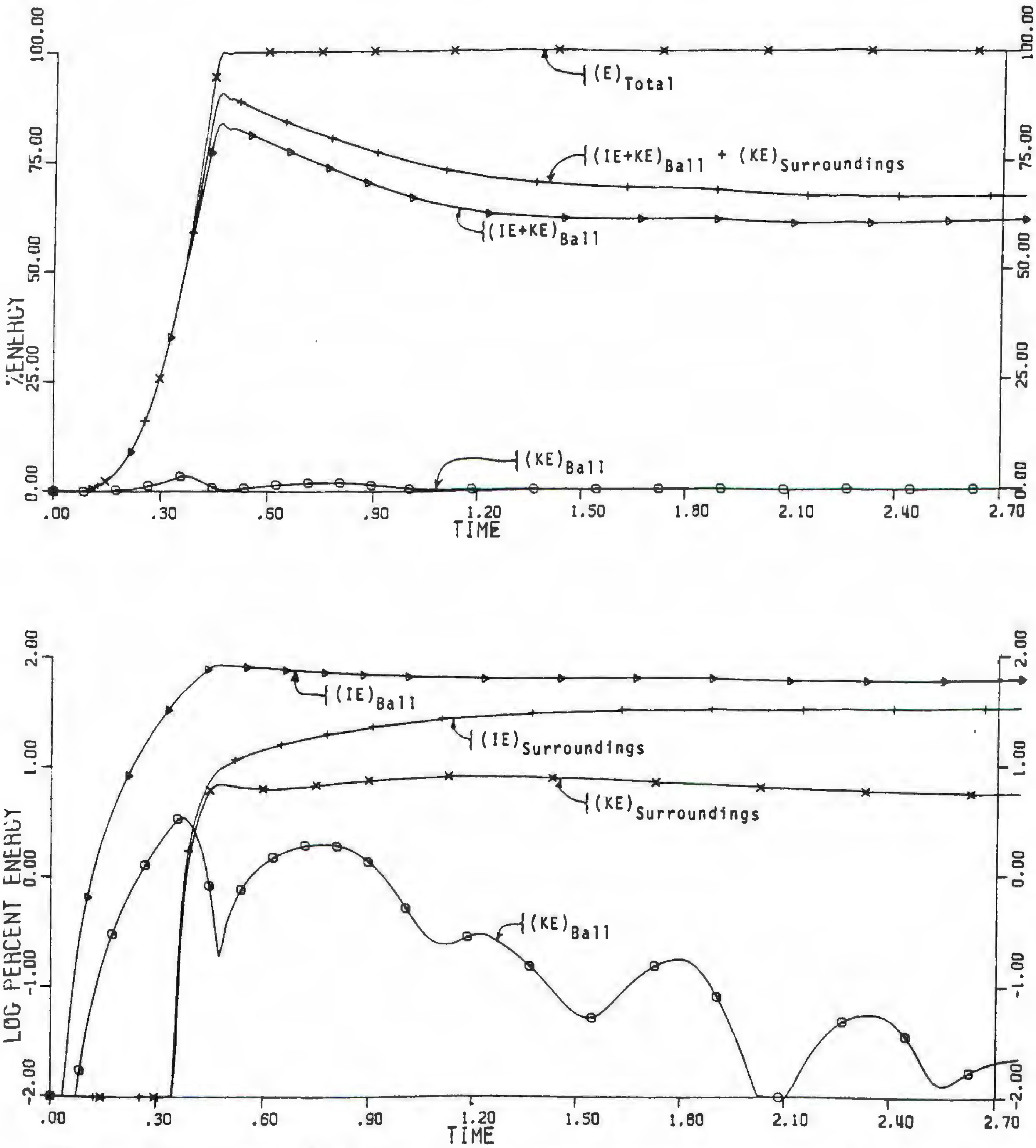

Figure 62. Energy distribution versus time behavior in a blast system generated by a Mach 2.0 energy wave.

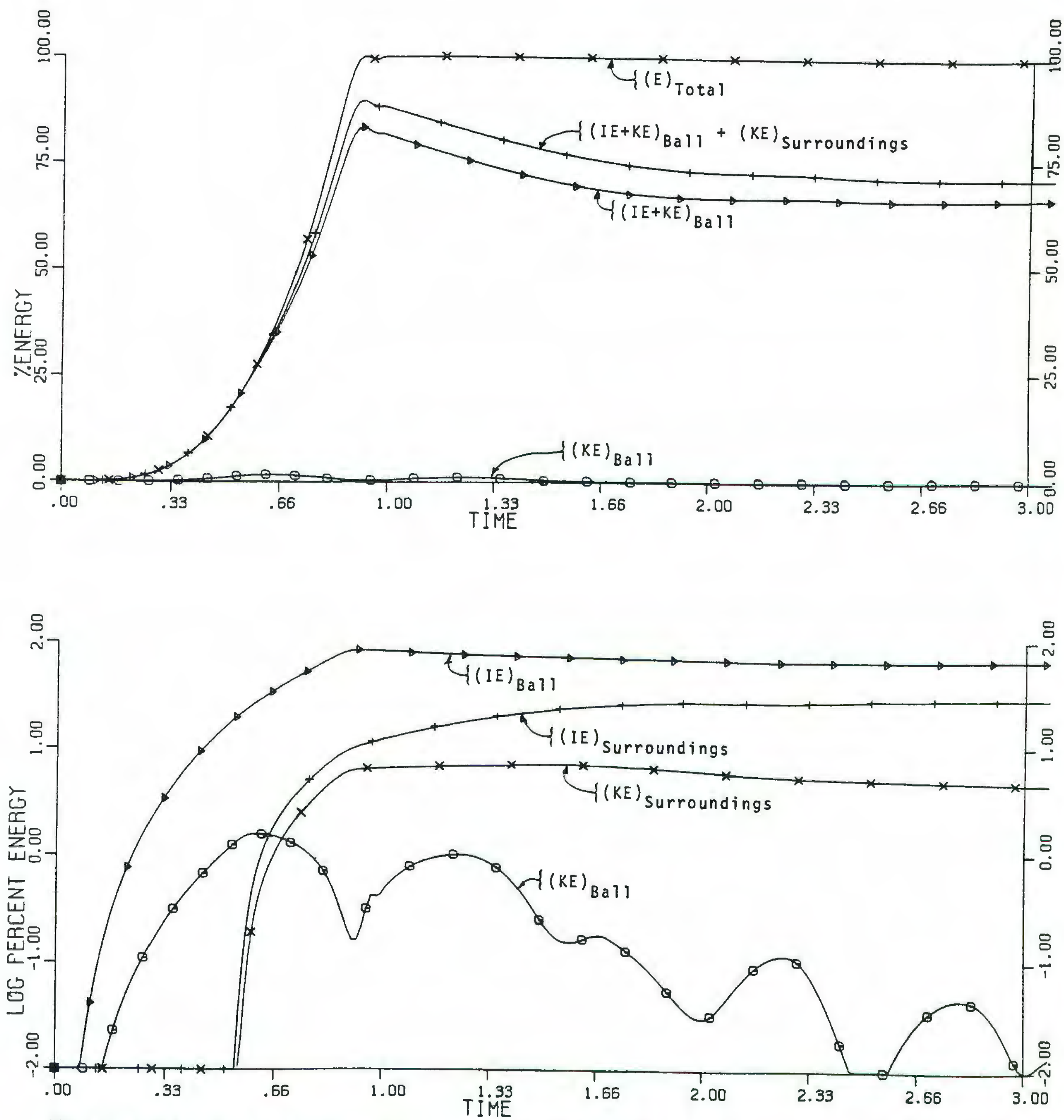

Figure 63. Energy distribution versus time behavior in a blast system generated by a Mach 1.0 energy wave.

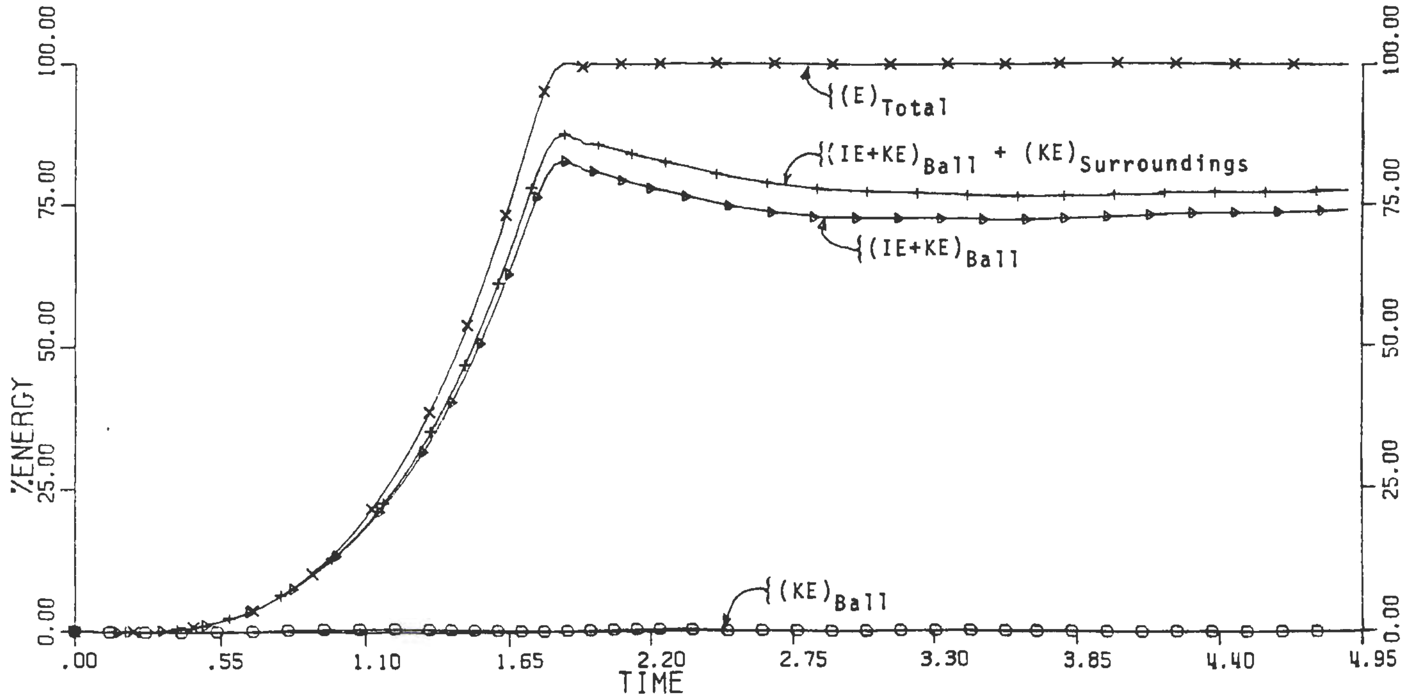

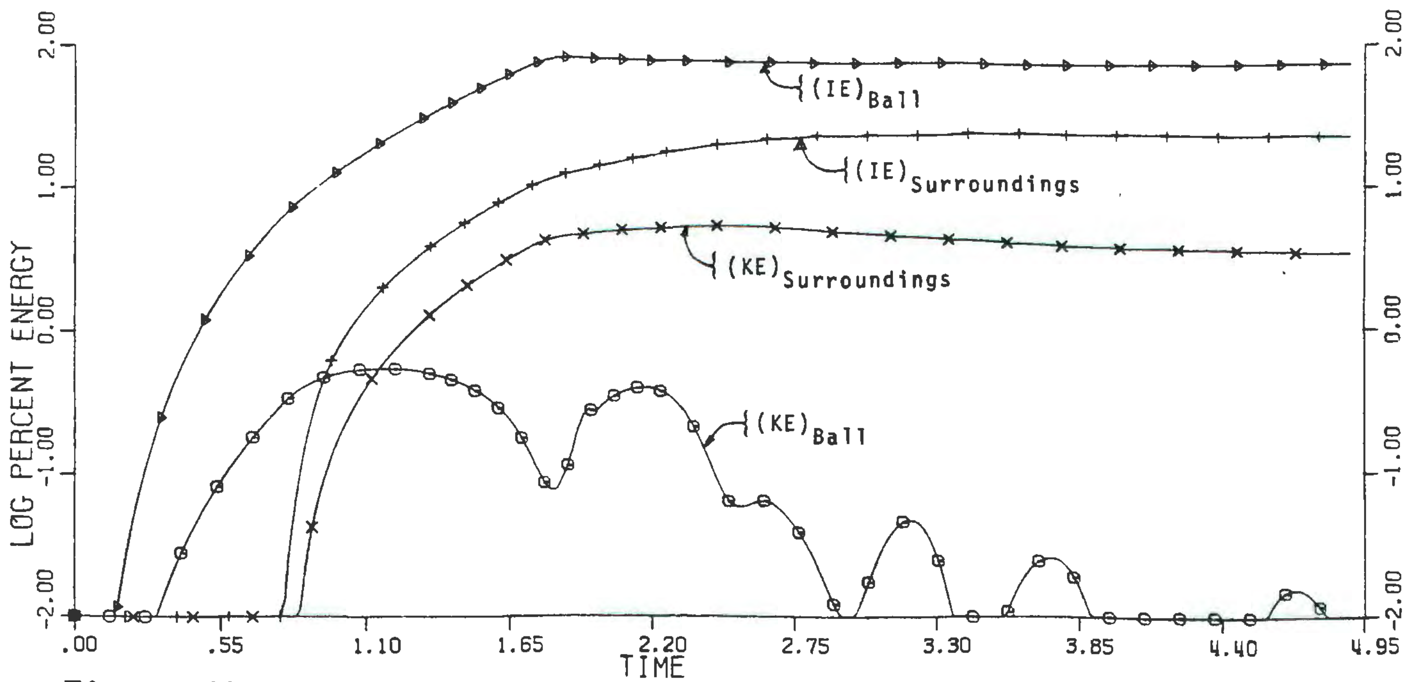

Figure 64. Energy distribution versus time behavior in a blast system generated by a Mach 0.5 energy wave.

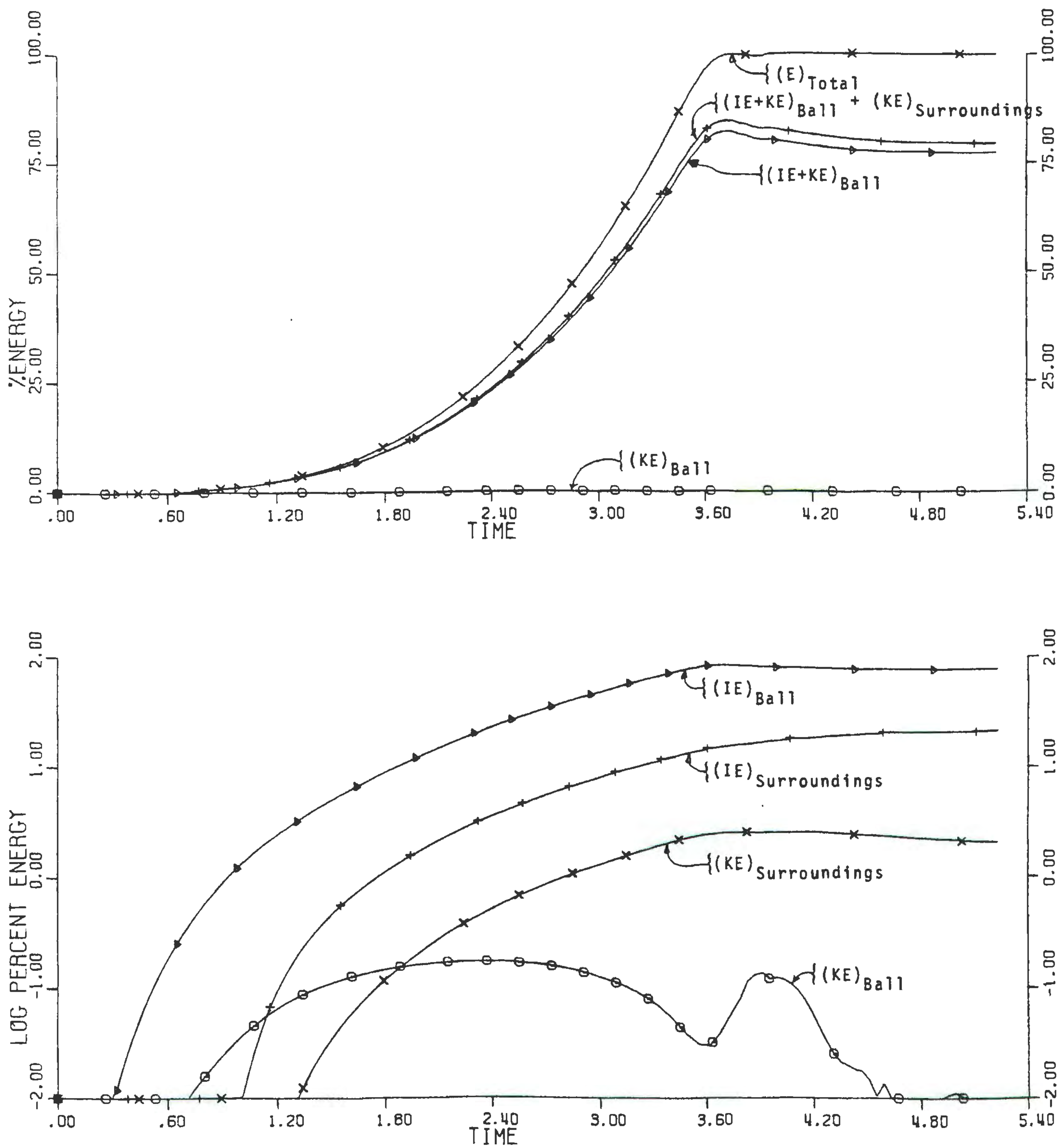

Figure 65. Energy distribution versus time behavior in a blast system generated by a Mach 0.25 energy wave.

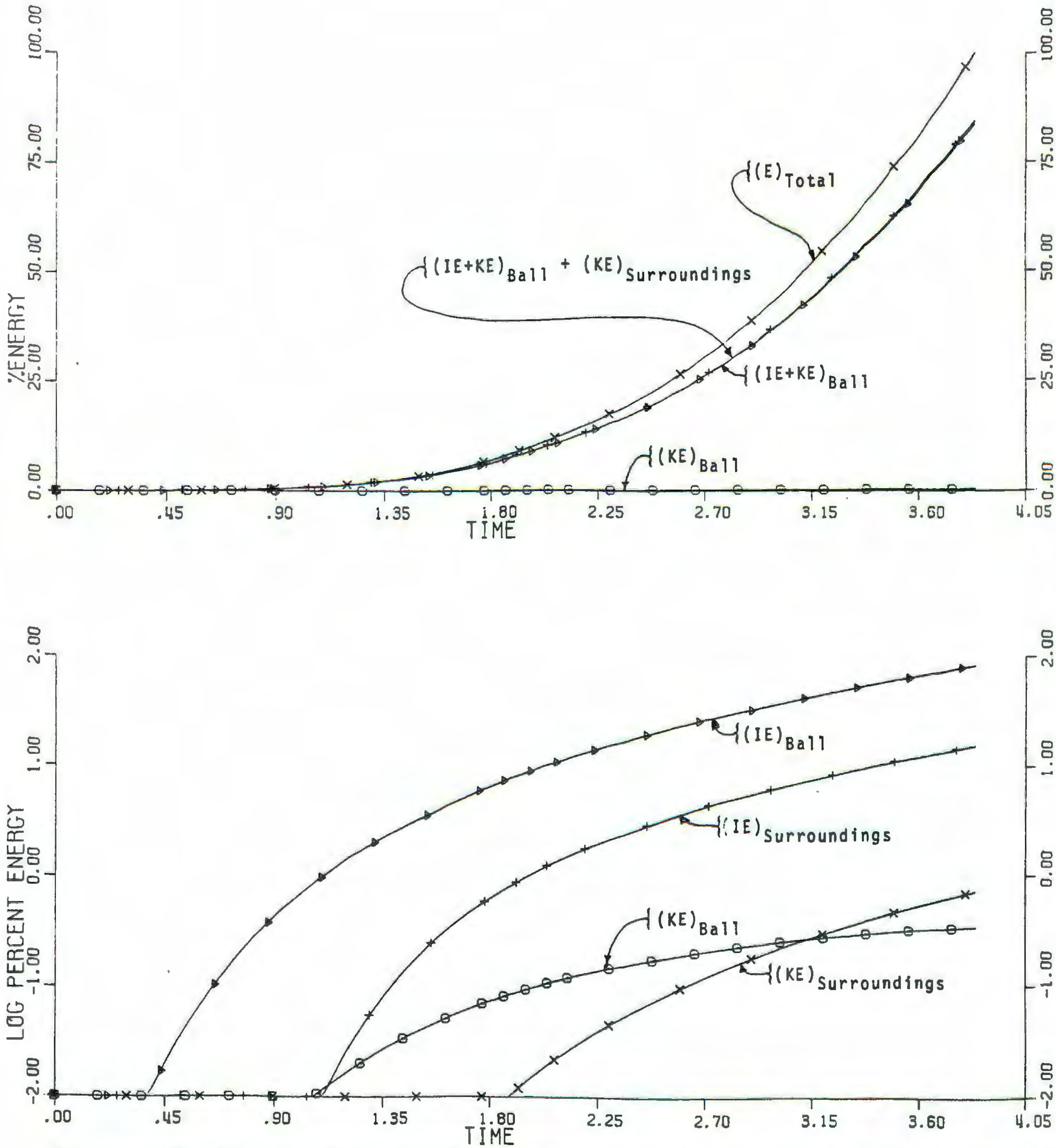

Figure 66. Energy distribution versus time behavior in a blast system generated by a Mach 0.125 energy wave.

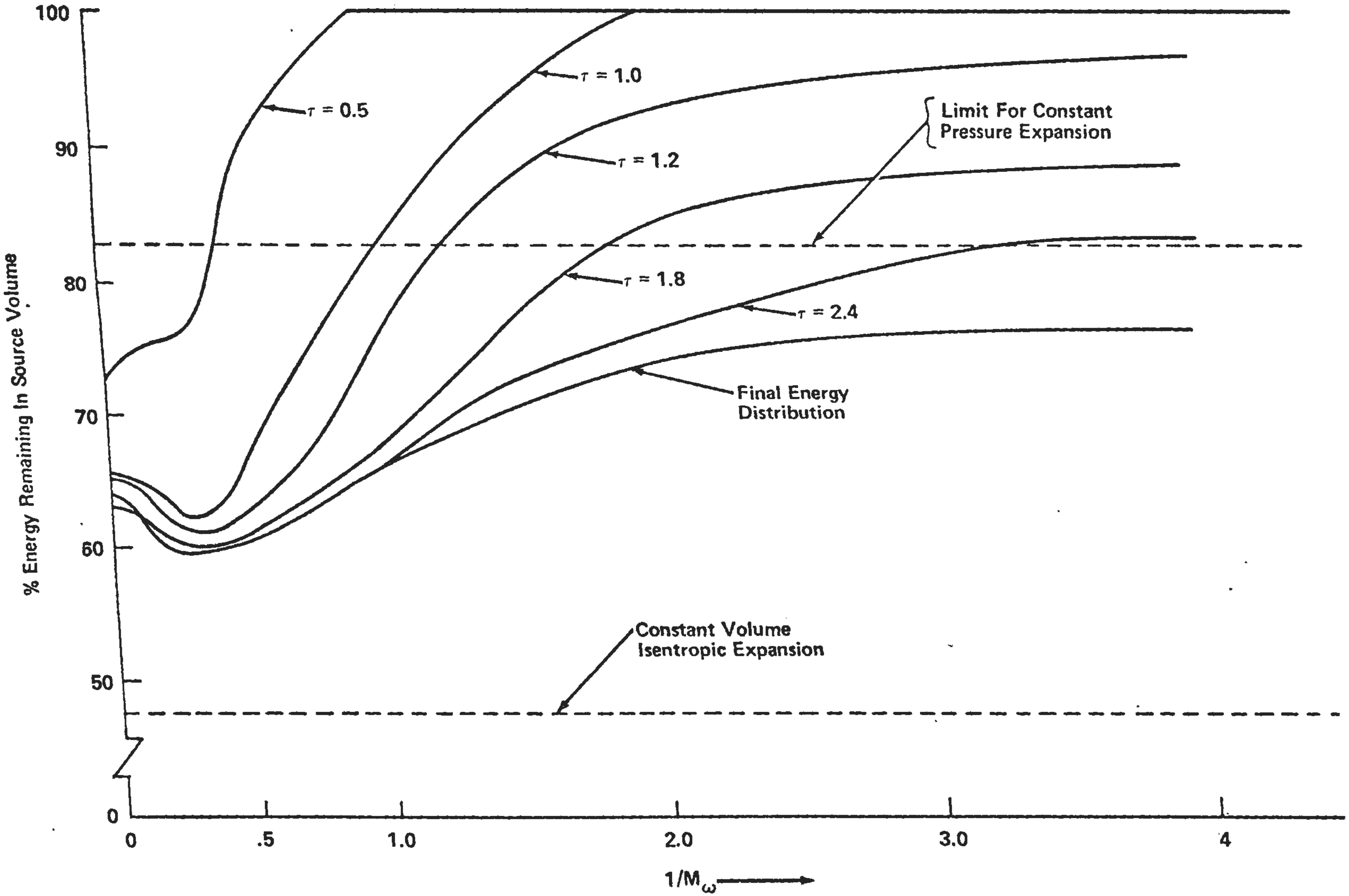

Figure 67. Energy Remaining in Source Volume Versus Reciprocal Mach Number of Energy Wave.

V. COMPARISONS

A. An Investigation Of Blast Waves Generated From Non-Ideal Energy Sources

Adamczyk[18] systematically studied the flow field of blast waves generated by the homogeneous deposition of energy (infinite velocity wave of infinite thickness with finite deposition time). Using a Von-Neumann/Richtmyer-type finite difference integration procedure he generated numerical solutions of the flow field parameters for planar, cylindrical, and spherical flow fields.

In the analysis, Adamczyk determined the time of energy deposition and the energy density within the source to be the two most critical parameters affecting the flow properties of the blast system. Since the calculations in this dissertation were all done at one energy density, these comparisons will only address his conclusions concerning deposition time.

For comparison with the homogeneous energy deposition investigated by Adamczyk, two cases with deposition times $\tau_D=0.2$ and $\tau_D=2.0$ were run. A shorter deposition time was not deemed necessary since the flow field approaches bursting sphere.

1. Flow Field Properties

Kernel Addition $\tau_D=0.2$

For the case of an energy deposition time of τ=0.2, figures* 68 and 69 show the pressure time history of the energy addition. As the energy is added, the flow field develops and an expansion wave propagates in from the kernel edge. When energy addition stops the expansion wave has progressed only about 50% of the distance into the kernel. Therefore, the sturcture of the system closely resembles that generated by a bursting sphere. Comparing figures 69 and 15, it can be seen that the flow fields are similar if the time for energy deposition is considered. The expansion wave has propagated 50% of the way into the bursting sphere at time 0.13 and 50% into the homogeneous energy addition at time 0.2. By adjusting the times for flow field behavior to reflect this time difference, the flow fields are similar.

This can also be seen by examining figure 75. The energy addition results in an initial expansion wave followed by a second shock reflected from the origin, similar to the bursting sphere. However, the expansion wave does not propagate into the source volume at constant velocity. The local velocity of sound is a function of the local temperature and gamma, both of which are functions of the energy addition.

Figure 71 shows that the center of the source volume experiences a constant volume energy addition, similar to the bursting sphere case. The cells on the edge of the source volume experience both a pressure rise and specific volume increase.

*Note: figures in this chapter are collected at the end to simplify comparison

The blast wave structure at fixed Eulerian radii is shown in figure 73. Inside the source volume η = 0.825 the pressure rises during energy addition, peaking when energy addition ends. The pressure decreases below ambient at τ=0.58. The blast wave behavior outside the source volume is similar to bursting sphere, figure 38.

Kernel Addition τ=2.0

In run 20 a homogeneous energy addition was done with a deposition time of τ=2.0 which is quite long in relation to the characteristic times of the system. For the case of no energy addition an ambient temperature acoustic wave would take a time of τ=0.85 to propagate from the edge of the source volume to the center. Since the energy addition takes place over a much larger time, the system distributes the energy as it is added. Figure 70 shows that during the energy addition an expansion wave forms which reaches the center at τ=0.68 with a maximum pressure of P=2.7. (note: the travel time of the expansion wave is decreased by the effects of temperature and gamma on the speed of sound.)

The expansion wave reflects from the center and an outward propagating pressure "hump" develops. Since the energy is being added slowly there is primarily a low pressure expansion of the source volume with the pressure wave propagating into the surroundings. When energy addition has been completed the specific volume of the cells in the source volume is approximately 7.0 which approaches the specific volume expected from a constant pressure expansion.

Figure 76 shows that since the energy addition continues during and after the arrival of the expansion wave at the center there is no second shock generated. The expansion of the flow field is a smooth continuous process.

In the very slow homogeneous addition of energy, $\tau=2.0$, figure 72 shows very unique behavior is the p-ν plane. Initially the energy addition results in a pressure rise in all cells. As the expansion wave propagates into the source volume the energy addition changes from a pressure increase to a specific volume increase. Expansion waves propagating through the source volume tend to equalize the pressure and the intersections of the p-ν curves indicate equal temperatures in the source volume. At the end of energy addition the individual cells have expanded to a specific volume of approximately 6.75 at $P = 1.1$.

The blast wave develops as a relatively slow pressure rise both inside and outside the source volume as shown in figure 74.

The pressure remains greater than ambient throughout the energy addition. An interesting behavior in this case is that the pressure drops below ambient first in the source volume and then propagates outward.

2. Damage Parameters

Figure 77 shows the overpressure from homogeneous addition of energy. For the rapid energy addition (τ_D=0.2) the pressure peak progresses from the edge of the source volume towards the center until a shock waves forms. As expected, the overpressure of shock approximates overpressure from the bursting sphere shock. For the very slow energy addition (τ=2.0) the peak pressure propagates from the edge of the source volume to the center and out as a shock is formed. However for this case the overpressures are significantly lower. These overpressures lie between those of the Mach 0.5 and Mach 0.25 cases plotted on figure 56. This would be expected since the times for energy addition in these cases are 1.859 and 3.719, respectively.

In Adamczyk's investigation the instantaneous deposition time produced the highest overpressures, whereas in the wave addition of energy the overpressures increase to a maximum at a finite time of deposition, τ_D=0.28. Figure 78 presents comparisons of the overpressures developed in the wave addition of energy and the homogeneous addition of energy. For the cases investigated the overpressure outside the source volume was greater than the overpressure from the homogeneous energy addition. However, in the source volume, as the deposition time becomes greater than τ=0.6 the overpressure in the source volume was greater for the homogeneous addition of energy than the wave addition of energy. This is not considered to be controlling since the overpressure is low ($P=5.0$) and the area would be subjected to extensive fire damage.

The impulse in the cases involving the kernel (homogeneous) addition of energy is shown in figure 57. For the rapid deposition of energy $\tau=0.2$ the impulse is slightly less than bursting sphere in the near field and slightly greater in the intermediate to far field. In the near field the impulse is lower because of the time required for the energy deposition. In the intermediate and far field the impulse is greater because the finite time of deposition extends the positive phase of the blast wave.

For the long kernel deposition time ($\tau=2.0$) the impulse is much lower because of the low peak pressures developed. The impulse curve lies between the Mach 0.5 and Mach 0.25 energy addition wave curves with $\tau_D=1.86$ and $\tau_D=3.72$, respectively.

3. Energy Distribution

With consideration given for the time of energy addition, the kernel addition with $\tau_D=0.2$, shown in figure 79, is similar to the case of bursting sphere. However, during energy addition the energy appears as kinetic and internal energy in both the source volume and the surroundings. The internal energies approach final values of 65% in the source volume and 36% in the surroundings.

As expected kernel energy deposition of long duration, τ_D=2.0, results in very inefficient energy transfer to the surroundings as shown in figure 80. The final distribution is 74.7% in the source volume and 25.3% in the surroundings. This can be compared to the energy distribution from a Mach 0.5 wave with 74.1% of the energy remaining in the source volume. This behavior appears reasonable, since for the Mach 0.5 energy wave the total time of energy deposition in the source volume is τ=1.859.

B. *Some Aspects of Blast from Fuel-Air Explosives*

Beginning with the finite differencing technique of the "Cloud" program written by Oppenheim[30], Fishburn[35] added a burn routine similar to that of Wilkins[29] to simulate the detonation process. Using the program he studied blast waves generated by (1) centrally initiated, self-similar Chapman-Jouguet detonation, (2) edge initiated spherical implosion, and (3) constant volume energy release followed by sudden venting to the environment.

Selecting MAPP gas, methyl-acetylene propadiene mixture, as a representative hydrocarbon, Fishburn used the "TIGER" program to calculate thermodynamic equilibrium for MAPP gas in the CJ plane. Using the calculated detonation pressure, the energy to be added and the detonation Mach number were calculated from the steady-state conservation equations (Equations II-36, II-37).

The energy was added linearly and gamma changed proportional to the energy release through the front. Several runs were done varying the front thickness and a final wave thickness of 10% of the energy addition zone was selected.

In figure 2 of Fishburn's paper the plot of a centrally initiated detonation has a constant pressure from the center to the edge of the source volume. This plot was based on known detonative behavior and not program calculations. Calculated pressures started near zero at the center and approached the CJ pressure as the energy addition approached the edge of the source volume.(36) This behavior is consistent with the results noted in this dissertation. Fishburn noted that the constant volume energy release produced lower peak pressures near the charge but slightly higher peak pressures than the centrally initiated detonation to radii greater than $R/R_c=2$. This behavior was also noted in this dissertation.

Fishburn also did an analysis of the energy distribution by determining the net work done by the detonation products on their environment by the following relationship:

$$\frac{\text{Work}}{\frac{4}{3}\pi R_c^3 \; p_o \; \frac{Q}{p_o v_o}} = 1 - \frac{\left[\frac{(R_f/R_c)^3}{\gamma_4 - 1} - \frac{1}{\gamma_o - 1}\right]}{(Q/p_o v_o)}$$

Where R_c is the initial radius of the change and R_f is the final radius of the source volume. His calculations showed the fraction of energy deposited transferred to the surroundings to be:

explosion = 0.378

high pressure = 0.336

In this dissertation the fraction of energy released which is transferred to the surroundings as kinetic and internal energy was:

Chapman-Jouguet = 0.385

Bursting Sphere = 0.361

The differences in the results may be attributed in part to the different technique used in the calculation. However, the results are comparable.

The conditions calculated by Fishburn were used as input parameters for a run using the program modified by the author. Figure 81 shows the development of the blast wave with time. Figure 82 is a pressure-specific volume plot. The particles near the edge of the source volume exhibit Rayleigh line behavior during the energy addition and appear to tangent the insentrope. This indicates that for the specified conditions the results approach the expected results from a CJ detonation.

C. Pressure Waves Generated by Steady Flames

Kuhl, Kamel, and Oppenheim[21] studied the self-similar behavior of the flow field associated with flames traveling at constant velocity. Their study was directed to the steady-state condition the system attains when the flame propagation velocity attains a constant velocity. They did not consider ignition, initial flame acceleration, or the pressure wave decay after the source volume is consumed by the flame.

Introducing reduced blast wave parameters as phase-plane coordinates, they determined appropriate integral curves on this plane. For one of their calculations they assumed a combustible mixture with a specific heat ratio of $\gamma_o=1.3$ ahead of the flame and $\gamma_4=1.2$ behind, a volumetric expansion ratio of 7 for a constant pressure deflagration, and an ambient sound speed of 345 m/sec..

For comparison these parameters were used as input variables in the program used for this dissertation. The results are plotted as figure 83.

In their analysis the flame was treated as a steady deflagration and a piston expanding at constant velocity was used as a representative case. Using subscript p to denote parameters corresponding to the locus of states at the piston face, solutions were obtained in terms of $\zeta = \gamma_1 Z_P$ as the parameter. By integration of the governing differential equations, the solution for a spherical flow field is:

$$
\begin{aligned}
Z_P &= Z\ F^{2/3} \\
&= [(t/r_\mu)a]^2[(t/r_\mu)u]^{2/3} \\
Z_P &= 5.67 \\
\zeta &= \gamma_1 Z_P \\
\zeta &= (1.3)(5.67) \\
&= 7.37
\end{aligned}
$$

An examination of figure 83a shows the blast wave approaching a self-similar solution with a nearly linear decrease in pressure from a pressure of 1.26 at leading edge of the flame front (X=0.42) to 1.02 near the shock front (X=0.95).

Comparing this to figure 7 of Kuhl, et al., the ζ=4 curve has a nearly linear pressure decrease from a pressure of 1.28 at X=0.45 to 1.02 at the shock front. Thus the finite differencing technique assymptotically approaches p_o but the similarity solution appears to begin to develop a shock front at the leading edge.

In figure 83b the energy transfer ahead of the flame can be seen. The calculations appear to be approaching a self-similar solution ahead of the flame front with a near linear decrease to Θ/Θ_o=1.005 at X=0.95. Figure 83c shows the particle velocity in the blast wave. From a maximum velocity at the flame front it asymptotically, decreases to zero at the shock front. Through the flame front it decreases rapidly and remains at nearly zero.

Comparing these results to the results of Kuhl, et al., the maximum values calculated with the finite difference technique at the flame front approach the values calculated by Kuhl, et al., for the ζ=4.0 case. However, the blast wave structure is more closely approximated by the ζ=7.0 case.

D. The Air Wave Surrounding an Expanding Sphere

The properties of the flow field generated by a sphere expanding at a velocity, slow relative to the ambient velocity of sound, were determined by Taylor[3]. He integrated the velocity potential equation and developed the following relationships for the pressure and particle velocity distribution outside the expanding sphere:

$$p - p_o = \frac{2\rho\, a^2 M_s^{\,3}}{(1-M_s^{\,2})} \left(\frac{at}{r} - 1\right)$$

$$u = \frac{a\, M_s^{\,3}}{(1-M_s^{\,2})} \left(\frac{a^2 t^2}{r^2} - 1\right)$$

where M_s is the Mach number of the surface of the expanding sphere:

$$M_s = \frac{R/t}{a}$$

and R(t) is the Eulerian position of the sphere.

The results calculated in case 10 (M_w = 0.125) were analyzed and compared to predicted results from Taylor's formulas. The leading edge of the energy wave was used to represent the surface of the expanding sphere. After the self similar flow field developed the Eulerian velocity and Mach number of the energy wave were calculated to be M_s=0.24.

Using this velocity the pressure and particle velocity distribution were plotted in figure 85 for comparison with the results calculated by Taylor for the case $\frac{R}{at} = 0.2$. The distributions are nearly identical indicating close agreement of the results calculated with theoretical predictions.

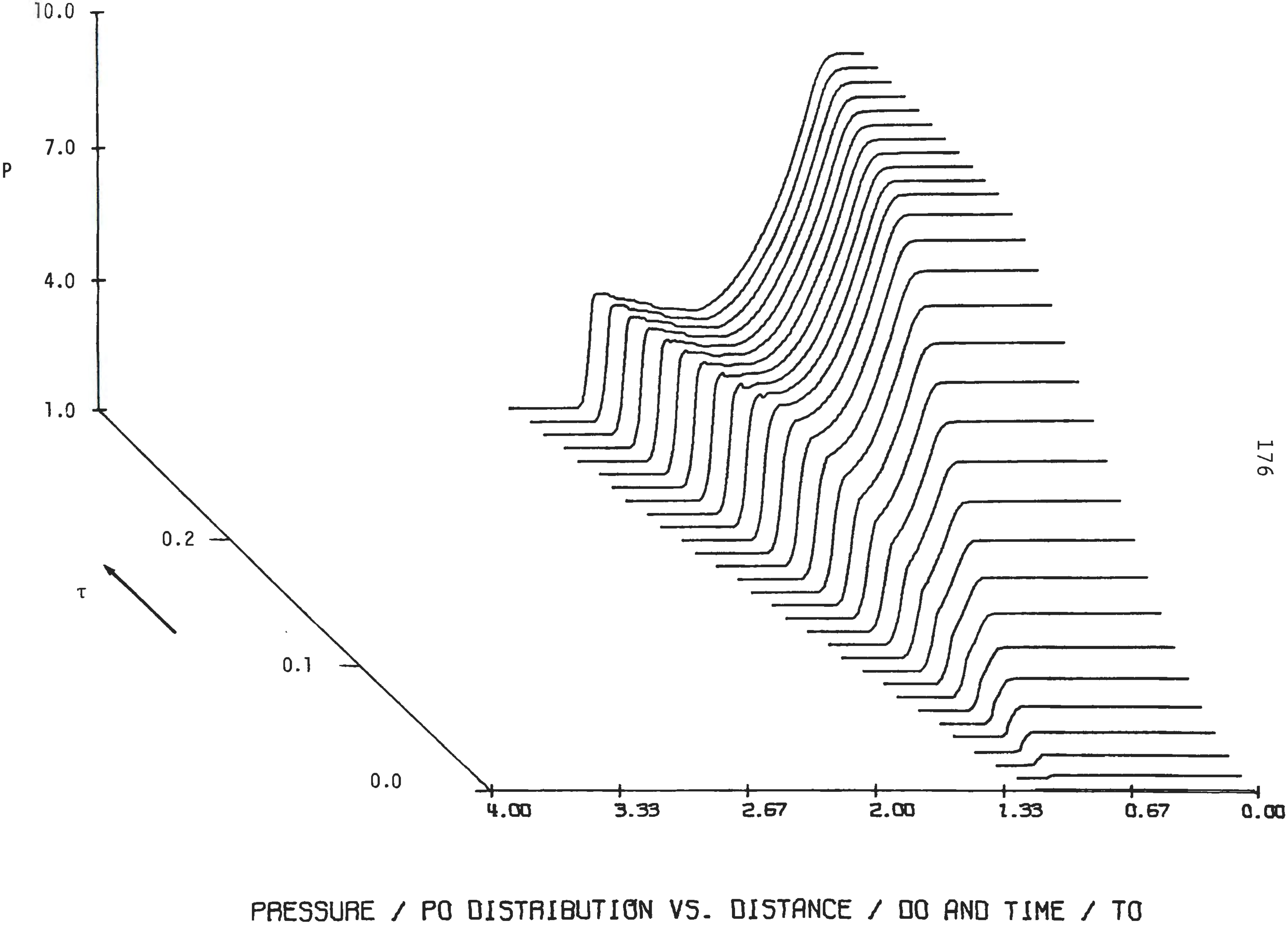

Figure 68. Pressure distribution versus Eulerian distance and time from a blast system generated by a $\tau_D = 0.2$ homogeneous energy addition.

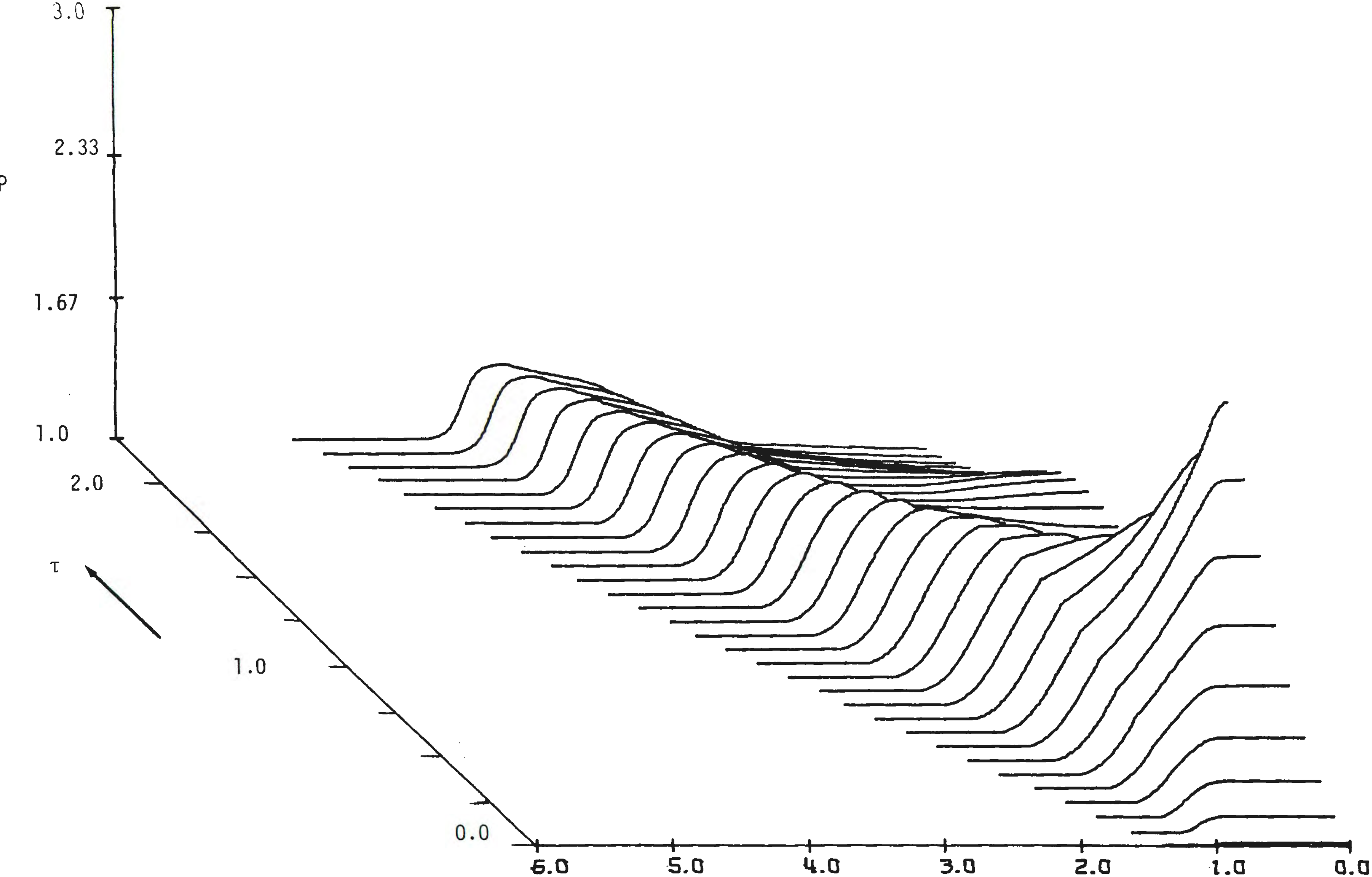

Figure 70. Pressure distribution versus Eulerian distance and time from a blast system generated by a τ_D = 2.0 homogeneous energy addition.

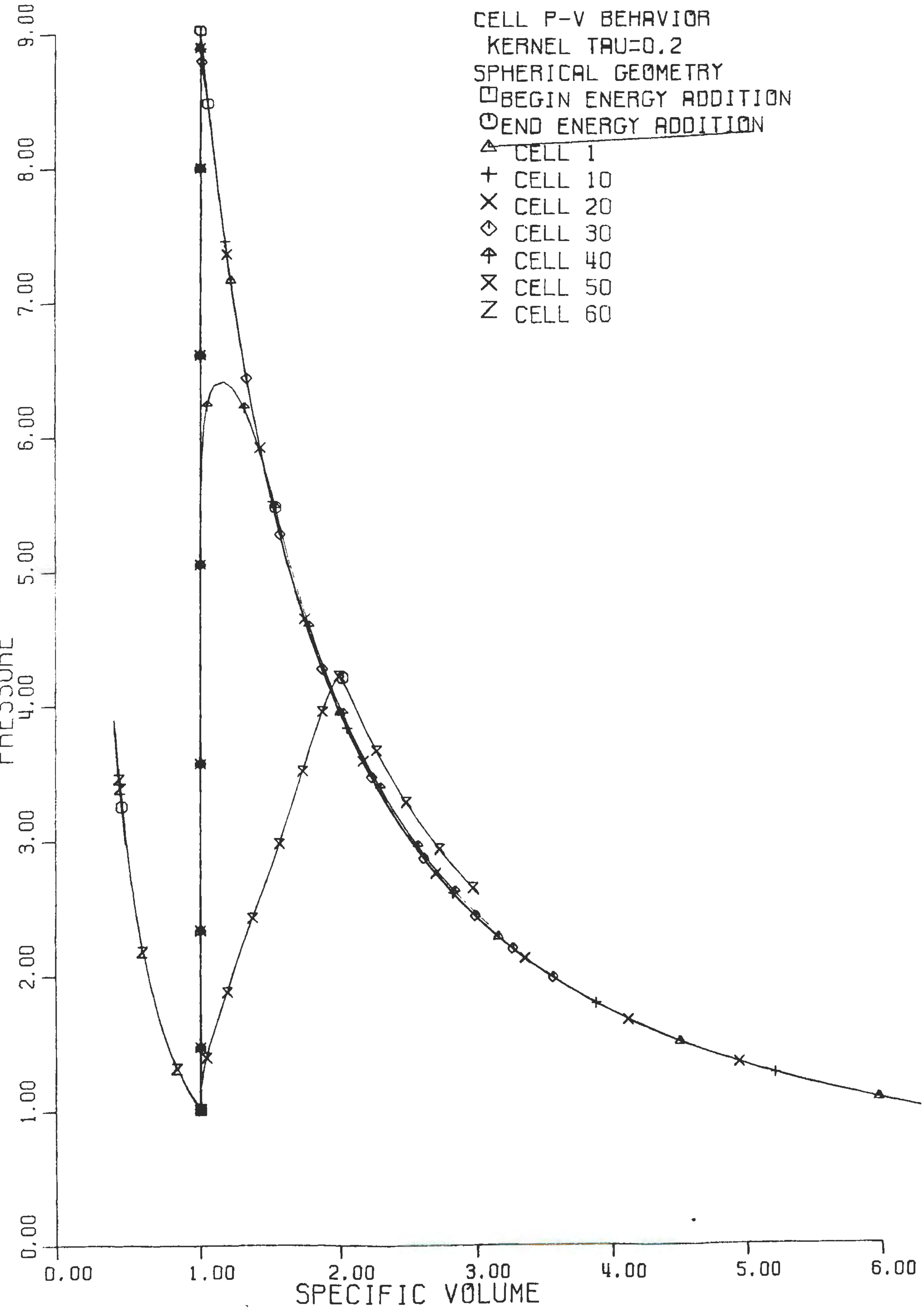

Figure 71. Pressure versus specific volume behavior from $\tau_D = 0.2$ homogeneous energy addition (D = 1.0 at cell 50)

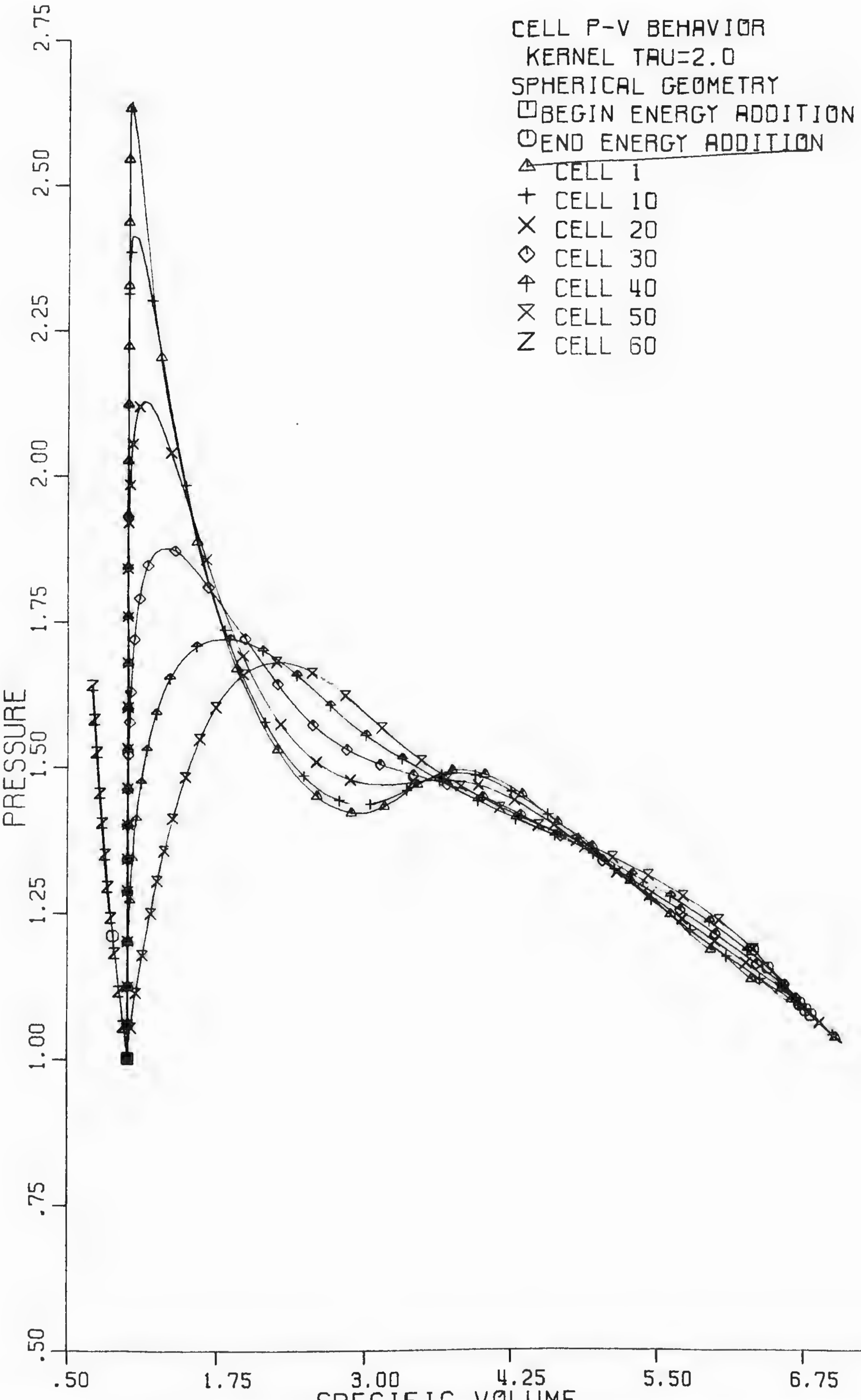

Figure 72. Pressure versus specific volume behavior from τ_D = 2.0

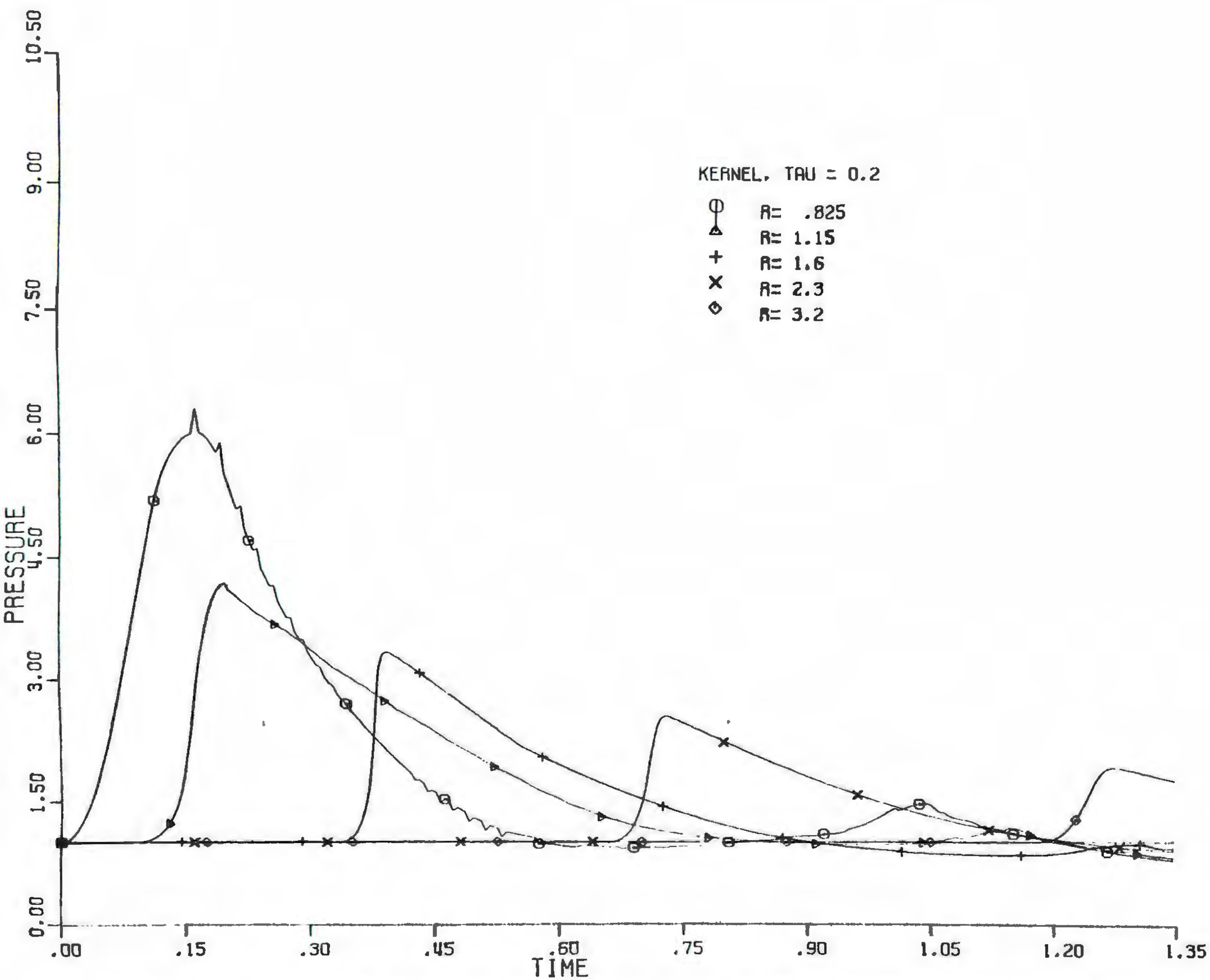

Figure 73. Pressure versus time behavior at fixed Eulerian radius from a blast system generated by a $\tau_D = 0.2$ homogeneous energy addition.

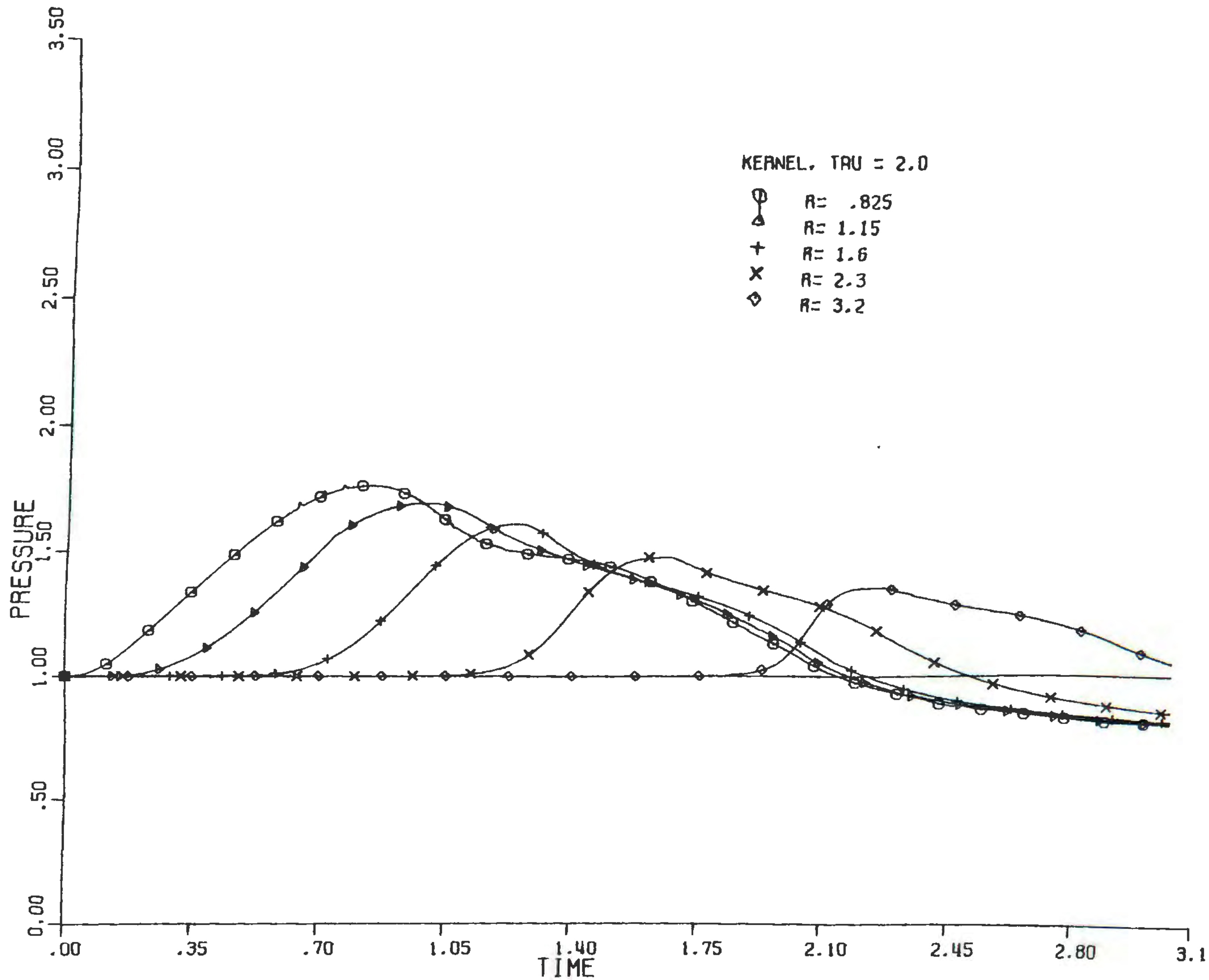

Figure 74. Pressure versus time behavior at fixed Eulerian radius from a blast system generated by τ_D = 2.0 homogeneous energy addition.

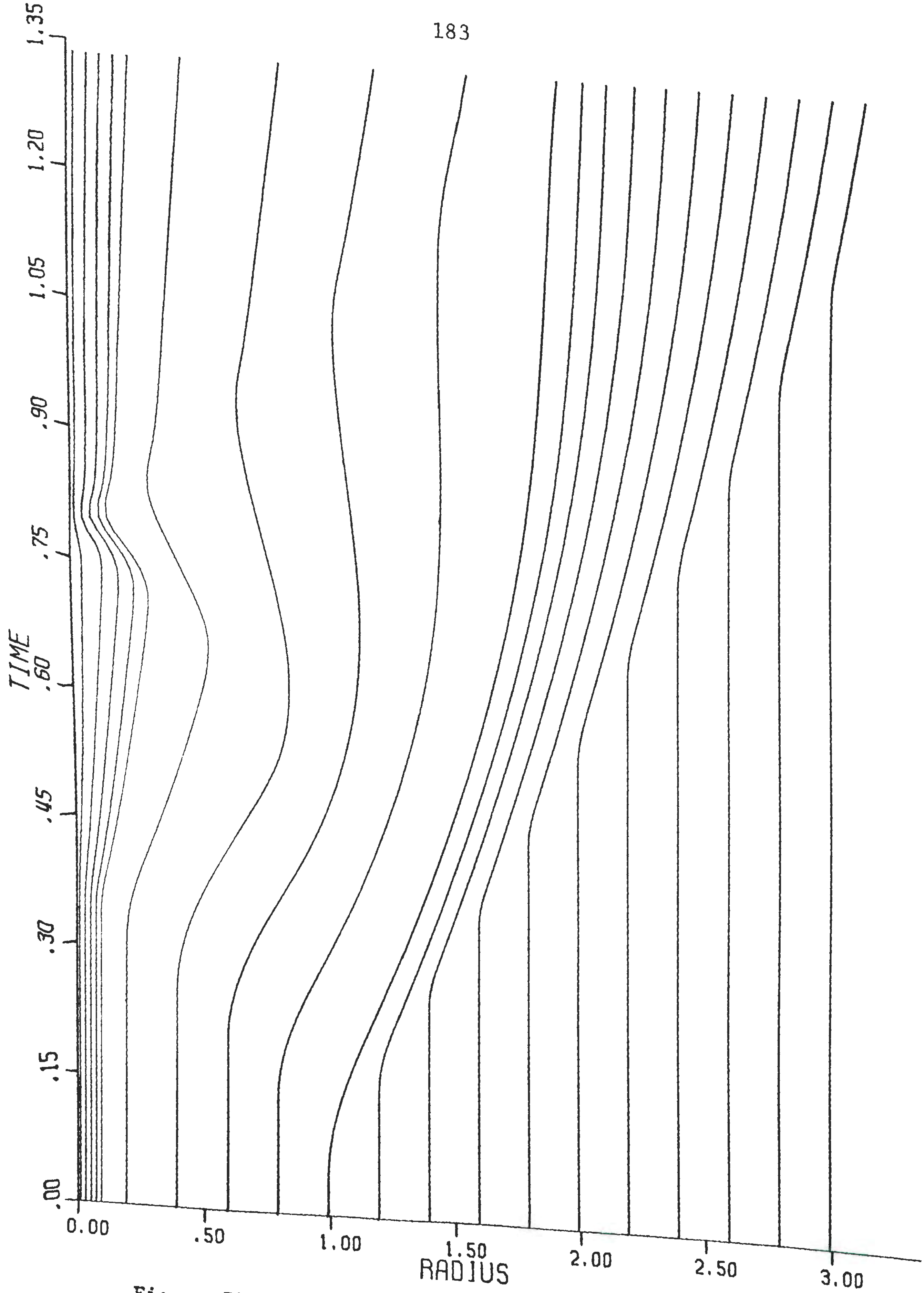

Figure 75. Particle position versus time in a blast system generated by a τ_D = 0.2 homogeneous energy addition

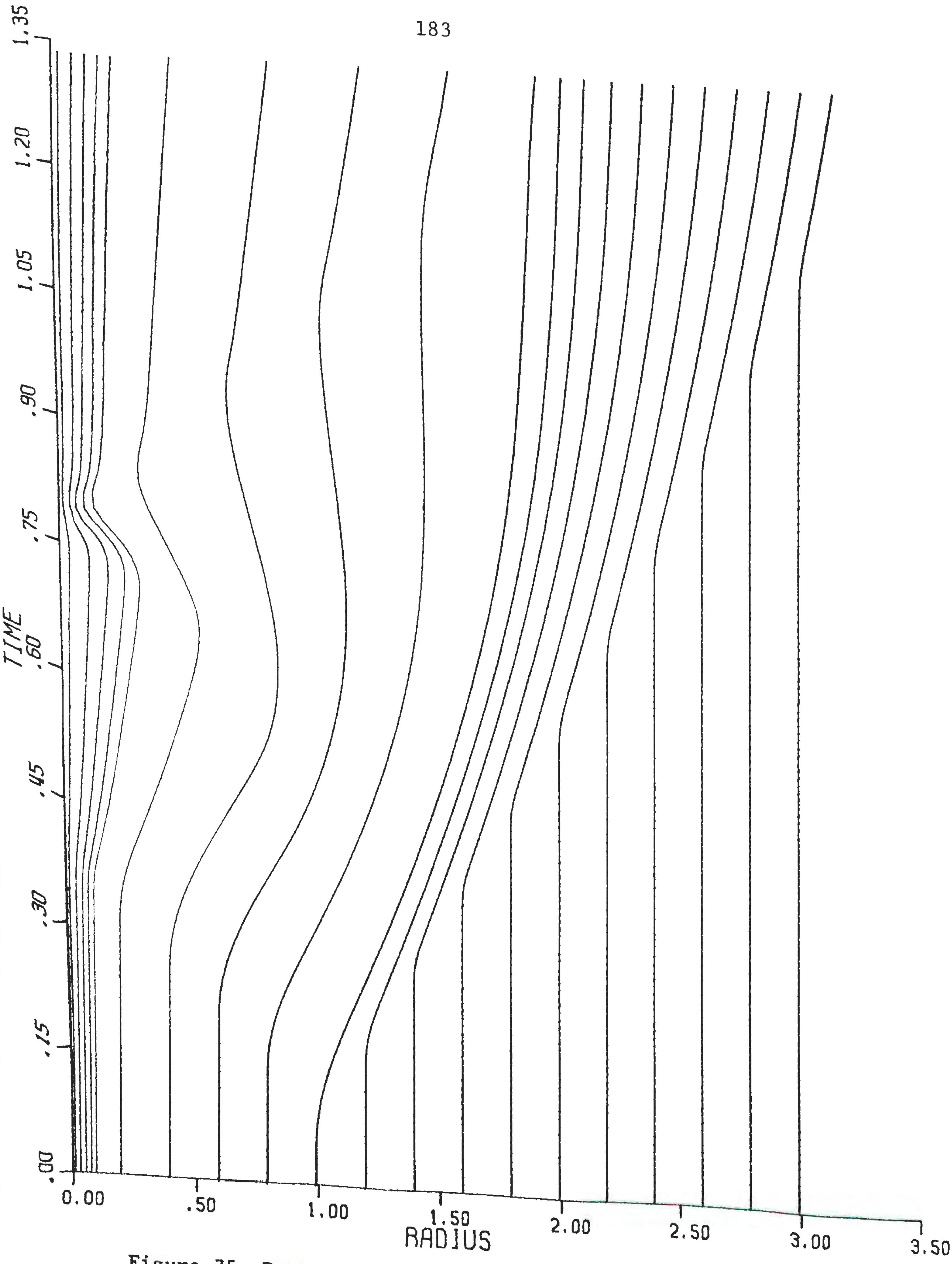

Figure 75. Particle position versus time in a blast system generated by a $\tau_D = 0.2$ homogeneous energy addition.

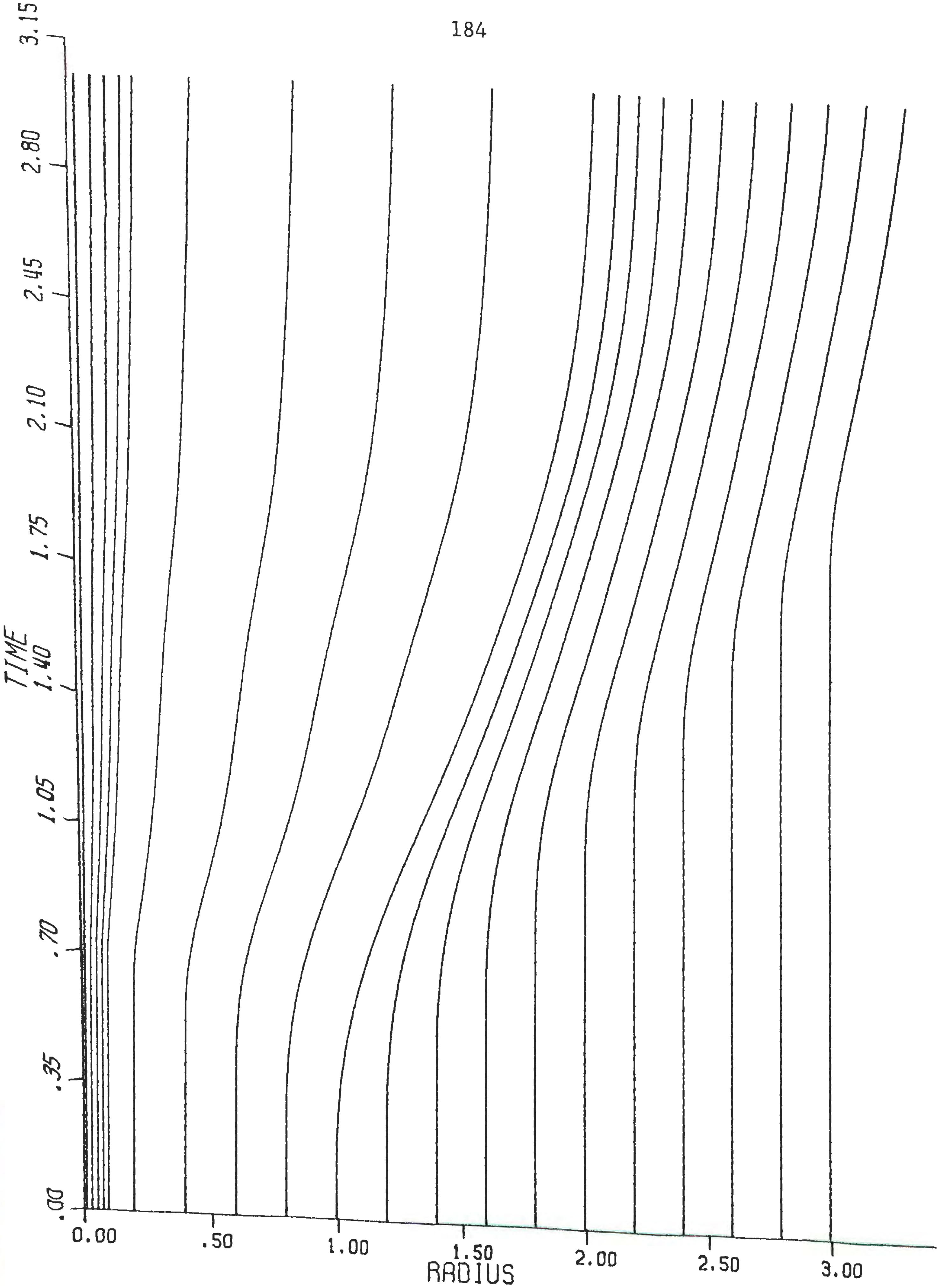

Figure 76. Particle position versus time in a blast system generated by a $\tau_D = 2.0$ homogeneous energy addition.

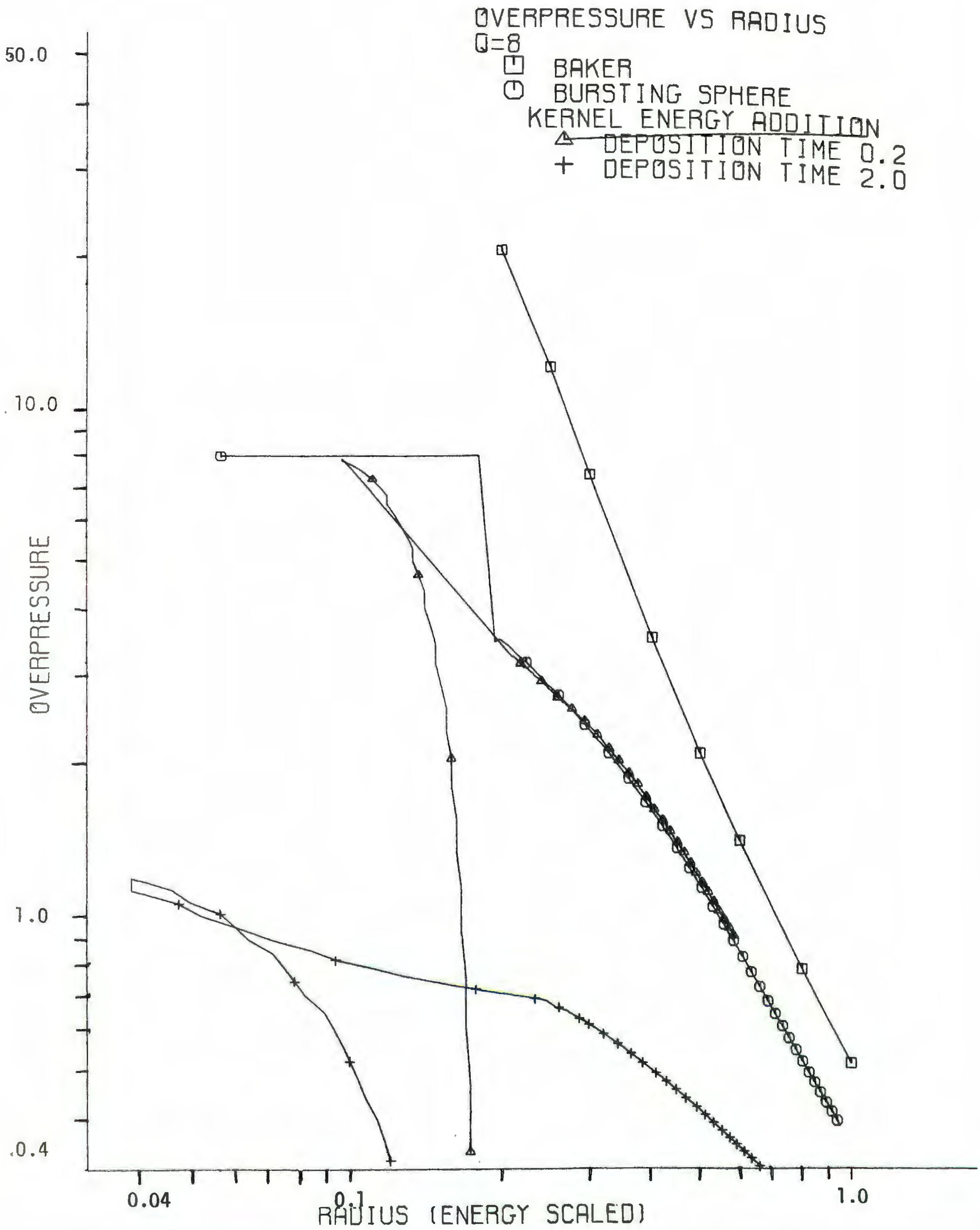

Figure 77. Overpressure versus energy scaled distance.

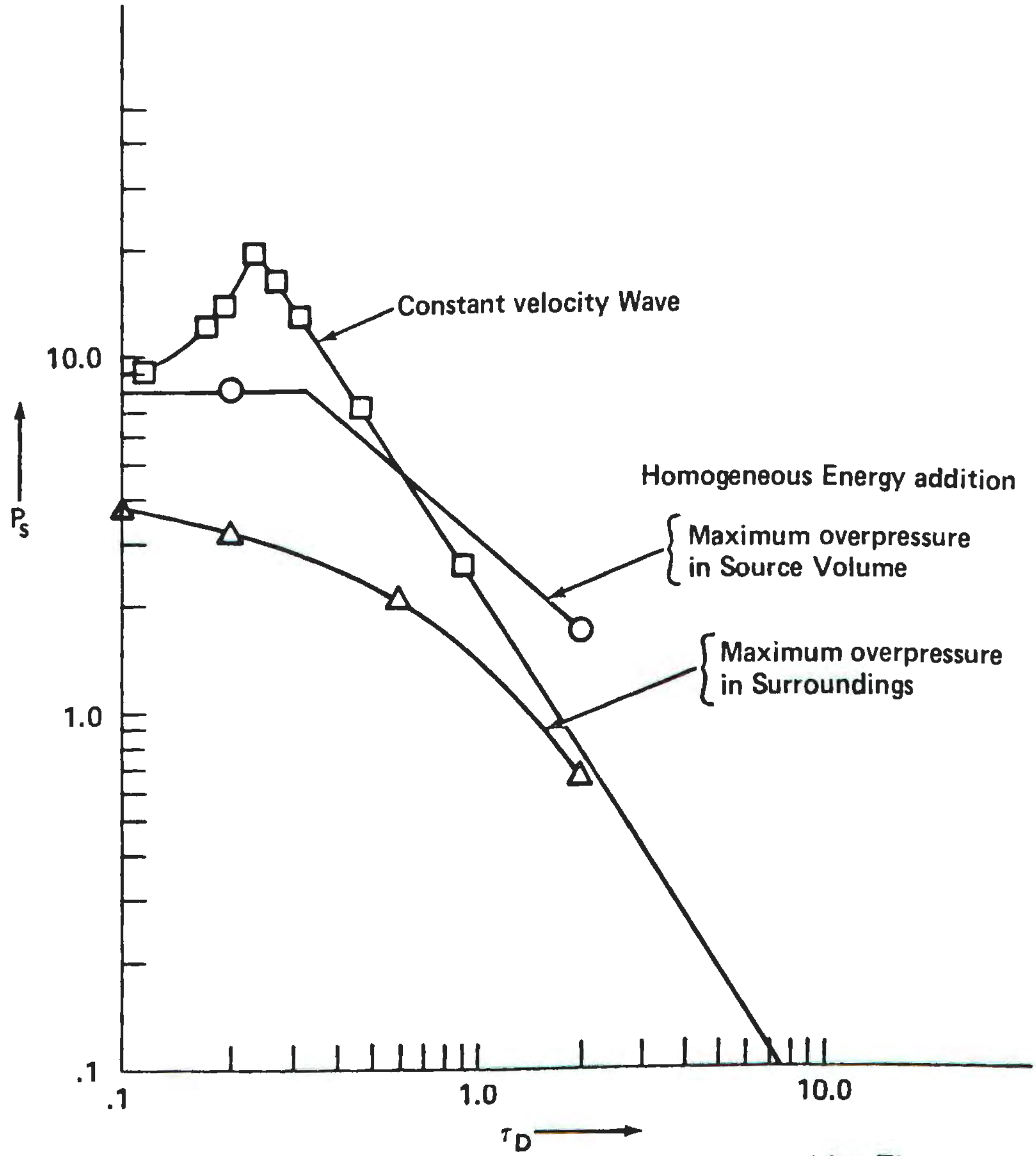

Figure 78. Maximum Overpressure vs Source Volume Deposition Time.

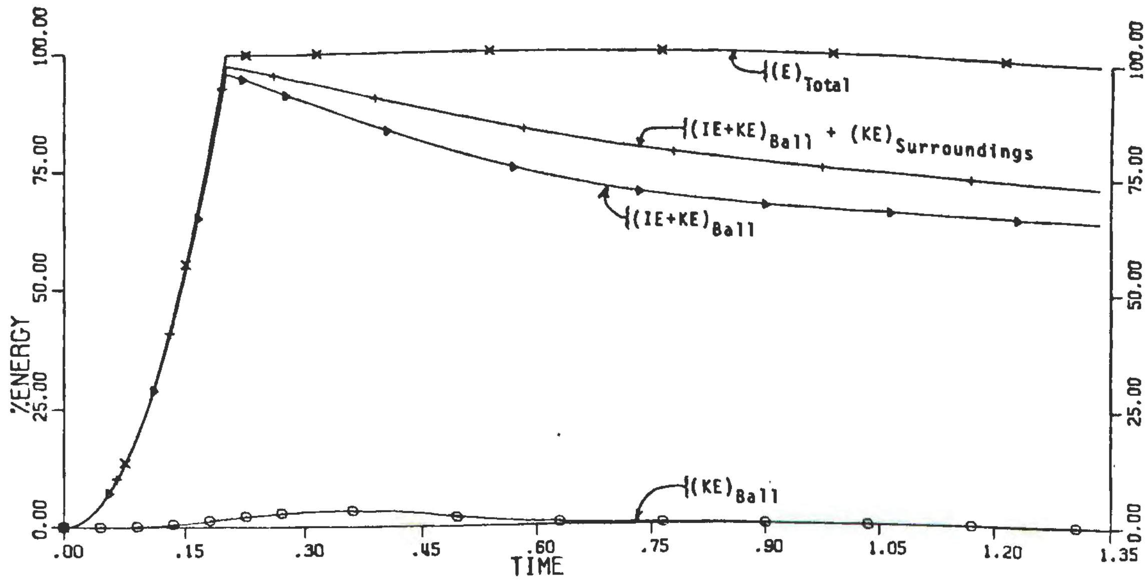

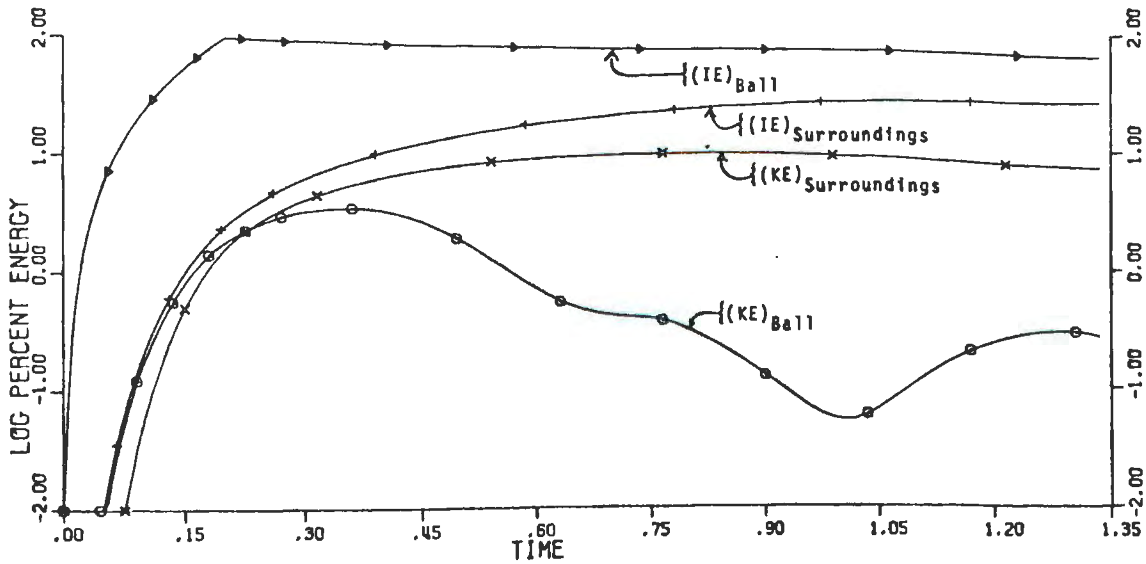

Figure 79. Energy distribution versus time behavior in a blast system generated by a τ_D=0.2 homogeneous energy addition.

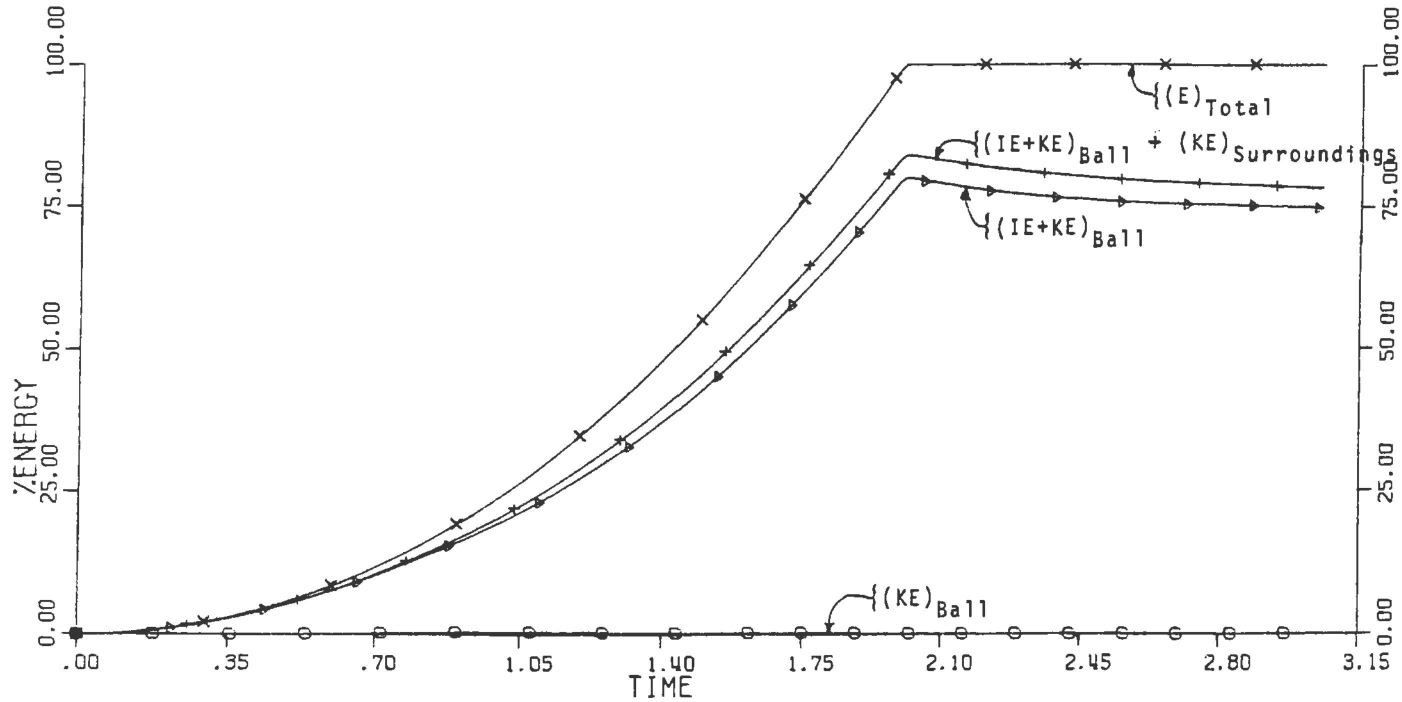

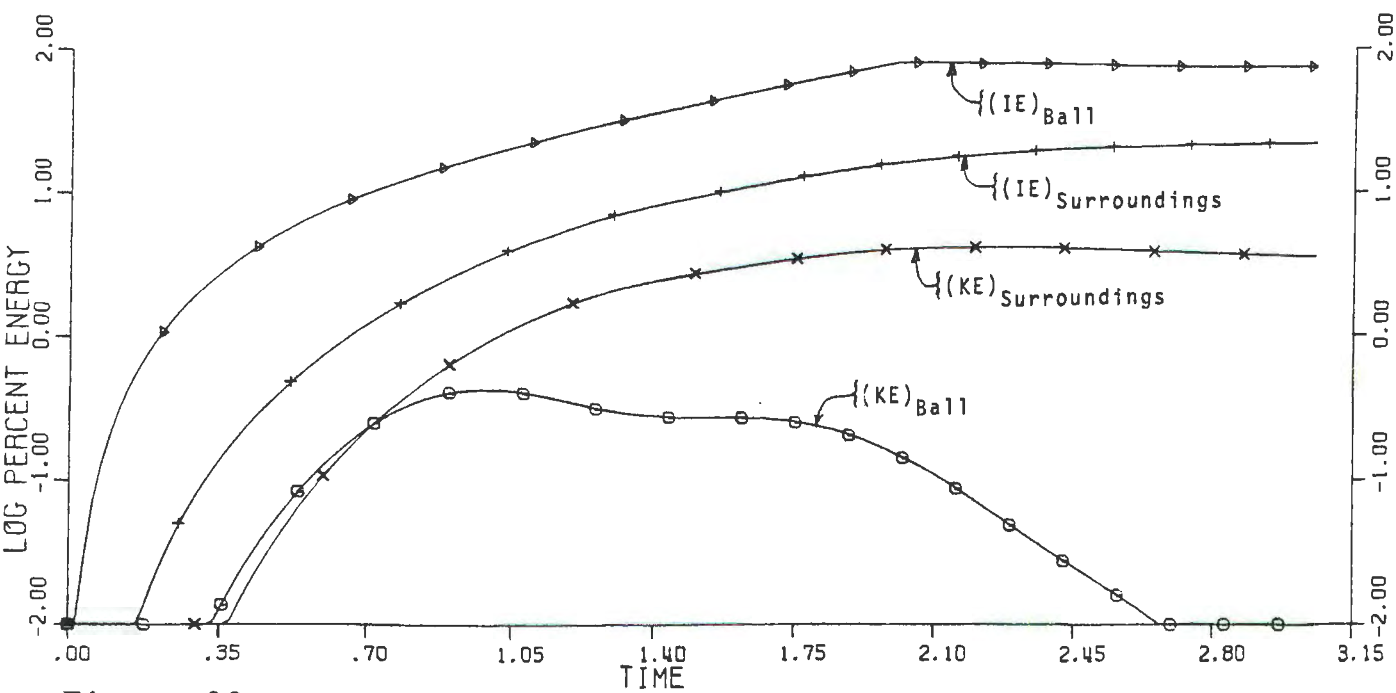

Figure 80. Energy distribution versus time behavior in a blast system generated by a τ_D=2.0 homogeneous energy addition.

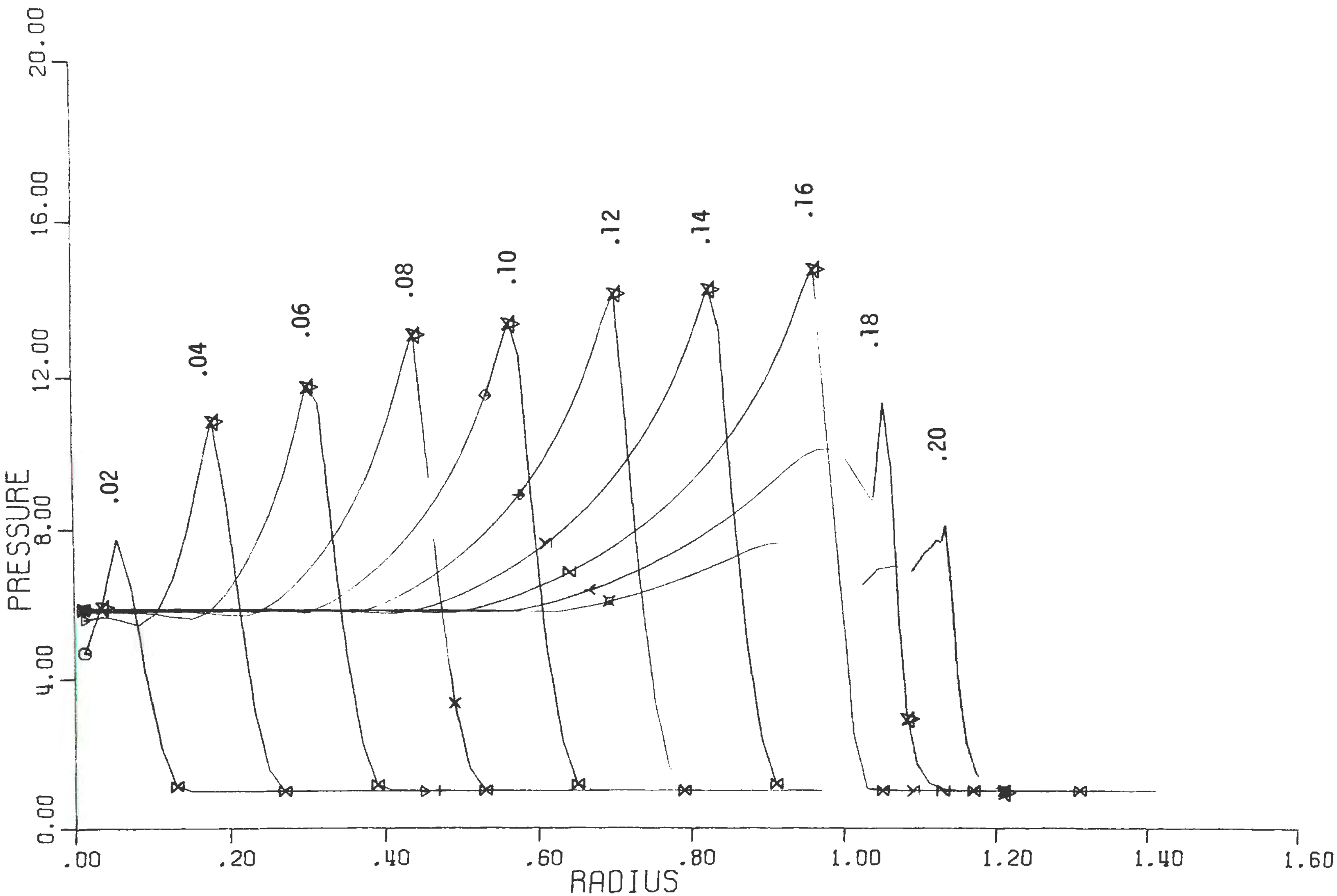

Figure 81. Pressure distribution versus Eulerian distance and tim[illegible] blast system generated by a Mach 5.55 energy addi ion wave (Fishburn's case study).

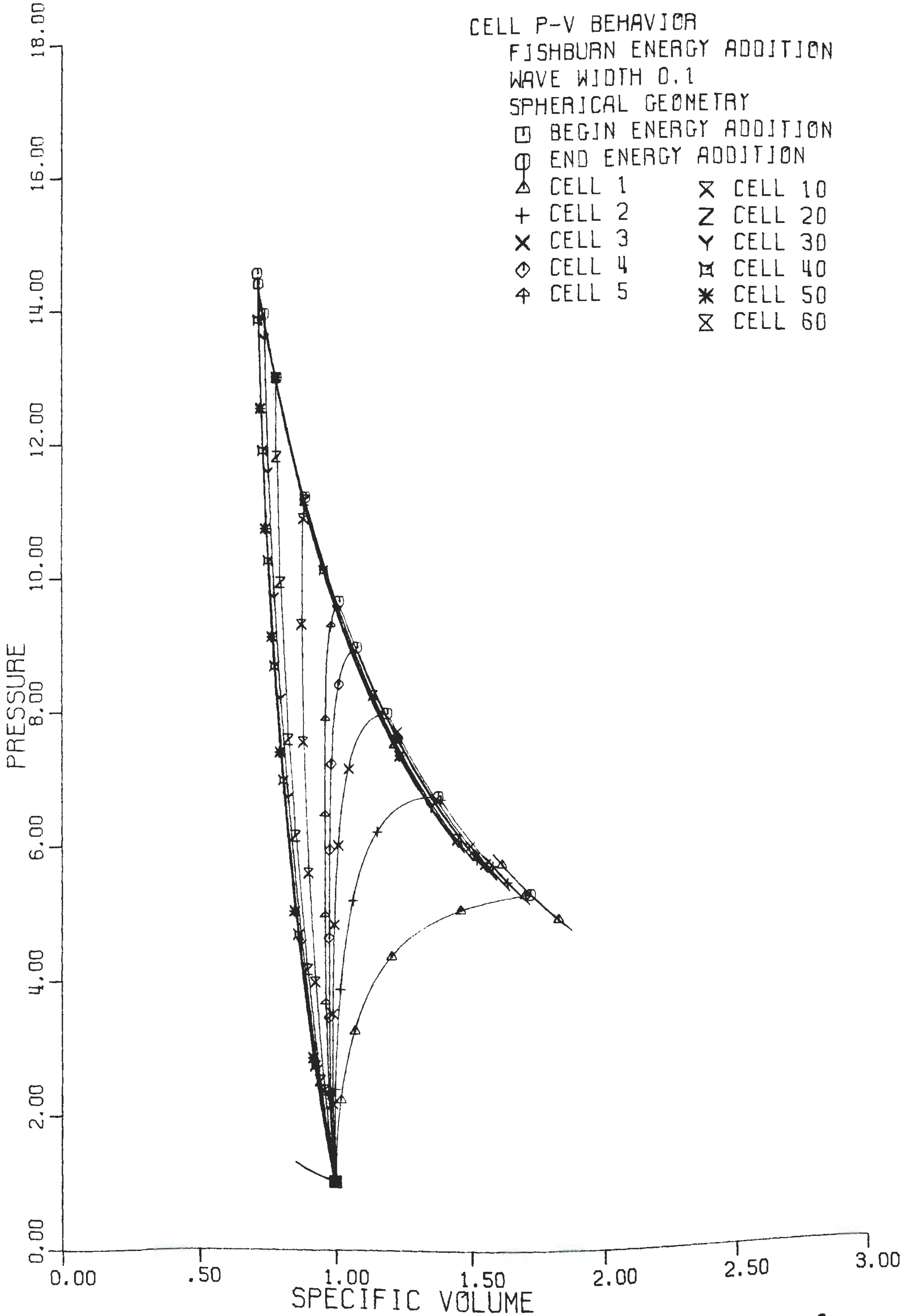

Figure 82. Pressure versus specific volume behavior from a Mach 5.55 energy wave (D = 1.0 at cell 50).

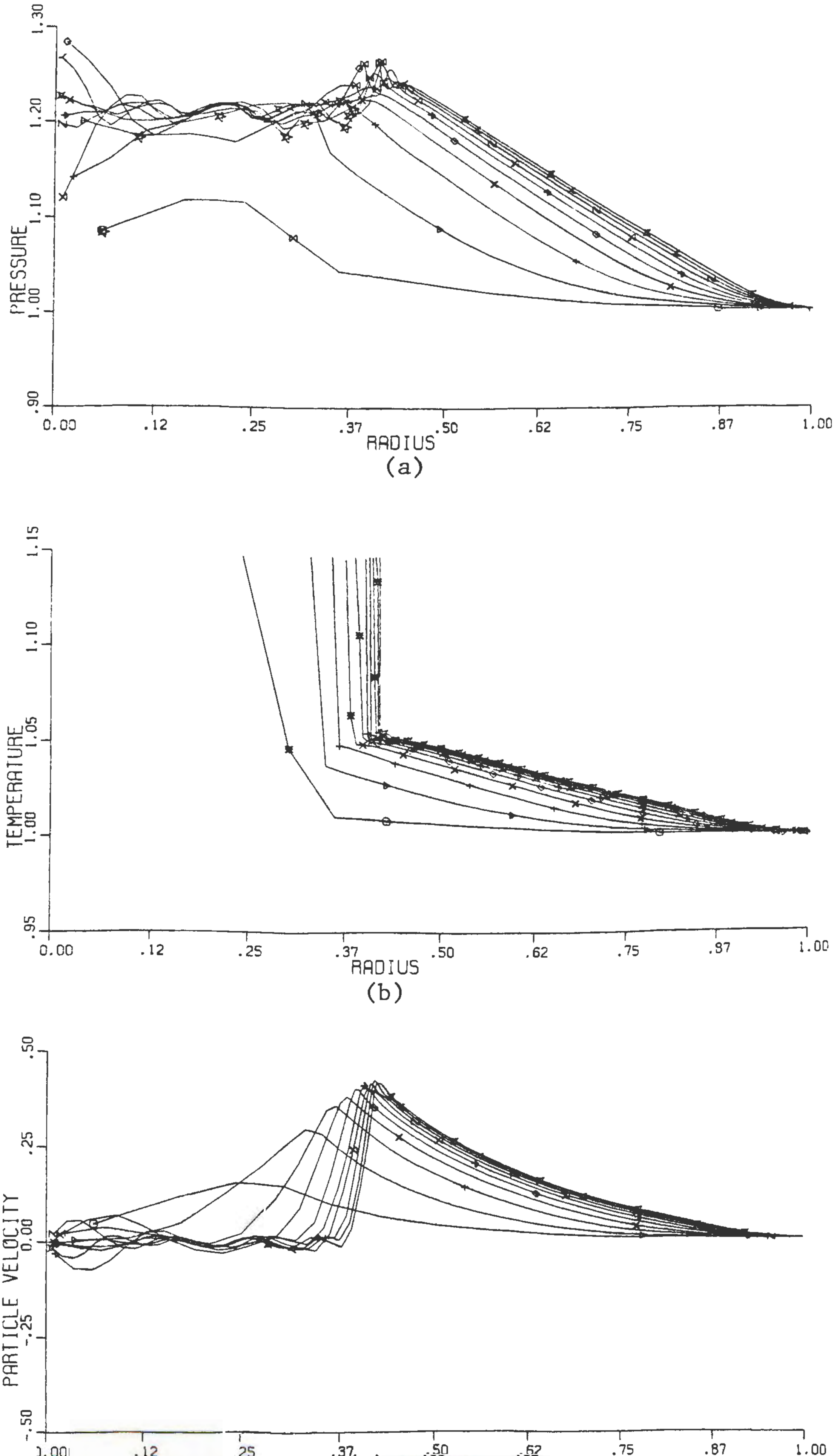

Figure 83. Pressure, temperature, and particle velocity versus similarity radius from energy addition

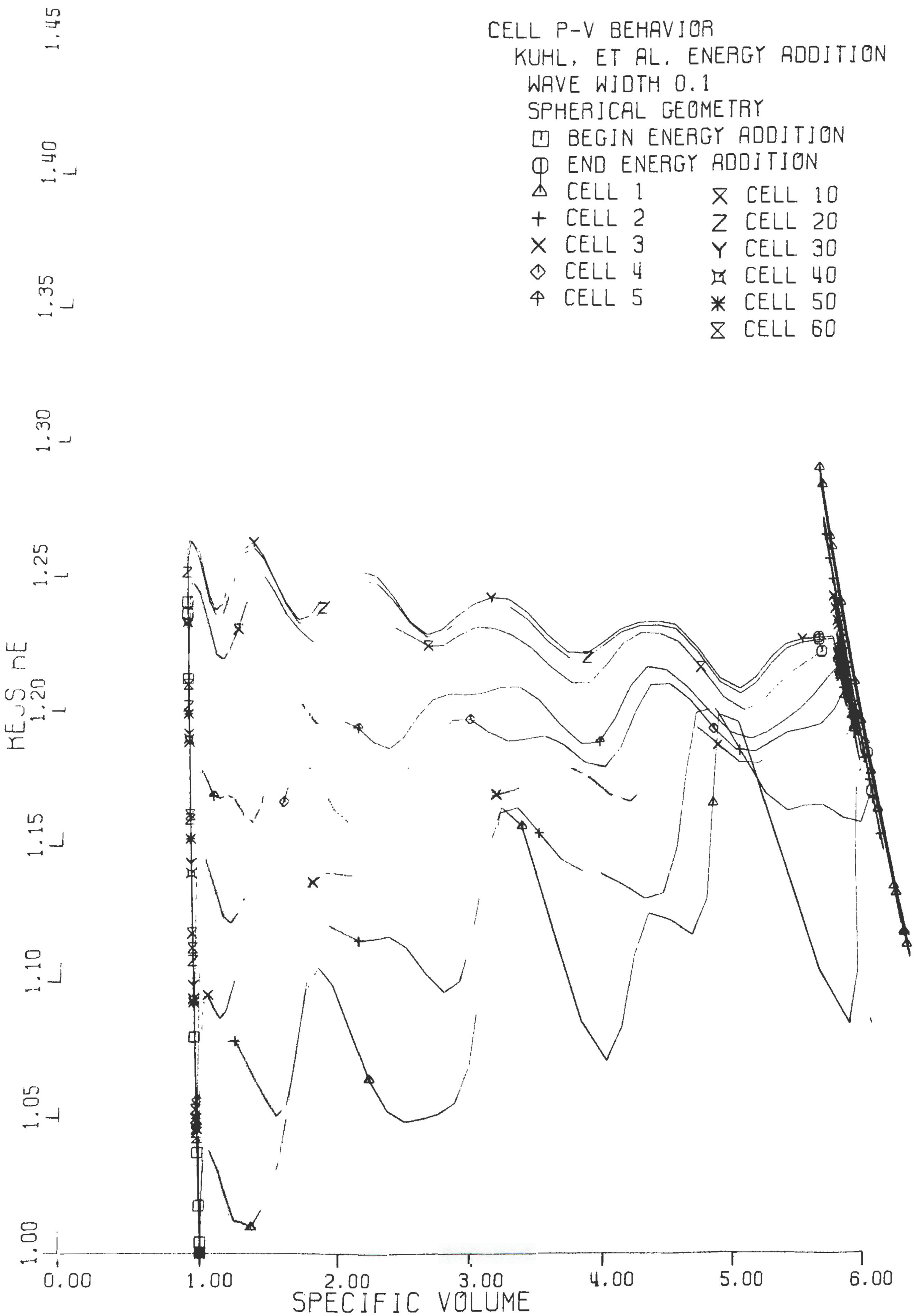

Figure 84. Pressure versus specific volume behavior from Kuhl, et al., case energy wave (D = 1.0 at cell 50).

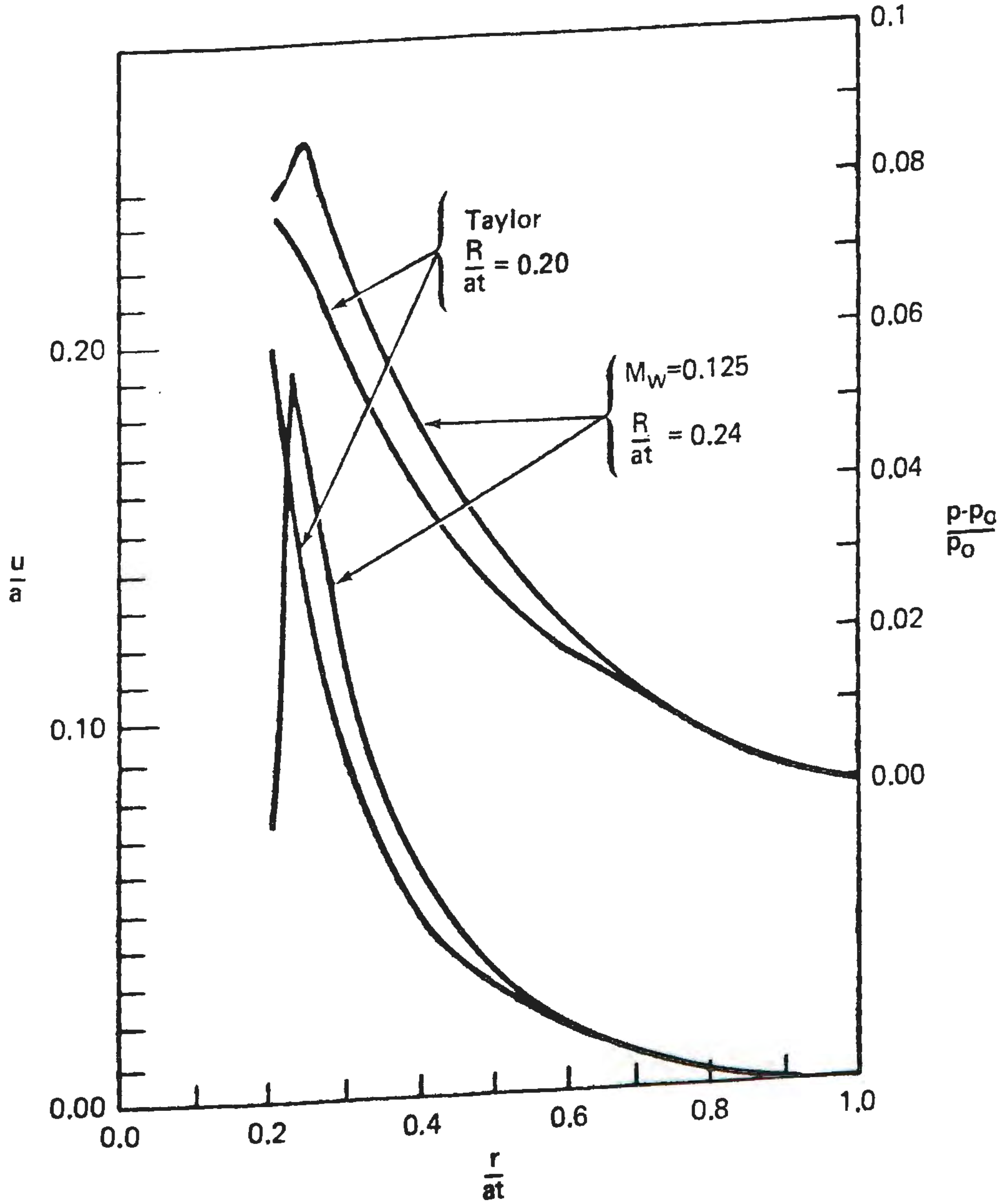

Figure 85. Comparison of pressure and particle velocity distribution of Mach 0.125 energy addition wave with results predicted by Taylor.

VI CONCLUSIONS AND RECOMMENDATIONS

In conclusion, this dissertation presents a systematic theoretical study of both the near and far field effects of constant velocity flames. Earlier studies included only the development of a self-similar solution during energy addition. None of the previous studies included blast wave behavior after the end of energy addition.

In this dissertation, the non-steady, one-dimensional fluid dynamic equations of motion with divergence and energy source terms, subject to the appropriate boundary conditions, were integrated using a Von Neumann/Richtmyer - type finite difference numerical integration procedure. The calculations yielded the thermodynamic changes and fluid-dynamic behavior associated with the propagation of the blast wave. Particular attention was directed to changes in peak pressure, positive impulse and energy distribution. In particular the relationship of non-steady behavior to steady-state behavior was noted.

A. Conclusions

On the basis of this investigation the following conclusions have been reached:

1. Near Field Behavior For Methane

a. In assessing potential damage from non-ideal explosions, preliminary estimates can be made from the values predicted by steady-state theory. For the cases of supersonic combustion from CJ velocity through infinite velocity (bursting sphere) the overpressures symptotically approach the values predicted by steady-state theory.

b. As the flame velocity decreases from infinite velocity, even through velocities impossible by steady-state theory, the pressure increases to a maximum of $P \simeq 20.0$ at a Mach number of 4.0.

1.) As the energy wave velocity increases above 4.0 the flame is moving so fast relative to the expansion behind the flame that the reinforcement of the pressure decreases.

2.) For flame velocities below Mach 4.0 a significant amount of the energy is taken up in the expansion through the flame front. This results in a decrease in the peak pressure as the Mach number decreases. For a 50% decrease in the wave velocity the following relationship holds:

overpressure(50% velocity) = 0.35{overpressure(100% velocity)}

3.) For flame velocities much less than the ambient velocity of sound the pressure and particle velocity distribution closely match the results originally predicted by Taylor [13].

2. Far Field Behavior For Methane

a. In the far field, the overpressure for all supersonic flame velocities approach 65% of high explosive at equivalent energy scaled radius.

b. At subsonic flame velocities the overpressure is significantly less than either the high explosive or the supersonic energy addition. When calculations were terminated, the Mach 0.5 case had reached 84% of the supersonic overpressure and the Mach 0.25 case had reached only 23% of the supersonic overpressure at $\eta=10.0$.

3. General Observations

a. For equal source volume deposition times the wave addition of energy produced greater overpressures than the homogeneous energy addition. This is attributed to the propagation of the energy addition wave interacting with the fluid dynamics of the flow field to develop greater overpressures. In the homogeneous energy addition there is no reinforcement of pressure.

b. In cases where the flow should reduce to a self-similar solution and/or show Rayleigh line behavior it did. The calculations showed that the flow field behaved normally where expected, and in the forbidden region, where steady-state behavior is not expected, non-steady behavior was observed.

c. Maximum energy transfer to the surroundings from the blast process occurs at a flame velocity of Mach 4.0, corresponding to the maximum overpressure in the flame.

1.) At flame velocities greater than Mach 4.0 the energy transfer to the surroundings decreased to the energy transfer associated with constant volume energy addition (bursting sphere) in the limit.

2.) At flame velocities less than Mach 4.0 the energy transfer to the surroundings decreased, approaching the energy transfer predicted for constant pressure deflagration.

d. For the energy density investigated, $q = 8.0$, the use of ideal (point source) theory results in an overestimation of the damage potential of these explosions.

e. In as much as the energy density, q, of most hydrocarbons are all approximately equal, the conclusions reached can be applied with reasonable confidence to other gases and flammable liquids having energy densities in the range of $6<q<10$.

f. Climatic conditions such as fog, mist, or rain could be accounted for in terms of an adjustment of the available energy. The determination of the energy density would include an accounting of the latent heat of evaporation of the water.

B. Recommendations

The findings of this dissertation lead to the following recommendations for future investigations:

1. Flame velocities are affected by the degree of mixing, chemical reaction kinetics, and the method of initiation of energy release. It is recommended that both experimental and theoretical studies by undertaken to determine the effect of these ignition related parameters on the development of constant velocity flames.

2. An important aspect of blast wave behavior not covered here is how the blast wave is established following ignition. It is recommended that theoretical experimental studies be initiated to evaluate the onset of blast conditions and include the limit cases of low energy ignition in a stagnant atmosphere through shock/thermal initialed ignition.

Appendix A

Computer Program for the Model

The computer program used for the calculation of blast wave properties consisted of a main program and eight subroutines. The main program, AMAIN, performed the finite differencing calculations. Subroutine BURST controlled the printing of the front and back cover pages of the printed output. Subroutine FIDIF controlled the printing of the data at selected intervals of time or selected iteration intervals. Subroutine GENDAT generated the initial conditions for the flow field. Subroutine INITIL determined the initial time step, and initialized program variables. Subroutine INT calculated the energy in the flow field. Subroutine PUDAT stored the data on tape at selected intervals of time or selected iteration intervals. Subroutine RESTAR stored the properties of the flow field at the last time line for continuing the run later. Subroutine SAMPLE calculated the location of the shock front.

For an initial run all input variables are read from unit 5. For a restart of an earlier run, the first card with LSTART = 1 is read from unit 5 and the RESTAR data file from the previous run is read as unit 15. The input variables for the program are:

<u>First Card</u>

LSTART: Run number for each case;
set to (0) for initial case
set to (1) for restart from stored data

OTRACE: Logical variable for printing intermediate calculations during error tracing.

Set to (T) for intermediate results

Set to (F) for no intermediate results

OTAPE: Logical variable to stop calculations When limits on storage space for results is approached

Set to (T) if there are no limits to storage space

Set to (F) if program is to stop after 10000 lines of data stored.

(Note: Value of maximum number of lines can be varied by changing main program.)

<u>Second Card</u>

NCYCLE: number of completed calculations along the time coordinate; Set to zero (0) for initial run.

NPUNCH: switch for punching or storing results at termination of the run. (0) implies no stored results. (1) implies store results for a restart.

NSTORE: Control for storage of results for analysis.
(0) implies no intermediate storage.
(1) implies storage for all cells.
(i greater than 1) implies store the results for i+e cells where there are (i) cells between the origin and the maximum of pressure, and (e) cells between the maximum of pressure and the limit of the pressure wave at the same intervals as for (i).

NS: Store results of every NSth cycle on tape.

<u>Third Card</u>

LABEL(7): Identification for leading and trailing title pages

Fourth Card

NSTEPS: A limit for the number of time lines to be calculated in the run.

NFINAL: A limit for the number of property cells (grid points) which may be used in the run.

NN: Print flag, Print result of every NNth cycle. The results are printed if NCYCLE is a multiple of NN. Note that the value of NCYCLE is carried along with the restart data.

NNN: Print flag, Print results of every NNNth cell at every NNth cycle. If NNN is negative, property values will be printed for 26 cells evenly spaced from the origin to the outer cell, including the outermost cell.
If NNN is greater than 1000 a variable NSAM is set equal to NNN-1000 and properties are printed at NSAM positions between the origin and the maximum pressure, at the same interval between the maximum pressure and the outermost cell and at the outermost cell.

TERMIN: Limit for the amount of central processor time the program may use for calculations in seconds. (This is the third means of terminating the calculations)

TIPUN: Print flag, print results at specified time intervals. Intermediate results are stored at multiples of TIPUN according to the spacing of NSTORE.

NBUFF: Switch for homogeneous energy addition.
(0) implies no homogeneous energy addition
(1) implies homogeneous energy addition

NFREQ: Dummy Variable, not used as input.

NWAVE: Switch for wave addition of energy
(0) implies no energy wave
(1) implies energy addition wave

Fifth Card

NDP: Current number of data points (used to define the number of initial time-line data cards)
(0) implies program to generate initial values at grid points.

J: Geometry Factor along time line
(0) - Planar
(1) - Cylindrical
(2) - Spherical

NLI: Cell number corresponding to a change in the value of gamma, largest cell number with G4

CL: Linear coefficient of artificial viscosity

CO: Quadratic coefficient of artificial viscosity

G: Gamma of the surrounding gas

G4: Gamma of the core gas (GF)

UL: Value of the flow velocity at the left boundary

UR: Value of the flow velocity at the right boundary

ENERGY KERNEL PROFILE CARD: (Inserted if (NBUFF .NE.0)) Specifies Homogeneous Source Parameters

SLOSOR: Slope constant in energy function

SOREXP: Shaping constant in the energy function

TMAXE: Non-dimensional maximum time of energy addition

ENMAX: Non-dimensional maximum amount of energy added

MINCOS: Cell number corresponding to the beginning of the spatial rounding function

MAXCOS: Cell number corresponding to the outermost edge of the energy function.

ENERGY WAVE PROFILE CARD (Inserted if (NWAVE.NE.0))

Specifies Energy wave parameters

WVEL: Non-dimensional Mach number of energy wave

WIDWAV: Thickness of energy wave as fraction of source volume

ENWAU: Non-dimensional maximum amount of energy added

WSLSOR: Slope constant in energy wave

WSREXP: Shaping constant in energy wave

MNWCOS: Cell number corresponding to the beginning of of the spatial rounding function

MXWCOS: Cell number corresponding to the outermost cell of the source volume.

PRESSURE BURST DATA CARD:

PRESS: Initial pressure ratio

TEMP: Initial temperature ratio

N: Cell number corresponding to the edge of the energy kernel

NDEC: Number of fairing cells in the pressure source rounding function

INITIAL TIME LINE DATA CARDS: IF (NDP .GT. 0) a series of N cards is expected to specify the necessary thermodynamic and fluid-dynamic parameters for each mesh point on the initial time line.

K: Cell number (must be numbered consecutively 1 - N.)

R(1,M): Position of the m^{th} cell inner boundary

U(1,M): Velocity of the m^{th} cell inner boundary

P(1,M): Pressure in the m^{th} cell

V(1,M): Specific volume in the m^{th} cell

Q(1,M): Artificial viscosity in the m^{th} cell

In addition to the printed output there are four data files in which results are stored. Unit 17 is the restart file in which the program variables and cell properties are stored for later continuing the run. Unit 18 stores the pressure and specific volume of selected cells at each time line for examining the p-v behavior. Unit 19 stores cell properties at selected time intervals or cycle intervals. Unit 20 stores the location and properties at the shock front.

```
@FLIST,E
UOM FILE LISTER   01/14/77   14:42:39
END FLIST  19 CARDS GENERATED.

@HDG,P  ******  AMAIN  ******

@ELT,L AMAIN
ELT 6B-01/14-14:42 AMAIN
      C********* THIS PROGRAM FILE IS FOR CHANGE OF GAMMA ACROSS
      C             THE ENERGY ADDITION*****************
            IMPLICIT DOUBLE PRECISION (A-H,P-Z),LOGICAL (O)
            REAL     TA,TB,TC,TD,THF,TAP,TCN,XCPU,XMEM
         11   COMMON / ARRAYS / U(2,201), R(2,201),V(2,201 ),Q(2,201),
          U                       P(2,201), X(201), E(2,201), NCELL(201),
          2                       WE2CL(201),WE1CL(201),A(201),GCOS(10)
         13  COMMON/ TIME / TERMIN , TIPUN, T, DT, DTL,
          *                       KRUN(3), LABEL(7)
            COMMON / PARAM / CI , CO, G, GF, UL, UR , GMW, GFMW, ENMAX, ET,
          3                       PJ1,SLOSOR, SOREXP, TMAXE, TWO, WUN, ZERO    ,
          4                       MINCOS, MAXCOS, J, JP1, N, NL, NL1,NOP,
          5                       NPART, NSTEPS, OFNI, OESOR, OPEAK, OPLANF,
          6                         OPRINT, OPUTI, OSKIP, OSPHER,OTRACE,
          7                MWTAIL,MWHEAD,WVEL,WIDWAV,ENWAV,RHEAD,RTAIL,
          8                WSLSOR,WSREXP,MNWCOS,MXWCOS,OFWAV,RFF,F2CL
         22 COMMON / ARGINT / INDEX, LSTART, NCYCLE, NFINAL, NSTORE, NS,
          7                       NN, NNN, NPEAK, NSAM, NSHIF,NBUFF,NFREQ,NWAVE
          2                ,NPUNCH
         23  DIMENSION LABEL(7)
         24  FORMAT()
         25  FORMAT(' ','164',3I5,10E10.4)
         26 FORMAT( )
         27 FORMAT(1H0,'COMPUTER TIME IS APPROACHING DESIGNATED MAXIMUM')          27
         28 FORMAT(1H0,'DIMENSION-LIMIT STOP')
         29 FORMAT(1H0,'TIME STEPS EQUAL DESIGNATED MAXIMUM')
         30 FORMAT( 1H0,'NON-POSITIVE TIME STEP')
         31  FORMAT(' ','AT TIME ',1PE12.6,' THE ENERGY INTEGRAL EQUALS ',
          1               E12.6,' WITH ',I4,' CELLS')
         32  FORMAT(' ','116',6I5,5D10.4)
         33  FORMAT('1',//)
         34  FORMAT(1H0,' LW  WCM  WAA  WSLSOR  WSREXP  WCM1',/I5,5D20.10)
         35  FORMAT(1H0,' THE  TA   TAP  TERMIN  ',/ 4E20.10)
         36  FORMAT(7A4)
         37  FORMAT(' ','224',I5,11E10.4)
         38  FORMAT(' ',' 205',I5,11E10.4)
         39  FORMAT(' ','M     DT           DTMIN          DTTES     GRADTA       ',
          1          'DEM         R2MP        R2M          BS2    BS1  BDOTN  AS2')
         40  FORMAT(I5,11E10.4)
         41  FORMAT(' ','234',2I5,7E15.9/8E15.9)
         42  FORMAT(' ','108',2I5,2E10.4)
         43  FORMAT(' ','186',I5,5E20.14/6E20.14)
         44  FORMAT(' ','204',I5,6E18.12)
         45  FORMAT(' ','247',2I5,4E20.14)
         46  FORMAT(' ','300',2I5,6E15.9)
         47  FORMAT(' ','305',I5,5E20.14)
         48  FORMAT(' ','LAGRANGIAN POSITION OF HEAD IS ',F12.6,
          1          ' AND TAIL IS ',F12.6)
         49  FORMAT(' ','THE SPECIFIC VOLUME OF CELL',I5,' IS NEGATIVE')
         50  FORMAT(' ',3I5,7E14.8)
         51  FORMAT(' ','STORAGE FILE OVERFLOW')
         52  FORMAT(' ','*********GAMMA CHANGES AT WAVE FRONT*******')
         53  FORMAT(' ',6E20.15/7E17.12)
         54  FORMAT(' ','EXIT FOR INSTABILITY IN TIME STEP')
         55  FORMAT(' ',2I5,7E15.8)
         56  FORMAT(' ','142',I5,6E15.7/7E15.7)
             WRITE(6,33)
      C****                      DETERMINE INITIAL OR RESTART CONDITIONS
                CALL MTIME(XCPU,XMEM)
             TA=XMEM
            INDEX = 0
            WUN = 1.D0
            ZERO = 0.D0
            TWO = 2.D0
            THREE = 3.D0
            EIGHT = 8.D0
```

```
              SIXTEE = 16.D0
              ENINE = 9.D0
               IST=0
                PI = DACOS(-WUN)
      C
               READ(5,24)LSTART,OTRACE,OTAPE
               OSTART = LSTART .EQ. 0
                  IF(OSTART)  GO TO 57
                  CALL RESTAR
                  GO TO 58
           57  READ( 5,26    )  NCYCLE, NPUNCH, NSTORE,NS
               READ(5,36) LABEL
      C
           58     CALL INITIL
      C                INITIL=611
                  IF(.NOT. OSTART)GO TO 59
               T=ZERO
               NPEAK=1
                  CALL PUDAT
               T=DT
               IST=IST+N
           59  WRITE(6,52)
              LSTART = LSTART + 1
               NFRPR=LSTART
                  IF(OTAPE)NFRPR=20
               TAP = TA + 30.
              THF = TERMIN- TWO
                  IF(OTRACE)WRITE(16,35)THE,TA,TAP,TERMIN
               IF(THE .LT. TA) THE = TAP
              OSPHER = J .EQ. 2
              OPLANE = J .EQ. 0
              OPRINT = .FALSE.
              ONOVIS = CL .LE. ZERO .AND. CO .LE. ZERO
              OPUN = .FALSE.
              OPUTI = TIPUN .GT. ZERO
              OSKIP = NS .LE. 0
              OADDEN = .FALSE.
               OFE=.FALSE.
               OFEND = .FALSE.
               OEXIT = .FALSE.
              OVFR = .TRUE.
               NPR=0
               NNFIN=201-11
                  IF(N .GE. NNFIN)GO TO 315
                  IF(NFINAL .GT. NNFIN)NFINAL = NNFIN
                  IF ( .NOT. OESOR )  GO TO 84
              ENSTEP = ENMAX / 100.D0
                     DO 81    L = 1,10
              AA2 = AA1
              AA1 = AA
               CM2 = CM1
              CM1 = CM
                  IF ( L - 2 ) 72, 74, 76
           72  AA = DLOG ( SLOSOR + WUN + WUN / SOREXP )
                  GO TO 77
           74  AA = .95D0 * AA
                  GO TO 77
           76  AA =AA1+(SLOSOR-CM1)*(AA2-AA1)/(CM2                      -CM1)
           77  CM=DEXP(AA)-WUN+(DEXP(-AA/SOREXP)-WUN)
            *            / SOREXP
                   IF ( DABS (( CM - SLOSOR ) / SLOSOR ) .LT. 1.0D-7 )
           *        GO TO 82
           81 CONTINUE
           82      IF(.NOT. OSTART)GO TO 83
               E2CL=ZERO
           83 SORSPA = MINCOS - MAXCOS
           84      IF( .NOT. OEWAV) GO TO 91
                   DO 89  LW = 1,10
               WAA2=WAA1
               WAA1 = WAA
               WCM2 = WCM1
               WCM1 = WCM
                   IF(LW - 2) 85,86,87
           85  WAA = DLOG(WSLSOR+WUN+WUN/WSREXP)
                   GO TO 88
           86  WAA = .95D0*WAA
```

****** AMAIN ******

```
              GO TO 88
   87   WAA = WAA1+(WSLSOR-WCM1)*(WAA2-WAA1)/(WCM2-WCM1)
   88   WCM = DEXP(WAA)-WUN+(DEXP(-WAA/WSREXP)-WUN)/WSREXP
              IF(DABS((WCM-WSLSOR)/WSLSOR) .LT. 1.0D-7) GO TO 90
   89 C O N T I N U E
   90   WSRSPA = MNWCOS-MXWCOS
              IF(OTRACE)WRITE(16,34)LW,WCM,WAA,WSLSOR,WSREXP,WCM1
        TWID = WIDWAV/WVEL
        ENMAX = ENWAV
        SLOSOR = WSLSOR
        TMAXE = TWID
        SOREXP = WSREXP
        ENSTEP = ENWAV/100.D0
        STWDWV = WIDWAV
        AA = WAA
        PHI = ZERO
              IF(NCYCLE .GT. 0)GO TO 91
        WT1 = T * WVEL
              IF(WT1 .LT. R(1,9))N = 10
C***           ***REMAINDER OF THESE WAVE CALCULATIONS AT 204*****
C
   91         IF ( .NOT. OPUTI )  GO TO 92
      M = T/TIPUN
      TNEX = M+ 1
        TLINE = TIPUN*TNEX
C(**             SET INDEX NUMBER
C
C***                *** CALCULATIONS FOR NEW TIME STEP ********
C
C
   92   INDEX = INDEX + 1
        NCYCLE = NCYCLE + 1
C *****CHECK STABILITY OF TIME STEP *****
              IF(.NOT. OEXIT) GO TO 95
       WRITE(6,54)
             GO TO 312
C 94                         CHECK CENTRAL PROCESSOR ELAPSED TIME
   95         CALL MTIME(XCPU,XMEM)
       TB = XMEM
      TC = TB-TA
      TCN=TC+TC/5.
      TD = THE - TB
      TA = TB
              IF ( TCN.LT. TD )  GO TO  99
       WRITE (6,27)
             GO TO  312
C ********* CHECK FOR STORAGE OVERFLOW ***********
   99   IF(OTAPE)GO TO 103
              IF(IST .LT. 10000)GO TO 103
        WRITE(6,51)
              GO TO 312
C***              CHECK NUMBER OF STEPS
  103         IF ( INDEX .LE. NSTEPS ) GO TO 107
        WRITE(6,29)
        GO TO 312
C 106                  CHECK FOR DIMENSION LIMIT STOP OR MESH EXPANSION
  107   NO = N
        NM2=N-2
        DELP = (P(1,NM2)-P(1,N))/TWO
              DO 111 I= NM2,NFINAL
        PABS = DABS(P(1,I)-WUN)
              IF(OTRACE)WRITE(16,42)I,N,PABS,V(1,I)
              IF ( PABS .LE. 9.0D-14) GO TO 115
        N = I + 4
        NL = N-1
        PNL=DABS(P(1,NL)-WUN)
        PN= DABS(P(1,N)-WUN)
              IF(PNL .LE. 9.0D-17)GO TO 108
              GO TO 109
  108         IF(PN .LE. 9.0D-17)GO TO 111
  109         DO 110 J=1,2
              DO 110 M=1,201
        WRITE(6,55)M,J,P(J,M),V(J,M),R(J,M),U(J,M),Q(J,M),E(J,M),WE2CL(M)
  110   CONTINUE
  111   CONTINUE
        WRITE (6, 28)
```

```
            GO TO 312
C 114               DETERMINE PROPERTIES AT NEW TIME
C 114
  115   NL=N-1
            IF(N .EQ. NO) GO TO 117
            DO 116 I = NO,N
        P(1,I) = P(1,I-1)-DELP
            IF(P(1,I) .GT. WUN) GO TO 116
        P(1,I) = WUN
            GO TO 117
  116   CONTINUE
  117 DTN = ( DT+DTL)/TWO
C***            MOMENTUM CONSERVATION
C***            CALCULATE NEW VELOCITIES AND TRAJECTORIES
C***            LEFT BOUNDARY CONDITIONS
      IF(OTRACE)WRITE(16,32)NCYCLE,INDEX,NL,N,I,NSTEPS,T,DT,DTL,DTN,PARS
      U(2,1) = UL
C***            FIRST SIGMA FORWARD
        SIGMAF = -P(1,1)-Q(1,1)
C***            FIRST F1
        F1 = (R(1,2)-R(1,1))/V(1,1)
        R(2,1) = R(1,1)+UL*DT
      R1MP = R(1,2)
C
C
C
            DO   142   M = 2,NL
C 127                 VELOCITY AT GENERAL POINT
C***             INTERMEDIATE SIGMA VALUES
        SIGMAB = SIGMAF
        SIGMAF = -P(1,M)-Q(1,M)
C***            PHI PARAMETER
        F0 = F1
        R1M = R1MP
        R1MP = R(1,M+1)
        F1 = (R1MP-R1M)/V(1,M)
        PHI = ( F1+F0 ) / TWO
C***            VELOCITY
        U2M = U(1,M)+(DTN/PHI)*(SIGMAF-SIGMAB)
        U(2,M) = U2M
C***            TRAJECTORY
        R(2,M) =  R1M+U2M*DT
            IF(OTRACE)WRITE(16,56)M,R(2,M),R1M,U2M,U(1,M),PHI,
     *                 SIGMAF,SIGMAB,F1,F0,R1MP,R1M,V(1,M),R(2,1)
  142   CONTINUE
C***            RIGHT BOUNDARY CONDITIONS
        U(2,N) = UR
        R(2,N)= R(1,N)+UR*DT
C***            CONTINUITY CONSERVATION
C***            CALCULATE NEW SPECIFIC VOLUMES BASED ON CONTINUITY
C 152                 CONTINUITY
        U13 = U(2,1)*U(2,1)*U(2,1)
            IF(.NOT. OESOR)GO TO 160
            IF(OEND)GO TO 159
       E1CL = E2CL
        PHI = T / TMAXE* AA
        E2CL = ( ENMAX / CLOSOR ) * (( DEXP ( PHI ) - WUN) +
     *         (DEXP( -PHI* SOREXP) - WUN ) / SOREXP)
        OEND=T .GT. TMAXE
        OADDEN = .TRUE.
            IF(OEND)E2CL=ENMAX
        DELENG = E2CL - E1CL
            GO TO 160
  159   OEE=.TRUE.
  160       IF ( .NOT. OEWAV) GO TO 163
            IF(OEEND) GO TO 163
        WIDWAV = STWDWV
        RRHEAD=T*WVEL + REF
            IF( RRHEAD .LT. WIDWAV) WIDWAV = RRHEAD
        RRTAIL = RRHEAD - WIDWAV
        PHIW = ZERO
        RLHEAD = RRHEAD/REF
        MWHEAD=RLHEAD
        RLTAIL = RRTAIL/REF
        MWTAIL = RLTAIL
        MWTM1 = MWTAIL - 1
```

```
000              IF(MWTAIL .EQ. MWHEAD) MWTAIL = MWTM1
000              IF(MWTM1 .LE. MXWCOS)GO TO 163
000          MWHEAD=0
000          MWTAIL=0
000          OFEND= .TRUE.
000      163 F1 = U(2,1)
000              IF ( .NOT. OPLANE ) F1 = F1*(((R(2,1)+R(1,1))/TWO)**J)
000          GAMW = GFMW
000          U2MP = U(2,1)
000          QBAR = ZERO
000          NX = (NCYCLE/NN)*NN
000          OPRINT = NX .EQ. NCYCLE
000              IF(OTRACE)WRITE(16,25)MWHEAD,MWTAIL,MWTM1,RRHEAD,
000        1           RRTAIL,RLHEAD,RLTAIL,U2MP,F1,U13,R(2,N),GFMW,GAMW
000     C
000     C
000     C***     ***DO LOOP TO CALCULATE CELL PROPERTIES*****
000     C 165 ***
000     C
000     C
000                   DO 235 M= 1,NL
000          U2M = U2MP
000          U2MP = U(2,M+1)
000          V1M = V(1,M)
000          CHI = ZERO
000     C***          CHI PARAMETER
000              IF ( .NOT. OSPHER   )  GO TO 178
000          U03 = U13
000          U13 = U2MP**3
000          CHI = DT*DT*(U13-U03)/ 12.D0
000      178 F0 = F1
000          F1 = U2MP
000              IF (OPLANE) GO TO 184
000          F1 = U2MP*(((R(2,M+1)+R(1,M+1))/TWO)**J)
000      184 V2M = V1M+DT*(F1-F0+CHI)/X(M)
000              IF(V2M .GE. ZERO)GO TO 185
000          WRITE(6,49)M
000          WRITE(6,50)M,NCYCLE,INDEX,V2M,V1M,F1,F0,CHI,U13,U03
000              GO TO 312
000      185 V(2,M) = V2M
000     C***          ARTIFICIAL VISCOSITY
000     C***          CALCULATE A DISSIPATION TERM
000              IF ( ONOVIS )  GO TO 204
000     C***N         EXISTENCE CRITERIA
000              IF ( U2MP .GE. U2M )  GO TO 202
000              IF ( V2M .GE. V1M ) GO TO 202
000     C             COMPLETELY CENTERED PARAMETERS
000              IF(OTRACE)WRITE(16,43)M,U2M,U2MP,CHI,U03,U13,F0,
000        1           F1,V2M,V1M,X(M),DT
000          AC = DSQRT(P(1,M)/TWO*(V2M+V1M))
000          HETAC = ((WUN/V2M)+(WUN/V1M))/TWO
000     C             LINEAR TERM
000          UDIF =  DABS(U2MP-U2M)
000          QL = CL*AC*HETAC*UDIF
000     C             QUADRATIC TERM
000          QQ = CQ*CQ*HETAC*UDIF*UDIF
000     C             TOTAL ARTIFICIAL VISCOSITY FOR 1/2 POSITION FORWARD
000          Q2M =  QL+QQ
000              GO TO 203
000      202 Q2M =  ZERO
000      203 Q(2,M) = Q2M
000              IF(OTRACE)WRITE(16,44)M,AC,HETAC,P(1,M),UDIF,QL,QQ
000     C                END OF VISCOSITY CALCULATIONS
000     C
000     C     ENERGY CONSERVATION OF PERFECT GAS
000     C             CALCULATE NEW SPECIFIC ENERGY AND PRESSURE
000     C
000          QBAR = ( Q2M+Q(1,M))/TWO
000      204 ENUM = E(1,M)-(P(1,M)/TWO+QBAR)*(V2M-V1M)
000              IF(OTRACE)WRITE(16,38)M,ENUM,E(1,M),P(1,M),Q(2,M),
000        1           Q(1,M),V(2,M),V(1,M),QQ,QL,UDIF,AC
000     C
000     C
000     C***     ***WAVE ENERGY ADDITION*****
000     C
000     C
```

```
              IF ( .NOT. OEWAV) GO TO 225
              IF(.NOT. OEEND) GO TO 210
         GAMW = GFMW
         MC = M - MNWCOS
              IF(M .GE. MXWCOS)GAMW = GMW
              IF(M .GT. MNWCOS .AND. M .LT. MXWCOS)GAMW = GCOS(MC)
              GO TO 225
  210         OWVEND = .FALSE.
         GAMW = GMW
              IF(M .GT. MXWCOS) GO TO 220
              IF(M .GT. MWHEAD)GO TO 220
         GAMW=GFMW
              IF(M .LE. MWTM1) GO TO 220
              IF(M .LT. MWTAIL) OWVEND = .TRUE.
C***        *** PHI CALCULATIONS FROM 154 *****
         WE1CL(M)=WE2CL(M)
         DR = (RLHEAD-M)*REF
         PHIW = DR * WAA / STWDWV
              IF(PHIW .GT. PHI) PHI = PHIW
         WE2CL(M) = (ENWAV/WSLSOR)*((DEXP(PHIW)-WUN)+
     1   (DEXP(-PHIW*WSREXP)-WUN)/WSREXP)
              IF(WE2CL(M) .GT. ENWAV) WE2CL(M) = ENWAV
              IF (OWVEND) WE2CL(M) = ENWAV
         WDLENG = WE2CL(M) - WE1CL(M)
         DG = (G-GF)*(WE2CL(M)/ENWAV)
         GAMW = GMW - DG
              IF(M.GT.MNWCOS) GO TO 219
         WADENG = WDLENG
              GO TO 223
  219    WSPAN = M - MXWCOS
         WSPAN = WSPAN/WSRSPA*PI
         WSF = (DCOS(THREE*WSPAN)-ENINE*DCOS(WSPAN)+
     1    EIGHT)/SIXTEE
         WADENG = WDLENG * WSF
         MC=M-MNWCOS
         GCOS(MC) = GMW - DG*WSF
         GAMW = GCOS(MC)
                   GO TO 223
  220    WADENG = ZERO
  223    ENUM = ENUM + WADENG
              IF(M .EQ. MWHEAD)RHEAD=(R(2,M))+DR*(R(2,M+1)-R(2,M))
              IF(M .NE.MWTAIL)  GO TO 224
         DDR=(RLTAIL-M)*REF
         RTAIL=(R(2,M)) +DDR*(R(2,M+1)-R(2,M))
  224         IF(OTRACE)WRITE(16,37)M,R(2,M),DR,PHIW,ENUM,WE2CL(M),
     1                 WE1CL(M),WADENG,P(1,M),QBAR,V(2,M),WSPAN
C*****
C***          ***** HOMOGENEOUS ENERGY SOURCE *****
C
  225         IF(.NOT. OESOR)GO TO 230
              IF(.NOT. OEE)GO TO 226
         GAMW=GFMW
         MC=M-MINCOS
              IF(M .GE. MAXCOS)GAMW=GMW
              IF(M .GT. MINCOS .AND. M .LT. MAXCOS)GAMW=GCOS(MC)
              GO TO 230
  226    GAMW=GMW
              IF ( .NOT. OADDEN ) GO TO 230
         OADDEN = M .LT. MAXCOS
              IF ( .NOT. OADDEN )  GO TO 230
         DG=(G-GF)*(E2CL/ENMAX)
         GAMW=GMW-DG
              IF ( M .GT. MINCOS )  GO TO 227
         ADDENG = DELENG
              GO TO 228
  227    SPAN = M - MAXCOS
        SPAN = SPAN / SORSPA * PI
         SF=(DCOS ( THREE * SPAN ) - ENINE * DCOS (SPAN )
     *        + EIGHT) / SIXTEE
         ADDENG=DELENG*SF
         MC=M-MINCOS
         GCOS(MC)=GMW-(DG*SF)
         GAMW=GCOS(MC)
  228    ENUM = ENUM+ ADDENG
C*****
  230    EDEM = WUN + GAMW*(WUN-V1M/V2M)/TWO
```

```
      ENEW = ENUM/EDEM
      E(2,M) = ENEW
      P(2,M) = GAMW*ENEW/V2M
      A(M)=DSQRT((WUN+GAMW)*P(2,M)*V(2,M))
  235    IF(OTRACE)WRITE(16,41)M,NL,A(M),GAMW,P(2,M),V2M,V1M,ENEW,
     *          EDEM,ADDENG,DELENG,SPAN,SORSPA,RTAIL,R(2,M),RHEAD,DDR
C
C
C***     *** END OF LOOP FOR CALCULATION CELL PROPERTIES*******
C***    *** BACK TO 165  *****
C
C
      WRITE(18,236)T,NCYCLE,MWHEAD,MWTAIL,(P(2,I),V(2,I),I=1,5),
     *    (P(2,II),V(2,II),II=10,60,10)
  236 FORMAT(' ',E10.3,3I5,10F9.5/12F9.5)
      OPEAK = NSAM .NE. 0
      OENT = .TRUE.
         IF ( OSKIP )  GO TO 237
      NSX = (NCYCLE/NS)*NS
      OPUN = NSX .EQ. NCYCLE
C
  237    IF(.NOT. OPRINT) GO TO 238
      CALL SAMPLE
      CALL INT
      CALL FIDIF
C*****          *** FIDIF = 433  ********
      WRITE(6,31)T,ET,N
      IF(OEWAV)WRITE(6,48)RRHEAD,RRTAIL
C
  238       IF(.NOT. OPUN)GO TO 240
         IF(OPRINT)GO TO 239
      CALL SAMPLE
      CALL INT
  239 CALL PUDAT
      IST = IST + N
C1238            PUDAT = 791
C          DETERMINE NEXT TSTEP,TIME AND REINITIAL PROPERTIES
  240     IF ( OVER )  GO TO 248
          IF(OPRINT)GO TO 241
          IF(OPUN)GO TO 241
      CALL SAMPLE
      CALL INT
  241 CALL PUDAT
C1247            PUDAT = 791
      IST=IST+N
      NX=(NPR/NFRPR)*NFRPR
          IF(NPR .EQ. NX)GO TO 246
          GO TO 247
  246 CALL FIDIF
C1242            FIDIF = 433
  247 NPR=NPR+1
      WRITE(6,31)T,ET,N
      OVER = .TRUE.
      DTL = DT
      DT = DTHOL
      TLAS = T
      OPRINT = .TRUE.
          IF(OTRACE)WRITE(16,45)NCYCLE,INDEX,T,DT,DTHOL,DTL
                GO TO 289
  248 TLAS = T
      DTL = DT
C          STABILITY CRITERIA
      R2MP = R(2,1)
      GF = GF
      OFLIT = .FALSE.
C
C
          IF(OTRACE)WRITE(16,39)
C
C
          DO 281 M= 1,NL
      R2M = R2MP
      R2MP = R(2,M+1)
      RDIF = R2MP-R2M
      V2 = V(2,M)
      V1 = V(1,M)
```

```
000            AS2 = P(2,M)*V2*GE
000            VDOTN = TWO*(V2-V1)/(V2+V1)/DTL
000               IF ( VDOTN .LT. ZERO )  GO TO 265
000            BS2 = ZERO
000               GO TO 267
000       265  BS1 = CO*RDIF*VDOTN
000            BS2 =  64.D0*BS1*BS1
000       267  S2 = AS2 + BS2
000               IF(S2 .GT. ZERO)GO TO 268
000            S2 = WUN
000            WRITE(6,53)DEM,S2,BS2,BS1,AS2,VDOTN,V1,V2,RDIF,R2MP,R2M,
000          *          CO,DTL
000            OEXIT = .TRUE.
000       268  DEM = 3.D0*DSQRT(S2)
000            DT = TWO*RDIF/DEM
000               IF( OFLIT )  GO TO 280
000            OFLIT = .TRUE.
000            DTMIN = DT
000               IF (OEWAV)  GO TO 270
000               IF ( .NOT. OESOR )  GO TO 280
000       270  GRADEN = ( ENMAX / SLOSOR * AA / TMAXE ) * ( DEXP ( PHI ) -
000          *          DEXP ( - PHI * SOREXP) )
000               IF(GRADEN .NE. ZERO)  GO TO 276
000               GO TO 280
000       276  GRADTA = WUN / GRADEN
000            DTTES = ENSTEP * GRADTA
000               IF(OTRACE)WRITE(16,40)M,DT,DTMIN,DTTES,GRADTA,DEM,R2MP,
000          1          R2M,BS2,BS1,VDOTN,GE
000               IF ( DTTES .GT. DTMIN )  GO TO 280
000            DTMIN = DTTES
000       280     IF ( DT .LT. DTMIN )  DTMIN = DT
000               IF(OTRACE)WRITE(16,40)M,DT,DTMIN,DTTES,GRADTA,DEM,R2MP,
000          1          R2M,BS2,BS1,VDOTN,GE
000       281     IF ( M .EQ. NLT )  GE = G
000       C
000       C
000            DT = DTMIN
000               IF ( DT .LE. ZERO )  GO TO  309
000       C 291    LIMITING CONSTRAINT
000       C
000               IF  (DTL .LE. ZERO )  GO TO  289
000       289  DTUP =  1.4 D0*DTL
000               IF ( DT .GT. DTUP )  DT = DTUP
000            T = T + DT
000               IF(OTRACE)WRITE(16,40)M,DT,DTUP,DTL,DTMIN,DTTES,
000          1          GRADEN,DEM,PHI,VDOTN,GE,RDIF
000       C 290    REINITIAL PROPERTIES
000       C
000                    DO 297 M = 1,NL
000            U(1,M) = U(2,M)
000            R(1,M) = R(2,M)
000            V(1,M) = V(2,M)
000            Q(1,M) = Q(2,M)
000            P(1,M) = P(2,M)
000            E(1,M) = E(2,M)
000       297  CONTINUE
000            U(1,N)= U(2,N)
000            R(1,N) = R(2,N)
000               IF(OTRACE)WRITE(16,46)NCYCLE,INDEX,T,TLINE,TLAS,
000          1          TNEX,TIPUN,DT
000               IF ( .NOT. OPUTI ) GO TO 92
000               IF ( TLINE .GT. T )  GO TO 92
000            DTHOL = DT
000            OVER = .FALSE.
000            DT = TLINE    - TLAS
000            T = TLINE
000            TNEX = TNEX + WUN
000            TLINE = TNEX*TIPUN
000               IF(OTRACE)WRITE(16,47)NCYCLE,T,DT,TLINE,TNEX,DTHOL
000                    GO TO 92
000       C***     *** RETURN FOR CALCULATION OF NEW TIME STEP ************
000       C
000       C
000       C
000       309  WRITE ( 6,30)
000                    GO TO 314
```

```
000   C 311        PUNCH RESTART AND TERMINATE
000     312     IF ( N .GT. 201 )  N = 201
000             IF(OEWAV)WIDWAV=STWDWV
000   C
000             IF ( NPUNCH .GT. 0 )  CALL RESTAR
000   C
000   C
000     314   INDEX = INDEX -1
000             IF (NPUNCH .LE. 0 )  T = T - DT
000             IF (NPUNCH .LE. 0 )  NCYCLE = NCYCLE - 1
000   C
000           CALL INITIL
000   C1317          INITIL = 611
000           CALL BURST
000   C1318          BURST = 322
000     315   CONTINUE
000           S T O P
000           END
```

```
@HDG,P   ******  BURST  ******

@ELT,L BURST
ELT 68-01/14-14:42 BURST
000              SUBROUTINE BURST
000   C 321            BURST
000            IMPLICIT DOUBLE PRECISION(A-H,P-Z), LOGICAL(O),INTEGER(L)
000            DOUBLE PRECISION TERMIN,TIPUN,T,DT,DTL
000          COMMON / TIME / TERMIN,TIPUN, T,DT , DTL,
000         *                KRUN(3), LABEL(7)
000            COMMON/PARAM/CL,CO,G,GF,UL,UR,GMW,GFMW,FNMAX,ET,PJ1,SLOSOR,
000         1          SOREXP,TMAXE,TWO,WUN,ZERO,MINCOS,MAXCOS,J,JP1,N,NL,
000         2          NLI,NDP,NPART,NSTEPS,OFNT,OESOR,OPEAK,OPLANE,OPRINT,
000         3          OPUTI,OSKIP,OSPHER,OTRACE,MWTAIL,MWHEAD,WVEL,WIDWAV,
000         4          ENWAV,RHEAD,RTAIL,WSLSOR,WSREXP,MNWCOS,MXWCOS,OEWAV,
000         5          REF,E2CL
000            COMMON/ARGINT/INDEX,LSTART,NCYCLE,NFINAL,NSTORE,NS,NN,NNN,NPEAK,
000         1          NSAM,NSHIF,NBUFF,NFREQ,NWAVE,NPUNCH
000     327  DIMENSION   MONTH(48),M(2),
000         *      OIST(12), LIB(12), NLL(5),OIL(20)
000     329  DIMENSION KLF(2), KRF(2) , KLB(2), KRB(2),
000         *          KRO(2),  KLO(2)
000     331  EQUIVALENCE (OIST(1), M(1)),
000         *            (OIL(1), NLL(1))
000     333  DATA MONTH / '      ',' JAN','UARY', 7,'      ','FEBR','UARY', 8,
000         1              '      ','   M','ARCH', 5,'      ','   A','PRIL', 5,
000         2              '      ','    ',' MAY', 3,'      ','    ','JUNE', 4,
000         3              '      ','    ','JULY', 4,'      ','  AU','GUST', 6,
000         4              S','EPTE','MBER', 9,'      ',' OCT','OBER', 7,
000         5              ',','NOVE','MBER', 8,'      ','DECE','MBER', 8/
000     339  DATA OOSY / '0' /
000     340  DATA ODE / .FALSE. /
000     343  DATA LIB / '01','02','03','04','05','06','07','08','09',
000         1              '10','11','12'   /
000     345  DATA KLF / ' FRO','NT  ' /, KRF / '  FI','RST ' /
000     346  DATA KLB / ' BAC','K   ' /, KRB / '   L','AST ' /
000          DATA NOM / ', 19' /
000     349  DATA OFOR  / .FALSE. /
000     350  DATA  ICHAR/64/
000     351  DATA  INSTR/4095/
000     352  DATA  ISHOV/16779215/
000     353  DATA LYR/'  19'/
000     354  DATA  LZERO/'  0'/
000     355  DATA  LBLAN/' '/
000     356  DATA LCOMM/'    ,'/
000               CALL ERTRAN(9,M(1),M(2))
000               IF (ODE )  GO TO 407
000          ODE = .TRUE.
000          IYEAR=AND(INSTR,M(1))
000          IBUFF = AND(ISHOV,M(1))
000          IDAY = XOR(IBUFF,IYEAR)
000          IADD = AND(ISHOV,LBLAN)
000          IMON = XOR(IBUFF,M(1))
000          IMON = OR(IMON,IADD)
000          IBUFF = AND (LYR,INSTR)
```

213

```
000          IBUFF = XOR(IBUFF,LYR)
000          IYEAR = OR(IYEAR,IBUFF)
000          ICOMM = AND(LCOMM,INSTR)
000          IDAY = OR(ICOMM,IDAY)
000          IZERO = AND(LZERO,ISHOV)
000          IZERO = IZERO*ICHAR
000          ISTRIP = AND (IZERO,ISHOV)
000          IZERO = XOR(IZERO,ISTRIP)
000          IDAY = IDAY*ICHAR
000          ISTRIP = AND(IDAY,ISHOV)
000          ITEST = XOR(ISTRIP,IDAY)
000          OSI=ITEST .EQ. IZERO
000          ILEFT = AND(LBLAN,ISHOV)
000          ILEFT = XOR(ILEFT,LBLAN)
000          ISTRIP = OR(ILEFT,ISTRIP)
000             IF(OSI)   IDAY=ISTRIP
000          IDAY = IDAY/ICHAR
000          IDAY = AND(IDAY,ISHOV)
000          IDAY = OR(IDAY,ILEFT)
000          IDAY = IDAY*ICHAR
000          IM = 1
000                 DO  361    I = 1, 12
000             IF ( IMON .EQ. LIB(I) )  IM = I
000     361  CONTINUE
000          K= 4*( IM-1)
000                 DO  364     I = 1,3
000     364  NLL(I) = MONTH(K+I)
000          NLL(4) = IDAY
000          NLL(5) = IYEAR*ICHAR
000     398  FORMAT(' ','********** GAMMA CHANGES @ ENERGY ADDITION ****')
000     399  FORMAT( ' ', 4A4,A5,  ' TOTOEOTOEOEOTOOTOEOEOT     DETONAT',
000        1 'ON WAVES      OTOEOTOEOTOO ', 3A4, 'EOE ',A6,' ',A6, )
000     400  FORMAT(' ',4A4,A5,' TOOEO',2A4,14X,3I5,9X,2A4,
000        1                 3A4,'EOT ',A6,' ',A6)
000     401  FORMAT(' ',4A4,A5,' TOTOE',2A4,4X,2F15.8,4X,2A4,
000        1                 3A4,'FOT ',A6,' ',A6)
000     402  FORMAT ( '1',// )
000     403  FORMAT (' ', 4A4,A5, ' ETOEO' , 2A4, 38X, 2A4,3A4,
000        1  'EOE '    ,A6,' ',A6)
000     404  FORMAT(' ',4A4,A5,' TOOOE',2A4,4X,6I5,4X,2A4,3A4,
000        1                 'EOT ',A6,' ',A6)
000     405  FORMAT ( ' ', 4A4,A5, ' TOOEO', 2A4, 6X, 7A4, 4X,2A4,
000        1     3A4, 'EOT ',  A6,' ',A6)
000     406  FORMAT(/)
000     407  OFOR =   .NOT. OFOR
000             IF ( OFOR )      GO TO 413
000                 DO    411     I = 1,2
000          KLO(I) = KLB(I)
000     411  KRO(I) = KRB(I)
000                 GO TO 416
000     413         DO  415     I = 1,2
000          KLO(I) = KLF(1)
000     415  KRO(I) = KRF(1)
000     416  ILIM = 15
000                 DO    430       K = 1,3
000          WRITE ( 6,402)
000          WRITE(6,398)
000                 DO 420     I = 1,8
000     420  WRITE ( 6, 399)  NLL, KRUN,M(1),M(2)
000                 DO 422         I = 1,9
000     422  WRITE ( 6, 403)  NLL, KLO,          KRO, KRUN,M(1),M(2)
000          WRITE( 6, 405 ) NLL, KLO, LABEL, KRO, KRUN,M(1),M(2)
000          WRITE(6,404)NLL,KLO,LSTART,NCYCLE,NPUNCH,NSTORF,NS,NSTEPS,KRO,
000        1                 KRUN,M(1),M(2)
000          WRITE(6,404)NLL,KLO,NFINAL,NN,NNN,NBUFF,NFREQ,NWAVE,
000        1                 KRO,KRUN,M(1),M(2)
000          WRITE(6,401)NLL,KLO,TERMIN,TIPUN,KRO,KRUN,M(1),M(2)
000          WRITE(6,401)NLL,KLO,G,GF,KRO,KRUN,M(1),M(2)
000          WRITE(6,400)NLL,KLO,J,NDP,NLI,KRO,KRUN,M(1),M(2)
000                 DO   426    I = 1,9
000     426  WRITE ( 6,403)  NLL,KLO, KRO,KRUN,M(1),M(2)
000                 DO    428      I = 1,ILIM
000     428  WRITE ( 6,399)NLL, KRUN,M(1),M(2)
000             IF(K .EQ. 2)GO TO 430
000             IF ( OFOR )  ILIM = 2
000     430  CONTINUE
```

```
000                 WRITE(6,406)
000                        RETURN
000     C1431              INITIL = 675
000     C2431              MAIN PROGRAM = 319
000                END
```

```
@HDG,P   ******  FIDIF  ******
```

```
@ELT,L FIDIF
ELT 68-01/14-14:42 FIDIF
000                   SUBROUTINE FIDIF
000     C 433                    FIDIF
000                IMPLICIT DOUBLE PRECISION (A-H,P-Z),LOGICAL (O)
000                DOUBLE PRECISION MACH
000           11    COMMON / ARRAYS / U(2,201), R(2,201),V(2,201 ),Q(2,201),
000            U                        P(2,201), X(201), E(2,201), NCELL(201),
000            2                          WE2CL(201),WE1CL(201),A(201),GCOS(10)
000           13   COMMON/ TIME / TERMIN , TIPUN, T, DT, DTL,
000            *                           KRUN(3), LABEL(7)
000               COMMON / PARAM / C1 , CO, G, GF, UL, UR , GMW, GFMW, FNMAX, FT,
000            3                          PJ1,SLOSOR, SOREXP, TMAXE, TWO, WUN, ZERO ,
000            4                          MINCOS, MAXCOS, J, JP1, N, NL, NLI,NDP,
000            5                          NPART, NSTEPS, OENT, OESOR, OPEAK, OPLANE,
000            6                            OPRINT, OPUTI, OSKIP, OSPHER,OTRACE,
000            7                MWTAIL,MWHEAD,WVEL,WIDWAV,ENWAV,RHEAD,RTAIL,
000            8                WSLSOR,WSREXP,MNWCOS,MXWCOS,OEWAV,REF,E2CL
000           22 COMMON / ARGINT / INDEX, LSTART, NCYCLE, NFINAL, NSTORE, NS,
000            7                          NN, NNN, NPEAK, NSAM, NSHIF,NBUFF,NFREQ,NWAVE
000            2                 ,NPUNCH
000          451 FORMAT ( ' TIME =', 1PD12.6, 3X, 'DT =', D12.6, 5X, 'INDEX =',
000            *                        I5, 8X, 'VTIMD =', D12.6, 7X, 'CYCLE =', I5 / )
000          453 FORMAT( '   CELL    CENTER DIST   CENTER PRESS     PRESS DIFF    ',
000            *             'CELL SP VOL     CENTER VEL       CELL VISC    ',
000            *             'CELL ENERGY  CONTINUITY CELL')
000          454   FORMAT(' ','THE ENERGY WAVE BEGINS AT',F14.9,
000            1           ' AND ENDS AT ',F14.9)
000          456   FORMAT(' ',I5,2F14.9,1PE14.4,0PF14.9,1P2E14.4,0PF14.9,F9.4,I5)
000          457   FORMAT( '0', 20X, 'THE LEADING MACH NUMBER =', F7.4 )
000          458   FORMAT ( 1H1)
000          459   FORMAT ( '+', 6X, 8( '*', 13X ), '* PEAK **' )
000          460   FORMAT('+', 6X, 8('$',13X),'$ HEAD $$')
000          461   FORMAT('+', 6X, 8('!',13X),'! TAIL !!')
000          462   FORMAT(1H0,'NO LEAD SHOCK WAVE YET')
000                VTIME = T - DT/TWO
000     C461              PRINT HEADERS
000                WRITE ( 6, 458)
000                WRITE ( 6, 451   ) T,DT,INDEX,VTIME, NCYCLE
000                WRITE ( 6,453   )
000     C *****             CALCULATE CURRENT PROPERTIES
000                MM = NFREQ
000                    IF(NFREQ.LE.0)  MM = NL/25
000                    IF ( MM.EQ.0) MM = 1
000                    IF(.NOT. OEWAV)GO TO 470
000                MWHP9 = MWHEAD + 9
000                MWTM5 = MWTAIL - 5
000         470    R2 = R(2,1)
000                U2 = U(2,1)
000                RPJ2 = R2**JP1
000                IJ = 0
000                        DO    492   M = 1,NL
000                R1 = R2
000                U1 = U2
000                R2 = R(2,M+1)
000                U2 = U(2,M+1)
000                PD = P(2,M)-WUN
000                DMID = (R1+R2)/TWO
000                UMUD = (U1+U2)/TWO
000                RPJ1 = RPJ2
000                RPJ2 = R2**JP1
000                    IF(M  .LT. 9)GO TO 485
000                    IF(M  .EQ. NPEAK)GO TO 485
000                    IF ( M .LT. MWTM5 ) GO TO 484
000                    IF ( M .LE. MWHP9 ) GO TO 485
000                    IF ( M.EQ. NL ) GO TO 485
```

```
000      484  MX = ( ( M-NSHIF )/MM ) * MM + NSHIF
000              IF ( MX .NE. M ) GO TO  492
000      485  CM = (RPJ2-RPJ1)/V(2,M)/PJ1/X(M)
000    C 486                PRINT CURRENT PROPERTIES
000           WRITE ( 6, 456 )  NCELL(M), DMID, P(2,M),PD,V(2,M),
000         *                   UMUD, Q(2,M), E(2,M), CM,M
000           IJ = IJ + 1
000              IF ( M .EQ. MWTAIL ) WRITE (6,461)
000              IF (M .EQ. MWHEAD ) WRITE(6,460)
000              IF   ( M .NE.NPEAK )   GO TO  491
000           WRITE ( 6, 459)
000           GA = G
000              IF(M .LT. MWHEAD)GA = GF
000             MACH = DSQRT ( ( P(2,M) - WUN )*(GA+WUN) / TWO/GA+WUN )
000      491     IF(IJ .GT. 60)GO TO 493
000      492  CONTINUE
000      493     IF(P(2,NPEAK) .GT. WUN) WRITE(6,457) MACH
000              IF(P(2,NPEAK) .LE. WUN) WRITE(6,462)
000              IF(OEWAV)WRITE(6,454)RHEAD,RTAIL
000           RETURN
000    C1494              INITIL = 730
000    C2494              MAIN PROGRAM 238
000    C3494              MAIN PROGRAM 242
000           END
```

@HDG,P ****** GENDAT ******

@ELT,L GENDAT
ELT 6B-01/14-14:42 GENDAT

```
000                SUBROUTINE GENDAT
000    C 496             GENDAT
000           IMPLICIT DOUBLE PRECISION (A-H,P-Z),LOGICAL (O)
000      11    COMMON / ARRAYS / U(2,201), R(2,201),V(2,201 ),Q(2,201),
000        U                      P(2,201), X(201), E(2,201), NCELL(201),
000        2                       WE2CL(201),WE1CL(201),A(201),GCOS(10)
000          COMMON / PARAM / C1 , C0, G, GF, UL, UR , GMW, GFMW, ENMAX, ET,
000        3                      PJ1,SLOSOR, SOREXP, TMAXE, TWO, WUN, ZERO ,
000        4                      MINCOS, MAXCOS, J, JP1, N, NL, NLI,NDP,
000        5                      NPART, NSTEPS, OENT, OESOR, OPEAK, OPLANE,
000        6                        OPRINT, OPUTI, OSKIP, OSPHER,OTRACE,
000        7              MWTAIL,MWHEAD,WVEL,WIDWAV,ENWAV,RHEAD,RTAIL,
000        8              WSLSOR,WSREXP,MNWCOS,MXWCOS,OEWAV,REF,E2CL
000      507  FORMAT()
000      508  FORMAT('0',10X,'KERNEL PRESSURE: P(KER.)/P(AMB.)=',F5.2,/
000        1           10X,'                T(KER.)/T(AMB.)=',F5.2,/
000        2          10X,'THERE ARE',I5,' CELLS WITH',I5,' FAIRING CELLS',/)
000      511  FORMAT ( '4', 5X, 'ENERGY SOURCE: ENERGY(SOR. MAX. ) / ENERGY',
000        *      '(INT. AMB.) = ', F8.1, '   FINAL ENERGY DEPOSITION TIME ',
000        *      '(TAU MAX.) = ', F5.2, / , 20X, ' SHAPING CONSTANT 1 = ',
000        3   F6.2, ' SHAPING CONSTANT 2 = ',F5.2, '   CELL NO OF RO = ',
000        4      F5.2, /, 21X, '(MIN.) CELL NO.  OF COS. DIST. = ', I4,
000        *       '  (MAX.) CELL NO. OF COS. DIST. = ', I4 )
000     C
000           READ (5,507)  PRESS, TEMP,    N, NDEC
000     C
000           WRITE ( 6, 508)  PRESS, TEMP, N, NDEC
000              IF(N .GE.201)GO TO 609
000           GGMW = GFMW
000              IF(OEWAV)GGMW = GMW
000              IF(OESOR)GGMW=GMW
000           NL = N-1
000           LIMIT=N-2*NDEC
000           BUFF = N-NDEC
000              IF ( OESOR ) WRITE( 6,   511) ENMAX, TMAXE, SLOSOR,
000         *            SOREXP, BUFF, MINCOS, MAXCOS
000           REF = WUN/BUFF
000           VOL = TEMP/PRESS
000           R1 = ZERO
000           R1J = ZERO
000           R(1,1) = R1
000           P(1,1) = PRESS
000           V(1,1) = VOL
000           NCELL(1) = 1
000           A(M)=DSQRT((WUN+GGMW)*P(1,M)*V(1,M))
```

```
000          E(1,1) = TEMP/GGMW
000             IF ( LIMIT .EQ. 1 ) GO TO 545
000                 DO   544  M =  2,LIMIT
000          R2J = R1J
000          BUFF = M-1
000          R1 = BUFF * REF
000          R1J =  R1**JP1
000          R(1,M) = R1
000          P(1,M) = PRESS
000          V(1,M) = VOL
000          X(M-1) = (R1J-R2J)/VOL/PJ1
000          NCELL(M) = M
000             IF(M .GT. NLI)GGMW = GMW
000          A(M)=DSQRT((WUN+GGMW)*P(1,M)*V(1,M))
000    544   E(1,M) = TEMP / GGMW
000    545   LL = LIMIT
000          XRMXO = NDEC
000          XRMXO = TWO*XRMXO*REF
000          PS = PRESS - WUN
000          TS = TEMP-WUN
000                 DO  568    I = 1, NDEC
000          M = LL + I
000          BUFF = M-1
000          R2J = R1J
000          R1 = BUFF*REF
000          R1J = R1**JP1
000          R(1,M) = R1
000          X(M-1) = (R1J-R2J)/VOL/PJ1
000          NCELL(M) = M
000          XMXO = I
000          XMXO = XMXO*REF
000          SCALE = TWO*((XMXO/XRMXO)**2)
000          PV = PRESS-SCALE*PS
000          TV = TEMP-SCALE*TS
000          VOL = TV/PV
000          V(1,M) = VOL
000          P(1,M) = PV
000             IF(M .GT. NLI)GGMW = GMW
000          A(M)=DSQRT((WUN+GGMW)*P(1,M)*V(1,M))
000    568   E(1,M) = TV/GGMW
000          LL = LL+NDEC
000                 DO    587    I = 1,NDEC
000          M= LL+I
000          BUFF = M-1
000          R2J = R1J
000           R1 = BUFF*REF
000          R1J = R1**JP1
000          X(M-1) = (R1J-R2J)/VOL/PJ1
000          R(1,M) = R1
000          NCELL(M) = M
000          XRMX = NDEC -I
000          XRMX = XRMX*REF
000          SCALE = TWO*((XRMX/XRMXO)**2)
000          PV = WUN+SCALE*PS
000          TV = WUN+SCALE*TS
000          VOL = TV/PV
000          P(1,M) = PV
000          V(1,M) = VOL
000             IF(M .GT.  NLI)GGMW = GMW
000          A(M)=DSQRT((WUN+GGMW)*P(1,M)*V(1,M))
000    587   E(1,M) = TV/GGMW
000          LL = N+1
000                 DO    599  M = LL, 201
000          BUFF = M-1
000          R1 = BUFF * REF
000          NCELL(M) = M
000          P(1,M) = WUN
000          V(1,M) = WUN
000             IF(M .GT. NLI)GGMW = GMW
000          E(1,M) = WUN/GMW
000          R2J = R1J
000          R1J = R1**JP1
000          R(1,M) = R1
000          A(M)=DSQRT((WUN+GGMW)*P(1,M)*V(1,M))
000    599   X(M-1) = (R1J-R2J)/PJ1
000                 DO     608   M = 1,201
```

```
000            U(1,M) = ZERO
000            U(2,M) = ZERO
000            Q(1,M) =  ZERO
000            Q(2,M) = ZERO
000            WE2CL(M) = ZERO
000            R(2,M) = R(1,M)
000            P(2,M) = P(1,M)
000            V(2,M) = V(1,M)
000      608   E(2,M) = E(1,M)
000      609   CONTINUE
000            RETURN
000     C1609          INITIL = 668
000            END
```

@HDG,P ****** INITIL ******

```
@ELT,L INITIL
ELT 68-01/14-14:42 INITIL
000               SUBROUTINE INITIL
000     C 611                INITIL
000            IMPLICIT DOUBLE PRECISION (A-H,P-Z),LOGICAL (O)
000            DOUBLE PRECISION MACH
000      11     COMMON / ARRAYS / U(2,201), R(2,201),V(2,201 ),Q(2,201),
000       U                       P(2,201), X(201), E(2,201), NCELL(201),
000       2                       WE2CL(201),WE1CL(201),A(201),GCOS(10)
000      13    COMMON/ TIME / TERMIN , TIPUN, T, DT, DTL,
000       *                       KRUN(3), LABEL(7)
000           COMMON / PARAM / CI , CO, G, GF, UL, UR , GMW, GFMW, FNMAX, ET,
000       3                       PJI,SLOSOR, SOREXP, TMAXF, TWO, WUN, ZERO ,
000       4                       MINCOS, MAXCOS, J, JP1, N, NL, NLI,NDP,
000       5                       NPART, NSTEPS, OFNT, OESOR, OPEAK, OPLANE,
000       6                         OPRINT, OPUTI, OSKIP, OSPHER,OTRACE,
000       7               MWTAIL,MWHEAD,WVEL,WIDWAV,ENWAV,RHEAD,RTAIL,
000       8               WSLSOR,WSREXP,MNWCOS,MXWCOS,OEWAV,REF,E2CL
000      22   COMMON / ARGINT / INDEX, LSTART, NCYCLE, NFINAL, NSTORE, NS,
000       7                       NN, NNN, NPEAK, NSAM, NSHIF,NBUFF,NFREQ,NWAVE
000       2               ,NPUNCH
000     627    DIMENSION KINIT(3),KREST(2),KNUM(9)
000     628    DATA KINIT / 'INIT','IAL ','RUN ' /,
000       *         KREST / 'REST','ART ' /,
000       *         KNUM / '1 TE','2 TE','3 TE','4 TE','5 TE',
000       *         '6 TE','7 TE','8 TE','9 TE' /
000     633    DATA ALLOW / 1.0D-5 /
000     634    FORMAT()
000     635    FORMAT()
000     636    FORMAT()
000     637    FORMAT()
000     638    FORMAT(/, 40X, 'FIRST TIME STEP =',F13.6/
000       2              40X, 'GAMMA1             =',F13.6/
000       3              40X, 'GAMMA4             =',F13.6)
000     639    FORMAT(30X,'PLANAR GEOMETRY')
000     640    FORMAT(30X,'CYLINDRICAL GEOMETRY')
000     641    FORMAT(30X,'SPHERICAL GEOMETRY')
000     642    FORMAT(30X,'DESIGNATED MAX TIME = ',I4,' SECONDS'/
000       1              30X,'NUMBER OF TIME STEPS  =',I5/)
000     643    FORMAT(10X,'RESULTS WILL BE STORED FOR RESTART')
000     644    FORMAT(15X,'LINEAR ARTIFICIAL VISCOSITY COFFFICIENT    =',D13.6/
000       1              15X,'QUADRATIC ARTIFICIAL VISCOSITY COEFFICIENT =',D13.6/)
000     645    FORMAT(10X,'RESULTS WILL NOT BE STORED FOR RESTARTING')
000     646    FORMAT(10X,'RESULTS OF EVERY',I5,' CYCLES ARE STORED ON TAPE')
000     647   FORMAT(70X,' ET =',D12.6)
000     648    FORMAT ( '0', 30X, ' THE SHOCK FRONT MACH NUMBER =',F7.4 )
000     649    FORMAT(10X,'THE MAXIMUM NUMBER OF CELLS IS ',I5,/
000       1              10X,'RESULTS ARE PRINTED EVERY',I5,' CYCLES',/
000       1              10X,'THE CURRENT NUMBER OF DATA POINTS IS',I5,/
000       1              10X,'GAMMA CHANGES AT CELL NUMBER',I5,/
000       1              10X,'THE FLOW VELOCITY AT THE LEFT BOUNDARY IS',F15.10,/
000       1              10X,'THE FLOW VELOCITY AT THE RIGHT BOUNDARY IS',F15.10,/)
000     650    FORMAT(10X,'THE ENERGY FUNCTION SLOPE CONSTANT EQUALS',F10.4,/
000       1              10X,'THE ENERGY SLOPING CONSTANT EQUALS',F10.4,/
000       2              10X,'THE MAXIMUM TIME OF ENERGY ADDITION IS',F10.4,/
000       3              10X,'THE MAXIMUM ENERGY ADDED IS',F10.4,/
000       4              10X,'THE SPATIAL ROUNDING FUNCTION BEGINS AT CELL',I5,/
000       5              10X,'THE OUTERMOST EDGE OF THE ENERGY FUNCTION IS AT '
```

```
      6             'CELL',I5)
  651  FORMAT()
  652  FORMAT(10X,'THE WAVE VELOCITY IS',1PE10.4,/
      2        10X,'THE WAVE FRONT WIDTH IS',F10.4,/
      3        10X,'THE ENERGY ADDED IS',E10.4,/
      4        10X,'THE WAVE SLOPE CONSTANT EQUALS',0PF10.4,/
      5        10X,'THE ENERGY SLOPE CONSTANT EQUALS',F10.4,/
      6        10X,'THE SPATIAL ROUNDING FUNCTION BEGINS AT CELL',I5,/
      7        10X,'THE LAST ENERGY CELL IS ',I5/)
  653  FORMAT(10X,'NO ENERGY ADDITION',/)
  654  FORMAT('0',30X,'THERE IS NO SHOCK WAVE  ',E10.4)
  655  FORMAT(10X,'RESULTS WILL BE STORED AT TIME INTERVALS',
      1        ' OF ',F10.6)
       OPASS = LSTART .NE. 0
          IF(OPASS) GO Tn 665
       NPART = 2000
       OENAD = .FALSE.
       T = ZERO
       DTL = ZERO
C
C654                  READ INPUT
C
       READ(5,634)NSTEPS,NFINAL,NN,NNN,TERMIN,TIPUN,NBUFF,NFREQ,NWAVE
C
       READ ( 5, 635)NDP,J,NLI,CL,CO,G,GF,UL,UR
          IF(OTRACE)WRITE(6,634)NSTEPS,NFINAL,NN,NNN,TERMIN,
      1         TIPUN,NBUFF,NFREQ,NWAVE
          IF(OTRACE)WRITE(6,635)NDP,J,NLI,CL,CO,G,GF,UL,UR
C
       OESOR = NBUFF .NE. 0
       OEWAV = NWAVE .NE. 0
          IF ( .NOT. OEWAV )  GO TO 660
           READ (5,651) WVEL,WIDWAV,ENWAV,
      1                  WSLSOR,WSREXP,MNWCOS,MXWCOS
       TISTO=WUN/(WVEL*5n0.0D0)
          IF(TIPUN .EQ. ZERO)TIPUN=TISTO
       OENAD= .TRUE.
  660        IF( .NOT. OESOR) GO TO 661
           READ (5,637) SLOSOR, SOREXP,TMAXE,ENMAX,
      *                 MINCOS,MAXCOS
       OENAD = .TRUE.
  661  GMW = G - WUN
       GFMW = GF - WUN
        NL=NDP-1
C****                  DEFINE INITIAL MESH POINTS AND CELL PARAMETERS
       JP1 = J+1
       PJ1 = JP1
       OALT = NDP.EQ. 0
          IF(INDEX .NE. n) GO TO 675
       KRUN(1) = KINIT(1)
       KRUN(2) = KINIT(2)
       KRUN(3) = KINIT(3)
          GO TO 670
  665        IF(INDEX .NE. 0) GO TO 728
       KRUN(1) = KREST(1)
       KRUN(2) = KREST(2)
       KRUN(3) = KNUM(LSTART)
  670        CALL BURST
C*****  ******BURST =  321 **********
  675        IF(OPASS) Go TO 715
       WRITE(6,649)NFINAL,NN,NDP,NLI,UL,UR
          IF( .NOT. OENAD) WRITE(6,653)
          IF ( OALT)  CALL GENDAT
C1667        GENDAT = 500
        IF ( OALT ) GO Tn  695
       R1 = ZERO
       GAMW = GFMW
             DO 694    M = 1,201
       NCELL(M) = M
       IF(M.GT.N) GO TO  679
       R2 = R1
C
       READ(5,636)K,R1,U(1,M),P(1,M),V(1,M),Q(1,M)
C
       R(1,M) = R1
       RDIF = R1-R2
```

```
      000               PHIGH = PEST
      000                GO TO 741
      000          747  PCAL = PEST/(ARGUE**POW      )
      000                   IF ( DABS(PCAL/PBASE-WUN) .LE.ALLOW)  GO TO 753
      000               OSWIT = PCAL .GT. PBASE
      000                   IF (OSWIT)  PHIGH = PEST
      000                   IF ( .NOT. OSWIT ) PLOW = PEST
      000                          GO TO 741
      000          753  MACH = DSQRT((PEST-WUN)*GPW/TWO/G+WUN       )
      000                   IF (PEST .GT. WUN) WRITE(6,648) MACH
      000                   IF (PEST .LE. WUN) WRITE(6,654)PEST
      000          755  T = T+DT
      000               RETURN
      000       C1756            MAIN PROGRAM = 58,317
      000               END
      000       C
```

@HDG,P ****** INT ******

```
@ELT,L INT
ELT 6B-01/14-14:42 INT
      000                  SUBROUTINE INT
      000       C 758                  INT
      000       C
      000                IMPLICIT DOUBLE PRECISION (A-H,P-Z),LOGICAL (O)
      000           11    COMMON / ARRAYS / U(2,201), R(2,201),V(2,201 ),Q(2,201),
      000             U                 P(2,201), X(201), E(2,201), NCELL(201),
      000             *        WE2CL(201),WE1CL(201),A(201),GCOS(10)
      000              COMMON / PARAM / C1 , CO, G, GF, UL, UR , GMW, GEMW, ENMAX, ET,
      000             3                 PJ1,SLOSOR, SOREXP, TMAXE, TWO, WUN, ZERO ,
      000             4                 MINCOS, MAXCOS, J, JP1, N, NL, NLI,NDP,
      000             5                 NPART, NSTEPS, OENT, OESOR, OPEAK, OPLANE,
      000             6                    OPRINT, OPUTI, OSKIP, OSPHER,OTRACE,
      000             7                    MWTAIL,MWHEAD,WVEL,WIDWAV,ENWAV,RHEAD,RTAIL,
      000             8                    WSLSOR,WSREXP,MNWCOS,MXWCOS,OFWAV,REF,E2CL
      000          776  FORMAT(2I5,4E12.5)
      000          777  FORMAT(' ',I5,10E12.5)
      000               ET = -(R(1,N)**JP1)/GMW
      000               R2P = R(1,1)**JP1
      000               U1MP= U(1,1)
      000                U2MP = U(2,1)
      000                  IF(OTRACE)WRITE(16,776)N,NL,U2MP,U1MP,R2P,R(1,N)
      000                          DO 781   M =  1,NL
      000               R1P = R2P
      000               R2P = R(1,M+1)**Jp1
      000               U1M = U1MP
      000               U2M = U2MP
      000               U1MP = U(1,M+1)
      000               U2MP = U(2,M+1)
      000               U2 =   (U1MP*U2MP+U1M*U2M)/TWO
      000                  IF(OTRACE)WRITE(16,777)M,ET,E(1,M),U2,R2P,R1P,V(1,M),
      000             *            U1MP,U2MP,U1M,U2M
      000          781  ET = ET  +(E(1,M)+U2/TWO)*(R2P-R1P)/V(1,M)
      000               RETURN
      000       C1782              INITIL = 716
      000       C2782              MAIN PROGRAM 238   ,
      000               END
      000       C
      000       C
```


@HDG,P ****** PUDAT ******

```
@ELT,L PUDAT
ELT 6B-01/14-14:42 PUDAT
      000                  SUBROUTINE PUDAT
      000       C 784                  PUDAT
      000              IMPLICIT DOUBLE PRECISION(A-H,P-Z),LOGICAL(O)
      000              REAL TTT
      000           11  COMMON / ARRAYS / U(2,201), R(2,201),V(2,201 ),Q(2,201),
      000             U                 P(2,201), X(201), E(2,201), NCELL(201),
      000             2                   WE2CL(201),WE1CL(201),A(201),GCOS(10)
      000           13  COMMON/ TIME / TERMIN , TIPUN, T, DT, DTL,
```

```
000          1                 KRUN(3), LABEL(7)
000     COMMON / PARAM / C1 , CO, G, GF, UL, UR , GMW, GFMW, ENMAX, ET,
000          3                 PJ1,SLOSOR, SOREXP, TMAXE, TWO, WUN, ZERO ,
000          4                 MINCOS, MAXCOS, J, JP1, N, NL, NLI,NDP,
000          5                 NPART, NSTEPS, OENT, OESOR, OPEAK, OPLANE,
000          6                   OPRINT, OPUTI, OSKIP, OSPHER,OTRACE,
000          7            MWTAIL,MWHEAD,WVEL,WIDWAV,ENWAV,RHEAD,RTAIL,
000          8            WSLSOR,WSREXP,MNWCOS,MXWCOS,OEWAV,REF,E2CL
000     22 COMMON / ARGINT / INDEX, LSTART, NCYCLE, NFINAL, NSTORE, NS,
000          7               NN, NNN, NPEAK, NSAM, NSHIF,NBUFF,NFREQ,NWAVE
000          2               ,NPUNCH
000     804  FORMAT(I5,E15.9,2I5,E15.9,I5,2E15.9)
000     805  FORMAT(I5,E15.9,I5,5E18.13)
000     806  FORMAT(' ',E10.3,2I5,10F9.5/12F9.5)
000     807  FORMAT(' ',E15.7,4I5,6E14.8)
000          OSAMP=NSTORE .GT. 1
000     C
000     C 811         STORE CURRENT PROPERTIES
000     C
000          MM = NFREQ
000             IF ( MM.EQ. 0 ) MM = 1
000          LCAR = 1
000          WRITE(19,804)LCAR,T,NL,NCYCLE,ET,NPEAK,G,GF
000          LCAR = 2
000          R2 = R(2,1)
000          U2 = U(2,1)
000          A2=A(1)
000             DO 847  M =  1,NL
000          R1 = R2
000          U1 = U2
000          A1=A2
000          R2 = R(2,M+1)
000          U2 = U(2,M+1)
000          A2=A(M+1)
000          DMID = (R1+R2)/TWO
000          UMUD = (U1+U2)/TWO
000          AMID=(A1+A2)/TWO
000             IF (.NOT. OSAMP ) GO TO 835
000             IF (M .EQ. NL )  GO TO 835
000          MX = (( M-NSHIF )/MM)*MM+NSHIF
000             IF (MX.NE.M)  GO TO 847
000     835  WRITE(19,805)LCAR,AMID,M,DMID,UMUD,P(2,M),V(2,M),E(2,M)
000          LCAR=LCAR+1
000     847     CONTINUE
000          TTT=T/TIPUN
000          IC=TTT
000          ICY=IC+1
000          WRITE(20,807)T,ICY,NCYCLE,NL,NPEAK,P(2,NPEAK),V(2,NPEAK),
000         *               R(2,NPEAK),E(2,NPEAK),U(2,NPEAK),A(NPEAK)
000          WRITE(18,806)T,ICY,MWHEAD,MWTAIL,P(2,1),V(2,1),P(2,2),
000         *   V(2,2),P(2,3),V(2,3),P(2,4),V(2,4),P(2,5),V(2,5),
000         *      P(2,10),V(2,10),P(2,20),V(2,20),P(2,30),V(2,30),P(2,40),
000         *   V(2,40),P(2,50),V(2,50),P(2,60),V(2,60)
000             RETURN
000     C1849         MAIN PROGRAM = 239
000     C2849         MAIN PROGRAM = 241
000          END
000     C
000     C

@HDG,P ****** RESTAR ******

@ELT,L RESTAR
ELT 6B-01/14-14:42 RESTAR
000             SUBROUTINE RESTAR
000     C 851             RESTAR
000          IMPLICIT DOUBLE PRECISION (A-H,P-Z),LOGICAL (O)
000     11     COMMON / ARRAYS / U(2,201), R(2,201),V(2,201 ),Q(2,201),
000          U                 P(2,201), X(201), E(2,201), NCELL(201),
000          2                   WE2CL(201),WE1CL(201),A(201),GCOS(10)
000     13   COMMON/ TIME / TERMIN , TIPUN, T, DT, DTL,
000          1                 KRUN(3), LABEL(7)
000      COMMON / PARAM / C1 , CO, G, GF, UL, UR , GMW, GFMW, ENMAX, ET,
000          3                 PJ1,SLOSOR, SOREXP, TMAXE, TWO, WUN, ZERO ,
```

```
000        4                   MINCOS, MAXCOS, J, JP1, N, NL, NLI,NDP,
000        5                   NPART, NSTEPS, OENT, OESOR, OPEAK, OPLANE,
000        6                      OPRINT, OPUTI, OSKIP, OSPHER,OTRACE,
000        7              MWTAIL,MWHEAD,WVEL,WIDWAV,ENWAV,RHEAD,RTAIL,
000        8              WSLSOR,WSREXP,MNWCOS,MXWCOS,OEWAV,REF,F2CL
000       22 COMMON / ARGINT / INDEX, LSTART, NCYCLE, NFINAL, NSTORE, NS,.
000        1                  NN,NNN,NPEAK,NSAM,NSHIF,NBUFF,NFREQ,NWAVE
000        2              ,NPUNCH
000      868  FORMAT(4I5,2D35.28,3I5)
000      869  FORMAT(5I5,7A4)
000      870  FORMAT(3I5,3D35.28/3D35.28,I5)
000      871  FORMAT(I4,4D28.18/2D28.18,I4,2D28.18)
000      872  FORMAT ( 3D35.28/D35.28,2I5,D35.28)
000      873  FORMAT ( 2D35.28, I5/2D35.28,2L2)
000      874  FORMAT(5D24.18/4D24.18)
000      875  FORMAT (3D35.28/2D35.28,4I5)
000              IF(INDEX.EQ.0)    GO TO   892
000     C***           **** STORE DATA FOR LATER RESTARTING RUN ********
000     C
000     C
000           NPUNCH = 1
000           NCYCLE = NCYCLE-1
000            T = T - DT
000           WRITE (17,869)LSTART,NCYCLE,NPUNCH,NSTORE,NS,LABEL
000            WRITE(17,868)NSTEPS,NFINAL,NN,NNN,TERMIN,TIPUN,NBUFF,NFREQ,NWAVE
000           WRITE (17,870) N,J,NLI,T,DT,DTL,UL,UR,REF,NPEAK
000           WRITE(17,873) CL,CO,NPART,GF,G,OESOR,OEWAV
000              IF ( .NOT. OEWAV) GO TO 886
000              WRITE(17,875) WVEL,WIDWAV,ENWAV,WSLSOR,
000        1                   WSREXP,MNWCOS,MXWCOS,MWTAIL,MWHEAD
000           WRITE(17,874)(GCOS(MC),MC=1,9)
000      886     IF(.NOT. OESOR)GO TO 887
000            WRITE(17,872) SLOSOR,SOREXP ,
000        *                   TMAXE, ENMAX,MINCOS,MAXCOS,F2CL
000           WRITE(17,874)(GCOS(MC),MC=1,9)
000      887     DO  889  M = 1,N
000            WRITE (17,871) M, R(1,M), P(1,M),V(1,M),
000        *                   U(1,M),Q(1,M),X(M),NCELL(M),WE2CL(M),E(1,M)
000      889  C O N T I N U E
000           ENDFILE 17
000           ENDFILE 17
000           ENDFILE 19
000           ENDFILE 19
000           GO TO 932
000      C *****                READ RESTART CARDS
000      892  READ(15,869)LSTART,NCYCLE,NPUNCH,NSTORE,NS,LABEL
000           READ(15,868)NSTEPS,NFINAL,NN,NNN,TERMIN,TIPUN,NBUFF,NFREQ,NWAVE
000           READ(15,870) N,J,NLI,T,DT,DTL,UL,UR,REF,NPEAK
000           NL = N-1
000           JP1 = J+1
000           PJ1 = JP1
000           READ(15,873) CL,CO,NPART,GF,G,OESOR,OEWAV
000           GMW = G-WUN
000           GFMW = GF-WUN
000           R1 = ZERO
000           GAMW = GMW
000              IF(.NOT. OEWAV)GO TO 895
000              READ(15,875) WVEL,WIDWAV,ENWAV,WSLSOR,
000        1                   WSREXP,MNWCOS,MXWCOS,MWTAIL,MWHEAD
000           READ(15,874)(GCOS(MC),MC=1,9)
000      895     IF( .NOT. OESOR)GO TO 896
000           READ (15, 872) SLOSOR,SOREXP,
000        *                   TMAXE, ENMAX,MINCOS,MAXCOS,F2CL
000           READ(15,874)(GCOS(MC),MC=1,9)
000      896     DO  928  M = 1,201
000              IF (M.GT.N) GO TO   913
000           R2 = R1
000           READ(15,871)  K,R1,P(1,M),V(1,M),U(1,M),
000        *                   Q(1,M), X(M),NCELL(M),WE2CL(M),E(1,M)
000           RDIF = R1-R2
000           R(1,M) = R1
000              GO TO 921
000      913  B2 = M-N
000           R(1,M) = R1+B2*RDIF
000           P(1,M) = WUN
000           V(1,M) = WUN
```

```
000                U(1,M) = ZERO
000                Q(1,M) = ZERO
000                NCELL(M) = M
000                WE2CL(M) = ZERO
000                X(M-1) = (R(1,M)**JP1-R(1,M-1)**JP1)/V(1,M-1)/PJ1
000                   IF(OEWAV)GAMW = GMW
000                E(1,M) = P(1,M)*V(1,M)/GAMW
000         921    R(2,M) = R(1,M)
000                U(2,M) = U(1,M)
000                P(2,M) = P(1,M)
000                V(2,M) = V(1,M)
000                Q(2,M) = Q(1,M)
000                E(2,M) = E(1,M)
000         928    CONTINUE
000                X(201) = ZERO
000         932    R E T U R N
000       C1932          MAIN PROGRAM = 53
000                   END
```

```
@HDG,P   ******  SAMPLE  ******

@ELT,L SAMPLE
ELT 6B-01/14-14:42 SAMPLE
000                     SUBROUTINE SAMPLE
000       C 933                   SAMPLE
000       C
000                IMPLICIT DOUBLE PRECISION (A-H,P-Z),LOGICAL (O)
000          11     COMMON / ARRAYS / U(2,201), R(2,201),V(2,201 ),Q(2,201),
000           U                      P(2,201), X(201), E(2,201), NCELL(201),
000           2                         WE2CL(201),WE1CL(201),A(201),GCOS(10)
000             COMMON / PARAM / C1 , CO, G, GF, UL, UR , GMW, GEMW, FNMAX, ET,
000           3                      PJ1,SLOSOR, SOREXP, TMAXE, TWO, WUN, ZERO ,
000           4                      MINCOS, MAXCOS, J, JP1, N, NL, NLI,NDP,
000           5                      NPART, NSTEPS, OENT, OESOR, OPEAK, OPLANE,
000           6                         OPRINT, OPUTI, OSKIP, OSPHER,OTRACE,
000           7                      MWTAIL,MWHEAD,WVEL,WIDWAV,FNWAV,RHEAD,RTAIL,
000           8                      WSLSOR,WSREXP,MNWCOS,MXWCOS,OEWAV,REF,E2CL
000          22 COMMON / ARGINT / INDEX, LSTART, NCYCLE, NFINAL, NSTORE, NS,
000           7                      NN, NNN, NPEAK, NSAM, NSHIF,NBUFF,NFREQ,NWAVE
000           2         ,NPUNCH
000         947    DATA GAIN /1.001D0 /
000                DATA TEST/1.00001D0/
000         949    FORMAT(' ','964',4I5,L5,5E15.5)
000         952    FORMAT(' ','968',L5,7I5,5E12.6)
000                URE = ZERO
000                UGE = WUN
000                FDIF = ZERO
000                OSET = .FALSE.
000                         DO  964   I = 5,NL
000                PRE = UGE
000                K = N-I
000                UGE = P(2,K)
000                   IF (OSET)  GO TO 962
000                PDIF = FDIF
000                FDIF = UGE-PRE
000                   IF(UGE .LT. TEST)GO TO 963
000                   IF (FDIF .GE.PDIF)    GO TO 963
000                OSET = .TRUE.
000         962       IF (UGE .LE.URE)  GO T O 965
000         963    URE = UGE*GAIN
000         964       IF(OTRACE)WRITE(16,949)N,I,K,NL,OSET,UGE,URE,FDIF,PDIF,PRE
000                K = N-2
000         965    K = K+1
000                NPEAK = K
000                   IF(NPEAK .EQ. NL) NPEAK = 1
000                NFREQ = K/NSAM
000                NSHIF = K-NFREQ*NSAM
000                   IF  (NFREQ.GT. 0 ) GO TO 968
000                NFREQ= 1
000                NSHIF = 0
000         968       IF(OTRACE)WRITE(16,952)OSET,N,NSHIF,NFREQ,K,NSAM,NPEAK,I,
000           1              URE,UGE,GAIN,FDIF,PDIF
000                   RETURN
000       C1969            FIDIF=465
```

224

Appendix B

Computer Program for Analyzing Data

The calculation of the impulse and the energy integrals were performed by the following program which read and analyzed data stored on tape by the model. The tape is read from unit 10 and the input variables are read from unit 5. The following unit 5 input variables must be specified:

FIRST CARD

ILINE: Number of time lines to be calculated

MXWCOS: Cell number corresponding to the outermost cell of the source volume

J: Geometry factor

(0) Planar
(1) Cylindrical
(2) Spherical

TSCALE: Dummy variable not used in this edition of program.

RMAX: Maximum dimensionless radius at which impulse is calculated.

TO: Value of last time line. Set to 0.0 for first data set.

In addition to the printed output from unit 6 there are four other output units in which the output data is stored. Output unit 11 is for the impulse calculations, unit 12 is for pressure-time behavior at fixed Eulerian radius, unit 13 is for the energy distribution calculations and unit 14 stores the positions of selected particles for plotting of particle displacement.

```
 AMAIN(19)
       IMPLICIT LOGICAL (O)
       DIMENSION P(401),R(401),U(401),V(401),E(401),A(401),
     *      BALKE(102),TBALE(102),BPAKE(102),ETOTAL(102),TT(102),
     *      BALIF(102),AIRKE(102),AIRIF(102),RPRT(102,24),
     *      RR(5),RL(105),AIMP(105),OIMP(105),PP(404,5),TIME(404)
       READ(5,9)ILINE,MXWCOS,J,TSCALE,RMAX,TO
       WRITE(6,9)ILINE,MXWCOS,J,TSCALE,RMAX,TO
    9  FORMAT()
       EMAX=0.
       PI=ACOS(-1.)
       ESCAL=(PI*160./3.)**(1./3.)
       ATSCAL=SQRT(1.4)/ESCAL
       MXWCP1=MXWCOS+1
       JP1=J+1
       IPLT=0
       IMAX=102-2
       ITEST=ILINE/IMAX+1
          DO 55 I=1,401
       P(I)=1.
   55  R(I)=(I*.02)-.01
       IRMAX=105-2
          DO 66 I=1,IRMAX
   66  OIMP(I)=.TRUE.
C***** ESTABLISH LOCATIONS FOR CALCULATING IMPULSE *****
       RMLG=LOG10(RMAX)
       RMNLG=LOG10(.05*ESCAL)
       DLOG=(RMLG-RMNLG)/IRMAX
       IP=1
       RLG=RMNLG
          DO 77 IR=1,IRMAX
       RL(IR)=10.**(RLG)
       RLG=RLG+DLOG
C      WRITE(6,80)IR,RLG,DLOG,RL(IR)
   80  FORMAT()
   77  CONTINUE
C***** ESTABLISH LOCATIONS FOR P-T CURVES *****
          DO 88 IR=40,88,12
       RR(IP)=RL(IR)
C      WRITE(6,87)IR,IP,RL(IR),RR(IP)
   87  FORMAT(2I5,2F10.5)
       IP=IP+1
       IT=0
   88  CONTINUE
C ***** READ IN DATA *****
       DO 979 IO=1,ILINE
       READ(10,95,END=991,ERR=989)LCAR,T,NL,NCYCLE,ET,NLI,G,GF
   95  FORMAT(I5,F15.9,2I5,E15.9,I5,2F15.9)
       OPLOT= .TRUE.
       IT=IT+1
       TIME(IT)=T
       TMAX=T
       DT=T-TO
       TO=T
       IP=1
          IF(IO .EQ. 1)GO TO 96
       JTEST=(IO/ITEST)*ITEST
          IF(IO .NE. JTEST)OPLOT= .FALSE.
   96  WRITE(6,98)IO,JTEST,NL,NCYCLE,IT,OPLOT,T,DT,TO,FT
   98  FORMAT(5I5,L5,4F10.5)
          DO 199 I=1,NL
       READ(10,159,END=991,ERR=989)LCAR,A(I),M,R(I),U(I),P(I),
     *      V(I),E(I)
  159  FORMAT(I5,E15.9,I5,5E18.13)
C      WRITE(6,159)LCAR,A(I),M,R(I),U(I),P(I),V(I),E(I)
  199  CONTINUE
       IR=1
          DO 249 I=1,401
C      WRITE(6,218)I,IR,IP,IT,OIMP(IR),R(I),RL(IR),RO,RR(IP),
C    *      P(I),PO
```

```
  218   FORMAT(4I5,L5,6F10.5)
C ***** STORE DATA FOR P-T CURVES *****
           IF(IP .GT. 5)GO TO 219
           IF(R(I) .LT. RR(IP))GO TO 219
        DR=R(I)-RO
        DR1=RL(IR)-RO
        DP=P(I)-PO
        PR=PO+(DP*DR1/DR)
        PP(IT,IP)=-PR
           IF(PR .GT. PMAX)PMAX=PR
        IP=IP+1

           IF(I .GT. NL)GO TO 249
C *****  CALCULATE IMPULSE *****
  219      IF(R(I) .LT. RL(IR))GO TO 241
  220      IF( .NOT. OIMP(IR))GO TO 239
        DR=R(I)-RO
        DR1=RL(IR)-RO
        DP=P(I)-PO
        PR=PO+(DP*DR1/DR)-1.
           IF(PR .LT. 0.)GO TO 229
        AIMP(IR)=AIMP(IR)+PR*DT
  229   IF(P(I) .LT. 1.)OIMP(IR) = .FALSE.
  239   IRM1=IR
        IR=IR+1
           IF(IR .GE. IRMAX)GO TO 259
  241   CONTINUE
C       WRITE(6,244)I,IR,IRM1,OIMP(IRM1),RO,PO,AIMP(IRM1),PR,DP,DR1,DR,
C     *      RL(IRM1),R(I),P(I)
           IF(RL(IR) .LT. R(I))GO TO 220
        PO=P(I)
        RO=R(I)
  244   FORMAT(3I5,L5,10F10.5)
  249   CONTINUE
  259      IF(.NOT. OPLOT)GO TO 979
        IPLT=IPLT+1
        TT(IPLT)=T
C *****  STORE DATA FOR PARTICLE PATHS *****
        J=0
           DO 310 I=1,5
C       WRITE(6,309)IO,I,J,IPLT,R(I),TT(IPLT)
  309   FORMAT(4I5,2F10.5)
  310   RPRT(IPLT,I)=R(I)
        J=5
           DO 410 I=10,50,5
        J=J+1
C       WRITE(6,409)I,J,RPRT(I)
  410   RPRT(IPLT,J)=R(I)
  409   FORMAT(2I5,F10.5)
           DO 510 I=60,150,10
        J=J+1
C       WRITE(6,509)I,J,R(I)
  509   FORMAT(2I5,F10.5)
  510   RPRT(IPLT,J)=R(I)
C ***** CALCULATE ENERGY INTEGRAL *****
        ROP=0.
        BTMASS=0.
        ATMASS=0.
        TMASS=0.
        BALKE(IPLT)=0.
        BALIE(IPLT)=0.
        AIRKE(IPLT)=0.
        AIRIE(IPLT)=0.
        AIRAMB=1./(G-1.)
        ROP=0.
        RJ=0.
           DO 599 MC=1,MXWCOS
        RNEW=2.*R(MC)-ROP
        RNP=RNEW**JP1
        RMASS=(RNP-RJ)/V(MC)
        USQ=U(MC)**2
        GAMW=P(MC)*V(MC)/E(MC)
           IF(IO .LT. 16 .OR. IO .GT. 20)GO TO 555
C       WRITE(6,549)IO,MC,RMASS,USQ,BALKE(IPLT),GAMW,RNEW,V(MC),
C     *      R(MC),U(MC),E(MC),P(MC)
  549   FORMAT(2I5,10E11.3)
```

```
  555   BALAMB=1./GAMW
        CELLKE=((USQ*RMASS)/2.)
        BALKE(IPLT)=BALKE(IPLT)+CELLKE
        CELLIE=(E(MC)-BALAMB)*RMASS
        BALIE(IPLT)=BALIE(IPLT)+CELLIE
        BTMASS=BTMASS+RMASS
        RJ=RNP
        ROP=RNEW
C       WRITE(6,588)IO,MC,IPLT,ROP,RJ,BTMASS,RMASS,BALIE(IPLT),
C    *     CELLIE,BALKE(IPLT),CELLKE,GAMW,USQ
  588   FORMAT(3I5,10F10.5)
           IF(MC .GE. NL)GO TO 709
  599   CONTINUE
  609      DO 699 MC=MXWCP1,NL
        RNEW=2.*R(MC)-ROP
        RNP=RNEW**JP1
        RMASS=(RNP-RJ)/V(MC)
        USQ=U(MC)**2
        GAMW=G-1.
        CELLKE=((USQ*RMASS)/2.)
        AIRKE(IPLT)=AIRKE(IPLT)+CELLKE
        CELLIE=(E(MC)-AIRAMB)*RMASS
        AIRIE(IPLT)=AIRIE(IPLT)+CELLIE
        ATMASS=ATMASS+RMASS
        RJ=RNP
        ROP=RNEW
C       WRITE(6,588)IO,MC,IPLT,ROP,AIRAMB,E(MC),RMASS,AIRIE(IPLT),
C    *     CELLIE,AIRKE(IPLT),CELLKE,GAMW,USQ
  699     CONTINUE
  709   ETOTAL(IPLT)=BALKE(IPLT)+BALIE(IPLT)+AIRKE(IPLT)+AIRIE(IPLT)
           IF(ETOTAL(IPLT) .GT. EMAX)EMAX=ETOTAL(IPLT)
        TMASS=ATMASS+BTMASS
        TBALE(IPLT)=BALKE(IPLT)+BALIE(IPLT)
        BPAKE(IPLT)=TBALE(IPLT)+AIRKE(IPLT)
C       WRITE(6,899)IO,IPLT,MC,NL,TT(IPLT),ETOTAL(IPLT),BPAKE(IPLT),
C    *     TBALE(IPLT),BALIE(IPLT),BALKE(IPLT),AIRIE(IPLT),
C    *     AIRKE(IPLT),TMASS,ATMASS,BTMASS
  899   FORMAT(4I5,11F9.5)
  979   CONTINUE
  989   WRITE(6,990)IO,LCAR,M,NL,T,A(I),E(I),P(I),V(I),U(I)
  990   FORMAT('FILE ERROR',4I5,6F10.5)
  991   WRITE(6,992)LCAR,T,NL,NCYCLE,ET,NLI,G,GF
  992   FORMAT('END OF FILE',I5,F10.5,2I5,F10.5,I5,2F10.5)
        WRITE(11,1008)IRMAX,AISCAL
 1008   FORMAT(I5,F10.5)
        WRITE(11,1009)(I,OIMP(I),RL(I),AIMP(I),I=1,IRMAX)
 1009   FORMAT(I5,L5,2F20.10)
        WRITE(12,1014)IT,(RR(I),I=1,5)
 1014   FORMAT(I5,5F10.5)
        WRITE(12,1019)(I,TIME(I),(J,PP(I,J),J=1,5),I=1,IT)
 1019   FORMAT(6(I5,F10.5))
        WRITE(13,1029)IPLT,EMAX
 1029   FORMAT(I5,F15.10)
        WRITE(13,1059)(I,TT(I),BALKE(I),BALIE(I),AIRIE(I),
     *     AIRKE(I),TBALE(I),BPAKE(I),ETOTAL(I),I=1,IPLT)
 1059   FORMAT(I5,8F15.10)
        WRITE(14,1069)IO,IPLT
 1069   FORMAT(2I5)
        WRITE(14,1079)(II,TT(II),(RPRT(II,I),
     *     I=1,24),II=1,IPLT)
 1079   FORMAT(I5,12F9.5/13F9.5)
        WRITE(6,1069)IO,IPLT
        WRITE(6,1079)(II,TT(II),(RPRT(II,I),I=1,24),II=1,IPLT)
        STOP
        END
```

NOMENCLATURE

Roman

a_0	Speed of sound--ambient
a_1	Speed of sound--ahead of(before) shock wave
a_4	Speed of sound--behind(after) energy addition
C_i	Concentration - mass fraction
C_p	Constant pressure heat capacity
C_v	Constant volume heat capacity
c_0	Newtonian speed of sound--ambient
CJ	Chapman Jouguet condition
D	Lagrangian distance
D_1	Beginning of rounding term in energy source volume--Lagrangian distance
D_0	Extent of energy source volume--Lagrangian distance
D_w	Width energy addition wave--Lagrangian distance
e	Internal energy
e_i^o	Energy of formation--species i
e_0	Internal energy--ambient
E	Non-dimensional internal energy
E_B	Energy remaining within the source
E_S	Energy transmitted to the surrounding gas
E_T	Total amount of energy deposited at the source
$\overline{f}$	Body force vector
h	Enthalpy
Δh_f^o	Effective zero point energy
ΔH_c	Heat of combustion
h_i	Enthalpy--species i
h'	Enthalpy-working fluid heat addition model

h_1	Enthalpy-ahead of shock front
h_4	Enthalpy-behind energy addition
i	Species
I_+	Positive phase impulse
$\bar{I}$	Non-dimensional positive phase impulse
j	Geometry factor
K	Linear spring constant
m_c	Mass
M	Mach number
M_1	Mach number-approach flow
M_s	Mach number-expanding sphere
M_w	Mach number-energy addition wave
n	moles of gas within the source volume
p	Pressure
p_s	Shock pressure
p_o	Pressure--ambient
p_1	Pressure--ahead of shock
p_2	Pressure--behind shock
p_3	Pressure--behind (ahead of (before) energy addition
p_4	Pressure--behind(after) energy addition
P	Non-dimensional pressure
P^*	Non-dimensional dissipative pressure
P_s	Non-dimensional shock overpressure
q	Source energy density
$\dot{Q}$	Heat transfer rate
Q	Heat release during a constant gamma process
Q_c	Heat release/unit mass of fuel

Q_f	Non-dimensional amount of energy deposited at the origin
Q_F	Energy/unit mass deposited at the origin
r	Radial distance coordinate
r_0	Initial source radius
R	Gas constant
R_ε	Energy-scaled shock position
R_s	Shock position
R_0	Energy scaling distance
t	Time
t_a	Time of shock arrival
t_d	Source deposition time
t_{max}	Time at which maximum structural displacement occurs
t_0	Characteristic acoustic propagating time
$t+$	Time end of positive phase
t^-	Time--end of negative phase
T	Characteristic loading time
u	Particle velocity
U	Non-dimensional particle velocity
U_w	Non-dimensional energy wave velocity
V	Volume of the source
V_0	Initial source volume
$\bar{V}$	Flow velocity vector
W	Wave width-energy addition wave
W_{TNT}	Comparable weight of tri-nitro-toulene
X	Weight of explosive material
X_c	Weight of hydrocarbon explosive
Y	Similarity lines

Greek

γ	Specific heat ratio
γ_0	Specific heat ratio--ambient
γ_1	Specific heat ratio--ahead of(before) energy addition
γ_4	Specific heat ratio--behind(after) energy addition
η	Non-dimensional distance coordinate
Θ	Temperature
Θ_0	Temperature--ambient
Θ_1	Temperature--ahead of shock front
Θ_2	Temperature--behind shock front
Θ_4	Temperature--behind energy addition
λ	Energy source term
Λ	Non-dimensional energy source term
ν	Specific volume
ν_f	Specific volume expansion ratio
ν_0	Specific volume--ambient
ξ	Energy addition wave parameter
Ξ	Energy wave structure parameter
Π	Artificial viscosity term
ρ	Density
ρ_0	Density--ambient
ρ_1	Density--ahead of shock front
ρ_2	Density behind the shock front
σ	Length scaling factor
τ	Non-dimensional time

τ_c	Non-dimensional cell deposition time
τ_D	Non-dimensional source volume deposition time
τ_T	Non-dimensional energy wave source volume transit time
ψ	Non-dimensional specific volume
ω	Natural frequency
Ω	Non-dimension energy wave Mach number

BIBLIOGRAPHY

1. Strehlow, R.A., "Unconfined Vapor-Cloud Explosions--An Overview," 14th Symposium (International) on Combustion, The Combustion Institute, pp 1189-1200(1973).

2. Baker, W.E., Explosions In Air, University of Texas Press, Austin, Texas (1973).

3. Taylor, G.I., "The Air Wave Surrounding an Expanding Sphere," Proc. Royal Society, A186, pp. 273-292 (1946).

4. Sedov, L.I., Similarity and Dimensional Methods in Mechanics, Academic Press, New York, N.Y. (1959).

5. Bethe, H.A., Fuchs, K., Hirschfelder, H.O., Magee, J.L., Peierls, R.E., and Von Neumann, J., "Blast Waves," LASL 2000, Los Alamos Scientific Laboratory (1947).

6. Sakurai, A., "Blast Wave Theory," in Basic Developments in Fluid Mechanics, Vol I, (Morris Holt, ed.), Academic Press, New York, N.Y. (1965).

7. Oshima, K., On Exploding Wires (W.B. Chance and H.K. Moore, eds.) Vol. 2, Plenum Press, New York, N.Y. (1967).

8. Liepmann, H.W. and Roshko, A., Elements of Gas Dynamics, John Wiley and Sons, Inc., New York, N.Y. (1967).

9. Von Neumann, J. and Richtmyer, R.D., "A Method for the Numerical Calculation of Hydrodynamic Shocks", J. of Appl. Phys., 21, pp 233-237 (1950).

10. Lax, P.D. and Wendroff, B., "Systems of Conservation Laws," Comm of Pure and Applied Math., 13, p 217 (1960).

11. Richtmyer, R.D. and Morton, K.W., Difference Methods for Initial Value Problems, Interscience Publishers, Inc., New York, N.Y. (1967).

12. Von Neumann, J. and Goldstine, H., "Blast Wave Calculation," Comm. Pure and Appl. Math., 8, pp 327-353 (1955).

13. Brode, H.L., "Numerical Solutions of Spherical Blast Waves," J. Appl. Phys., 26, pp 766-775 (1955).

14. Ricker, R., "Blast Waves from Bursting Pressurized Spheres," M.S. Thesis, Aeronautical and Astronautical Engineering Dept., Univ. of Illinois, Urbana-Champaign, Ill. (1975).

15. Zajac, L.J. and Oppenheim, A.K., "The Dynamics of an Explosive Reaction Center," AIAA Journal, 9, pp 545-553 (1971).

16. Freeman, R.A., "Variable Energy Blast Waves," British Journal of Appl. Phys., Ser. 2, 1, pp 1697-1710 (1968).

17. Dabora, E.K., "Variable Energy Blast Waves," AIAA Journal, 10, pp 1384-5 (1972).

18. Adamczyk, A.A., "An Investigation of Blast Waves from Non-ideal Energy Sources," Ph.D. Thesis, Aeronautical and Astronautical Engineering Dept., Univ. of Ill, Urbana Champaign, Ill. (1975).

19. Rudinger, G., Nonsteady Duct Flow, Dover Publications, Inc., New York, N.Y. (1969).

20. Oppenheim, A.K., Kuhl, A.L., Lundstrom, E.A., and Kamel, M.M., "A Parametric Study of Self-similar Blast Waves," J. Fluid Mech., 52-4, pp 657-682 (1972).

21. Kuhl, A.L., Kamel, M.M., and Oppenheim, A.K., "Pressure Waves Generated by Steady Flames," XIV Symposium (International) on Combustion, The Combustion Institute, pp 1201-1215 (1973).

22. Strehlow, R.A., "Blast Waves Generated by Constant Velocity Flames: A Simplified Approach," Combustion and Flame, 24, pp 257-261 (1975).

23. Williams, F.A., Combustion Theory, Addison-Wesley Publishing Company, Inc., Reading, Ma.(1965).

24. Strehlow, R.A., Fundamentals of Combustion, International Textbook Company, Scranton, Pa. (1968).

25. Zajac, L.J. and Oppenheim, A.K., "Thermodynamic Computations for the Gasdynamic Analysis of Explosion Phenomena," Combustion and Flame, 13, pp 537-550 (1969).

26. Hopkinson, B., British Ordnance Board Minutes, 13565 (1915).

27. Strehlow, R.A., and Baker, W.E., "The Characterization and Evaluation of Accidental Explosions," Report NASA CR-134779 (1975).

28. Baker, W.E., Westine, P.S. and Dodge, F.T., Similarity Methods in Engineering Dynamics: Theory and Practice of Scale Modelling, Spartan Books, Rochelle Park, N.J. (1973).

29. Wilkins, M.L., "Calculation of Elastic-Plastic Flow," UCRL-7322, 7, Rev. 1, Lawrence Radiation Laboratory, Livermore, CA (1969).

30. Oppenheim, A.K., "Elementary Blast Wave Theory and Computations," Proceedings of the Conference on Mechanisms of Explosion and Blast Waves, Paper No. 1, Yorktown, Va (1973).

31. Boyer, D.W., Brode, H.L., Glass, I.I., and Hall, J.G., "Blast From a Pressurized Sphere," UTIA Report No. 48 (1958).

32. Huang, S.L., and Chou, P.C., "Calculations of Expanding Shock Waves and Late-Stage Equivalence," Final Report 125-12, Drexel Institute of Technology, Philadelphia, Pa. (April 1968).

33. Brode, H.L., "Blast Wave From a Spherical Charge," Physics of Fluids, 2, pp 217-229 (1959).

34. Brinkley, S.R., "Determination of Explosive Yields," AIChE Loss Prevention, 3, pp 79-82 (1969).

35. Fishburn, B.D., "Some Aspects From Fuel-Air Explosions," Acta Astronautica (in press (1977)).

36. Fishburn, B.D., Private Communication (1977).

CURRICULUM VITAE

Name: Robert Thomas Luckritz.

Permanent address: 90-36 Avenue North
Clinton, Iowa 52732.

Degree and date to be conferred: Ph.D., 1977.

Date of birth: February 24, 1943.

Place of birth: Clinton, Iowa.

Secondary education: Clinton High School
Clinton, Iowa
11 June 1961.

Collegiate institutions attended	Dates	Degree	Date of Degree
United States Coast Guard Academy	1961-1965	B.S.	June 9, 1965
University of Maryland	1969-1971	M.S.	June 5, 1971
University of Maryland	1971-1976	Ph.D.	May 14, 1977

Major: Chemical Engineering.

Professional positions held: June 1973-Dec. 1975
Lieutenant Commander
U.S. Coast Guard
Cargo and Hazardous Materials Division
U.S. Coast Guard Headquarters
Washington, D.C. 20590.